

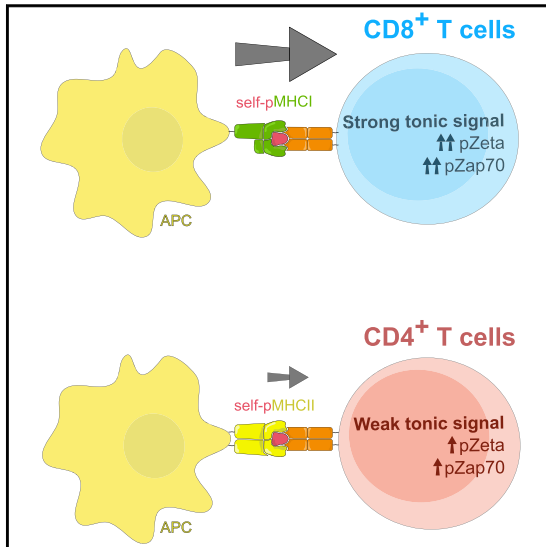
## **Attachment 1**

Dynamics of the Coreceptor-LCK  
Interactions during T Cell Development  
Shape the Self-Reactivity of Peripheral CD4  
and CD8 T Cells

# Cell Reports

## Dynamics of the Coreceptor-LCK Interactions during T Cell Development Shape the Self-Reactivity of Peripheral CD4 and CD8 T Cells

### Graphical Abstract



### Authors

Veronika Horkova, Ales Drobek, Daniel Mueller, ..., Carolyn G. King, Dietmar Zehn, Ondrej Stepanek

### Correspondence

ondrej.stepanek@img.cas.cz

### In Brief

Horkova et al. reveal dynamic regulation of the coreceptor-LCK interaction during T cell development, establishing the self-reactivity of mature T cells. Differences between CD8 and CD4 coreceptors cause peripheral CD8<sup>+</sup> T cells to be more self-reactive than CD4<sup>+</sup> T cells.

### Highlights

- Coupling of CD8-LCK but not CD4-LCK increases upon T cell maturation
- Dynamics of coreceptor-LCK coupling stoichiometry establish T cell self-reactivity
- CD8<sup>+</sup> T cells are more self-reactive than CD4<sup>+</sup> T cells



Horkova et al., 2020, Cell Reports 30, 1504–1514  
February 4, 2020 © 2020 The Author(s).  
<https://doi.org/10.1016/j.celrep.2020.01.008>

CellPress

# Dynamics of the Coreceptor-LCK Interactions during T Cell Development Shape the Self-Reactivity of Peripheral CD4 and CD8 T Cells

Veronika Horkova,<sup>1</sup> Ales Drobek,<sup>1</sup> Daniel Mueller,<sup>2</sup> Celine Gubser,<sup>2,3</sup> Veronika Niederlova,<sup>1</sup> Lena Wyss,<sup>2,4</sup> Carolyn G. King,<sup>2</sup> Dietmar Zehn,<sup>5</sup> and Ondrej Stepanek<sup>1,6,\*</sup>

<sup>1</sup>Laboratory of Adaptive Immunity, Institute of Molecular Genetics of the Czech Academy of Sciences, 14220 Prague, Czech Republic

<sup>2</sup>Department of Biomedicine, University Hospital and University of Basel, 4031 Basel, Switzerland

<sup>3</sup>Peter Doherty Institute, University of Melbourne, Melbourne, Australia

<sup>4</sup>Institute for Immunology, Biomedical Center (BMC) Munich, Ludwig-Maximilians-University, Munich, Germany

<sup>5</sup>Division of Animal Physiology and Immunology, School of Life Sciences Weihenstephan, Technical University of Munich, Freising, Germany

<sup>6</sup>Lead Contact

\*Correspondence: [ondrej.stepanek@img.cas.cz](mailto:ondrej.stepanek@img.cas.cz)

<https://doi.org/10.1016/j.celrep.2020.01.008>

## SUMMARY

Overtly self-reactive T cells are removed during thymic selection. However, it has been recently established that T cell self-reactivity promotes protective immune responses. Apparently, the level of self-reactivity of mature T cells must be tightly balanced. Our mathematical model and experimental data show that the dynamic regulation of CD4- and CD8-LCK coupling establish the self-reactivity of the peripheral T cell pool. The stoichiometry of the interaction between CD8 and LCK, but not between CD4 and LCK, substantially increases upon T cell maturation. As a result, peripheral CD8<sup>+</sup> T cells are more self-reactive than CD4<sup>+</sup> T cells. The different levels of self-reactivity of mature CD8<sup>+</sup> and CD4<sup>+</sup> T cells likely reflect the unique roles of these subsets in immunity. These results indicate that the evolutionary selection pressure tuned the CD4-LCK and CD8-LCK stoichiometries, as they represent the unique parts of the proximal T cell receptor (TCR) signaling pathway, which differ between CD4<sup>+</sup> and CD8<sup>+</sup> T cells.

## INTRODUCTION

T cells are involved in most adaptive immune responses. The hallmark of T cell responses is the variability of T cell receptors (TCRs) among individual T cell clones. The interaction between the TCR and its cognate antigen (i.e., a peptide bound to major histocompatibility complex class I [MHC I] or MHC II molecules) on the surface of an antigen-presenting cell (APC) leads to the activation of the T cell and the initiation of the immune response.

There are two basic types of T cells, MHC I-restricted CD8<sup>+</sup> T cells and MHC II-restricted CD4<sup>+</sup> T cells. CD8<sup>+</sup> T cells are involved in direct killing of infected cells, whereas CD4<sup>+</sup> T cells orchestrate immune responses by acting on other immune cells. Invariant coreceptors CD4 and CD8 bind to MHC I and MHC II, respectively, to promote the TCR signaling. One of the major

roles of the coreceptors is to recruit a kinase LCK to the TCR signaling complex, which, in turn, leads to the phosphorylation of the TCR-associated chains and the initiation of the downstream signaling (Artyomov et al., 2010; van Oers et al., 1996; Rudd et al., 2010; Veillette et al., 1988; Barber et al., 1989). The interaction between the coreceptor and LCK regulates the sensitivity of T cells to the antigen (Erman et al., 2006; Stepanek et al., 2014; Drobek et al., 2018).

Besides their key role in protective immunity, T cells can induce harmful autoimmunity, depending on whether they respond to foreign or self-antigens. A central mechanism establishing self-tolerance is the negative selection of highly self-reactive T cells during their maturation in the thymus. However, a certain level of self-reactivity of mature T cells is required because only the self-pMHC-restricted pool of T cells can efficiently recognize foreign antigens. This is achieved by positive selection of developing T cells with moderate reactivity to self-antigens in the thymus. The stoichiometry of the coreceptor-LCK interaction sets up the "selection window" by establishing the thresholds for positive and negative selection of developing T cells (Erman et al., 2006; Stepanek et al., 2014).

There is an increasing amount of evidence showing that the actual level of self-reactivity largely determines T cell responses to foreign cognate antigens. It has been shown that the level of self-reactivity correlates with the ability of T cells to recognize foreign antigens with high affinity (Mandi et al., 2013). A comparison of two CD4<sup>+</sup> T cell clones with identical affinity for the cognate antigen revealed that the less self-reactive clone expanded more in the primary response, whereas the more self-reactive clone dominated the recall response (Weber et al., 2012; Persaud et al., 2014). Other studies showed that priming of T cells by self-antigens enhances their subsequent responses to foreign antigens and that highly self-reactive T cells have an advantage over weakly self-reactive T cells in this respect (Fulton et al., 2015; Swee et al., 2016; Stefanová et al., 2002). Overall, the self-reactivity of T cells is beneficial for immune protection, but at the same time, it represents the risk for the onset of autoimmunity. Apparently, there is an optimal level of self-reactivity that balances these two counteracting phenomena. This optimal level of self-reactivity can be established by correct setting of the thresholds for positive and negative selection in the thymus



and/or by eventual changes in the sensitivity of the TCR signaling machinery during T cell maturation. Considering fundamental differences in the roles of CD8<sup>+</sup> and CD4<sup>+</sup> T cells, it is very plausible that the optimal levels of self-reactivity might substantially differ between these two populations.

We and others showed that CD4-LCK and CD8-LCK binding stoichiometry is a limiting factor for signaling induced by suboptimal self-antigens in immature thymocytes (Erman et al., 2006; Stepanek et al., 2014). Moreover, we have recently revealed that the CD8-LCK binding frequency regulates tonic TCR signaling in peripheral T cells and the generation of virtual memory T cells from relatively highly self-reactive CD8<sup>+</sup> T cells (Drobek et al., 2018). However, the stoichiometry of CD4-LCK and CD8-LCK interactions in mature T cells has not been addressed in detail.

In this study, we observed that the stoichiometry of the CD8-LCK, but not CD4-LCK, interaction is dynamically regulated during development. The percentage of CD8 molecules carrying LCK is substantially higher in mature T cells than in thymocytes at the double positive (DP) stage, where the positive selection and most of the negative selection takes place. Consequently, CD8<sup>+</sup> T cells increase their responsiveness to antigens with suboptimal affinity upon maturation. Moreover, CD8<sup>+</sup> T cells are, on average, more self-reactive than CD4<sup>+</sup> T cells. Our observation seems to be a result of an evolutionary adaptation that took advantage of the different use of coreceptors by MHC-I and MHC-II-restricted T cells to tune the optimal level of self-reactivity for these two subsets independently.

## RESULTS

### CD8-LCK Coupling Frequency Is Dynamically Regulated during T Cell Maturation

The stoichiometry of the CD4-LCK and CD8-LCK interactions has been previously analyzed using a semiquantitative method of immunoprecipitation followed by flow cytometry (FC-IP) in preselection DP thymocytes (Stepanek et al., 2014). In this study, we applied this method to mature peripheral T cells. This method is based on the immunoprecipitation of CD4 or CD8 by using antibody-coated beads, followed by the detection of coreceptor and LCK molecules by flow cytometry. We used NP-40S detergent for cell lysis that extracted the vast majority of CD4, CD8, and LCK molecules from thymocytes and lymph node (LN) cells (Figure S1A), excluding the possibility that our results are influenced by a potential insolubility of these proteins. We used an anti-CD8 $\beta$  antibody for pull down and anti-CD8 $\alpha$  for detection to exclude eventual CD8 $\alpha\alpha$  homodimers that do not promote TCR signaling (Witte et al., 1999). For the pull down and detection of CD4, two non-competing antibody clones were used (Figures S1B–S1D). The concentration of the detection antibodies was titrated to use saturating concentrations (Figure S1E).

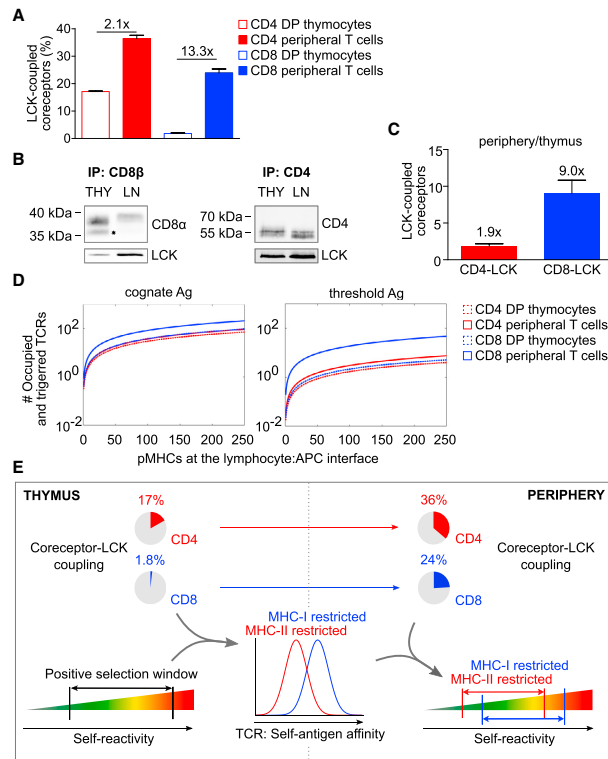
In agreement with the previous study (Stepanek et al., 2014), we observed a substantially higher frequency of LCK-coupled CD4 coreceptors than CD8 coreceptors in DP thymocytes (Figure 1A). Interestingly, the difference between CD4-LCK and CD8-LCK interactions was much less pronounced in mature peripheral T cells than in DP thymocytes (Figure 1A). Upon T cell maturation, the CD8-LCK binding stoichiometry increased

~13-fold, whereas the percentage of CD4 molecules coupled to LCK increased only ~2-fold (Figure 1A).

We addressed the relative changes of coreceptor-LCK binding stoichiometries between thymocytes and mature T cells by using an independent technique. We performed conventional immunoprecipitation from cell lauryl-maltoside lysates followed by immunoblotting (Figures 1B and 1C). We observed differences in the apparent molecular weight of CD8 $\alpha$  between thymocytes and peripheral T cells (Figure 1B). First, the apparent molecular weight of CD8 $\alpha$  was lower in thymocytes than in peripheral T cells. This shift is caused by more intensive sialylation of CD8 in peripheral cells than in thymocytes (Daniels et al., 2001; Merry et al., 2003; Moody et al., 2001). Accordingly, the removal of the sialic acid chains by neuraminidase normalized the apparent molecular weight of CD8 $\alpha$  but did not substantially affect the relative intensities of the detecting antibodies in immunoblotting or flow cytometry (Figures S1F and S1G). Second, there was an additional lower band detected exclusively in the thymocytes (Figure 1B). This band corresponds to the truncated isoform CD8 $\alpha'$  (Zamoyska et al., 1989; Zamoyska and Parnes, 1988). The analysis of the LCK to coreceptor ratio in this experiment showed that upon T cell maturation, the CD8-LCK binding stoichiometry increased ~9-fold, whereas the percentage of CD4 molecules coupled to LCK increased only ~2-fold. Thus, these results were in a good agreement with the FC-IP data.

The dramatic changes in CD8-LCK coupling frequency upon maturation is most likely caused by two factors. First, we and others observed that the truncated isoform CD8 $\alpha'$  devoid of the LCK-binding site is present in thymocytes but not in peripheral T cells (Figure 1B). Interestingly, the expression of CD8 $\alpha'$  is regulated post-transcriptionally, as there is almost no difference in the CD8 $\alpha'$ -encoding RNA levels between the two T cell stages (Figure S1H) (Zamoyska and Parnes, 1988). However, CD8 $\alpha'$  constitutes only ~30% of the total CD8 $\alpha$  in thymocytes (Figure S1I), suggesting that there must be an additional mechanism for the dynamic regulation of CD8-LCK coupling. Because the vast majority of LCK molecules are coupled to CD4 or CD8 in DP thymocytes (Van Laethem et al., 2007) and because CD4 has been shown to have higher affinity to LCK than CD8 has *in vitro* (Kim et al., 2003), CD4 sequesters LCK from CD8 at the DP stage, which does not occur in mature CD8<sup>+</sup> T cells.

We previously developed the “LCK come&stay/signal duration model” to predict TCR signaling output by using a set of parameters including TCR density, antigen affinity, and coreceptor-LCK stoichiometry (Stepanek et al., 2014). The model is based on the kinetic proof-reading principle (McKeithan, 1995). It assumes that LCK recruitment and phosphorylation of the TCR/ZAP70 complex must be accomplished during the interaction of the TCR with the pMHC to trigger the TCR. The model assumes that the triggered TCR continuously transduces the signal downstream as long as it is occupied by the antigen. This model was the only one among a couple of constructed models that could explain the importance of the coreceptor-LCK binding in the antigen affinity discrimination in DP thymocytes, which was observed experimentally (Stepanek et al., 2014). We use this relatively simplistic model here to obtain testable predictions of how the dynamics of CD4-LCK and CD8-LCK coupling regulates the T cell responses to antigens. To assess how the differences



**Figure 1. The Dynamics of the Coreceptor-LCK Coupling Predicts Self-Reactivity**

(A) Mature T cells or DP thymocytes were lysed and incubated with beads coated with antibodies to CD4 (RM4-4) or CD8 $\beta$  (53-5.8). Beads were probed with PE-conjugated antibodies to LCK (3a5), CD8 $\alpha$  (53-5.7), or CD4 (H129.19) and analyzed by flow cytometry. Calculated CD4-LCK or CD8-LCK stoichiometry for thymocytes and mature T cells is shown. Mean  $\pm$  SEM; n = 3–5 mice in 3–4 independent experiments.

(B and C) CD4 (H129.19) or CD8 $\beta$  (53-5.8) were immunoprecipitated from lysates of thymocytes or enriched peripheral CD8 $^+$  and CD4 $^+$  T cells from WT mice, followed by immunoblotting using anti-CD4 (D7D2Z), anti-CD8 $\alpha$  (D4W2Z), and anti-LCK (3a5) antibodies. (B) Representative experiments for CD8 $\beta$  and CD4 immunoprecipitation. CD8 $\alpha$  truncated isoform is marked with an asterisk. (C) Ratio of LCK-coupled coreceptors (periphery/thymus). Mean  $\pm$  SEM; n = 3–5 samples (pooled 2–3 mice) in 3–4 independent experiments.

(D) TCR signal intensity predicted by the “LCK come&stay/signal duration model” (Stepanek et al., 2014) induced by strong cognate or suboptimal antigens (at the threshold for negative selection) in MHC-I- or MHCII-restricted DP or mature T cells. The TCR signal intensity corresponds to the number of signaling TCRs and is shown as a function of antigen density. The input data correspond to the parameters obtained from monoclonal OT-I and B3K508 T cells (Stepanek et al., 2014).

(E) Schematic illustration of the prediction of the mathematical model applied to the process of T cell selection. The coreceptor-LCK coupling in the thymocytes sets the self-antigen affinity window of the positively selected T cell, resulting in higher affinity to self-antigens in the MHC-I-restricted than in the MHCII-restricted T cells. Increased CD8-LCK, but not CD4-LCK, coupling frequency in mature T cells leads to the increased sensitivity of peripheral CD8 T cells to suboptimal antigens. Altogether, mature CD8 $^+$  T cells have, on average, higher level of self-reactivity than CD4 $^+$  T cells. See also Figure S1, Table S1, and Data S1.

in the dynamics of CD4-LCK and CD8-LCK coupling influences the TCR signaling, we used our experimental CD4- and CD8-LCK stoichiometry data as well as the quantification of the percentage of phosphorylated LCK molecules, and the TCR levels on mature CD4 $^+$  and CD8 $^+$  T cells (Figures S1J–S1M, Table S1) as inputs for the LCK come&stay/signal duration model.

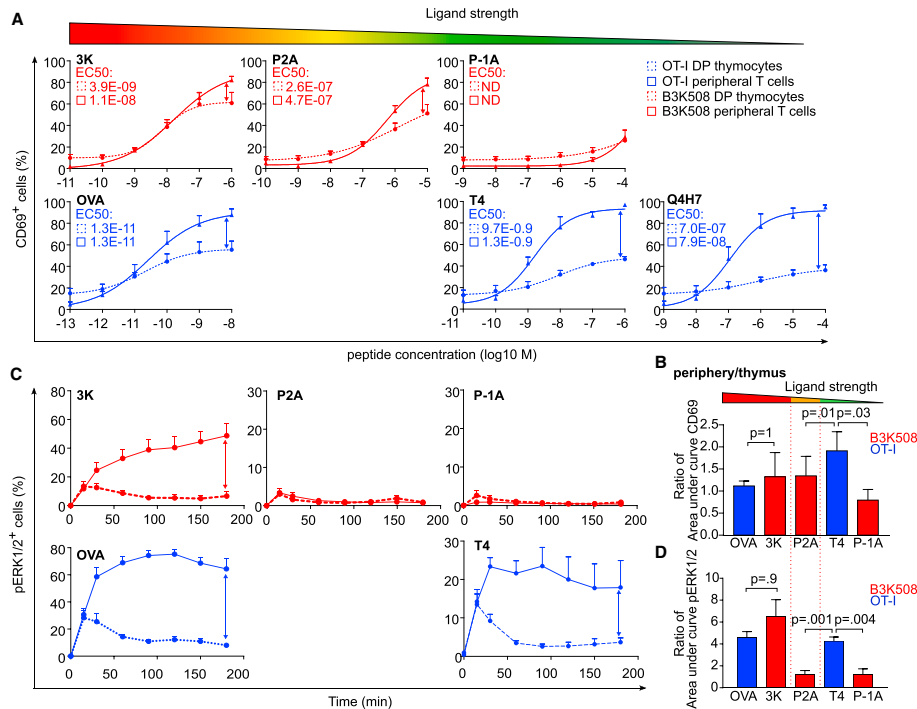
The model predicts that MHC-I- and MHCII-restricted T cells and DP thymocytes exhibit comparable responses to their high-affinity cognate antigens (Figure 1D). However, the stoichiometry of the coreceptor-LCK interaction was shown to be limiting, specifically for signaling induced by suboptimal antigens (Erman et al., 2006; Stepanek et al., 2014; Drobek et al., 2018). We took advantage of the fact that the affinities to self-antigens at the threshold for negative selection are known for both MHC-I-restricted and MHCII-restricted thymocytes (Daniels et al., 2006; Naeher et al., 2007; Stepanek et al., 2014), and we used these parameters in the mathematical model. The model predicts that partial-negative-selecting antigens induce stronger TCR

signaling in CD8 $^+$  mature peripheral T cells than in peripheral CD4 $^+$  T cells or in MHC-I- and MHCII-restricted DP thymocytes (Figure 1D). These results suggest that peripheral MHC-I-restricted CD8 $^+$  T cells, but not MHCII-restricted CD4 $^+$  T cells, could be activated by positive selecting or only partial negative selecting self-antigens.

#### CD8 $^+$ T Cells Are More Reactive to Suboptimal Antigens Than CD4 $^+$ T Cells *Ex Vivo*

Based on the dynamics of the CD4- and CD8-LCK binding stoichiometry and the predictions of the mathematical model, we hypothesize that MHC-I-restricted T cells, but not MHCII-restricted T cells, increase their sensitivity to suboptimal antigens upon maturation. We reasoned that CD8 $^+$  T cells are, therefore, on average more self-reactive than CD4 $^+$  T cells (Figure 1E). In the next steps, we addressed our hypothesis experimentally.

We used monoclonal mature T cells and thymocytes from *Rag2*-deficient mice bearing either MHC-I-restricted



### Figure 2. CD8<sup>+</sup> T Cells Are More Sensitive to Suboptimal Antigens Than CD4<sup>+</sup> T Cells *In Vitro*

LN T cells or thymocytes from OT-I mice (blue) or B3K508 mice (red) were stimulated by BMDCs loaded with indicated concentrations of indicated peptides overnight.

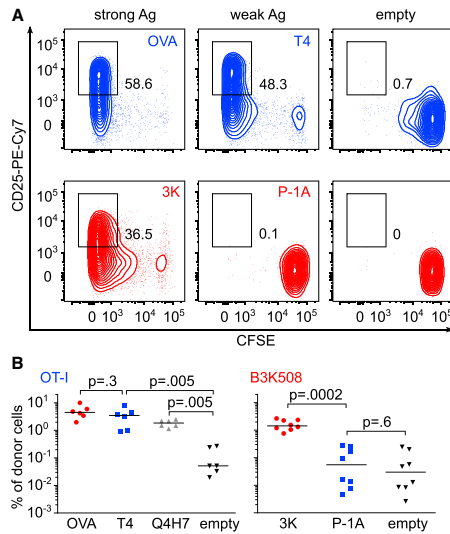
(A and B) CD69 levels on T cells were analyzed by flow cytometry. EC<sub>50</sub> concentrations of peptides are indicated (A). The ratio of the area under curve of the % CD69<sup>+</sup> T cells in the periphery versus thymus (B). Mean + SEM; n = 4 mice in 4 independent experiments.

(C and D) The cells were stimulated by BMDCs loaded with a 10<sup>-8</sup>-M concentration of indicated peptides, fixed at indicated time points, and analyzed for phosphorylation of ERK1/2 by flow cytometry. Mean + SEM; n = 6–10 independent experiments (C). The ratio of area under curve of % pERK1/2<sup>+</sup> T cells in the periphery versus thymus. Mean + SEM, n = 6–10 mice in 6–10 independent experiments (D). Statistical analysis was performed using 2-tailed Mann-Whitney test. See also Figure S2.

OT-I-transgenic TCR (specific to H-2K<sup>b</sup>-SIINFEKL; OVA) or MHCII-restricted B3K508-transgenic TCR (specific to H-2A<sup>b</sup>-FEAQKAKANKAKAVD; 3K) as our experimental model. The advantage of these monoclonal models is that there is a wide range of well-characterized cognate-altered peptide ligands covering negative selectors, partial negative selectors, and positive selectors (Daniels et al., 2006; Huseby et al., 2006; Keck et al., 2014; Stepanek et al., 2014; Figure S2A). TCR expression is higher in B3K508 T cells than in OT-I T cells, mimicking the situation in polyclonal T cells (Figures S1M and S2B).

Upon overnight stimulation with bone-marrow-derived dendritic cells (BMDCs) pulsed with the cognate peptides or their lower affinity variants, we measured the expression of an activation marker, CD69, in the monoclonal T cells and thymocytes

(Figures 2A, 2B, S2C, and S2D). We compared CD69 upregulation in mature T cells and DP thymocytes by calculating the ratio of the corresponding areas under curve for each antigen (Figure 2B) or the ratio of the maximal response (Figure S2D). The responses of OT-I and B3K508 mature T cells and DP thymocytes to the high-affinity antigens (OVA and 3K, respectively) were comparable. However, the mature OT-I T cells exhibited stronger responses than DP thymocytes when stimulated with suboptimal antigens T4 and Q4H7, a partial negative selector and a positive selector, respectively (Figures 2A, 2B, S2C, and S2D). In the case of B3K508 mice, the mature T cells and DP thymocytes showed comparable responses to suboptimal antigens P2A and P-1A, a relatively weak negative selector and a partial negative selector, respectively (Figures 2A, 2B, S2C, and S2D).



**Figure 3. CD8<sup>+</sup> T Cells Are More Sensitive to Suboptimal Antigens Than CD4<sup>+</sup> T Cells *In Vivo***

CFSE-loaded LN cells from OT-I mice and B3K508 mice were injected into congenic Ly5.1 WT mice. The mice were infected with transgenic *Lm* expressing indicated peptides. Four days after the infection, viable splenic donor T cells (gated as CD3<sup>+</sup> CD4<sup>+</sup> Va2<sup>+</sup> Ly5.2<sup>+</sup> for B3K508 T cells and CD3<sup>+</sup> CD8<sup>+</sup> Va2<sup>+</sup> Ly5.2<sup>+</sup> for OT-I T cells) were analyzed for proliferation (CFSE) and CD25 expression by flow cytometry.

(A) Representative animals out of 6–8 per group.  
(B) The percentage of donor cells among all splenic CD4<sup>+</sup> or CD8<sup>+</sup> T cells is shown. n = 6–8 mice in 4 independent experiments. Statistical analysis was performed using 2-tailed Mann-Whitney test. See also Figure S3.

In a next step, we studied a proximal TCR signaling event, a phosphorylation of kinases ERK1 and ERK2 (Figures 2C, 2D and S2E–S2G). As the mature T cells and DP thymocytes had distinct kinetics of ERK1/2 phosphorylation, we used the overall response calculated as the area under curve (Figure 2D) or maximal response (Figure S2G) for quantification. We calculated the mature T cell/DP thymocytes ratio for each antigen. In the case of OT-I T cells, mature T cells showed an ~4.5-fold stronger overall response than DP thymocytes to both the high-affinity antigen OVA and the suboptimal antigen T4 (Figures 2C and 2D). However, B3K508 mature T cells showed a substantially stronger response to the high-affinity antigen than DP thymocytes (~6.5-fold), but the responses of B3K508 mature T cells and DP thymocytes to suboptimal antigens P2A and P-1A were comparable (Figures 2C and 2D).

Overall, CD69 upregulation and pERK1/2-phosphorylation were in line with the mathematical model predicting that the responses to suboptimal antigens are augmented upon maturation of MHCII-restricted, but not MHCII-restricted, T cells. However, it

should be noted here that the responses of B3K508 T cells to P2A (pERK1/2) and P-1A (both pERK1/2 and CD69) were weak, which limits our conclusions.

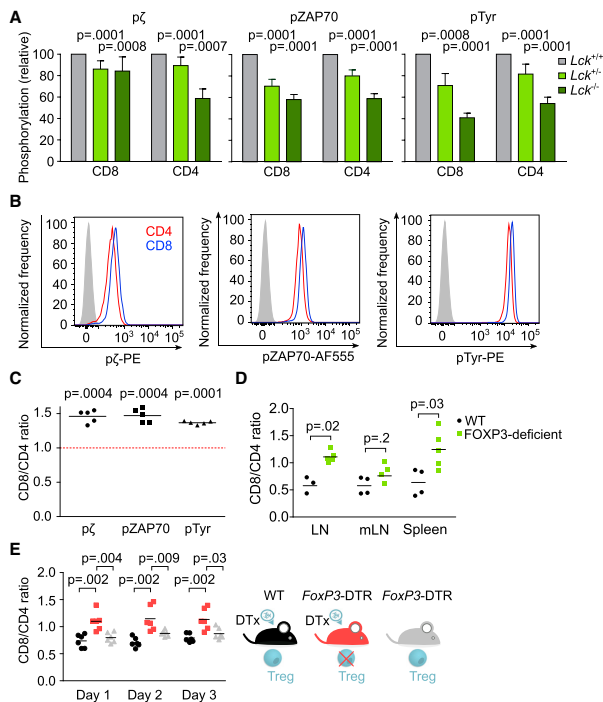
### CD8<sup>+</sup> T Cells Are More Reactive to Suboptimal Antigens Than CD4<sup>+</sup> T Cells *In Vivo*

We next examined the activation of T cells *in vivo*. In this assay, we took advantage of the fact that the ability of particular antigens to induce negative selection in OT-I and B3K508 thymocytes has been established previously (Daniels et al., 2006; Huseby et al., 2006; Keck et al., 2014; Stepanek et al., 2014; Wyss et al., 2016). Thus, we could monitor T cell responses to high-affinity cognate antigens and partial-negative-selecting antigens in the periphery. We transferred CFSE-labeled OT-I and B3K508 peripheral T cells into congenic Ly5.1 mice. Subsequently, we infected the mice with *Listeria monocytogenes* (*Lm*) expressing the cognate antigens for the transferred T cells. We analyzed the expansion, proliferation, and CD25 upregulation in the donor T cells 4 days later. Both OT-I and B3K508 T cells exhibited strong proliferation, expansion, and CD25 upregulation upon infection, with *Lm* carrying the respective high-affinity cognate antigens (OVA and 3K) (Figures 3A and 3B; Figures S3A–S3D). In the case of OT-I T cells, *Lm* carrying the partial-negative-selecting antigen T4 or even a positive-selecting antigen Q4H7 induced substantial expansion, proliferation, and CD25 upregulation, whereas non-cognate empty *Lm* did not induce a detectable response (Figures 3A and 3B; Figures S3A and S3B). In striking contrast to OT-I T cells, B3K508 T cells did not respond to *Lm* expressing the partial-negative-selecting antigen P-1A (Figures 3A and 3B; Figures S3A and S3B). Collectively, these data reveal that peripheral CD8<sup>+</sup> T cells show a robust *in vivo* response to antigens with low affinity as partial negative selectors or even positive selectors, whereas peripheral CD4<sup>+</sup> T cells are not able to respond to partial-negative-selecting antigens at all.

### CD8<sup>+</sup> T Cells Experience Stronger Homeostatic TCR Signals Than CD4<sup>+</sup> T Cells

The results of *in vitro* and *in vivo* assays using monoclonal MHCII- and MHCII-restricted T cells corresponded well to the predictions of the mathematical model. If we translate these findings to the polyclonal repertoire, we can hypothesize that the CD8<sup>+</sup> T cell population is, on average, more self-reactive than the CD4<sup>+</sup> population because only the CD8<sup>+</sup> subset contains T cells that are able to respond to the positive- and partial-negative-selecting self-antigens at the periphery.

The self-reactivity of peripheral T cells determines the intensity of homeostatic signaling at the basal state. We generated and analyzed LCK-deficient mice to (1) validate our tools for the detection of proximal signaling intermediates of tonic signaling by using phospho-specific antibodies by flow cytometry and (2) to address the role of LCK in the homeostatic TCR signaling. The *Lck*<sup>-/-</sup> thymocytes showed partial blocks in the  $\beta$  selection and positive selection (Figure S4A), as previously reported (Molina et al., 1992). Reduced LCK levels in heterozygous *Lck*<sup>+/-</sup> and in *Lck*<sup>-/-</sup> mice lead to a gradual decrease in TCR $\zeta$  and ZAP70 phosphorylation and overall tyrosine phosphorylation in both CD4 and CD8 peripheral T cells (Figure 4A). These results



**Figure 4. Polyclonal CD8<sup>+</sup> T Cells Show Stronger Homeostatic TCR Signaling Than CD4<sup>+</sup> T Cells**

(A–C) Fixed and permeabilized LN T cells from WT mice were stained with antibodies to TCR $\beta$ , CD4, CD8, pTCR $\zeta$  chain, pZAP70, and overall tyrosine phosphorylation and analyzed by flow cytometry. Comparison of basal signaling in CD8<sup>+</sup> CD44<sup>+</sup> and CD4<sup>+</sup> CD44<sup>+</sup> T cells from *Lck*<sup>+/+</sup>, *Lck*<sup>+/-</sup>, and *Lck*<sup>-/-</sup> mice. Phosphorylation level (geometric mean fluorescence intensity [gMFI]) relative to *Lck*<sup>+/+</sup> mice is shown. Mean  $\pm$  SEM; n = 7 mice in 7 independent experiments. Statistical analysis was performed by one sample t test (hypothetical mean value = 1) (A). Comparison of basal signaling in CD4<sup>+</sup> and CD8<sup>+</sup> T cells. A representative experiment out of 5 independent experiments in total (B). Ratio of phosphorylation levels (gMFI) of CD8<sup>+</sup> versus CD4<sup>+</sup> peripheral T cells in pTCR $\zeta$ , pZAP70, and overall tyrosine phosphorylation for each mouse. Mean; n = 5 mice in 4 independent experiments. Statistical analysis was performed by one sample t test (hypothetical mean value = 1) (C). (D) The LN, mLN, and splenic T cells of *Foxp3*-deficient mice and their WT littermates were analyzed by flow cytometry. The ratio of CD8<sup>+</sup> to CD4<sup>+</sup> T cells is shown. Mean; n = 4–5 mice from 2 experiments. Statistical analysis was performed by 2-tailed Mann-Whitney test. (E) The peripheral LN T cells from *Foxp3*-DTR mice after the administration of diphtheria toxin, untreated *Foxp3*-DTR mice, and WT mice after the administration of diphtheria toxin were analyzed. The ratio of CD8<sup>+</sup> to CD4<sup>+</sup> T cells is shown. n = 6 mice in 3 independent experiments; mean. Statistical analysis was performed by 2-tailed Mann-Whitney test. See also Figure S4.

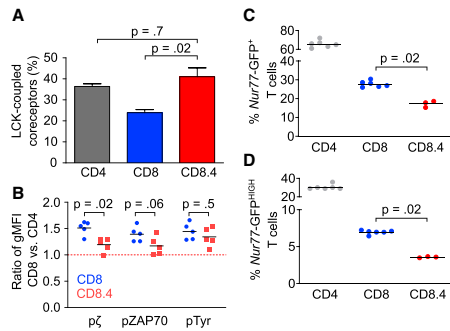
show that LCK is a major factor regulating the strength of the homeostatic TCR signaling in resting peripheral T cells, which is in line with our model.

We examined the intensity of homeostatic TCR signaling to compare the level of self-reactivity of polyclonal peripheral CD4<sup>+</sup> and CD8<sup>+</sup> T cells. Higher levels of TCR $\zeta$  and ZAP70 phosphorylation and overall tyrosine phosphorylation in CD8<sup>+</sup> T cells than in CD4<sup>+</sup> T cells suggested that CD8<sup>+</sup> T cells receive stronger homeostatic signals from self-antigens than CD4<sup>+</sup> T cells (Figures 4B and 4C). These observations were not substantially influenced by the inclusion of CD4<sup>+</sup> regulatory T cells (Tregs), as the comparison of CD8<sup>+</sup> T cells to conventional FOXP3<sup>-</sup> CD4<sup>+</sup> T cells showed similar results (Figures S4B and S4C). Moreover, the higher intensity of basal TCR signaling in CD8<sup>+</sup> T cells than in CD4<sup>+</sup> T cells was not caused by higher surface TCR levels in CD8<sup>+</sup> T cells. On the contrary, CD8<sup>+</sup> T cells have a lower surface TCR expression than CD4<sup>+</sup> T cells (Figure S1M). Overall, these data supported the hypothesis that CD8<sup>+</sup> T cells are more self-reactive than CD4<sup>+</sup> T cells.

The higher level of self-reactivity of CD8<sup>+</sup> T cells than of CD4<sup>+</sup> T cells indicates that CD8<sup>+</sup> T cells might be more sus-

ceptible to hyperproliferation than CD4<sup>+</sup> T cells. To address this hypothesis, we used Treg deficiency as a model for a systemic breakdown of peripheral tolerance. We observed that the ratio of CD8<sup>+</sup>/CD4<sup>+</sup> T cells is significantly higher in FOXP3-deficient 2- to 3-week-old mice devoid of Tregs than in the healthy littermates (Figure 4D). In a complementary assay, we observed the effect of acute depletion of Tregs by injecting diphtheria toxin (DT) into *Foxp3*-DTR mice, expressing the DT receptor in FOXP3<sup>+</sup> T cells (Kim et al., 2007). The CD8<sup>+</sup>/CD4<sup>+</sup> T cell ratio significantly increased in adult Treg-depleted mice compared to untreated *Foxp3*-DTR mice and to wild-type (WT) mice injected with the DT (Figure 4E). These results are consistent with the hypothesis that the polyclonal CD8<sup>+</sup> T cell population receives stronger signals from self-antigens than the CD4<sup>+</sup> T cell population and that CD8<sup>+</sup> T cells are more prone to hyperproliferation than CD4<sup>+</sup> T cells when the Treg-mediated tolerance fails. However, we cannot exclude that additional differences between CD8<sup>+</sup> versus CD4<sup>+</sup> (e.g., differential expression of cytokine receptors) play a role in this assay.





**Figure 5. Role of Coreceptor-LCK Coupling in Self-Reactivity of T Cell Subpopulations**

(A) CD4-LCK, CD8-LCK, or CD8.4-LCK stoichiometry in LN T cells of WT and CD8.4 mice was analyzed. Mean  $\pm$  SEM; n = 4–9 mice from 4–8 independent experiments. Statistical analysis was performed by 2-tailed Mann-Whitney test. The CD4-LCK and CD8-LCK stoichiometries are the same as that shown in Figure 1A.

(B) Ratio of MFI levels of pTCR $\zeta$ , pZAP70, and overall tyrosine phosphorylation in CD8<sup>+</sup> versus CD4<sup>+</sup> peripheral T cells in WT and CD8.4 chimeric mice is shown. Mean, n = 5 mice in 3 independent experiments. Statistical analysis was performed by 2-tailed Mann-Whitney test. See Figure S5D for similar data. (C and D) LN T cells from *Nur77*-GFP reporter mice were analyzed by flow cytometry. The CD8<sup>+</sup> CD44<sup>−</sup> CD62L<sup>+</sup> or CD8.4<sup>+</sup> CD44<sup>−</sup> CD62L<sup>+</sup> T cells were analyzed for the expression of the *Nur77*-GFP. The percentage of *Nur77*-GFP<sup>+</sup> and *Nur77*-GFP<sup>HIGH</sup> cells is shown. Mean; n = 3–6 mice in 3–6 independent experiments. Statistical analysis was performed by 2-tailed Mann-Whitney test. See also Figure S5.

### The Self-Reactivity of CD8<sup>+</sup> T Cells Is Regulated by the Dynamics of the CD8-LCK Coupling

The previous experiments and the prediction of the mathematical model show substantial differences between CD8<sup>+</sup> and CD4<sup>+</sup> T cells in terms of their response to suboptimal antigens and the basal signaling. In a next step, we addressed the link between the coreceptor-LCK coupling and the self-reactivity of mature T cells directly. We took advantage of a previously developed CD8.4 knockin mouse model (Drobek et al., 2018; Erman et al., 2006; Stepanek et al., 2014). In this mouse, MHC-I-restricted T cells express a chimeric CD8.4 coreceptor that has the intracellular domain of CD8 $\alpha$  replaced by the intracellular domain of the CD4 coreceptor. The coupling of CD8.4 coreceptor to LCK is comparable to CD4 both in the thymus and at the periphery (Stepanek et al., 2014) (Figure 5A). The basal phosphorylation of TCR $\zeta$  in CD8.4 T cells was significantly lower than in CD8<sup>+</sup> T cells, and the difference in the ZAP70 phosphorylation was close to significant (Figure 5B), indicating that peripheral CD8<sup>+</sup> T cells are, on average, more self-reactive than CD8.4<sup>+</sup> T cells. We obtained similar results when we repeated this key experiment in a different animal facility (Figure S5D). Because the phosphorylation of ZAP70 and TCR $\zeta$  and overall tyrosine phosphorylation were only slightly increased in CD8.4<sup>+</sup> compared with CD4<sup>+</sup> T cells, we concluded that the changes in coreceptor-LCK stoichiometry during development are a ma-

ior cause of the differences in basal TCR signaling between CD8<sup>+</sup> and CD4<sup>+</sup> T cells.

Expression of an orphan nuclear receptor, *Nur77*, is very sensitive even to weak TCR signaling. For this reason, the *Nur77*-GFP reporter mouse has been used to study TCR signals induced by self-antigens (Moran et al., 2011). The *Nur77*-GFP signal is stronger in CD4<sup>+</sup> than in CD8<sup>+</sup> T cells (Moran et al., 2011) (Figures S5A and S5B), suggesting that CD4<sup>+</sup> T cells might have stronger TCR signaling than CD8<sup>+</sup> T cells. Because these results are contradictory to our analysis of basal TCR signaling (Figures 4B and 4C), we addressed it in a greater detail. We compared GFP expression in CD8<sup>+</sup> *Nur77*-GFP and CD8.4<sup>+</sup> *Nur77*-GFP T cells. We observed a significantly higher frequency of GFP<sup>+</sup> and GFP<sup>HIGH</sup> cells among CD8<sup>+</sup> than among CD8.4<sup>+</sup> T cells (Figures 5C and 5D; Figure S5C), supporting our previous data that the dynamics of the coreceptor-LCK stoichiometry sets the level of T cell self-reactivity. In the light of these data, we suggest that the previously reported higher expression of *Nur77* in CD4<sup>+</sup> T cells than in CD8<sup>+</sup> T cells reflects a differential regulation of this gene in these two very different T cell types rather than the differences in basal TCR signaling per se.

The sizes of CD4, CD8, and CD8.4 naive T cells are comparable in terms of cellular dry mass (Figure S5E) and forward scatter signal (Figure S5F). The TCR levels are the highest in CD4 T cells and comparable in CD8 and CD8.4 T cells (Figures S1M and S5G). The expression level of ZAP70 is comparable among these cell types (Figure S5H). Thus, we could exclude the possibility that the cell size variation or TCR or ZAP70 expression is responsible for the observed differences in the homeostatic TCR signaling.

Altogether, our data indicate that the stoichiometry of the CD4- and CD8-LCK interactions and their changes during T cell development establish the level of self-reactivity of mature T cells. The dynamic regulation of the CD8-LCK stoichiometry causes CD8<sup>+</sup> T cells to be, on average, more self-reactive than CD4<sup>+</sup> T cells.

## DISCUSSION

Our results show that the developmental dynamics of CD4-LCK and CD8-LCK stoichiometries differ substantially in mice. A relatively high number of CD4 molecules are coupled to LCK in developing DP thymocytes (Stepanek et al., 2014), and this coupling is only mildly increased during the maturation of CD4<sup>+</sup> T cells. In contrast, CD8-LCK stoichiometry is relatively low in DP thymocytes (Stepanek et al., 2014) when positive selection and most of the negative selection occurs. The number of CD8 molecules carrying LCK dramatically increases upon maturation. This is partially caused by the expression of the truncated CD8 $\alpha'$  variant (Zamoyska et al., 1989). CD8 $\alpha'$  is expressed only on the surface of thymocytes but not of mature T cells (Zamoyska and Parnes, 1988). However, the major mechanism causing the low CD8-LCK coupling in DP thymocytes is the preferential sequestering of LCK (Van Laethem et al., 2007) by CD4, which has a higher affinity for LCK than CD8 (Kim et al., 2003).

The stoichiometry between the coreceptors and LCK is a limiting factor for triggering the TCR signaling by suboptimal antigens (Stepanek et al., 2014). Our mathematical model (Stepanek et al., 2014) made two interesting predictions: (1) mature

peripheral CD8<sup>+</sup> T cells, but not CD4<sup>+</sup> T cells, are more sensitive to suboptimal cognate antigens than DP thymocytes with the same specificity and (2) mature CD8<sup>+</sup> T cells are more self-reactive than mature CD4<sup>+</sup> T cells. Our experimental data using well-defined monoclonal MHCI- and MHCII-restricted T cells as well as polyclonal murine T cells supported the predictions of the model. The experiments using T cells expressing the chimeric CD8.4 coreceptor showed that the higher self-reactivity of CD8<sup>+</sup> T cells compared to CD4<sup>+</sup> T cells is at least partially caused by the differential developmental kinetics of the CD8-LCK versus CD4-LCK stoichiometries.

One of the key mechanisms of self-tolerance is the removal of overtly self-reactive T cell clones during negative selection in the thymus. However, the self-reactivity of positively selected mature T cells is beneficial for their survival and immune responses (Mandl et al., 2013; Fulton et al., 2015; Swee et al., 2016; Stefanová et al., 2002). These two counteracting mechanisms generate a pressure for an optimal level of self-reactivity of mature T cells. Because the effector roles of CD4<sup>+</sup> and CD8<sup>+</sup> T cells in the immune responses are very different, it is very likely that the optimal level of self-reactivity differs between these two populations. However, the proximal TCR signaling pathway is identical in CD8<sup>+</sup> and CD4<sup>+</sup> T cells, which limits the possibilities of tuning the optimal level of self-reactivity for CD4<sup>+</sup> and CD8<sup>+</sup> T cells individually by evolutionary processes. The coreceptors represent the exceptional part of the TCR signaling machinery that differs between CD4<sup>+</sup> and CD8<sup>+</sup> T cells, and thus, it represents the ideal target for the evolutionary tuning of optimal self-reactivity of CD4<sup>+</sup> and CD8<sup>+</sup> T cells separately. The increase in CD8-LCK, but not CD4-LCK, stoichiometry during the maturation contributes to setting the higher level of self-reactivity of mature CD8<sup>+</sup> T cells than of mature CD4<sup>+</sup> T cells. Because CD4<sup>+</sup> helper T cells modulate immune responses by acting on many other leukocytes, an autoimmune response of a CD4<sup>+</sup> T cell might be more harmful than an autoimmune response of a CD8<sup>+</sup> T cell. This might explain why we observed a buffering gap between the self-antigen affinity required for negative selection and affinity required for inducing an immune response in CD4<sup>+</sup> T cells. In contrast, CD8<sup>+</sup> T cells are able to induce a robust response to partial negative selectors and even to positive selectors. In the case of CD8<sup>+</sup> T cells, the benefit from having a higher level of self-reactivity might overcome the risk of inducing autoimmunity.

Our findings were surprising because previous studies often suggested the opposite, i.e., that mature peripheral T cells are less sensitive to antigens than DP thymocytes (Ebert et al., 2009; Li et al., 2007; Lucas et al., 1999) and that peripheral CD4<sup>+</sup> T cells are more self-reactive than CD8<sup>+</sup> T cells (Moran et al., 2011).

Our data highlight the role of CD8-LCK stoichiometry as the main cause of the increase in the responsiveness to suboptimal antigens, including self-antigens, upon maturation of CD8<sup>+</sup> T cells. Moreover, pre-selection DP thymocytes exhibit substantially lower levels of surface TCR than mature T cells, which might also contribute to their lower sensitivity. In contrast, multiple mechanisms selectively enhancing the responses of thymocytes or suppressing the signaling in mature T cells were proposed (reviewed in Gaud et al., 2018). These mechanisms include sialya-

tion of CD8 in peripheral T cells (Starr et al., 2003) and higher expression of positive regulators of TCR signaling, a voltage-gated sodium channel (Lo et al., 2012), Themis (Choi et al., 2017; Fu et al., 2009; Johnson et al., 2009), TESPA1 (Wang et al., 2012; Liang et al., 2017), and miRNA-181a (Li et al., 2007; Ebert et al., 2009) in thymocytes than in mature T cells.

Because our data concerning MHCII-restricted T cells do not show substantial differences between the immature and mature T cells, they are not in dramatic contrast to previous studies (Ebert et al., 2009; Li et al., 2007; Lucas et al., 1999). However, our data showing that CD8<sup>+</sup> T cells increase their sensitivity to suboptimal antigens upon maturation are contradictory to some previous reports (Davey et al., 1998; Starr et al., 2003). Most likely, differences in the experimental *ex vivo* protocols caused the discrepancy. For instance, the expression of costimulatory and inhibitory ligands on the APCs might selectively regulate responses of thymocytes and/or mature T cells. Thus, the usage of different cells as APCs could be the source of the inconsistencies among different studies. For this and other reasons, we believe that the *in vivo* data are more relevant than the *ex vivo* experiments. We showed that partial-negative-selecting and positive-selecting antigens are able to trigger a significant activation of CD8<sup>+</sup>, but not CD4<sup>+</sup> T cells, *in vivo*. These experiments are in a very good agreement with previously published *in vivo* studies (Keck et al., 2014; King et al., 2012; Koehli et al., 2014; Zehn et al., 2009; Enouz et al., 2012), although a side-by-side comparison of CD8<sup>+</sup> and CD4<sup>+</sup> T cells has not been carried out previously.

The higher self-reactivity of CD4<sup>+</sup> T cells than CD8<sup>+</sup> T cells has been suggested based on the higher expression of *Nur77*-GFP and CD5 in CD4<sup>+</sup> T cells than in CD8<sup>+</sup> T cells (Moran et al., 2011; Hogquist and Jameson, 2014). However, it is possible that the transcription of these reporter genes is regulated in a cell-type-specific manner (Moran et al., 2011). In such scenario, the markers are not reliable for a comparison between different T cell subsets. To avoid comparing apples and oranges, we examined CD8<sup>+</sup> T cells and CD8.4<sup>+</sup> T cells expressing a chimeric coreceptor, recapitulating the dynamics of CD4-LCK, but selecting MHCII-restricted T cells. CD8.4<sup>+</sup> T cells showed lower basal expression of *Nur77*-GFP than CD8<sup>+</sup> T cells. These results indicate that the changes in the coreceptor-LCK stoichiometry during maturation determine the self-reactivity of T cells. Moreover, the data suggest that the *Nur77*-GFP reporter is most likely differentially regulated in CD8<sup>+</sup> and CD4<sup>+</sup> T cells. To avoid artifacts caused by unique gene expression programs in CD4<sup>+</sup> and CD8<sup>+</sup> T cells, we focused on the basal TCR-dependent phosphorylation of TCR $\zeta$  and ZAP70. We believe that this analysis of the proximal TCR signaling is the most reliable approach for the comparison of basal TCR signaling among different T cell subsets. It should be noted here that we cannot formally exclude that, besides LCK, other potential interacting partners of CD4 and/or CD8 might contribute to the differences between the CD8WT<sup>+</sup> and CD8.4<sup>+</sup> T cells.

Data about the coreceptor-LCK coupling in human immature and mature T cells are not available. Moreover, the level of self-reactivity of human CD4<sup>+</sup> and CD8<sup>+</sup> T cells has not been addressed. These parameters can be very different from mice.

However, the principle of tuning the self-reactivity by the regulation of coreceptor-LCK stoichiometry could be very general because it represents an ideal target to set up the optimal self-reactivity of CD4<sup>+</sup> and CD8<sup>+</sup> T cells separately. Subsequent work should focus on the link between self-reactivity and coreceptor-LCK stoichiometry in human T cells.

Mice with point mutations disabling the CD8-LCK and/or CD4-LCK interactions would be required for a thorough understanding of the role of the coreceptor-LCK interaction in the T cell biology. However, our data suggest that targeting the CD4- and CD8-LCK interactions might reduce T cell self-reactivity. Thus, these interactions represent a potential target for the therapy of autoimmune diseases.

## STAR★METHODS

Detailed methods are provided in the online version of this paper and include the following:

- [KEY RESOURCES TABLE](#)
- [LEAD CONTACT AND MATERIALS AVAILABILITY](#)
- [EXPERIMENTAL MODEL AND SUBJECT DETAILS](#)
  - Mice
  - Bone marrow-derived dendritic cells (BMDC)
- [METHOD DETAILS](#)
  - Flow cytometric immunoprecipitation assay
  - Analysis of soluble and insoluble fractions
  - Immunoprecipitation of surface coreceptors
  - Neuraminidase treatment
  - Quantitative PCR
  - Mathematical model
  - T cell enrichment
  - Flow cytometry analysis and sorting
  - Determination of LCK phosphorylation status
  - Determination of TCR and coreceptor levels
  - Antigen presentation assay
  - Listeria infection
  - Quantitative phase imaging
  - Antibody competition binding assay
- [QUANTIFICATION AND STATISTICAL ANALYSIS](#)
- [DATA AND CODE AVAILABILITY](#)

## SUPPLEMENTAL INFORMATION

Supplemental Information can be found online at <https://doi.org/10.1016/j.celrep.2020.01.008>.

## ACKNOWLEDGMENTS

We thank Ladislav Cupak, Barbara Hausmann, and Rosmarie Lang for their technical assistance and genotyping of mice. We thank Light Microscopy and Flow Cytometry at Institute of Molecular Genetics, namely, Zdenek Cimbrek and Dr. Matyas Sima for cell sorting and Dr. Ivan Novotny for assistance with microscopy experiments. We thank Dr. Inken Beck and Dr. Petr Kasperek from the Czech Centre of Phenogenomics for generating *Lck*<sup>-/-</sup> mice. We thank Prof. Ed Palmer for his multilateral support to the project. We thank Prof. Alfred Signer for providing us with CD8.4 mice. We thank Dr. Tomas Brdicka for providing us with hybridoma-produced antibodies (anti-CD4, anti-CD11b). We thank Dr. Peter Draber for comments on the manuscript. This project was supported by the Swiss National Science Foundation

(Promys, IZ1120\_166538), the Czech Science Foundation (GJ19-03435Y), ERC Starting Grant (FunDIT) to O.S., and ERC Starting Grant (ProtectC) to D.Z. L.W. is supported by SNSF Early Postdoc Mobility Scholarship (P2BSP3\_168719). C.G. is supported by Novartis Foundation. The Group of Adaptive Immunity at the Institute of Molecular Genetics in Prague is supported by an EMBO Installation grant, the Institute of Molecular Genetics of the Czech Academy of Sciences (RVO 68378050), and the J.E. Purkyně Fellowship by the Czech Academy of Sciences (to O.S.). V.H. is a student of the Faculty of Science, Charles University, Prague. The animal facility of the IMG is a part of the Czech Centre for Phenogenomics, and the work there was supported, in part, by grants LM2015040, OP RDI CZ.1.05/2.1.00/19.0395, and OP RDI BIOCEV CZ.1.05/1.1.00/02.0109 provided by the Czech Ministry of Education, Youth and Sports and the European Regional Development Fund. Quantitative phase microscopy was performed in the Microscopy Centre - Light Microscopy Core Facility, IMG ASCR, Prague, Czech Republic, supported by grants (Czech-Bioimaging, MEYS LM2015062), "Centre of Model Organisms" OPK (CZ.2.16/3.1.00/21547), and "Biomodels for health" (LO1419).

## AUTHOR CONTRIBUTIONS

V.H. and O.S. planned experiments. V.H., A.D., D.M., C.G., L.W., V.N., and O.S. performed and analyzed experiments. C.G.K. and D.Z. contributed with unique biological material. O.S. performed the mathematical calculations. V.H. and O.S. wrote the manuscript. All authors reviewed the manuscript. O.S. conceived the study.

## DECLARATION OF INTERESTS

The authors declare no competing interests.

Received: December 18, 2018  
Revised: May 31, 2019  
Accepted: January 2, 2020  
Published: February 4, 2020

## REFERENCES

- Artyomov, M.N., Lis, M., Devadas, S., Davis, M.M., and Chakraborty, A.K. (2010). CD4 and CD8 binding to MHC molecules primarily acts to enhance Lck delivery. *Proc. Natl. Acad. Sci. USA* *107*, 16916–16921.
- Barber, E.K., Dasgupta, J.D., Schlossman, S.F., Trevillyan, J.M., and Rudd, C.E. (1989). The CD4 and CD8 antigens are coupled to a protein-tyrosine kinase (p56lck) that phosphorylates the CD3 complex. *Proc. Natl. Acad. Sci. USA* *86*, 3277–3281.
- Choi, S., Warzecha, C., Zvezdova, E., Lee, J., Argente, J., Lesourne, R., Aravind, L., and Love, P.E. (2017). THEMIS enhances TCR signaling and enables positive selection by selective inhibition of the phosphatase SHP-1. *Nat. Immunol.* *18*, 433–441.
- Daniels, M.A., Devine, L., Miller, J.D., Moser, J.M., Lukacher, A.E., Altman, J.D., Kavathas, P., Hogquist, K.A., and Jameson, S.C. (2001). CD8 binding to MHC class I molecules is influenced by T cell maturation and glycosylation. *Immunity* *15*, 1051–1061.
- Daniels, M.A., Teixeira, E., Gill, J., Hausmann, B., Roubaty, D., Holmberg, K., Werlen, G., Holländer, G.A., Gascoigne, N.R.J., and Palmer, E. (2006). Thymic selection threshold defined by compartmentalization of Ras/MAPK signalling. *Nature* *444*, 724–729.
- Davey, G.M., Schober, S.L., Endrizzi, B.T., Dutcher, A.K., Jameson, S.C., and Hogquist, K.A. (1998). Preselection thymocytes are more sensitive to T cell receptor stimulation than mature T cells. *J. Exp. Med.* *188*, 1867–1874.
- Drobek, A., Moudra, A., Mueller, D., Huranova, M., Horkova, V., Pribikova, M., Ivanek, R., Oberle, S., Zehn, D., McCoy, K.D., et al. (2018). Strong homeostatic TCR signals induce formation of self-tolerant virtual memory CD8 T cells. *EMBO J.* *37*, e98518.

- Ebert, P.J.R., Jiang, S., Xie, J., Li, Q.J., and Davis, M.M. (2009). An endogenous positively selecting peptide enhances mature T cell responses and becomes an autoantigen in the absence of microRNA miR-181a. *Nat. Immunol.* **10**, 1162–1169.
- Enouz, S., Carrié, L., Merkler, D., Bevan, M.J., and Zehn, D. (2012). Autoreactive T cells bypass negative selection and respond to self-antigen stimulation during infection. *J. Exp. Med.* **209**, 1769–1779.
- Erman, B., Alag, A.S., Dahle, O., van Laethem, F., Sarafova, S.D., Guintier, T.I., Sharrow, S.O., Grinberg, A., Love, P.E., and Singer, A. (2006). Coreceptor signal strength regulates positive selection but does not determine CD4/CD8 lineage choice in a physiologic *in vivo* model. *J. Immunol.* **177**, 6613–6625.
- Fontenot, J.D., Dooley, J.L., Farr, A.G., and Rudensky, A.Y. (2005). Developmental regulation of Foxp3 expression during ontogeny. *J. Exp. Med.* **202**, 901–906.
- Fu, G., Vallée, S., Rybak, V., McGuire, M.V., Ampudia, J., Brockmeyer, C., Salek, M., Fallen, P.R., Hoerter, J.A.H., Munshi, A., et al. (2009). Thymis controls thymocyte selection through regulation of T cell antigen receptor-mediated signaling. *Nat. Immunol.* **10**, 848–856.
- Fulton, R.B., Hamilton, S.E., Xing, Y., Best, J.A., Goldrath, A.W., Hogquist, K.A., and Jameson, S.C. (2015). The TCR's sensitivity to self peptide-MHC dictates the ability of naive CD8(+) T cells to respond to foreign antigens. *Nat. Immunol.* **16**, 107–117.
- Gaud, G., Lesourne, R., and Love, P.E. (2018). Regulatory mechanisms in T cell receptor signalling. *Nat. Rev. Immunol.* **18**, 485–497.
- Hogquist, K.A., and Jameson, S.C. (2014). The self-obsession of T cells: how TCR signaling thresholds affect fate 'decisions' and effector function. *Nat. Immunol.* **15**, 815–823.
- Hogquist, K.A., Jameson, S.C., Heath, W.R., Howard, J.L., Bevan, M.J., and Carbone, F.R. (1994). T cell receptor antagonist peptides induce positive selection. *Cell* **76**, 17–27.
- Huseby, E.S., White, J., Crawford, F., Vass, T., Becker, D., Pinilla, C., Marrack, P., and Kappler, J.W. (2005). How the T cell repertoire becomes peptide and MHC specific. *Cell* **122**, 247–260.
- Huseby, E.S., Crawford, F., White, J., Marrack, P., and Kappler, J.W. (2006). Interface-disrupting amino acids establish specificity between T cell receptors and complexes of major histocompatibility complex and peptide. *Nat. Immunol.* **7**, 1191–1199.
- Johnson, A.L., Aravind, L., Shulzhenko, N., Morgan, A., Choi, S.Y., Crockford, T.L., Lambe, T., Domaschenz, H., Kucharska, E.M., Zheng, L., et al. (2009). Thymis is a member of a new metazoan gene family and is required for the completion of thymocyte positive selection. *Nat. Immunol.* **10**, 831–839.
- Kasperek, P., Krausova, M., Haneckova, R., Kriz, V., Zbodakova, O., Korinek, V., and Sedlacek, R. (2014). Efficient gene targeting of the Rosa26 locus in mouse zygotes using TALE nucleases. *FEBS Lett.* **588**, 3982–3988.
- Keck, S., Schmalzer, M., Ganter, S., Wyss, L., Oberle, S., Huseby, E.S., Zehn, D., and King, C.G. (2014). Antigen affinity and antigen dose exert distinct influences on CD4 T-cell differentiation. *Proc. Natl. Acad. Sci. USA* **111**, 14852–14857.
- Kim, P.W., Sun, Z.Y., Blacklow, S.C., Wagner, G., and Eck, M.J. (2003). A zinc clasp structure tethers Lck to T cell coreceptors CD4 and CD8. *Science* **301**, 1725–1728.
- Kim, J.M., Rasmussen, J.P., and Rudensky, A.Y. (2007). Regulatory T cells prevent catastrophic autoimmunity throughout the lifespan of mice. *Nat. Immunol.* **8**, 191–197.
- King, C.G., Koehli, S., Hausmann, B., Schmalzer, M., Zehn, D., and Palmer, E. (2012). T cell affinity regulates asymmetric division, effector cell differentiation, and tissue pathology. *Immunity* **37**, 709–720.
- Koehli, S., Naeher, D., Galati-Fournier, V., Zehn, D., and Palmer, E. (2014). Optimal T-cell receptor affinity for inducing autoimmunity. *Proc. Natl. Acad. Sci. USA* **111**, 17248–17253.
- Li, Q.J., Chau, J., Ebert, P.J.R., Sylvester, G., Min, H., Liu, G., Braich, R., Manoharan, M., Soutschek, J., Skare, P., et al. (2007). miR-181a is an intrinsic modulator of T cell sensitivity and selection. *Cell* **129**, 147–161.
- Liang, J., Lyu, J., Zhao, M., Li, D., Zheng, M., Fang, Y., Zhao, F., Lou, J., Guo, C., Wang, L., et al. (2017). Tespa1 regulates T cell receptor-induced calcium signals by recruiting inositol 1,4,5-trisphosphate receptors. *Nat. Commun.* **8**, 15732.
- Lin, W., Truong, N., Grossman, W.J., Haribhai, D., Williams, C.B., Wang, J., Martin, M.G., and Chatila, T.A. (2005). Allergic dysregulation and hyperimmunoglobulinemia E in Foxp3 mutant mice. *J. Allergy Clin. Immunol.* **116**, 1106–1115.
- Lo, W.L., Donermeyer, D.L., and Allen, P.M. (2012). A voltage-gated sodium channel is essential for the positive selection of CD4(+) T cells. *Nat. Immunol.* **13**, 880–887.
- Lucas, B., Stefanová, I., Yasutomo, K., Dautigny, N., and Germain, R.N. (1999). Divergent changes in the sensitivity of maturing T cells to structurally related ligands underlies formation of a useful T cell repertoire. *Immunity* **10**, 367–376.
- Mandl, J.N., Monteiro, J.P., Vriskoop, N., and Germain, R.N. (2013). T cell-positive selection uses self-ligand binding strength to optimize repertoire recognition of foreign antigens. *Immunity* **38**, 263–274.
- McKeithan, T.W. (1995). Kinetic proofreading in T-cell receptor signal transduction. *Proc. Natl. Acad. Sci. USA* **92**, 5042–5046.
- Merry, A.H., Gilbert, R.J., Shore, D.A., Royle, L., Miroshnychenko, O., Vuong, M., Wormald, M.R., Harvey, D.J., Dwek, R.A., Classon, B.J., et al. (2003). O-glycan sialylation and the structure of the stalk-like region of the T cell co-receptor CD8. *J. Biol. Chem.* **278**, 27119–27128.
- Molina, T.J., Kishihara, K., Siderovski, D.P., van Ewijk, W., Narendran, A., Timms, E., Wakeham, A., Paige, C.J., Hartmann, K.U., Veillette, A., et al. (1992). Profound block in thymocyte development in mice lacking p56lck. *Nature* **357**, 161–164.
- Moody, A.M., Chui, D., Reche, P.A., Priatel, J.J., Marth, J.D., and Reinherz, E.L. (2001). Developmentally regulated glycosylation of the CD8alpha beta coreceptor stalk modulates ligand binding. *Cell* **107**, 501–512.
- Moran, A.E., Holzapfel, K.L., Xing, Y., Cunningham, N.R., Maltzman, J.S., Punt, J., and Hogquist, K.A. (2011). T cell receptor signal strength in Treg and iNKT cell development demonstrated by a novel fluorescent reporter mouse. *J. Exp. Med.* **208**, 1279–1289.
- Naeher, D., Daniels, M.A., Hausmann, B., Guillaume, P., Luescher, I., and Palmer, E. (2007). A constant affinity threshold for T cell tolerance. *J. Exp. Med.* **204**, 2553–2559.
- Persaud, S.P., Parker, C.R., Lo, W.L., Weber, K.S., and Allen, P.M. (2014). Intrinsic CD4+ T cell sensitivity and response to a pathogen are set and sustained by avidity for thymic and peripheral complexes of self peptide and MHC. *Nat. Immunol.* **15**, 266–274.
- Rudd, C.E., Trevillyan, J.M., Dasgupta, J.D., Wong, L.L., and Schlossman, S.F. (2010). The CD4 receptor is complexed in detergent lysates to a protein-tyrosine kinase (pp59) from human T lymphocytes. *J. Immunol.* **185**, 2645–2649.
- Ruedi, C., Khameneh, H.J., and Karjalainen, K. (2008). Manipulation of immune system via immortal bone marrow stem cells. *Int. Immunol.* **20**, 1211–1218.
- Schrum, A.G., Gil, D., Dopfer, E.P., Wiest, D.L., Turka, L.A., Schamel, W.W., and Palmer, E. (2007). High-sensitivity detection and quantitative analysis of native protein-protein interactions and multiprotein complexes by flow cytometry. *Sci. STKE* **2007**, pl2.
- Shen, F.W., Saga, Y., Litman, G., Freeman, G., Tung, J.S., Cantor, H., and Boyse, E.A. (1985). Cloning of Ly-5 cDNA. *Proc. Natl. Acad. Sci. USA* **82**, 7360–7363.
- Shinkai, Y., Rathbun, G., Lam, K.P., Oltz, E.M., Stewart, V., Mendelsohn, M., Charron, J., Datta, M., Young, F., Stall, A.M., et al. (1992). RAG-2-deficient mice lack mature lymphocytes owing to inability to initiate V(D)J rearrangement. *Cell* **68**, 855–867.
- Sommers, C.L., Dejarnette, J.B., Huang, K., Lee, J., El-Khoury, D., Shores, E.W., and Love, P.E. (2000). Function of CD3 epsilon-mediated signals in T cell development. *J. Exp. Med.* **192**, 913–919.

- Starr, T.K., Daniels, M.A., Lucido, M.M., Jameson, S.C., and Hogquist, K.A. (2003). Thymocyte sensitivity and supramolecular activation cluster formation are developmentally regulated: a partial role for sialylation. *J. Immunol.* *171*, 4512–4520.
- Stefanová, I., Dorfman, J.R., and Germain, R.N. (2002). Self-recognition promotes the foreign antigen sensitivity of naïve T lymphocytes. *Nature* *420*, 429–434.
- Stepanek, O., Kalina, T., Draber, P., Skopцова, T., Svojič, K., Angelisova, P., Horejsi, V., Weiss, A., and Brdicka, T. (2011). Regulation of Src family kinases involved in T cell receptor signaling by protein-tyrosine phosphatase CD148. *J. Biol. Chem.* *286*, 22101–22112.
- Stepanek, O., Prabhakar, A.S., Osswald, C., King, C.G., Bulek, A., Naeher, D., Beaufils-Hugot, M., Abanto, M.L., Galati, V., Hausmann, B., et al. (2014). Coreceptor scanning by the T cell receptor provides a mechanism for T cell tolerance. *Cell* *159*, 333–345.
- Swee, L.K., Tan, Z.W., Sanecka, A., Yoshida, N., Patel, H., Grotenbreg, G., Frickel, E.M., and Ploegh, H.L. (2016). Peripheral self-reactivity regulates antigen-specific CD8 T-cell responses and cell division under physiological conditions. *Open Biol.* *6*, 160293.
- Van Laethem, F., Sarafova, S.D., Park, J.H., Tai, X., Pobezinsky, L., Guinter, T.I., Adoro, S., Adams, A., Sharrow, S.O., Feigenbaum, L., and Singer, A. (2007). Deletion of CD4 and CD8 coreceptors permits generation of alpha-beta T cells that recognize antigens independently of the MHC. *Immunity* *27*, 735–750.
- van Oers, N.S., Killeen, N., and Weiss, A. (1996). Lck regulates the tyrosine phosphorylation of the T cell receptor subunits and ZAP-70 in murine thymocytes. *J. Exp. Med.* *183*, 1053–1062.
- Veillette, A., Bookman, M.A., Horak, E.M., and Bolen, J.B. (1988). The CD4 and CD8 T cell surface antigens are associated with the internal membrane tyrosine-protein kinase p56lck. *Cell* *55*, 301–308.
- Wang, D., Zheng, M., Lei, L., Ji, J., Yao, Y., Qiu, Y., Ma, L., Lou, J., Ouyang, C., Zhang, X., et al. (2012). *Tespa1* is involved in late thymocyte development through the regulation of TCR-mediated signaling. *Nat. Immunol.* *13*, 560–568.
- Weber, K.S., Li, Q.J., Persaud, S.P., Campbell, J.D., Davis, M.M., and Allen, P.M. (2012). Distinct CD4+ helper T cells involved in primary and secondary responses to infection. *Proc. Natl. Acad. Sci. USA* *109*, 9511–9516.
- Witte, T., Spoerl, R., and Chang, H.C. (1999). The CD8beta ectodomain contributes to the augmented coreceptor function of CD8alphabeta heterodimers relative to CD8alphaalpha homodimers. *Cell. Immunol.* *197*, 90–96.
- Wyss, L., Stadinski, B.D., King, C.G., Schallenberg, S., McCarthy, N.I., Lee, J.Y., Kretschmer, K., Terracciano, L.M., Anderson, G., Surh, C.D., et al. (2016). Affinity for self antigen selects Treg cells with distinct functional properties. *Nat. Immunol.* *17*, 1093–1101.
- Zamoyska, R., and Parnes, J.R. (1988). A CD8 polypeptide that is lost after passing the Golgi but before reaching the cell surface: a novel sorting mechanism. *EMBO J.* *7*, 2359–2367.
- Zamoyska, R., Derham, P., Gorman, S.D., von Hoegen, P., Bolen, J.B., Veillette, A., and Parnes, J.R. (1989). Inability of CD8 alpha' polypeptides to associate with p56lck correlates with impaired function in vitro and lack of expression in vivo. *Nature* *342*, 278–281.
- Zehn, D., Lee, S.Y., and Bevan, M.J. (2009). Complete but curtailed T-cell response to very low-affinity antigen. *Nature* *458*, 211–214.

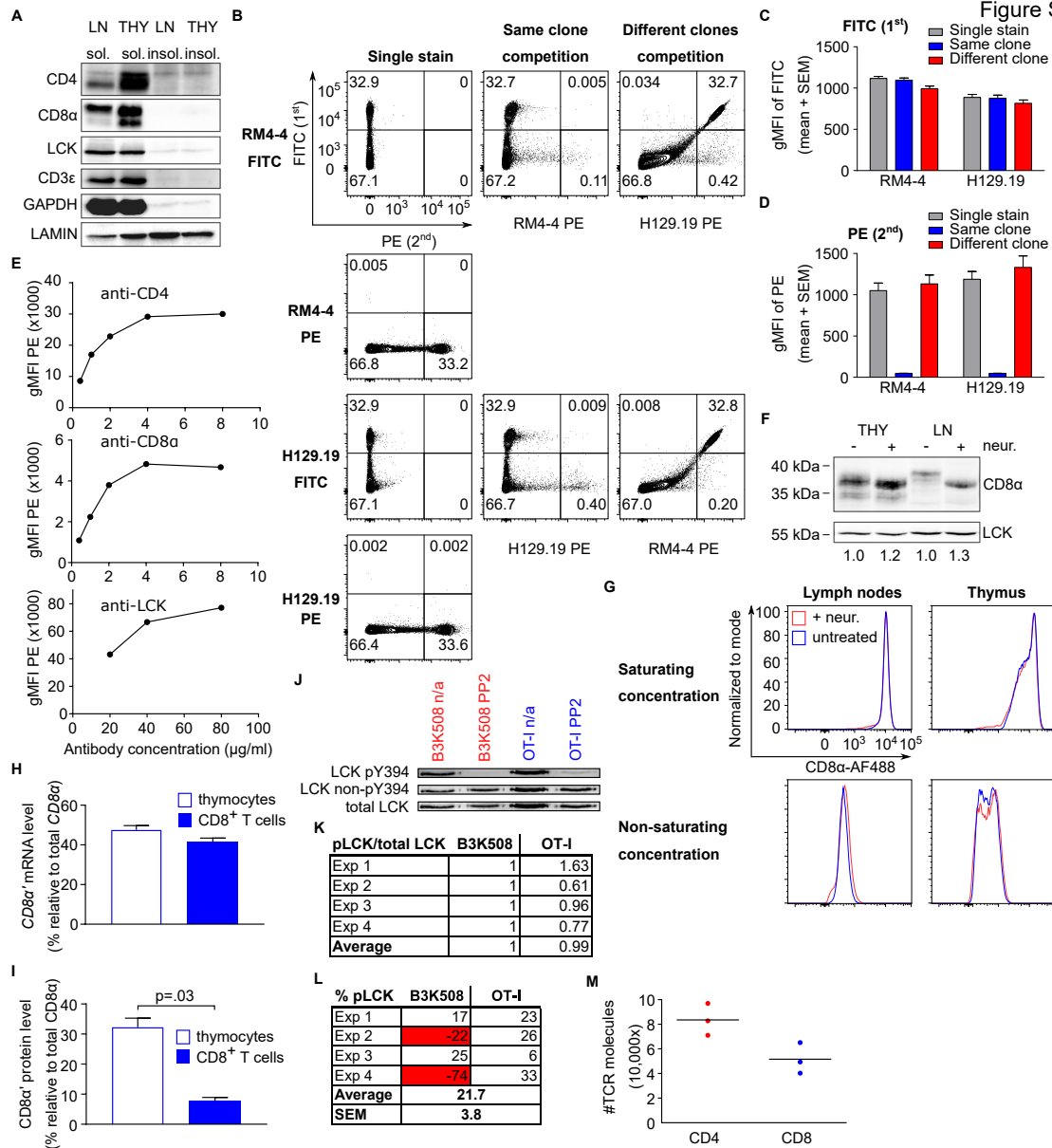
Cell Reports, Volume 30

**Supplemental Information**

**Dynamics of the Coreceptor-LCK Interactions  
during T Cell Development Shape the  
Self-Reactivity of Peripheral CD4 and CD8 T Cells**

Veronika Horkova, Ales Drobek, Daniel Mueller, Celine Gubser, Veronika Niederlova, Lena Wyss, Carolyn G. King, Dietmar Zehn, and Ondrej Stepanek

Figure S1

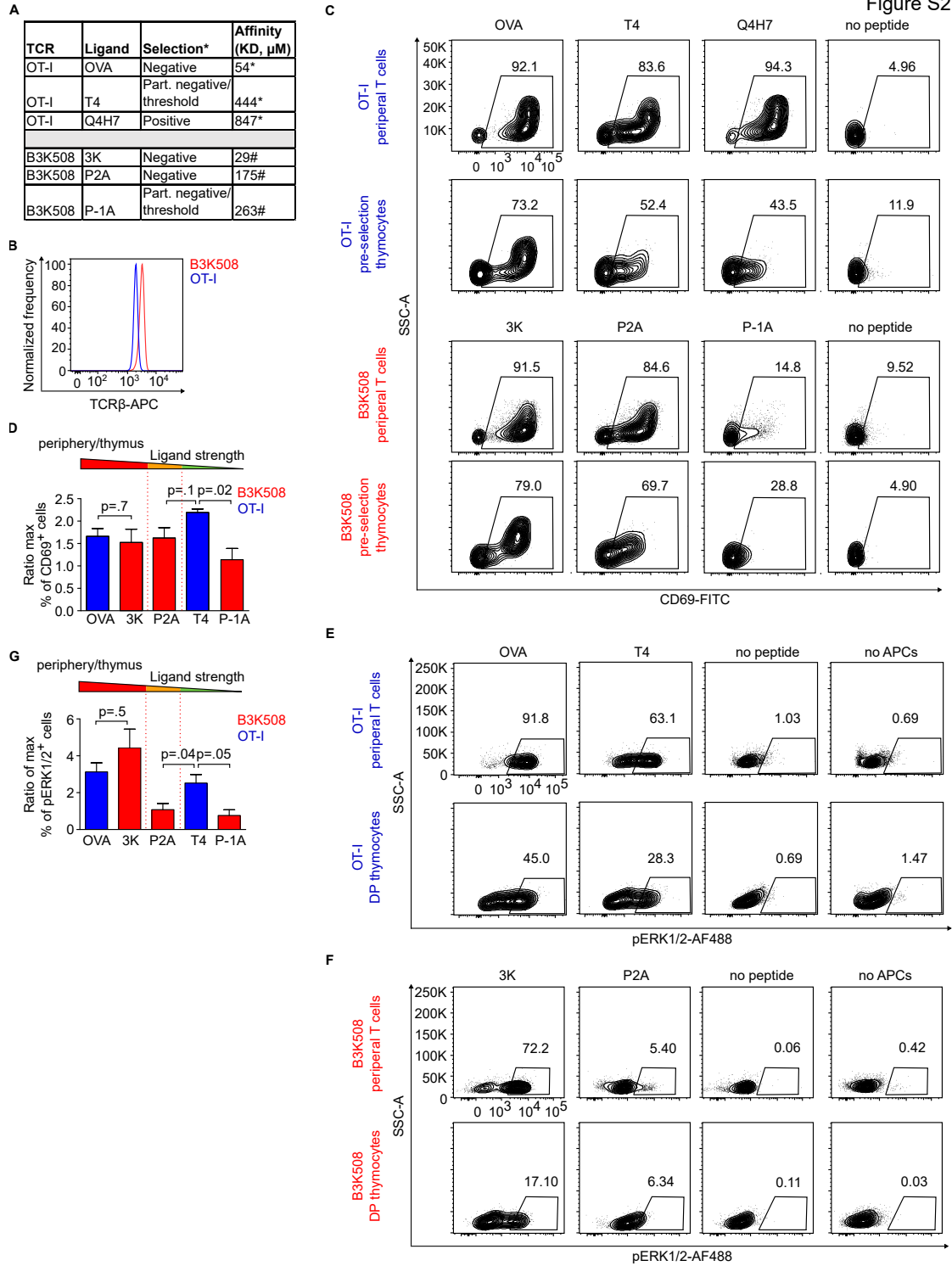


**Fig. S1. Related to Figure 1.**

(A) Soluble and insoluble fraction of lysate (1% NP-40S) from full LN and thymus were analyzed by immunoblotting. The membranes were stained with antibodies specific for CD4 (D7D2Z), CD8 $\alpha$  (D4W2Z), LCK (3a5), CD3 $\epsilon$  (goat polyclonal), GAPDH (rabbit polyclonal), LAMIN B1 (119D5-F1) (B-D) The LN T cells were stained first with FITC-conjugated antibodies (H129.19 or RM4-4). After the antibody was washed out the cells were stained with PE-conjugated antibodies specific for CD4 (H129.19 or RM4-4) in all 4 combinations. To address whether these two antibody clones compete with each other, we compared the fluorescence intensities from single stained cells, cell stained sequentially with the same antibody clone coupled to two different fluorophores, and cells stained sequentially with two different clones coupled to two different fluorophores. (B) A representative experiment out of 3 independent experiments. (C) gMFI levels of FITC. Mean + SEM, n = 3 mice (D) gMFI levels of PE. Mean + SEM, n = 3 mice. (E) Titration of antibodies used for the analysis of FC-IP experiments. A representative experiment out of 2 independent experiments is shown. (F) Thymocytes and peripheral T cells were treated with neuraminidase or not and analyzed by immunoblotting. The membranes were probed with antibodies specific for CD8 $\alpha$  (D4W2Z) and LCK (3a5). Change in the anti-CD8 $\alpha$  signal (normalized to LCK expression) relative to non-treated controls is indicated. Representative experiment out of 4 independent experiments. (G) Thymocytes and LN cells were treated with neuraminidase or not and analyzed by flow cytometry. The cells were stained with a saturating concentration of anti-CD8 $\beta$ -APC (4  $\mu$ g/ml, clone 53-5.8), together with anti-CD8 $\alpha$ -AlexaFluor488 (clone 53-6.7) at a saturating concentration of 20  $\mu$ g/ml or a non-saturating concentration of 32 ng/ml. The CD8 $\alpha$  signal on CD8 $\beta$ <sup>+</sup> cells is shown. A representative experiment out of 2 in total. (H) Quantitative PCR analysis was performed on total thymocytes vs peripheral CD8<sup>+</sup> T cells. Mean + SEM, n = 3 mice (I) Quantitative analysis of surface CD8 $\alpha$  protein level in thymus and in peripheral CD8<sup>+</sup> T cells from experiments in Fig.1B-C. Mean + SEM, n = 5 mice in 4 independent experiments. (J-L) LCK was immunoprecipitated from lysates from non-treated (NT) or 20  $\mu$ M PP2-treated B3K508 or OT-I peripheral LN T cells. Phosphorylation of LCK was analyzed by immunoblotting using simultaneous staining with antibodies specific for phosphorylated or non-phosphorylated Y394. The membrane was re-probed with antibody to total LCK. (J) Representative image out of 4 independent experiments is shown. (K) Signal of phospho-LCK to total LCK for B3K508 and OT-I T cells is shown. Data were normalized to B3K508 in each experiment. n = 4. (L) Percentage of phosphorylated LCK molecules in B3K508 and OT-I peripheral T cells was calculated for each experiment. For B3K508, two calculations led to negative values that were excluded from the final calculation, because such values make no biological and mathematical sense and were apparently caused by the error in the measurement. The average of the remaining 6 values was used for the estimation of the percentage of phosphorylated LCK molecules. (M) The peripheral CD4<sup>+</sup> and CD8<sup>+</sup> T cells were analyzed for their expression of CD3/TCR by flow cytometry.

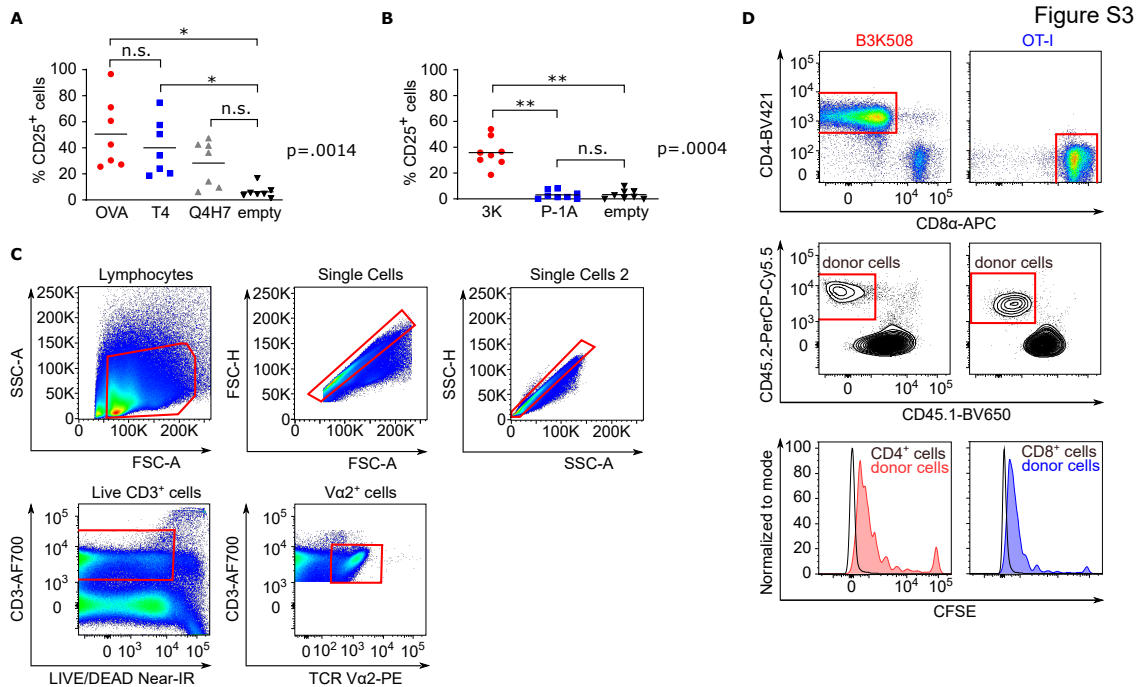


Figure S2



**Fig. S2. Related to Figure 2.**

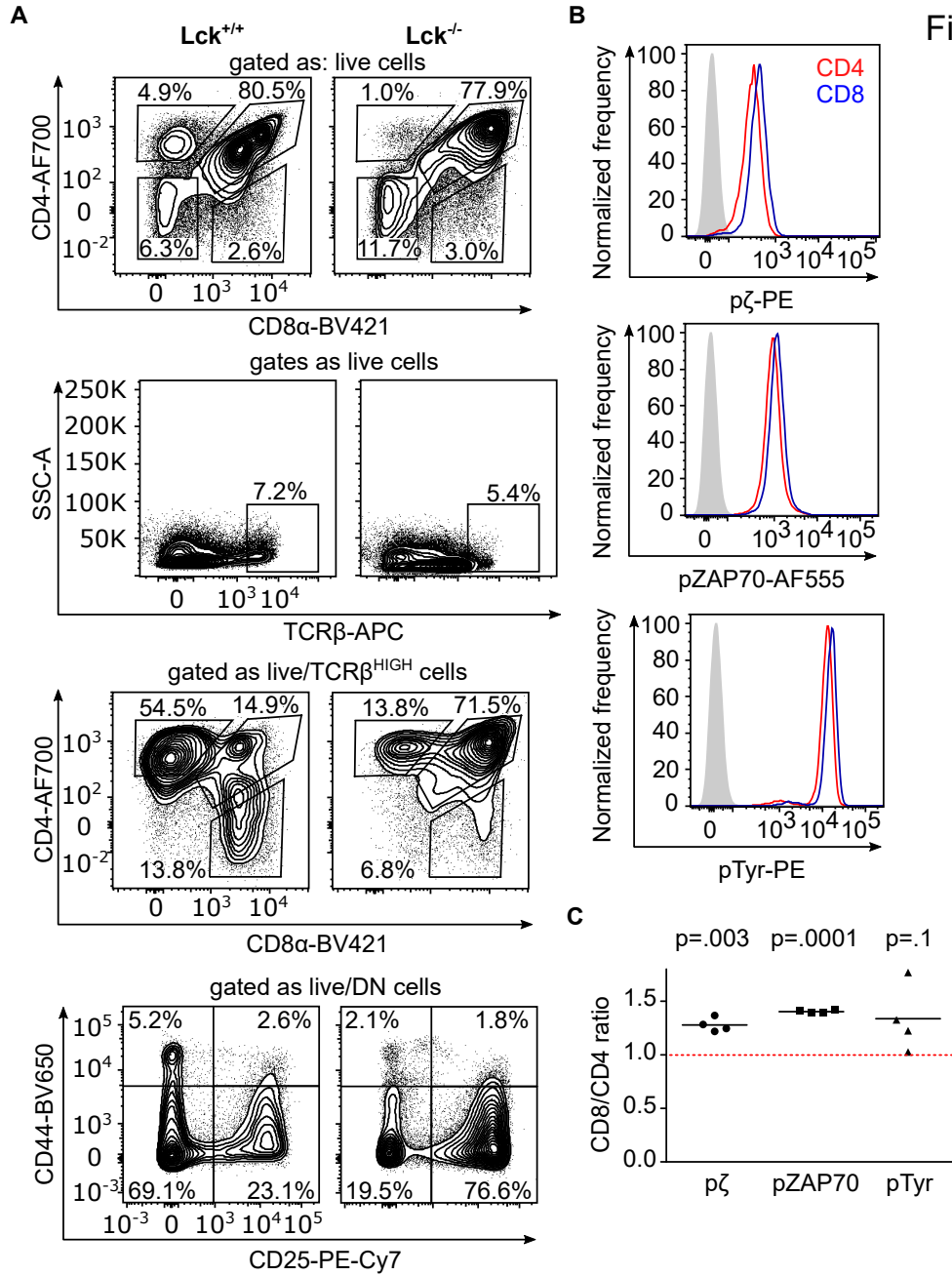
(A) List of ligands to corresponding transgenic TCR used in Fig. 2A-D. The measured dissociation constant  $K_d$  (Stepanek et al., 2014) # (Huseby et al., 2006) and their ability to induce the thymic selection is denoted. (B) TCR $\beta$  expression on CD8 $^+$ CD44 $^+$  OT-I and CD4 $^+$ CD44 $^+$  B3K508 T cells. A representative experiment out of 4 in total. (C) Representative data from experiments shown in Fig. 2A are shown. (D) The ratio of maximum activation (% of CD69 $^+$  cells) of the T cells in periphery vs. thymus. Mean + SEM, n = 4 mice in 4 independent experiments. (E-F) Alternative analysis of experiments shown in Figure 2. Representative data from experiments shown in Fig. 2C are shown. (G) The ratio of maximum activation (% of CD69 $^+$  cells) of the T cells in periphery vs thymus. Mean + SEM. n = 6-10 mice in 6-10 independent experiments.



**Fig. S3. Related to Figure 3.**

(A-B) Quantification of % CD25<sup>+</sup> monoclonal T cells from experiment in Fig.3A-B. Statistical analysis was performed using Kruskal-Wallis test with Dunn's Multiple Comparison post-tests (\* p<0.05, \*\* p<0.01). (C-D) Gating strategy for the experiments in Fig.3A-B. (C) Initial gating strategy used for all samples. (D) Additional gating strategy for B3K508 (Lm-3K) or OT-1 (Lm-T4) cells. The CFSE signals on donor cells are shown as histograms.

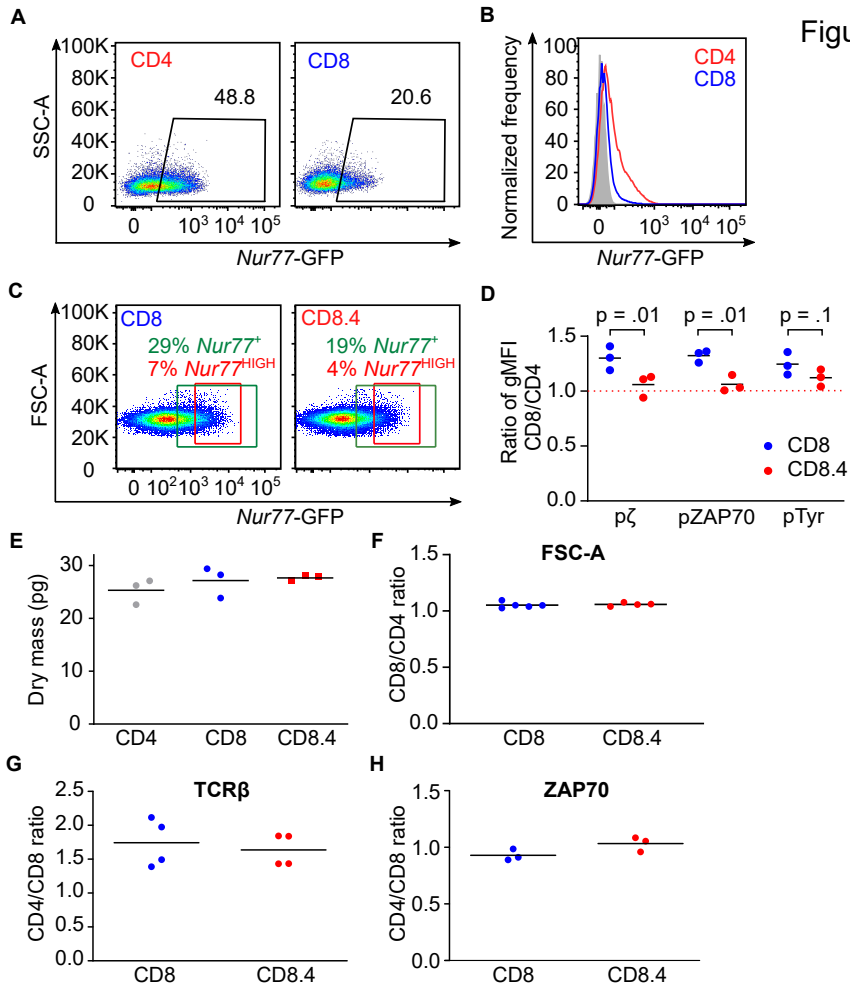
Figure S4



**Fig. S4. Related to Figure 4.**

(A) Flow cytometry analysis of thymocytes from *Lck<sup>+/+</sup>* and *Lck<sup>-/-</sup>* mice using indicated antibodies and LIVE/DEAD near-IR staining. A representative experiment out of 3 in total. (B-C) Fixed and permeabilized LN T cells from *Foxp3-GFP* mice were stained with antibodies to CD4, CD8, TCR $\beta$ , pTCR $\zeta$ , pZAP70, and overall tyrosine phosphorylation and analyzed by flow cytometry. Only GFP-negative cells are shown. A representative experiment out of 3 mice in 2 independent experiments in total.

Figure S5



**Fig. S5. Related to Figure 5.**

(A) Representative data from the CD4<sup>+</sup> and CD8<sup>+</sup> T cells gated for *Nur77*-GFP<sup>+</sup>. Data out of 5 independent experiments are shown. (B) Representative data on *Nur77* expression of the CD4<sup>+</sup> and CD8<sup>+</sup> T cells. The data are the same as in Fig. S5A. (C) Representative data from CD8 WT and CD8.4 naïve T cells gated for *Nur77*-GFP<sup>+</sup> and *Nur77*-GFP<sup>High</sup>. (D) Independent repetition of experiment in Fig. 5B performed in Prague. Statistical significance was calculated using paired T test. n = 3 mice in 3 independent experiments. (E) Peripheral LN T cells from C57Bl/6J and CD8.4 mice were analyzed on Tescan Q-Phase microscope. Dry mass of individual populations is displayed. Mean. n = 3 mice in 3 independent experiments. (F) Peripheral LN T cells from C57Bl/6J and CD8.4 mice were analyzed by flow cytometry and gated as CD44<sup>+</sup> CD4<sup>+</sup> or CD44<sup>+</sup> CD8<sup>+</sup> cells. The relative size (gMFI of FSC-A) of CD8<sup>+</sup> or CD8.4<sup>+</sup> cells to CD4<sup>+</sup> cells is displayed. Mean. n = 4-5 mice in 4-5 independent experiments. (G) Relative expression (gMFI) of *Zap70* in CD8<sup>+</sup> or CD8.4<sup>+</sup> T cells compared to CD4<sup>+</sup> T cells is shown. Mean. n = 3 mice in 3 independent experiments.

Table S1. Related to Fig. 1: Parameters for the mathematical model related to Fig.1C.

Parameter	diffusion (D)	coreceptor-MHC offrate (Ku)	lattice spacing (l)	coreceptor-MHC onrate (Kb)	pLck coupling (f)	number of TCRs/3 (T)	Area	$k_{on}$	$k_p$	phosphorylation
Units	$\mu\text{m}^2 \text{s}^{-1}$	$\text{s}^{-1}$	$\mu\text{m}$	$\text{s}^{-1}$	%		$\mu\text{m}^2$	$\mu\text{m}^2 \text{s}^{-1}$	$\text{s}^{-1}$	
CD4 DP thymocytes	0.08	200	0.01	1000	0.051	697	26.18	0.1	5	5
CD4 LN T cells	0.08	200	0.01	1000	0.108	27861	26.18	0.1	5	5
CD8 DP thymocytes	0.08	20	0.01	1000	0.0054	697	26.18	0.1	5	5
CD8 LN T cells	0.08	20	0.01	1000	0.072	17203	26.18	0.1	5	5



**Data S1 Related to Fig.1: Source code for 'Lck come&stay/signal duration' model (MatLab).**

**% Main script**

```
% calculates Come%Stay model from given parametes using essentially 4
% conditions (can vary in coupling), the result are 4 matrices where X is
% DOSE and Y is dwell time

%dwelldtimes=zeros(100,100);
%for j=1:10 % makes an array of dwell times, always in columns from 0.05 to 20 in 0.025 steps, 1000 columns (all are the same)
%dwelldtimes(:,j)=i*0.1;
%end

%antigens=zeros(100,100); %makes an array of antigen numbers from 1 to 1000, 800 rows (all are the same)
%for j=1:100
%antigens(j,:)=j;
%end

antigens=1:250;

sourcedata1=fopen('comenstaydata_5_6_P.txt','r'); %opens file with source data (dataDIAOTI.txt) and calls it sourcedata1
Dat=fscanf(sourcedata1,'%f', [10,4]) % reads data from the file
Cordata=Dat;
Data1=Cordata(1,:); % condition 1
Data2=Cordata(2,:); % condition 2
Data3=Cordata(3,:); % condition 3
Data4=Cordata(4,:); % condition 4

dw1=0.86; % antigen dwell time (CD4s) 0.2 for threshold Ag, 0.86 FOR 3K
dw2=10.5; % antigen dwell time (CD8s) 0.9 for threshold Ag, 10.5 for OVA (approx. for thymus)

res1=dataprocess(Data1, dw1, antigens); % calls data process function for datasets 1-4
res2=dataprocess(Data2, dw1, antigens);
res3=dataprocess(Data3, dw2, antigens);
res4=dataprocess(Data4, dw2, antigens);

semilogy(antigens.res1, 'red', 'LineWidth',2.5)
set(gca, 'FontSize', 17);

hold on % to draw all lines to the same graph
semilogy(antigens.res2, 'red', 'LineWidth', 2.5)
semilogy(antigens.res3, 'blue', 'LineWidth', 2.5)
semilogy(antigens.res4, 'blue', 'LineWidth', 2.5)
xlabel('Number of antigens', 'fontSize', 15, 'FontWeight', 'bold')
ylabel('# TCRs triggered', 'fontSize', 15, 'FontWeight', 'bold')
hold off
```

```

% Functions
function [lam] = markovchain ( D, Ku, l, Kb, f)
% Gives lambda parameter from an analytical Markov Chain solution
% lambda is the rate of Lck recruitment to the TCR via coreceptors
% Describes output of the coreceptor scanning mechanism
% D is a diffusion coefficient for membrane proteins, std 0.08 um^2
% x s-1
% cor_Koff is the coreceptor Koff from the MHC molecule, std 20s-1 for
% CD8, 200s-1 for CD4
% l is a lattice spacing of the model, std 0.01 um
% cor_Kon is on-rate of the coreceptor-MHC interaction, std 1000s-1
lam = (f.*D.*Ku)/(D+l.^2.*Kb);
end

function [hotTCR] = dataprocess( dataValues, dwelltimeValue, antigenNumber )
% uses input data in a horizontal vector (reading from a file) and
% calculates the output of the comenstay, i.e. calculates lambda and then
% number of triggered and occupied TCRs

lambda=markovchain(dataValues(1,1), dataValues(1,2),dataValues(1,3), dataValues(1,4),dataValues(1,5))
hotTCR=comenstay(lambda, antigenNumber, dataValues(1,6), dataValues(1,7), dwelltimeValue, dataValues(1,8), dataValues(1,9), dataValues(1,10));

end

function [ R ] = comenstay( la, L, T, A, t, kon, kp, n )

%Gives abverage number of occupied and triggered TCRs at the equilibrium
% from Stepanek et al. Cell 2014
% la is lambda (rate of Lck recruitment, calculated by markov chain model)
% L is number of antigen (pMHC) molecules in the contact area, varied
% T is number of TCRs in the contact area
% A is the area of the T cell/APC inteface, std 26 um^2
% t is dwell-time, i.e. half-life (varied)
% kon is the on-rate of the antigen, std 0.1 um^2s-1
% kp is the phosphorylation rate, std 5s-1
% n is the required number of phosphorylation steps

%la=ones(100)*la1; %to have it in matrices (optional), change THE INPUT
%variables accordigly
%T=ones(100)*T1;
%A=ones(100)*A1;
%kon=ones(100)*kon1;
%kp=ones(100)*kp1;
%n=ones(100)*n1;

```

af=log(2)/(kon\*t); % Affinity, to simplify the final equation ln2/(kon x t)  
koff=log(2)/t; % koff calculated

ProbTrig=la/(la+koff)\*(kp/(kp+koff))^n; %probability that a single TCR/MHC interaction leads to the TCR triggering

OccTCRs = (L/A+T/A+af-(L/A+T/A+af)^2-4\*L\*T/A^2)^0.5/A; %average number of antigen occupied by MHC antigens in equilibrium, . removed when not necessary

R= ProbTrig\*OccTCRs; % number of triggered and occupied TCRs at the equilibrium, OUTPUT of the Come&Stay model



## **Attachment 2**

# Unique Roles of LCK in CD4 and CD8 T cells

## **Title: Unique roles of LCK in CD4 and CD8 T cells**

**Authors:** Veronika Horkova<sup>1</sup>, Ales Drobek<sup>1</sup>, Darina Paprczkova<sup>1</sup>, Daniela Glatzova<sup>1</sup>, Markus Kraller<sup>2</sup>, Avishek Prasai<sup>1</sup>, Katerina Krizova<sup>1</sup>, Rene Platzer<sup>2</sup>, Johannes B. Huppa<sup>2</sup>, Ondrej Stepanek<sup>1\*</sup>

### **Affiliations:**

<sup>1</sup>Laboratory of Adaptive Immunity, Institute of Molecular Genetics of the Czech Academy of Sciences; Prague, Czech Republic.

\*Corresponding author. Email: [ondrej.stepanek@img.cas.cz](mailto:ondrej.stepanek@img.cas.cz)

<sup>2</sup> Institute for Hygiene and Applied Immunology, Center for Pathophysiology, Infectiology and Immunology, Medical University of Vienna, Vienna, Austria.

### **Abstract:**

The kinase LCK and CD4/CD8 co-receptors initiate T-cell receptor (TCR) signaling, leading to key T-cell fate decisions. Despite decades of research, the importance of CD4- and CD8-LCK interactions for TCR triggering remains largely unknown. In this study, we generated animal models expressing modified LCK to uncover whether and how coreceptor-bound LCK drives TCR signaling. We show that CD4-coupled LCK is crucial for proper development and responses of helper T cells largely in a kinase-independent manner, whereas its catalytic activity is required only for signaling induced by weak antigens. Conversely, CD8-coupled LCK relies on its kinase activity completely to fine-tune the development and effector response of cytotoxic T cells to suboptimal antigens. Our findings reveal differential mechanisms of CD4-LCK and CD8-LCK in promoting T-cell responses.

### **One-Sentence Summary:**

The LCK kinase associated with T-cell co-receptors has kinase-dependent and kinase-independent roles in T-cell activation.

### **Main Text:**

T-cells use their antigen receptor (TCR) to mediate adaptive immune responses to infection and cancer, but also to trigger autoimmunity. Cytotoxic CD8<sup>+</sup> and helper CD4<sup>+</sup> T cells have different functions in the immune system, but their TCR signaling pathways are very similar. One notable difference is the usage of CD8 or CD4 invariant coreceptors recognizing MHCI and MHCII, respectively. Both coreceptors interact with a Src-family kinase, LCK, which initiates the TCR signal transduction inside the cells by phosphorylating tyrosine motifs in the TCR complex. Although CD8 and CD4 have different affinities for MHCI/II and different stoichiometry of the interaction with LCK [1, 2], they are supposed to play largely analogical roles in the TCR triggering [3].

It has been proposed that the interaction of coreceptors with LCK increases the sensitivity of TCR signaling [1, 2, 4], sets the threshold for negative and positive selection [2], mediates the selection of self-MHC-restricted T cells [5], and defines the productive antigen docking polarity [6]. However, the mechanism of how coreceptor-LCK contributes to TCR triggering is unclear. The original and intuitive model is that a coreceptor recruits LCK to the antigen-engaged TCR and this LCK subsequently phosphorylates the TCR/CD3 complex [2, 7, 8]. An alternative model proposes

that this phosphorylation is preferentially carried out by 'free' LCK [9, 10]. In this scenario, coreceptor-bound LCK physically stabilizes the TCR:antigen interaction from inside the cell [11].

In this study, we developed and characterized mouse models tailored to resolve the function of the coreceptor-LCK interaction in the development and immune responses of T cells. We generated knock-in mouse strains with C20A/C23A (CA) or K273R (KR) amino acid substitutions in LCK together with *Lck*<sup>KO/KO</sup> mice (Fig. S1A-C). LCK<sup>CA</sup> does not interact with CD4 and CD8 [5, 12] (Fig. S1D-E), whereas LCK<sup>KR</sup> lacks enzymatic activity [13]. To uncouple the putative catalytic and adaptor roles of LCK, we produced *Lck*<sup>CA/KR</sup> compound heterozygotes expressing one pool of active LCK<sup>CA</sup> unable to bind to coreceptors and a pool of kinase-dead LCK<sup>KR</sup> interacting with coreceptors (Fig. S1F).

As reported previously [14], *Lck*<sup>KO/KO</sup> mice showed partial developmental blocks at CD4<sup>-</sup> CD8<sup>-</sup> double negative (DN) 3 and CD4<sup>+</sup> CD8<sup>+</sup> double positive (DP) stages (Fig. 1A, S2A-D). *Lck*<sup>KR/KR</sup> showed even more severe phenotype, suggesting that LCK<sup>KR</sup> is a dominant negative variant preventing the phosphorylation of the TCR complex by other kinases, such as Fyn [14]. As expected, *Lck*<sup>CA/CA</sup> mice did not show the block at the DN stage, documenting the normal activity of this kinase in T cells without coreceptors (Fig. S2A-C). *Lck*<sup>CA/CA</sup> mice had a partial block in the positive selection, which was more pronounced in mature single positive (mSP) CD4<sup>+</sup> than in mSP CD8<sup>+</sup> thymocytes (Fig. 1A, S2A,D). *Lck*<sup>CA/KR</sup> mice showed higher numbers of mSP CD4<sup>+</sup> than *Lck*<sup>CA/CA</sup> mice, but the numbers of mSP CD8<sup>+</sup> thymocytes were comparable in these two strains (Fig. 1A, S2D). These observations suggested a kinase-independent role of coreceptor-bound LCK in CD4<sup>+</sup> T cells, but not in CD8<sup>+</sup> T cells.

The numbers of mature CD4<sup>+</sup> and CD8<sup>+</sup> T cells in the periphery reflected their maturation in the thymus (Fig. 1B, S2E). The exception was comparable numbers of mature CD8<sup>+</sup> T cells in *Lck*<sup>CA/CA</sup> and *Lck*<sup>WT/WT</sup> mice, probably because homeostatic proliferation of peripheral T cells compensated for the moderately decreased thymic output of *Lck*<sup>CA/CA</sup> mice.

To study the intrinsic role of LCK variants in the development of CD4<sup>+</sup> and CD8<sup>+</sup> T cells, we generated mixed bone marrow (BM) chimeras. We transferred BM cells from congenic WT Ly5.1 mice and from indicated *Lck* variant strains (Ly5.2) at 1:1 ratio into Ly5.1/Ly5.2 host mice. We observed reduced numbers of peripheral *Lck*<sup>CA/CA</sup> CD4<sup>+</sup> and CD8<sup>+</sup> T cells in comparison to WT cells (Fig. 1C, S2G-H). The coreceptor-bound kinase-dead LCK in *Lck*<sup>CA/KR</sup> background partially rescued this developmental defect in CD4<sup>+</sup> T cells, but not in CD8<sup>+</sup> T cells (Fig. 1C, S2G-H).

We assessed the *Lck* variant mice for their anti-viral and anti-tumor immune protection abilities, which are largely mediated by cytotoxic CD8<sup>+</sup> T cells. *Lck*<sup>KR/KR</sup> mice cleared Lymphocytic choriomeningitis virus (LCMV) inefficiently (Fig. 1D). *Lck*<sup>CA/KR</sup> showed higher LCMV titers than WT mice as well, whereas *Lck*<sup>CA/CA</sup> mice were comparable to *Lck*<sup>WT/WT</sup>. The fastest growth of implanted MC-38 carcinoma [15] was detected in *Lck*<sup>KR/KR</sup> followed by *Lck*<sup>KO/KO</sup> and *Lck*<sup>CA/KR</sup> mice (Fig. 1E, S2I). *Lck*<sup>CA/CA</sup> mice showed slightly reduced, but not significant, anti-tumor effects than WT mice (Fig. 1E, S2I). Overall, the heterozygous *Lck*<sup>CA/KR</sup> mice showed impaired anti-tumor and anti-viral responses in comparison to *Lck*<sup>WT/WT</sup> and *Lck*<sup>CA/CA</sup> mice, suggesting that the CD8-coupled kinase-dead LCK blocks, not promotes, TCR activation.

To study roles of CD4- and CD8-bound LCK separately, we crossed *Lck* variant strains to MHCII-restricted and MHCII-restricted transgenic TCR *Rag2*<sup>KO/KO</sup> mice. First, we analyzed the effect of LCK variants in CD8<sup>+</sup> OT-I T cells specific to ovalbumin-derived K<sup>b</sup>-SIINFEKL antigen (OVA). *Lck*<sup>KO/KO</sup> and *Lck*<sup>KR/KR</sup> OT-I mice showed a severe developmental impairment, whereas *Lck*<sup>WT/WT</sup>, *Lck*<sup>CA/CA</sup>, and *Lck*<sup>CA/KR</sup> mice did not have an apparent block in T-cell maturation (Fig. S3A-D).

We activated OT-I T cells with antigen presenting cells loaded with OVA peptide or its lower affinity variants (Q4R7, Q4R7, T4, G4, E4, E1) *ex vivo* and measured the magnitude of the antigenic response as the percentage of CD69<sup>+</sup> positive OT-I T cells. *Lck*<sup>CA/CA</sup> OT-I T cells showed

a normal response to a high-affinity antigen, OVA, but a weak response to low-affinity OVA variants (Fig. 2A), which was in line with our previous reports that the CD8-LCK interaction facilitates signaling induced particularly by suboptimal antigens [2]. *Lck*<sup>CA/KR</sup> OT-I T cells exhibited even weaker responses than *Lck*<sup>CA/CA</sup> OT-I T cells (Fig. 2A), documenting the inhibitory role of kinase-dead CD8-bound LCK.

In the next step, we adoptively transferred *Lck* variant OT-I T cells into congenic Ly5.1 mice followed by infection with transgenic *Listeria monocytogenes* (Lm) expressing OVA or its lower affinity variants (T4, G4). The expansion of OT-I T cells on day 5 post-infection followed the hierarchy *Lck*<sup>WT/WT</sup> > *Lck*<sup>CA/CA</sup> > *Lck*<sup>CA/KR</sup> (Fig. 2B). Again, the differences were more pronounced upon stimulation with low-affinity antigens.

We examined the ability of *Lck* variant OT-I T cells to hamper tumor progression upon their adoptive transfer into T-cell deficient CD3ε<sup>-/-</sup> mice bearing small MC-38 OVA tumors. The anti-tumor activity of OT-I cells followed the hierarchy *Lck*<sup>WT/WT</sup> > *Lck*<sup>CA/CA</sup> > *Lck*<sup>CA/KR</sup> again (Fig. 2C, S3E).

Overall, these *ex vivo* and *in vivo* experiments documented that the catalytic activity of CD8-bound LCK enhances signaling by suboptimal antigens, such as antigens with low affinity or antigens presented in weak immunogenic conditions such as anti-tumor responses. In contrast, the interaction of CD8 with kinase dead LCK inhibits TCR signaling. It has been proposed that CD8-LCK interaction might stabilize the antigen binding [11]. We assessed the role of CD8-LCK in antigen avidity using three different assays. Whereas the K<sup>b</sup>-OVA and K<sup>b</sup>-T4 tetramer staining (Fig. S3F) and the on-cell *k<sub>off</sub>* measurement [16] (Fig. S3G) indicated that CD8-LCK indeed stabilizes the TCR:antigen interaction, 2D affinity measurements using the antigen nested in a lipid bilayer did not reveal substantial differences (Fig. 3H). Although the results from these assays were not conclusive and require further investigation, the potential CD8-LCK-mediated stabilization of the TCR:antigen binding does not explain the differences in our functional assays, because *Lck*<sup>CA/KR</sup> OT-I T cells showed intermediate antigen binding, but the weakest antigenic responses.

To study the role of the CD4-LCK interaction in CD4<sup>+</sup> T-cell antigenic responses, we crossed our collection of *Lck* variant mice with I-A<sup>b</sup>-3K-specific B3K508 T cells [17]. *Lck*<sup>KO/KO</sup> and *Lck*<sup>KR/KR</sup> B3K508 thymocytes showed a developmental block, whereas *Lck*<sup>WT/WT</sup>, *Lck*<sup>CA/CA</sup>, and *Lck*<sup>CA/KR</sup> had normal T-cell maturation (Fig. S4A-D). *Lck*<sup>CA/CA</sup> B3K508 T cells exhibited weaker *ex vivo* antigenic responses to the cognate 3K peptide and its intermediate- and low-affinity variants (P5R and P2A, respectively) than WT B3K508 T cells (Fig. 3A). *Lck*<sup>CA/KR</sup> B3K508 T cells partially rescued defective responses to high-affinity 3K and intermediate-affinity P5R antigens, but not to low-affinity antigen P2A (Fig. 3A). Accordingly, we observed weaker response of *Lck*<sup>CA/CA</sup> B3K508 T cells to Lm expressing 3K or low-affinity P2A *in vivo* (Fig. 3B). *Lck*<sup>CA/KR</sup> rescued the responses to Lm-3K, but not to P2A (Fig. 3B). These data indicated that CD4-coupled LCK has a kinase-independent role and, at the same time, the response to low-affinity antigens require the catalytic activity of CD4-bound LCK.

To address the kinase-independent role of CD4-LCK in T-cell development (Fig. 1) and antigenic responses (Fig. 3A-B), we focused on the role of LCK in CD4 localization. We observed that LCK stabilizes surface expression of CD4 in a kinase-independent manner whereas CD8 levels were less affected by the absence of LCK or its inability to interact with coreceptors (Fig. 3C, S4E-G). We noticed that *LCK*<sup>KO</sup> Jurkat cell line [18] expresses very low CD4 surface levels (Fig. S4H). Expression of *LCK*<sup>WT</sup> or *LCK*<sup>KR</sup>, but not *LCK*<sup>CA</sup>, substantially increased surface CD4 in *LCK*<sup>KO</sup> Jurkat cells (Fig. 3D). The down-regulation of CD4 in the absence of LCK coupling was mediated by protein kinase C (PKC), as the treatment of CD4<sup>+</sup> T cells isolated from *Lck*<sup>CA/CA</sup>, but not *Lck*<sup>WT/WT</sup> or *Lck*<sup>CA/KR</sup>, mice with PKC inhibitor elevated CD4 levels (Fig. 3E, Fig. S4I). We hypothesized that the absence of the CD4-LCK interaction regulates the localization of CD4



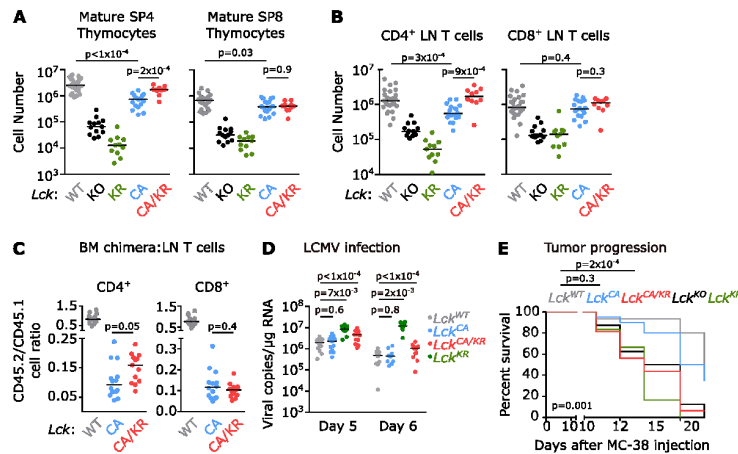
within the plasma membrane. The analysis of CD4 membrane distribution by electron microscopy revealed that LCK is present in clusters in *Lck<sup>CA/CA</sup>* CD4<sup>+</sup> T cells, but is relatively uniform in *Lck<sup>WT/WT</sup>* CD4<sup>+</sup> T cells (Fig. 3F-G).

Overall, our data indicate that the interaction of LCK with the coreceptors is required for proper T-cell development and immune responses, although the defects observed in mice with disrupted CD8- and CD4-LCK interactions were more subtle than in mice deficient in LCK or expressing kinase dead LCK. Our experiments with monoclonal TCR transgenic mice revealed that the interactions of LCK with CD8 and CD4 are not essential for maturation of conventional MHC/II-restricted T cells, but it is still plausible that they give a selective advantage to these T cells over T cells expressing MHC-independent TCRs.

The roles of CD8-LCK and CD4-LCK interactions differ. CD8-LCK facilitates TCR responses of CD8<sup>+</sup> T cells only to suboptimal stimulation (i.e., low-affinity antigens, low immunogenic environment), in a kinase-dependent manner. *Lck<sup>CA/KR</sup>* CD8<sup>+</sup> T cells with kinase-dead LCK interacting with CD8 show impaired responses *ex vivo* and *in vivo*, although they possess another pool of kinase active LCK unable to bind to CD8. Overall, our data do not reveal the putative kinase-independent adaptor role of CD8-bound LCK in TCR triggering for T-cell biology.

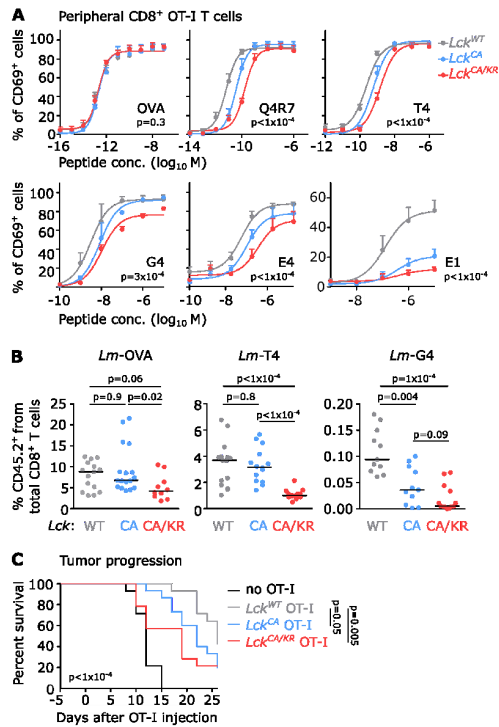
In contrast, CD4-LCK interaction has both kinase-dependent and kinase-independent roles. CD4<sup>+</sup> T cells depend on coreceptor-LCK binding more than CD8<sup>+</sup> T cells. Maturation and activation of CD4<sup>+</sup> T cells can be largely restored with a pool of CD4-interacting kinase-dead LCK. The kinase-independent role of LCK is coupled with the stabilization of surface CD4 and promoting its homogenous distribution in the plasma membrane. The regulation of CD4 stability and trafficking by LCK was reported in cells lines previously [19, 20], but its importance for T-cell biology was not investigated before. The responses to low-affinity antigens still require the kinase activity of CD4-bound LCK analogically to CD8<sup>+</sup> T cells.

Overall, our study resolves the enigmatic roles of coreceptor-LCK interactions in T-cell biology.



**Figure 1. Coreceptor-bound LCK promotes T-cell development and anti-tumor protection.**

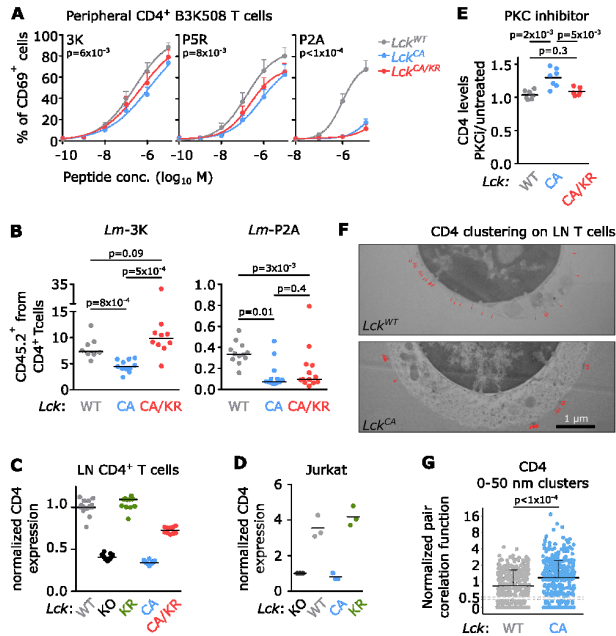
Indicated *Lck* variant mouse strains were analyzed. (A) mSP4 (TCR $\beta^+$  CD24 $^-$  CD4 $^+$  CD8 $\alpha^+$ ) and mSP8 (TCR $\beta^+$  CD24 $^-$  CD4 $^-$  CD8 $\alpha^+$ ) thymocytes were quantified by flow cytometry. n=25 *Lck*<sup>WT/WT</sup>, 13 *Lck*<sup>KO/KO</sup>, 11 *Lck*<sup>KR/KR</sup>, 18 *Lck*<sup>CA/CA</sup>, 11 *Lck*<sup>CA/KR</sup> mice. (B) CD4 $^+$  (viable TCR $\beta^+$  CD4 $^+$  CD8 $\alpha^+$ ) and CD8 $^+$  (viable TCR $\beta^+$  CD4 $^-$  CD8 $\alpha^+$ ) T cells in lymph nodes were quantified by flow cytometry. n=25 *Lck*<sup>WT/WT</sup>, 13 *Lck*<sup>KO/KO</sup>, 11 *Lck*<sup>KR/KR</sup>, 18 *Lck*<sup>CA/CA</sup>, 10 *Lck*<sup>CA/KR</sup> mice. (C) Bone marrow cells from indicated *Lck* variant strains mixed with bone marrow cells from congenic Ly5.1 WT mice were transplanted into Ly5.1/Ly5.2 WT mice at 1:1 ratio. n= 13 *Lck*<sup>WT/WT</sup>, 14 *Lck*<sup>CA/CA</sup>, 13 *Lck*<sup>CA/KR</sup> mice from 3 independent experiments. The ratio of lymph node CD4 $^+$  or CD8 $^+$  T cells derived from Ly5.1 and Ly5.2 bone marrow 8 weeks after transplantation. (D) Indicated *Lck* variant mice were infected with LCMV and the viral titres in the spleens were determined on day 5 or 6 post-infection by RT-qPCR. n= 16 *Lck*<sup>WT/WT</sup>, 15 *Lck*<sup>CA/CA</sup>, 13 *Lck*<sup>CA/KR</sup>, 13 *Lck*<sup>KR/KR</sup> mice in 6 independent experiments on day 5, n= 12 *Lck*<sup>WT/WT</sup>, 11 *Lck*<sup>CA/CA</sup>, 13 *Lck*<sup>CA/KR</sup>, 10 *Lck*<sup>KR/KR</sup> mice in 5 independent experiments on day 6 after infection. (A-D) Results from individual mice and medians are shown. Statistical significance was calculated using Mann-Whitney test. (E)  $0.5 \times 10^6$  MC-38 carcinoma cells were injected into indicated mice subcutaneously and the tumor growth was monitored. The percentage of mice with a tumor smaller than 500 mm<sup>3</sup> in time is shown. n =15 *Lck*<sup>WT/WT</sup>, 20 *Lck*<sup>CA/CA</sup>, 16 *Lck*<sup>CA/KR</sup>, 8 *Lck*<sup>KO/KO</sup>, 6 *Lck*<sup>KR/KR</sup> mice in 2 (*Lck*<sup>KR/KR</sup> mice) or 4 (other strains) independent experiments. The statistical significance was tested using Long-rank (Mantel-Cox) Test (all groups) and Gehan-Breslow-Wilcoxon test (individual groups).



**Figure 2. Kinase activity of CD8-bound LCK is drives responses to suboptimal antigens.**

T cells were isolated from lymph nodes of indicated *Lck* variant OT-I *Rag2*<sup>-/-</sup> mice and characterized. (A) T cells were activated *ex vivo* with T2-Kb cells loaded with OVA peptide or its variants with decreasing affinity (OVA>Q4R7>T4>G4>E4>E1) overnight and analyzed for expression of CD69 by flow cytometry. Mean values + SEM are shown. n = 3 independent experiments for OVA and Q4R7, n=4 independent experiments for T4, G4, E4 a E1. Differences in the slope and/or maximum of the fitted curves were tested using extra sum-of-squares F test. (B) T cells were transferred into Ly5.1 congenic mice followed by infection with *Lm* expressing OVA, T4, or G4. Expansion of OT-I T cells was measured as their percentage among total CD8<sup>+</sup> T cells on day 5 post-infection by flow cytometry. Results for individual mice and medians are shown. Statistical significance was calculated using Mann-Whitney test. n= 15 *Lck*<sup>WT/WT</sup>, 17 *Lck*<sup>CA/CA</sup>, 10 *Lck*<sup>CA/KR</sup> mice in 4 (*Lck*<sup>CA/KR</sup>) or 6 (other strains) independent experiments for *Lm*-OVA challenge. n= 15 *Lck*<sup>WT/WT</sup>, 14 *Lck*<sup>CA/CA</sup>, 14 *Lck*<sup>CA/KR</sup> mice in 4 independent experiments for *Lm*-T4 challenge. n= 12 *Lck*<sup>WT/WT</sup>, 12 *Lck*<sup>CA/CA</sup>, 14 *Lck*<sup>CA/KR</sup> mice in 3 independent experiments for *Lm*-G4 challenge. (C) 0.5x10<sup>6</sup> MC-38 carcinoma cells were injected into CD3ε<sup>-/-</sup> mice subcutaneously. 0.2x10<sup>6</sup> OT-I T cells were adoptively transferred into these mice 5 days later and the size of the tumor was measured. The percentage of mice with a tumor smaller than 500 mm<sup>3</sup>

in time is shown. The statistical significance was tested using Long-rank (Mantel-Cox) Test (all groups) and Gehan-Breslow-Wilcoxon test (individual groups).



**Figure 3. CD4-bound LCK has both kinase-dependent and kinase-independent roles in TCR signaling.**

(A-B) T cells were isolated from lymph nodes of indicated *Lck* variant B3K508 *Rag2*<sup>-/-</sup> mice and functionally characterized. (A) T cells were activated *ex vivo* with splenocytes from Ly5.1 mice loaded with 3K peptide or its variants with decreasing affinity (3K > P5R > P2A) overnight and analyzed for expression of CD69 by flow cytometry. Mean values + SEM are shown. Number of independent experiments: 7 (*Lck*<sup>CA/KR</sup>) or 8 (other strains) for 3K; n= 5 for P5R; 6 (*Lck*<sup>CA/KR</sup>) or 8 (other strains) for P2A. Differences in the slope and/or maximum of the fitted curves were tested using extra sum-of-squares F test. (B) T cells were transferred into Ly5.1 WT mice followed by infection with Lm expressing 3K or P2A. Expansion of B3K508 T cells was measured as their percentage among total CD4<sup>+</sup> T cells on day 5 post-infection by flow cytometry. Results for individual mice and medians are shown. Statistical significance was calculated using Mann-Whitney test. n = 8 *Lck*<sup>WT/WT</sup>, 11 for *Lck*<sup>CA/CA</sup>, 10 for *Lck*<sup>CA/KR</sup> mice from 3 independent experiments for Lm-3K, n = 12 *Lck*<sup>WT/WT</sup>, 13 for *Lck*<sup>CA/CA</sup>, 13 for *Lck*<sup>CA/KR</sup> mice from 3 independent experiments for Lm-P2A. (C) Relative CD4 surface levels on CD4<sup>+</sup> T cells isolated from indicated *Lck* variants were determined by flow cytometry. Individual mice and medians are shown. n=25 *Lck*<sup>WT/WT</sup>, 13 *Lck*<sup>KO/KO</sup>, 11 *Lck*<sup>KR/KR</sup>, 18 *Lck*<sup>CA/CA</sup> and 10 *Lck*<sup>CA/KR</sup> mice. (D) Normalized surface CD4 levels on *LCK*<sup>KO</sup> Jurkats cells transduced or not with indicated *LCK* variants were determined by flow

cytometry. Individual experiments and means are shown. n= 3 independent experiments. (E) Lymph node T cells of indicated *Lck* variants were incubated with PKC inhibitor overnight. CD4 expression was analyzed by flow cytometry. n= 7 individual experiments for *Lck*<sup>WT/WT</sup> and *Lck*<sup>CA/CA</sup>, n= 6 for *Lck*<sup>CA/KR</sup>. Individual experiments and means are shown. (F-G) CD4 on lymph node CD4<sup>+</sup> T cells from *Lck*<sup>WT/WT</sup> or *Lck*<sup>CA/CA</sup> B3K508 *Rag2*<sup>-/-</sup> was visualized with gold-labelled antibodies using transmission electron microscopy. (F) Representative cells are shown. The arrows indicate CD4 molecules. (G) Normalized pair correlation function values for CD4 clustering (clusters of 0-50 nm) were calculated for each cell. Individual values and medians + SD are shown. n= 358 *Lck*<sup>WT/WT</sup> and 422 *Lck*<sup>CA/CA</sup> cells from 3 independent experiments. The statistical significance was tested using Mann-Whitney test.

#### **Acknowledgments:**

We thank Ladislav Cupak for his technical assistance and genotyping of mice. We thank Dr. Inken Beck and Dr. Petr Kasperek from the Czech Centre of Phenogenomics for generating mice with genetic variants of *Lck*. We thank the Electron Microscopy Core Facility of Institute of Molecular Genetics for generation of electron microscopy data. We thank professor Daniel Pinschewer (European Virus Archive Global) for LCMV. We thank professor Dirk H. Busch from Technical University Munich, Germany for monomeric K<sub>b</sub>-OVA molecules. We thank professor Václav Hořejší for anti-LAT antibody. We thank Light Microscopy and Flow Cytometry at Institute of Molecular Genetics, namely, Zdenek Cimburek and Dr. Matyas Sima for cell sorting.

#### **Funding:**

This project was supported by the

Swiss National Science Foundation grant Promys, IZ11Z0\_166538 (OS)

Czech Science Foundation grant GJ19-03435Y (OS)

ERC Starting Grant FunDiT (OS)

Institute of Molecular Genetics of the Czech Academy of Sciences RVO 68378050 (OS)

J.E.Purkyne Fellowship by the Czech Academy of Sciences (OS)

VH, AP, DP are students of the Faculty of Science, Charles University, Prague.

Parts of this project were carried out at IMG facilities funded by following grants:

Czech Ministry of Education, Youth and Sports grant LM2015042 (Czech Centre for Phenogenomics)

Operational program of Czech Ministry of Education, Youth and Sport and the European Regional Development Fund RDI CZ.1.05/2.1.00/19.0395 (Czech Centre for Phenogenomics)

Operational program of Czech Ministry of Education, Youth and Sport and the European Regional Development Fund RDI BIOCEV CZ.1.05/1.1.00/02.0109 (Czech Centre for Phenogenomics)

Operational program of Czech Ministry of Education, Youth and Sport and the European Structural and Investment Funds CZ.02.1.01/0.0/0.0/16\_013/0001789 (Czech Centre for Phenogenomics)

Czech Ministry of Education, Youth and Sports grant LM2018129 (Czech-BioImaging)

Operational program of Czech Ministry of Education, Youth and Sport and the European Regional Development Fund CZ.02.1.01/0.0/0.0/18\_046/0016045 (Czech-BioImaging)

Operational program of Czech Ministry of Education, Youth and Sport and the European Regional Development Fund CZ.02.1.01/0.0/0.0/16\_013/0001775 (Czech-BioImaging)

#### Author contributions:

VH, AD, MK, RP, JBH and OS planned experiments. VH, AD, AP, DP, DG, KK, MK and RP performed and analyzed experiments. VH and OS wrote the manuscript. All authors reviewed the manuscript. OS conceived the study.

#### Competing interests:

Authors declare that they have no competing interests.

#### References:

1. Horkova, V., et al., *Dynamics of the Coreceptor-LCK Interactions during T Cell Development Shape the Self-Reactivity of Peripheral CD4 and CD8 T Cells*. Cell Reports, 2020. **30**(5): p. 1504-+.
2. Stepanek, O., et al., *Coreceptor scanning by the T cell receptor provides a mechanism for T cell tolerance*. Cell, 2014. **159**(2): p. 333-45.
3. Morch, A.M., et al., *Coreceptors and TCR Signaling - the Strong and the Weak of It*. Front Cell Dev Biol, 2020. **8**: p. 597627.
4. Erman, B., et al., *Coreceptor signal strength regulates positive selection but does not determine CD4/CD8 lineage choice in a physiologic in vivo model*. J Immunol, 2006. **177**(10): p. 6613-25.
5. Van Laethem, F., et al., *Lck Availability during Thymic Selection Determines the Recognition Specificity of the T Cell Repertoire*. Cell, 2013. **154**(6): p. 1326-1341.
6. Zareie, P., et al., *Canonical T cell receptor docking on peptide-MHC is essential for T cell signaling*. Science, 2021. **372**.
7. Artyomov, M.N., et al., *CD4 and CD8 binding to MHC molecules primarily acts to enhance Lck delivery*. Proceedings of the National Academy of Sciences of the United States of America, 2010. **107**(39): p. 16916-16921.
8. Rudd, C.E., *How the Discovery of the CD4/CD8-p56(lck) Complexes Changed Immunology and Immunotherapy*. Front Cell Dev Biol, 2021. **9**: p. 626095.
9. Casas, J., et al., *Ligand-engaged TCR is triggered by Lck not associated with CD8 coreceptor*. Nature Communications, 2014. **5**.
10. Wei, Q.R., et al., *Lck bound to coreceptor is less active than free Lck*. Proceedings of the National Academy of Sciences of the United States of America, 2020. **117**(27): p. 15809-15817.
11. Hong, J.S., et al., *A TCR mechanotransduction signaling loop induces negative selection in the thymus*. Nature Immunology, 2018. **19**(12): p. 1379-+.
12. Turner, J.M., et al., *Interaction of the unique N-terminal region of tyrosine kinase p56lck with cytoplasmic domains of CD4 and CD8 is mediated by cysteine motifs*. Cell, 1990. **60**(5): p. 755-65.

13. Carrera, A.C., K. Alexandrov, and T.M. Roberts, *The conserved lysine of the catalytic domain of protein kinases is actively involved in the phosphotransfer reaction and not required for anchoring ATP*. Proc Natl Acad Sci U S A, 1993. **90**(2): p. 442-6.
14. van Oers, N.S., et al., *alpha beta T cell development is abolished in mice lacking both Lck and Fyn protein tyrosine kinases*. Immunity, 1996. **5**(5): p. 429-36.
15. Corbett, T.H., et al., *Tumor induction relationships in development of transplantable cancers of the colon in mice for chemotherapy assays, with a note on carcinogen structure*. Cancer Res, 1975. **35**(9): p. 2434-9.
16. Nauerth, M., et al., *TCR-ligand koff rate correlates with the protective capacity of antigen-specific CD8+ T cells for adoptive transfer*. Sci Transl Med, 2013. **5**(192): p. 192ra87.
17. Huseby, E.S., et al., *How the T cell repertoire becomes peptide and MHC specific*. Cell, 2005. **122**(2): p. 247-60.
18. Courtney, A.H., et al., *A Phosphosite within the SH2 Domain of Lck Regulates Its Activation by CD45*. Mol Cell, 2017. **67**(3): p. 498-511.e6.
19. Foti, M., et al., *p56Lck anchors CD4 to distinct microdomains on microvilli*. Proc Natl Acad Sci U S A, 2002. **99**(4): p. 2008-13.
20. Pelchen-Matthews, A., et al., *The protein tyrosine kinase p56lck inhibits CD4 endocytosis by preventing entry of CD4 into coated pits*. J Cell Biol, 1992. **117**(2): p. 279-90.
21. Shen, F.W., et al., *Cloning of Ly-5 cDNA*. Proc Natl Acad Sci U S A, 1985. **82**(21): p. 7360-3.
22. Sommers, C.L., et al., *Function of CD3 epsilon-mediated signals in T cell development*. J Exp Med, 2000. **192**(6): p. 913-19.
23. Shinkai, Y., et al., *RAG-2-deficient mice lack mature lymphocytes owing to inability to initiate V(D)J rearrangement*. Cell, 1992. **68**(5): p. 855-67.
24. Hogquist, K.A., et al., *T cell receptor antagonist peptides induce positive selection*. Cell, 1994. **76**(1): p. 17-27.
25. Kasperek, P., et al., *Efficient gene targeting of the Rosa26 locus in mouse zygotes using TALE nucleases*. FEBS Lett, 2014. **588**(21): p. 3982-8.
26. Lo, W.-L., et al., *Lck promotes Zap70-dependent LAT phosphorylation by bridging Zap70 to LAT*. Nature immunology, 2018. **19**(7): p. 733-741.
27. Alexander, J., et al., *Differential transport requirements of HLA and H-2 class I glycoproteins*. Immunogenetics, 1989. **29**(6): p. 380-8.
28. Zhang, W., et al., *LAT: The ZAP-70 Tyrosine Kinase Substrate that Links T Cell Receptor to Cellular Activation*. Cell, 1998. **92**(1): p. 83-92.
29. Keck, S., et al., *Antigen affinity and antigen dose exert distinct influences on CD4 T-cell differentiation*. Proc Natl Acad Sci U S A, 2014. **111**(41): p. 14852-7.
30. Zehn, D., S.Y. Lee, and M.J. Bevan, *Complete but curtailed T-cell response to very low-affinity antigen*. Nature, 2009. **458**(7235): p. 211-4.
31. Zehn, D., et al., *Lack of original antigenic sin in recall CD8(+) T cell responses*. J Immunol, 2010. **184**(11): p. 6320-6.
32. Nauerth, M., et al., *Flow cytometry-based TCR-ligand Koff-rate assay for fast avidity screening of even very small antigen-specific T cell populations ex vivo*. Cytometry A, 2016. **89**(9): p. 816-25.
33. Schober, K., et al., *Reverse TCR repertoire evolution toward dominant low-affinity clones during chronic CMV infection*. Nat Immunol, 2020. **21**(4): p. 434-441.

34. Göhring, J., et al., *Temporal analysis of T-cell receptor-imposed forces via quantitative single molecule FRET measurements*. Nat Commun, 2021. **12**(1): p. 2502.
35. Garboczi, D.N., D.T. Hung, and D.C. Wiley, *HLA-A2-peptide complexes: refolding and crystallization of molecules expressed in Escherichia coli and complexed with single antigenic peptides*. Proc Natl Acad Sci U S A, 1992. **89**(8): p. 3429-33.
36. Huppa, J.B., et al., *TCR-peptide-MHC interactions in situ show accelerated kinetics and increased affinity*. Nature, 2010. **463**(7283): p. 963-967.



## Supplementary Materials:

### Materials and Methods:

#### Mice

All mice had C57BL/6J background. For the isolation of thymi for immunoblotting 4-8 weeks old mice were used. In other experiments, 6-12 weeks old mice were used. Both males and females were used for experiments. Mice were bred in our SPF facility (Institute of Molecular Genetics) in accordance with the laws of the Czech Republic. Animal protocols were approved by the Czech Academy of Sciences, Czech Republic. The used strains were: Ly5.2, Ly5.1 [21], *Cd3e*<sup>-/-</sup> [22], OT-I *Rag2*<sup>-/-</sup> [23, 24], B3K508 *Rag2*<sup>-/-</sup> [17], *Lck*<sup>-/-</sup> [1]. Mice were kept in the animal facility with 12 hours of light and dark cycle with food and water ad libitum.

*Lck*<sup>C20.23A</sup> and *Lck*<sup>K273R</sup> knock-in mice and *Lck*<sup>-/-</sup> mice were generated on C57BL/6N background in the Czech Centre for Phenogenomics, Institute of Molecular Genetics, ASCR. The mice were generated by pronuclear microinjection of Cas9 mRNA and gRNA (*Lck*<sup>C20.23A</sup>: TTGCTGTCCAGTGGGACTAT GGG; *Lck*<sup>K273R</sup>: CTACAACGGACACACGAAGG TGG) at concentration 100 ng/ml, together with ssODN templates (*Lck*<sup>C20.23A</sup>: GTGTCTGCAGCTCAAACCCTGAAGATGACTGGATGGAGAACATTGACGTG gccGAAAACgcctCAtTAcCCtATcGTgCCACTGGACAGCAAGATCTCGGTAAGAGGAAG; *Lck*<sup>K273R</sup>: AGGCGTCGGGGACATGCTCCCTTGTTTCAGACTCCGCACGGCGACCTTCGT GTGGCCGTTGTAGTACCCTGATGGGGTACG) into one-cell-stage murine embryos as described previously [25]. The founders were back-crossed on C57BL/6J background for at least 5 generations. Genotyping primers used for detection of the mutations were as follows:

Common FW primer 5'-AGGTAGTCCCCCAAAGGAGG paired with RV primer for *Lck*<sup>WT</sup> 5'-GGGATAGTGGCAGTTTTTCAACA or RV primer for *Lck*<sup>C20.23A</sup> 5'-AGGGTAATGAGCGTTTTTCGGC.

Common FW primer 5'-ACAAAGTTGAGCCGTCCTTGC paired with RV primer for *Lck*<sup>WT</sup> 5'-TTCAGACTTTCACCGCCAC or RV primer for *Lck*<sup>K273R</sup> 5'-CAGACTCCGCACGGCGA

#### Cell counting and cell culture

Cells were counted using Z2 Coulter Counter Analyzer (Beckman Coulter) or Cytex Aurora flow cytometer (Cytex).

Primary T cells were cultured in IMDM. Jurkat cells were cultured in RPMI. Media were supplemented with 10% FBS (GIBCO), 100 U/ml penicillin (BB Pharma), 100 mg/ml streptomycin (Sigma Aldrich), 40 mg/ml gentamicin (Sandoz).

The LCK-deficient human leukemic Jurkat T cell line with murine OT-I TCR [26] was transduced with human *LCK* variants (*LCK*<sup>WT</sup> [26], *LCK*<sup>C20.23A</sup>, *LCK*<sup>K273R</sup>) containing C-terminal FLAG tag in retroviral vector pMSCV-IRES-LNGFR.

#### Ex vivo activation assay

Human lymphoblast T2-Kb cell line expressing murine H2-K<sup>b</sup> [27] was used for antigen presentation to OT-I T cells. Splenocytes from Ly5.1 mice were used for activation of B3K508 T

cells. The antigen-presentation cells were pulsed with indicated concentrations of indicated peptides and co-cultured with isolated T cells at 1:2 ratio overnight. CD69 expression was detected by flow cytometry analysis. The results were fitted with log(agonist) vs. response (i.e., percentage of CD69<sup>+</sup> T-cells) function (least squares method) using PRISM (GraphPad Software).

#### **Flow cytometry analysis**

Live cells were stained with relevant antibodies and LIVE/DEAD Near-IR viability dye (ThermoFisher) on ice. For the analysis of murine thymocytes and T cells, following antibodies were used: anti-CD4 (clone RM4-5), anti-CD5 (clone 53-7-3), anti-CD8 $\alpha$  (clone 53-6.7), anti-CD8 $\beta$  (clone YTS156.7.7), anti-CD24 (clone M1/69), anti-CD25 (clone PC61), anti-CD44 (clone IM7), anti-CD45.1 (clone A20), anti-CD45.2 (clone 104), anti-CD49d (clone R1-2), anti-CD69 (clone H1.2F3), anti-TCR $\beta$  (clone H57-597). For analysis of Jurkat cell lines anti-CD4 (clone MEM-241), anti-CD8 (clone MEM-31), and anti-CD271 (clone ME20.4) were used. Antibodies were conjugated with various fluorophores and used according manufacturer instructions (Biolegend, BD Pharmingen). The samples were analyzed using a Cytex Aurora or BD FACSSymphony flow cytometers.

#### **PKC inhibition assay**

Live cells were incubated with PKC inhibitor Ro-32-0432 (Sigma Aldrich, cat# 557525) at concentration 5 $\mu$ M/ml overnight. The CD4 expression was analyzed by flow cytometry (antibody clone RM4-5).

#### **Surface coreceptor immunoprecipitation and immunoblotting**

Total thymocytes were used for immunoprecipitation. 2-3  $\times 10^7$  of live cells were stained with biotinylated anti-CD8 $\beta$  (53-5.8) or purified anti-CD4 (GK1.5 or H129.19) antibodies. Cells were lysed in 1 mL lysis buffer (1% Lauryl- $\beta$ -D-maltoside (Thermo Fisher Scientific), 30 mM Tris, 120 mM NaCl, 2 mM KCl, 10% glycerol, complete protease inhibitors (Roche), phosphoSTOP phosphatase inhibitors (Roche)), lysate was cleared by centrifugation and supernatant was incubated with Streptavidin Mag Sepharose (GE Healthcare) or Protein A/G Plus Agarose (Santa Cruz) for 2 hr at 4°C. Washed beads were lysed in Laemmli sample buffer. Samples were subjected to immunoblotting with murine anti-LCK (3A5, Santa Cruz) and rabbit mAb anti-CD8 $\alpha$  (D4W2Z, Cell Signaling) or anti-CD4 (D7D2Z, Cell Signaling).

For determination of endogenous LCK expression, 10<sup>7</sup> thymocytes or LN T cells were lysed in 100  $\mu$ l of lysis buffer, incubated 30 min on ice, cleared by centrifugation and diluted in Laemmli sample buffer. Samples were subjected to immunoblotting with murine anti-LCK (3A5, Santa Cruz), rabbit anti- $\beta$  actin (4967, Cell Signaling) and rabbit polyclonal anti-LAT antiserum [28].

Both immunoprecipitation samples and lysates were visualized with goat anti-rabbit or goat anti-mouse antibodies conjugated with horse-radish peroxidase (Jackson ImmunoResearch Labs) on Azure c200 (Azure Biosystems) or Fusion Solo S (Vilber).

#### **Bone marrow chimeras**

Bone marrows were isolated from 6-8 week old mice bearing Lck wild-type or two knock-in variants and mixed with supporting bone marrow cells from Ly5.1 mice in 1:1 ratio. Two million cells were transferred to lethally irradiated Ly5.1/Ly5.2 heterozygous donor mice. The mice

received dose of 6 Gy in X-RAD 225XL Biological irradiator (Precision X-Ray). T-cell development was analyzed 8 weeks after transplantation by flow cytometry.

#### **Listeria infection**

LN T cells were isolated from B3K508 and OT-I mice. The cells were adoptively transferred to Ly5.1 congenic host mice. The mice were injected with 5000 CFU of transgenic *Listeria monocytogenes* (Lm) expressing OVA, T4, G4, 3K, P5R, and P-2A antigens as described previously [29-31]. Expansion of the responsive cells was analyzed by flow cytometry.

#### **Lymphocytic choriomeningitis virus (LCMV) infection**

LCMV (Armstrong) was obtained from Prof. Daniel Pinschewer (European Virus Archive Global). For batch production, hamster BHK-21 cells were infected at MOI=0.01 and virus containing supernatant was harvested 48 hours after infection. Mice infections were done by intraperitoneal (i.p.) injection of  $2 \times 10^5$  plaque-forming units (PFU). Detection of LCMV in tissues was performed by qPCR and quantified against standard curve from cloned S-segment of LCMV.

(Primers: cDNA synthesis: 5'-AAGAACTGATGTCTCTTG; LCMV-qPCR FWD: 5'-CGCTGGCCTGGGTGAATTG; LCMV-qPCR REV: 5'-GTGAAGGATGGCCATACATAGC)

#### **Tumor growth**

Murine MC-38 cell line derived from C57BL/6 colon adenocarcinoma [15] was transduced with ovalbumin protein via retroviral vector pMSCV-IRES-LNGFR. 500,000 cells were injected subcutaneously (s.c.) to the left side of the mouse. When *Cd3ε*<sup>-/-</sup> mice were used as hosts, 200,000 OT-I cells were injected intravenously (i.v.) 5 days after tumor injection. The endpoint was tumor volume exceeding 500 mm<sup>3</sup> or the end of the experiment (day 22 post MC-38 injection for polyclonal mice, day 31 for *Cd3ε*<sup>-/-</sup> mice).

#### **Flow cytometry-based TCR-ligand $k_{off}$ -rate assay**

TCR-ligand  $k_{off}$ -rate experiments were performed as described previously [32]. Briefly, samples from *Lck* variant OT-I mice were multiplexed by combination of staining with PE- and PerCP-Cy5.5-conjugated CD45.2 antibodies. The cells were then stained with Streptactin (IBA Lifesciences, Cat.No. 6-5010-001) multimerized with Alexa Fluor 488-conjugated pMHC I K<sup>b</sup>-OVA molecules [33]. Samples were measured at 5 °C and after 30 s of measurement, the same volume of cold 2 mM D-biotin was added. Dissociation of the antigen was measured for additional 10 min. For analysis, Streptactin and monomer fluorescence values of CD8<sup>+</sup> OT-I T cells were exported from FlowJo to PRISM (GraphPad Software). The  $t_{1/2}$  was calculated by fitting one phase exponential decay curve.

#### **Tetramer binding**

Tetramers were produced in house by refolding biotinylated monomers using streptavidin-phycoerythrin conjugate in molar ratio 1:3. Streptavidin was added in three doses with 20 min incubation on ice after each step. Peripheral T cells were isolated from OT-I *Rag2*<sup>-/-</sup> mice, incubated with phycoerythrin-cojugated tetramers containing SIINFEKL (OVA) or SIITEKL (T4) peptide for 20 min on ice. The supernatant was replaced with PBS + 2% FBS and cells were immediately analyzed using a sample cooling system.

#### **Electron microscopy**

LN cells were stained with anti-CD4 antibody (clone RM4-5, Biolegend), washed and stained with 6 nm Colloidal Gold-AffiniPure Goat Anti-Rat antibody (Jackson ImmunoResearch) on ice. Prior to processing, cell suspensions were diluted in 20% BSA and rotated at 1180 rpm for 5 minutes in cooled centrifuge. Subsequent cryofixation was done using Leica EM ICE high-pressure freezer. Approximately 1  $\mu$ l of each cell suspension variant was put into each of 4 type A 3mm HPF carrier sandwiches, which were rapidly frozen and then dehydrated using Leica EM AFS2 automatic freeze substitution unit under temperature slowly increasing from -90°C to 0°C over 4 days in 100% acetone enriched with 0,2% uranyl acetate, 0,2% glutaraldehyde, 0,01% osmium tetroxide and 5% water. Samples were then removed from AFS2, infiltrated with 100% ethanol on ice and then with Quetol 651 resin diluted in 100% ethanol at 4°C. Afterwards, cells were embedded in Quetol - NSA resin. After polymerization for 72 hours at 60 °C, resin blocks were cut into 80 nm ultrathin sections using Leica UC6 Ultra microtome with a diamond knife (Diatome Ltd.), collected on copper slots with formvar membrane and air dry. After additional contrasting with 2% uranyl acetate in water, sections were examined in JEOL JEM-1400Flash transmission electron microscope operated at 80 kV equipped with Matataki Flash sCMOS camera (JEOL Ltd.).

Electron microscopy images were analyzed using open access application Pattern (pattern.img.cas.cz) developed by Electron Microscopy Core Facility at Institute of Molecular Genetics, Prague. Images were analyzed using 1D analysis, where ROI was manually traced along the membrane. Size calibration was defined as 1.189 nm in 1px. Clustering of golden particles was determined as pair correlation function (PCF) value. Values were normalized to predicted maximum standard deviation of simulated PCF value for analyzed density of individual cell staining.

#### **Ensemble FRET measurements**

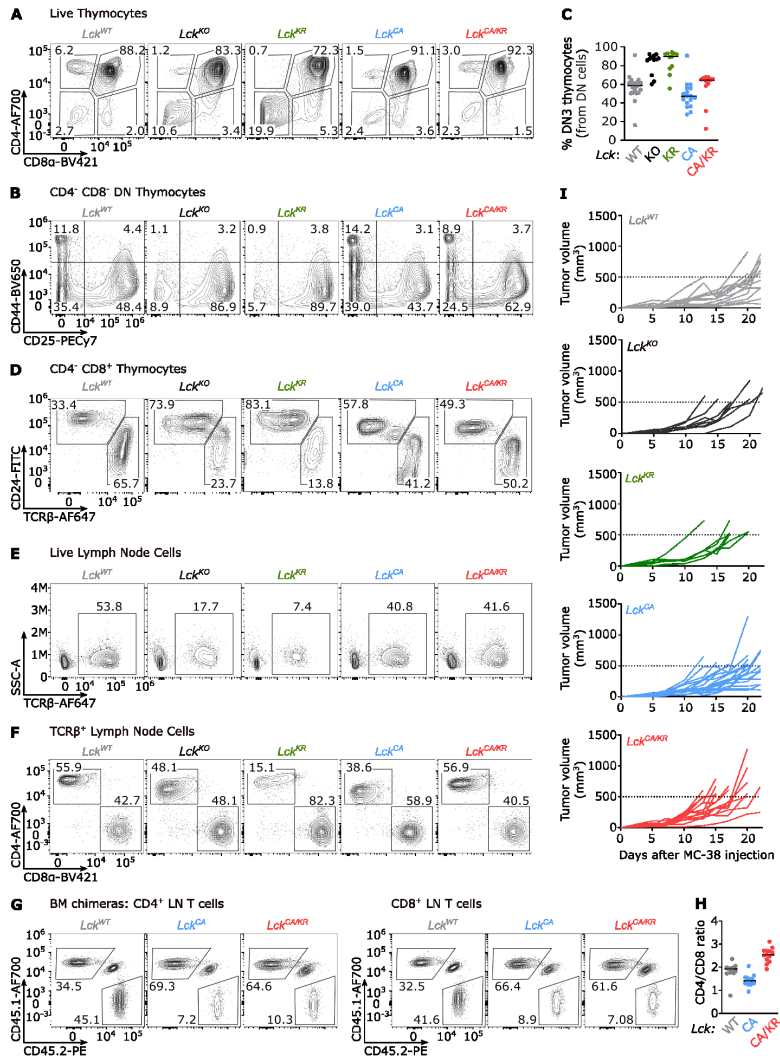
Functionalized lipid bilayers were prepared as described previously [34]. Shortly, small unilamellar vesicles (97.5 mol-% 1-palmitoyl-2-oleoyl-glycero-3-phosphocholine, 2 mol-% 1,2-dioleoyl-sn-glycero-3-[(N-(5-amino-1-carboxypentyl)iminodiacetic acid)succinyl], 0.5 mol-% PEG5000-DOPE (= 18:1 PEG5000 PE)) were used to form the bilayers on plasma-cleaned coverslips glued to 8-well chambers. K<sup>b</sup>-OVA conjugated with AF647 (1.5 ng/well) and ICAM-1 (0.1 ng/well) proteins were added to the bilayers. Only ICAM-1 was added to the control bilayers. The K<sup>b</sup>-OVA molecular density of 40-80 molecules per  $\mu$ m<sup>2</sup> was determined by dividing the fluorescence signal per pixel by the single molecule brightness recorded at the same settings, considering the effective pixel width of 160 nm. The K<sup>b</sup>-OVA, and ICAM-1 were produced as previously described [35, 36].

Fresh LN T cells were incubated with TCR $\beta$ -reactive scFV of the H57-597 conjugated with AF555 (0.25 mg/ml) [36]. The cells were added to the lipid bilayers and FRET efficiencies were determined using donor recovery after acceptor photobleaching. For this, an image of the donor channel was recorded before and after acceptor photobleaching, and the pixel-averaged fluorescence signal  $f_{pre}$  (before bleaching) and  $f_{post}$  (after bleaching), respectively, was calculated for each cell. The FRET efficiency was then given by  $E = (f_{post} - f_{pre}) / (f_{post} - \text{camera background})$ . Bleaching time was 250 ms. Illumination time was 50 ms, with 18 ms delay. Time lag between images of donor before and after bleaching was 550 ms.

In the microscopy system, excitation was achieved by coupling a 532 nm (OBIS LS, Coherent) and a 640 nm (iBeam smart, Toptica Photonics) laser line into a Ti-E inverted microscope (Nikon, Japan) via a dichroic mirror ZT405/488/532/640rpc (Chroma) into a 100 $\times$  objective (SR Apo



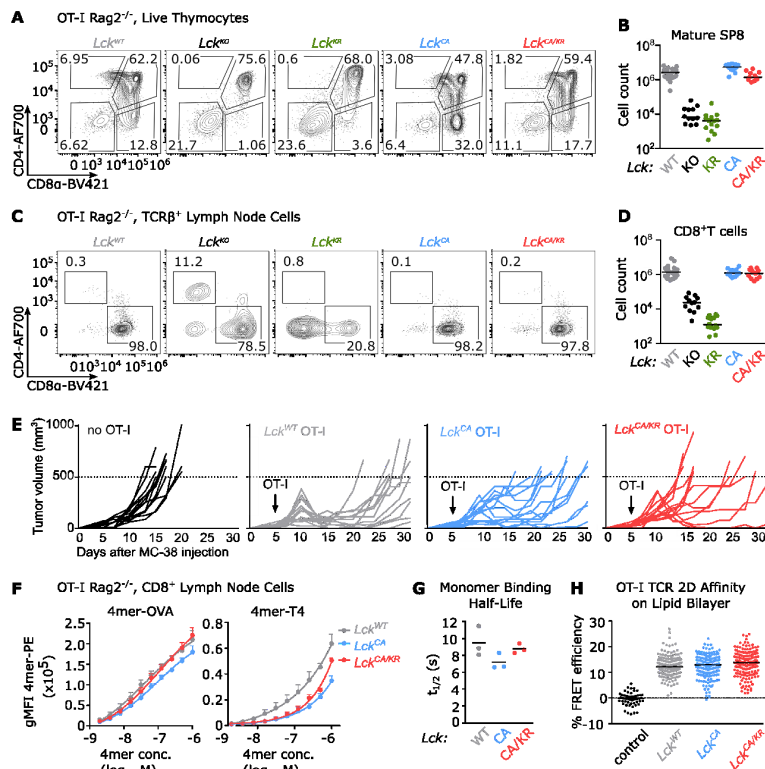
the comparable expression of *Lck* in these strains.  $\beta$ -actin detection was used as a loading control. LAT detection was used as control for thymocyte derived proteins in the lysates. (D-E) Immunoprecipitation of CD8 $\beta$  (D) or CD4 (E) followed by detection of LCK by immunoblotting documents that LCK<sup>WT</sup> and LCK<sup>KR</sup>, but not LCK<sup>CA</sup>, interacts with coreceptors. (F) Schematic representation of *Lck* variant strains including *Lck*<sup>CA/KR</sup> compound heterozygote.



**Supplemental Figure 2. Characterization of the T-cell compartment in *Lck* variant mice**

(A-D) Thymocytes from indicated *Lck* variant mice were analyzed by flow cytometry. Expression of indicated markers is shown. (A, D) Representative mice for Figure 1A. (B) Percentage of cells at the DN3 stage (CD4<sup>+</sup> CD25<sup>+</sup>) out of all DN (viable CD4<sup>+</sup> CD8 $\alpha$ <sup>-</sup>) thymocytes is shown.

Individual values and medians are shown.  $n=21$   $Lck^{WT/WT}$ ,  $12$   $Lck^{KO/KO}$ ,  $11$   $Lck^{KR/KR}$ ,  $17$   $Lck^{CA/CA}$ ,  $11$   $Lck^{CA/KR}$  mice. (E-F) Lymph node cells from indicated  $Lck$  variant mice were analyzed by flow cytometry. Expression of indicated markers is shown. Representative mice for Figure 1B. (G-H) Analysis of mixed bone marrow chimeric mice described in Figure 1C. (G) Representative mice. (H) Ratio of  $CD4^+ / CD8^+$  T cells derived from bone marrow of  $Lck^{WT/WT}$ ,  $Lck^{CA/CA}$ , and  $Lck^{CA/KR}$  donors. Individual values and medians are shown. (I) Tumor growth in individual mice for Figure 1D is shown.

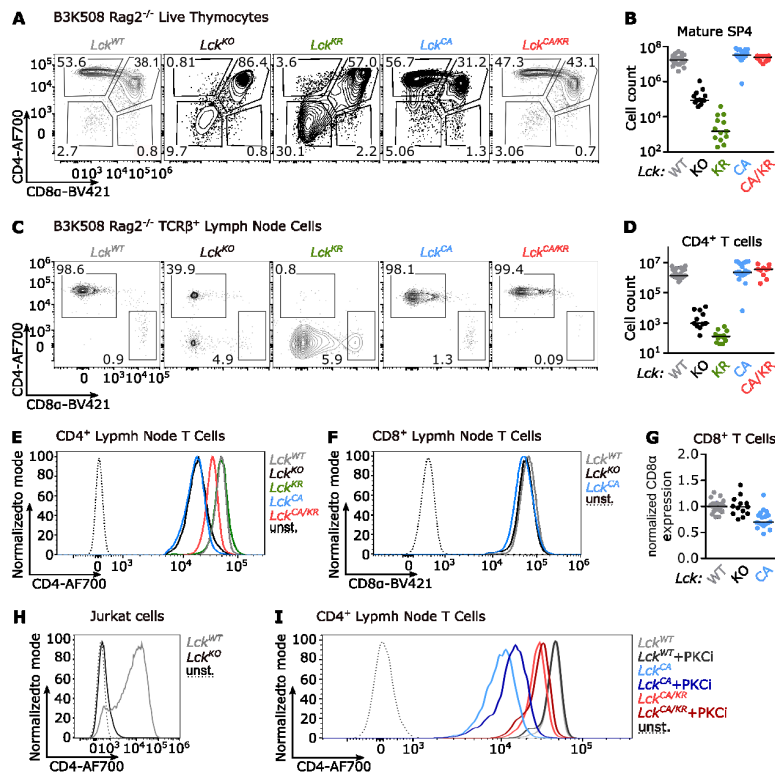


### Supplemental Figure 3. Characterization of $CD8^+$ T-cell responses of $Lck$ variant mice.

(A-B) Thymi of OT-I  $Rag2^{-/-}$   $Lck$  variant mice were analyzed by flow cytometry. (A) Expression of CD4 and CD8 $\alpha$  in representative mice. (B) Numbers of mSP8 (viable  $CD4^+ CD8\alpha^+ CD24^- TCR\beta^+$ ) T cells.  $n=22$   $Lck^{WT/WT}$ ,  $12$   $Lck^{KO/KO}$ ,  $14$   $Lck^{KR/KR}$ ,  $13$   $Lck^{CA/CA}$  and  $11$   $Lck^{CA/KR}$  mice. Individual mice and medians are shown. (C-D) Lymph nodes of OT-I  $Rag2^{-/-}$   $Lck$  variant mice were analyzed by flow cytometry. (D) Numbers of  $CD8^+$  T cells.  $n=23$   $Lck^{WT/WT}$ ,  $12$   $Lck^{KO/KO}$ ,  $14$   $Lck^{KR/KR}$ ,  $13$   $Lck^{CA/CA}$  and  $11$   $Lck^{CA/KR}$  mice. Individual mice and medians are shown. (E) Tumor



growth in individual mice for Figure 1E is shown. (F) CD8<sup>+</sup> T cells from OT-I *Rag2*<sup>-/-</sup> *Lck* variant mice were stained with a dilution series of fluorescently labeled K<sup>b</sup>-OVA and K<sup>b</sup>-T4 tetramer. Tetramer binding was measured by flow cytometry. Mean values + SEM are shown. (G) CD8<sup>+</sup> T cells from OT-I *Rag2*<sup>-/-</sup> *Lck* variant mice were stained with K<sup>b</sup>-OVA-streptactin multimers. Dissociation of K<sup>b</sup>-OVA monomer after the addition of free biotin was measured by flow cytometry. Individual experiments and means are shown. (H) CD8<sup>+</sup> T cells from OT-I *Rag2*<sup>-/-</sup> *Lck* variant mice were stained with fluorescently labeled anti-TCRβ Fab fragment and added to lipid bilayer containing ICAM-1 molecules and fluorescently labeled K<sup>b</sup>-OVA monomers. Relative TCR occupancy was measured as a fluorescence resonance energy transfer between the fluorophores. *Lck*<sup>WT/WT</sup> OT-I *Rag2*<sup>-/-</sup> T cells adhered to the lipid bilayer without K<sup>b</sup>-OVA monomers were used as a negative control. Individual cells and medians are shown.



**Supplemental Figure 4. Characterization of CD4<sup>+</sup> T-cell responses of *Lck* variant mice.**

(A-B) Thymi of B3K508 *Rag2*<sup>-/-</sup> *Lck* variant mice were analyzed by flow cytometry. (A) Expression of CD4 and CD8α in representative mice. (B) Numbers of mSP4 (viable CD4<sup>+</sup> CD8α<sup>+</sup>




CD24<sup>-</sup> TCRβ<sup>+</sup> T cells. n = 24 *Lck*<sup>WT/WT</sup>, 12 *Lck*<sup>KO/KO</sup>, 13 *Lck*<sup>KR/KR</sup>, 19 *Lck*<sup>CA/CA</sup>, 10 *Lck*<sup>CA/KR</sup> mice. Individual mice and medians are shown. (C-D) Lymph nodes of B3K508 *Rag2*<sup>-/-</sup> *Lck* variant mice were analyzed by flow cytometry. (D) Numbers of CD4<sup>+</sup> T cells. n = 26 *Lck*<sup>WT/WT</sup>, 11 *Lck*<sup>KO/KO</sup>, 13 *Lck*<sup>KR/KR</sup>, 20 *Lck*<sup>CA/CA</sup> and 10 *Lck*<sup>CA/KR</sup> mice. Individual mice and medians are shown. (E) Surface levels of CD4 on lymph node CD4<sup>+</sup> T cells in indicated *Lck* variant mice. A representative experiment for Figure 3C. (F-G) Surface levels of CD8α on lymph node CD8<sup>+</sup> T cells in indicated *Lck* variant mice. (F) A representative experiment. (G) Relative surface levels. n = 25 *Lck*<sup>WT/WT</sup>, 13 *Lck*<sup>KO/KO</sup>, 18 *Lck*<sup>CA/CA</sup> mice. Individual mice and medians are shown. (H) CD4 surface levels on WT Jurkat and *LCK*<sup>KO</sup> Jurkat cells were analyzed by flow cytometry. A representative experiment out of 3 in total. (I) A representative experiment showing CD4 surface levels on CD4<sup>+</sup> T cells upon overnight treatment with PKC inhibitor in Fig. 3E is shown.

## **Attachment 3**

Strong Homeostatic TCR Signals Induce  
Formation of Self-tolerant Virtual Memory  
CD8 T cells



# Strong homeostatic TCR signals induce formation of self-tolerant virtual memory CD8 T cells

Ales Drobek<sup>1,†</sup> , Alena Moudra<sup>1,†</sup>, Daniel Mueller<sup>2</sup>, Martina Huranova<sup>1</sup> , Veronika Horkova<sup>1</sup>, Michaela Pribikova<sup>1</sup>, Robert Ivanek<sup>2,3</sup>, Susanne Oberle<sup>4,‡</sup>, Dietmar Zehn<sup>4,5</sup>, Kathy D McCoy<sup>6,§</sup>, Peter Draber<sup>1</sup> & Ondrej Stepanek<sup>1,2,\*</sup> 

## Abstract

Virtual memory T cells are foreign antigen-inexperienced T cells that have acquired memory-like phenotype and constitute 10–20% of all peripheral CD8<sup>+</sup> T cells in mice. Their origin, biological roles, and relationship to naïve and foreign antigen-experienced memory T cells are incompletely understood. By analyzing T-cell receptor repertoires and using retrogenic monoclonal T-cell populations, we demonstrate that the virtual memory T-cell formation is a so far unappreciated cell fate decision checkpoint. We describe two molecular mechanisms driving the formation of virtual memory T cells. First, virtual memory T cells originate exclusively from strongly self-reactive T cells. Second, the stoichiometry of the CD8 interaction with Lck regulates the size of the virtual memory T-cell compartment via modulating the self-reactivity of individual T cells. Although virtual memory T cells descend from the highly self-reactive clones and acquire a partial memory program, they are not more potent in inducing experimental autoimmune diabetes than naïve T cells. These data underline the importance of the variable level of self-reactivity in polyclonal T cells for the generation of functional T-cell diversity.

**Keywords** gene expression profiling of T-cell subsets; retrogenic T cell; self-reactivity; T-cell receptor repertoire; virtual memory T cells

**Subject Categories** Immunology

**DOI** 10.15252/embo.201798518 | Received 28 October 2017 | Revised 11 March 2018 | Accepted 9 April 2018

The EMBO Journal (2018) e98518

## Introduction

Immunological memory is one of the hallmarks of adaptive immunity. During infection, pathogen-specific naïve T cells differentiate

into short-lived effector and memory T cells. The latter facilitate long-standing protection against a secondary infection of the same pathogen. CD8<sup>+</sup> CD44<sup>+</sup> CD62L<sup>+</sup> central memory (CM) T cells have the capability of expansion, self-renewal, and generation of cytotoxic effector T cells upon repeated encountering of their cognate antigen (Graef *et al.*, 2014).

Interestingly, some T cells with an apparent memory phenotype are specific to antigens which the host organism has not been exposed to (Haluszczak *et al.*, 2009; Su *et al.*, 2013). There are two possible explanations of their origin: (i) They could be cross-reactive T cells that have encountered another foreign cognate antigen previously (Su *et al.*, 2013) or (ii) they are generated via homeostatic mechanisms independently of the exposure to any foreign antigens (Haluszczak *et al.*, 2009). The strong evidence for the role of homeostatic mechanisms in generation of CD8<sup>+</sup> memory-like T cells was provided by the detection of these cells in germ-free mice. Since these T cells had limited prior exposure to foreign antigens, they were called virtual memory (VM) T cells (Haluszczak *et al.*, 2009).

Generation and/or maintenance of VM T cells depends on transcription factors Eomes and IRF4, type I interferon signaling, IL-15 and/or IL-4 signaling, and CD8 $\alpha$ <sup>+</sup> dendritic cells (Akue *et al.*, 2012; Sosinowski *et al.*, 2013; Kurzweil *et al.*, 2014; Tripathi *et al.*, 2016; White *et al.*, 2016). It has been shown that VM T cells express slightly higher levels of CD122 (IL-2R $\beta$ ) and lower levels of CD49d (integrin  $\alpha$ 4, a subunit of VLA-4) than true (i.e., foreign antigen-experienced) CM T cells (Sosinowski *et al.*, 2013). Based on these markers, VM T cells constitute for a majority of memory-phenotype CD8<sup>+</sup> T cells in unimmunized mice and around 10–20% of total CD8<sup>+</sup> T cells in lymphoid organs. Moreover, it has been proposed that memory-phenotype T cells, that accumulate in aged mice, are VM T cells (Chiu *et al.*, 2013). However, with the notable exception of the very initial study that identified CD44<sup>+</sup> CD62L<sup>+</sup> CM T cells in germ-free mice (Haluszczak *et al.*, 2009), all other published

<sup>1</sup> Laboratory of Adaptive Immunity, Institute of Molecular Genetics of the Czech Academy of Sciences, Prague, Czech Republic

<sup>2</sup> Department of Biomedicine, University Hospital and University of Basel, Basel, Switzerland

<sup>3</sup> Swiss Institute of Bioinformatics, Basel, Switzerland

<sup>4</sup> Swiss Vaccine Research Institute, Epalinges, Switzerland

<sup>5</sup> Division of Animal Physiology and Immunology, School of Life Sciences Weihenstephan, Technical University of Munich, Freising, Germany

<sup>6</sup> Department of Clinical Research (DKF), Inselspital, University of Bern, Bern, Switzerland

\*Corresponding author. Tel.: +420 241062155; E-mail: ondrej.stepanek@img.cas.cz

<sup>†</sup>These authors contributed equally to this work

<sup>‡</sup>Present address: Sanofi Genzyme, Baar, Switzerland

<sup>§</sup>Present address: Department of Physiology and Pharmacology, Cumming School of Medicine, University of Calgary, Calgary, AB, Canada

experiments used specific pathogen-free (SPF) mice that have significant exposure to microbial antigens. There are three major hypotheses of how virtual memory T cells might be formed in a homeostatic manner: (i) The differentiation into VM T cells occurs purely on a stochastic basis, (ii) lymphopenic environment in newborns induces differentiation of the first wave of thymic emigrants into VM T cells (Akue et al, 2012), or (iii) the VM T cells are generated from relatively highly self-reactive T cells that receive strong homeostatic TCR signals at the periphery (White et al, 2016). However, none of these hypotheses has been addressed in detail.

Although VM T cells form a large CD8<sup>+</sup> T cell population, their biological role is still unknown. VM T cells share some functional properties with true CM cells, including rapid production of IFN $\gamma$  upon stimulation with a cognate antigen or cytokines (Haluszczak et al, 2009; Lee et al, 2013). On a per cell basis, ovalbumin-specific VM T cells provide a protection to ovalbumin-expressing *Listeria monocytogenes* (Lm), comparable to true CM T cells, and surpass naive T cells with the same specificity (Lee et al, 2013). In addition, it has been proposed that VM T cells are capable of by-stander protection against infection, i.e., independently of their cognate antigen exposure (Chu et al, 2013; White et al, 2016). Altogether, these data pointed toward the superior role of VM T cells in protective immunity to infection. In a marked contrast to the above-mentioned findings, Decman et al showed that CD44<sup>+</sup> CD8<sup>+</sup> T-cell receptor (TCR) transgenic T cells isolated from unprimed mice (i.e., putative VM T cells) expand less than CD44<sup>-</sup> CD8<sup>+</sup> T cells expressing the same TCR upon antigenic stimulation *in vivo* (Decman et al, 2012). Likewise, VM T cells from aged mice were shown to be hyporesponsive to their cognate antigens in comparison with their naive counterparts, mostly because of their susceptibility to apoptosis (Decman et al, 2012; Renkema et al, 2014).

As VM T cells develop independently of infection, the understanding of mechanisms that guide their development is critical in order to elucidate their biological roles. One hint is the observation that levels of CD5 (a marker of self-reactivity) on naive T cells correlate with their ability to differentiate into VM T cells (White et al, 2016). In this study, we demonstrate that virtual memory T cells originate exclusively from relatively highly self-reactive T-cell clones and acquire only a partial memory gene expression program. Moreover, the interaction between CD8 and Lck (and possibly the overall intrinsic sensitivity of the TCR signaling machinery) determines the size of the virtual memory compartment. These data highlight the virtual memory T-cell formation as a T-cell fate decision checkpoint, when the intensity of TCR signals induced by self-antigens plays a central role in the decision-making process. Although virtual memory T cells show augmented responses to their foreign cognate antigen in some experimental setups in comparison with naive T cells, the potency of VM T cells to induce pathology in an experimental model of autoimmune diabetes is not higher than that of naive T cells.

## Results

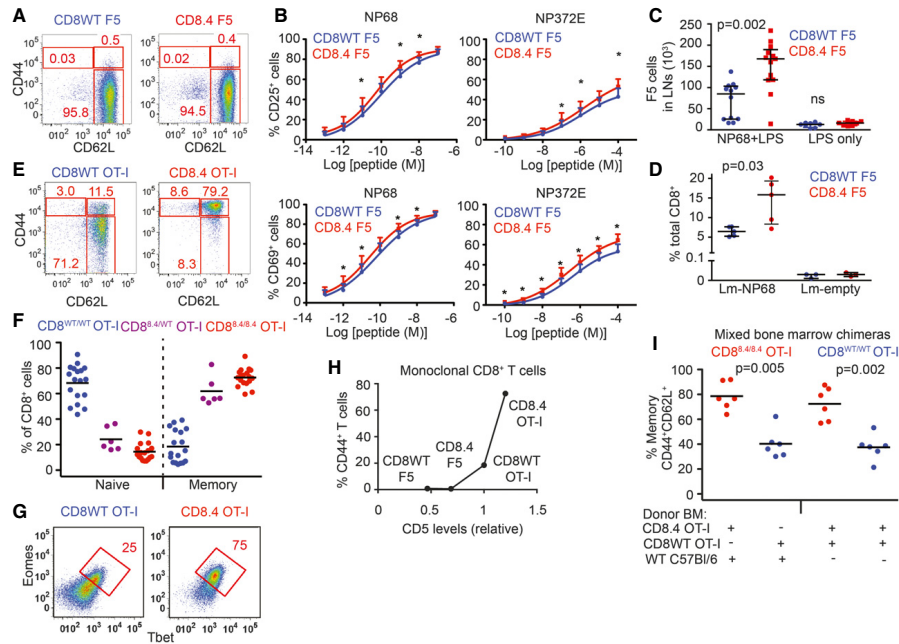
### Strong homeostatic TCR signaling induces virtual memory T cells

In this work, we aimed to understand why some mature CD8<sup>+</sup> T cells differentiate into VM T cells and some maintain their naive

phenotype. The peripheral T-cell pool of polyclonal mice consists of clones with different level of self-reactivity. To test the hypothesis that the level of self-reactivity plays a role in the formation of virtual memory T cells, we took advantage of previous observations that coupling frequency (or stoichiometry) of CD8 coreceptor to Lck kinase is a limiting factor for the TCR signaling in thymocytes (Erman et al, 2006; Stepanek et al, 2014). We used T cells from CD8.4 knock-in mouse strain, that express a chimeric CD8.4 coreceptor, consisting of the extracellular portion of CD8 $\alpha$  fused to the intracellular part of CD4 (Erman et al, 2006). In comparison with WT CD8 $\alpha$ , the chimeric CD8.4 coreceptor is more strongly binding Lck, a kinase initiating the TCR signal transduction. As a consequence, higher fraction of CD8.4 coreceptors molecules than CD8 coreceptors are loaded with Lck (Erman et al, 2006; Stepanek et al, 2014). Because the self-antigen triggered TCR signaling is stronger in CD8.4 T cells than CD8WT T cells (Park et al, 2007; Kimura et al, 2013; Stepanek et al, 2014), we use the CD8.4 T cells as a model to address the role of self-reactivity in virtual memory T-cell formation.

First, we compared monoclonal F5 Rag<sup>-/-</sup> T cells (henceforth CD8WT F5) and CD8.4 knock-in F5 Rag<sup>-/-</sup> T cells (henceforth CD8.4 F5) from unimmunized animals. The F5 TCR is specific for influenza NP68 and has been shown to have a very low level of self-reactivity (Ge et al, 2004; Hogan et al, 2013). We observed that CD8.4 F5 T cells had lower levels of CD8 and TCR and elevated levels of CD5 and IL-7R in comparison with CD8WT F5 T cells (Fig EV1A). Because the downregulation of CD8 and expression of CD5 and IL-7R correlate with the intensity of homeostatic TCR signaling (Park et al, 2007), we could conclude that CD8.4 indeed enhances homeostatic TCR signaling. However, we did not detect upregulation of memory markers, CD44, CD122, and LFA-1 on CD8.4 F5 T cells (Figs 1A and EV1A). CD8.4 F5 T cells showed slightly stronger antigenic responses, measured as CD25 and CD69 upregulation, than CD8WT F5 T cells *in vitro* upon activation with the cognate antigen, NP68, or a lower affinity antigen, NP372E (Shotton & Attaran, 1998; Fig 1B). Accordingly, CD8.4 F5 T cells expanded more than CD8WT F5 T cells after the immunization with NP68 peptide (Fig 1C). Infection with transgenic *Listeria monocytogenes* expressing NP68 (Lm-NP68) induced stronger expansion and formation of larger KLRG1<sup>+</sup>IL-7R<sup>-</sup> short-lived effectors and KLRG1<sup>+</sup>IL-7R<sup>+</sup> memory-precursor subsets in CD8.4 F5 than in CD8WT F5 T cells (Figs 1D and EV1B). Collectively, these data showed that CD8-Lck coupling frequency sets the sensitivity of peripheral T cells to self-antigens during homeostasis and to foreign cognate antigens during infection. However, supraphysiological CD8-Lck coupling in CD8.4 F5 T cells does not induce differentiation into memory-phenotype T cells in unimmunized mice.

Whereas the level of self-reactivity of F5 T cells is very low, transgenic OT-I T cells, specific for chicken ovalbumin (OVA), exhibit a relatively high level of self-reactivity (Ge et al, 2004; Hogan et al, 2013). We tested whether a combination of a relatively highly self-reactive OT-I TCR and supraphysiological CD8-Lck coupling is sufficient to induce VM T cells. For this reason, we compared monoclonal OT-I Rag<sup>-/-</sup> T cells (henceforth CD8WT OT-I) and CD8.4 knock-in OT-I Rag<sup>-/-</sup> T cells (henceforth CD8.4 OT-I) from unimmunized animals. As expected, CD8.4 OT-I T cells exhibited signs of stronger homeostatic TCR signaling than CD8WT OT-I



**Figure 1. Supraphysiological CD8-Lck coupling induces differentiation into VM T cells in a clone-specific manner.**

- A LN cells isolated from CD8WT F5 and CD8.4 F5 mice were analyzed by flow cytometry (gated as viable CD8<sup>+</sup>CD4<sup>+</sup>). A representative experiment out of 4 in total.
- B LN cells isolated from CD8WT F5 and CD8.4 F5 mice were stimulated with antigen-loaded DCs overnight and CD69 or CD25 expression was analyzed by flow cytometry. Mean  $\pm$  SEM.  $n = 7$  independent experiments. \* $p < 0.05$ .
- C  $2 \times 10^6$  CD8WT F5 or CD8.4 F5 LN T cells were adoptively transferred into Ly5.1 WT host 1 day prior to immunization with NP68 peptide and LPS or LPS only. Three days after the immunization, donor Ly5.2<sup>+</sup> Ly5.1<sup>-</sup> CD8<sup>+</sup> T cells from LN of the host mice were analyzed by flow cytometry and counted. Median  $\pm$  interquartile range.  $n = 8-13$  mice from seven independent experiments.
- D  $1 \times 10^5$  CD8WT F5 or CD8.4 F5 LN T cells were adoptively transferred into Ly5.1 WT hosts and immunized with WT Lm (empty) or Lm-NP68. Six days after the immunization, the percentage of donor Ly5.2<sup>+</sup> Ly5.1<sup>-</sup> CD8<sup>+</sup> T cells among all CD8<sup>+</sup> T cells was determined. Median  $\pm$  interquartile range.  $n = 3-5$  mice from three independent experiments.
- E, F LN cells isolated from CD8WT OT-I, CD8.4 OT-I, and heterozygous CD8<sup>WT/CD8.4</sup> mice were analyzed by flow cytometry (gated as viable CD8<sup>+</sup>CD4<sup>+</sup>). Percentages of naive (CD44<sup>-</sup>CD62L<sup>+</sup>) and memory (CD44<sup>+</sup>CD62L<sup>-</sup>) CD8<sup>+</sup> T cells were determined.  $n = 6-18$  mice per group from at least five independent experiments.
- G Expression of Eomes and Tbet in CD8<sup>+</sup> LN T cells isolated from CD8WT OT-I and CD8.4 OT-I mice was determined by flow cytometry. A representative experiment out of 3 in total.
- H Relationship between relative CD5 levels (CD5 on CD8WT OT-I was arbitrarily set as 1) percentage of VM T cells (CD44<sup>+</sup>CD62L<sup>+</sup>) using the data from indicated TCR transgenic strains. Mean value of  $n = 5-8$  mice per group from at least five independent experiments.
- I Irradiated Rag2<sup>-/-</sup> host mice were transplanted with B-cell and T-cell depleted bone marrow from Ly5.1 C57Bl/6 together with CD8.4 OT-I or CD8WT OT-I bone marrow in 1:1 ratio (first two datasets) or, with bone marrow from CD8.4 OT-I and CD8WT OT-I mice in 1:1 ratio (last two datasets). Eight weeks later, LN cells were isolated and analyzed by flow cytometry.  $n = 6$  mice per group from three independent experiments.

Data information: Statistical significance was determined using two-tailed Wilcoxon signed-rank test (B) and Mann-Whitney test (C, D, I). Source data are available online for this figure.

T cells, including downregulation of TCR, CD8, and increased levels of CD5 and CD127 (Fig EV1C and D). Interestingly, the majority of the CD8.4 OT-I T cells exhibited CM phenotype including CD44<sup>+</sup>CD62L<sup>+</sup> double positivity, increased levels of CD122 and LFA-1, increased forward-scatter signal, and expression of transcription factors Tbet and Eomes (Figs 1E-G and EV1C), which was in a striking contrast with analogical experiments with CD8WT/CD8.4 F5 T

cells (Figs 1A and EV1A). The CD8<sup>WT/CD8.4</sup> heterozygous OT-I T cells showed an intermediate frequency of memory T cells (Fig 1F). Because CD8.4 OT-I T cells exhibited features of memory T cells without encountering their foreign cognate antigen, we concluded that CD8.4 induced a differentiation of OT-I T cells into VM cells. When we compared monoclonal T cells from all four transgenic mouse strains tested, we identified a relationship between surface

levels of CD5, a commonly used marker of self-reactivity, and the frequency of VM T-cell formation. However, the dependency was not linear, but showed a threshold behavior, indicating that only the most self-reactive T cells have the potential to develop into VM T cells (Figs 1H and EV1E).

To address whether CD8.4 induces VM T-cell formation in OT-I T cells in a T-cell intrinsic manner, we generated mixed bone marrow chimeric animals where both CD8.4 and CD8WT populations were present. We transplanted bone marrow cells from Ly5.1 WT mouse together with bone marrow cells from either Ly5.2 CD8WT OT-I or Ly5.2 CD8.4 OT-I mice into an irradiated Rag2<sup>-/-</sup> recipient. CD8.4 OT-I T cells generated substantially more VM T cells than CD8WT OT-I T cells (Fig 1I). In an alternative setup, we cotransferred mixed bone marrow cells from Ly5.1 CD8WT OT-I and Ly5.2 CD8.4 OT-I animals into an irradiated Rag2<sup>-/-</sup> recipient to compare these two subsets in a single mouse. Again, CD8.4 OT-I T cells generated significantly more VM T cells than CD8WT OT-I T cells (Fig 1I). These experiments showed that CD8.4 OT-I T cells intrinsically trigger the memory differentiation program.

#### CD8-Lck coupling frequency regulates the size of virtual memory compartment in polyclonal repertoire

In a next step, we addressed how the CD8-Lck stoichiometry regulates the size of virtual memory compartment in a polyclonal T-cell pool. Interestingly, CD8.4 polyclonal mice showed significantly higher frequency of VM CD8<sup>+</sup> T cells than CD8WT control animals, although most CD8.4 T cells still showed a naïve phenotype (Fig 2A and B). Thus, CD8.4 induced the VM T-cell formation only in a subset of polyclonal CD8<sup>+</sup> T cells, implying that enhanced CD8-Lck coupling has clone-specific effects. The VM T cells from both CD8WT and CD8.4 mice rapidly produced IFN $\gamma$  after stimulation with PMA/ionomycin, showing that CD8WT and CD8.4 VM T cells are indistinguishable in this functional trait, typical for memory T cells (Fig EV2A). Importantly, the analysis of mice in germ-free condition showed elevated frequency of CD44<sup>+</sup> and Tbet/Eomes double-positive T cells in CD8.4 mice when compared to CD8WT (Fig 2C and D), demonstrating that supraphysiological CD8-Lck coupling indeed promotes formation of VM T cells independently of the exposure to foreign antigens.

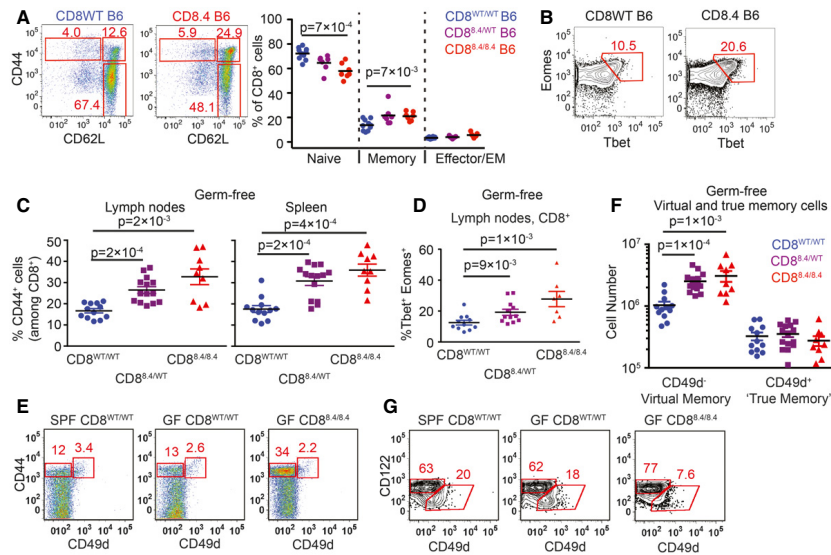
Although the VM and true CM T cells are very similar in many aspects, VM T cells were previously reported to express lower levels of CD49d and slightly higher levels of CD122 than true CM T cells (Haluszczak et al, 2009; Chiu et al, 2013; Sosinowski et al, 2013; White et al, 2016). However, CD49d as a marker discriminating VM and true CM T cells has not been validated using T cells from germ-free animals. For the first time, we could show that CD49d<sup>-</sup> and CD49d<sup>+</sup> T cells within the CD44<sup>+</sup> compartment of SPF and germ-free mice occur at comparable frequencies (Fig 2E). Only the CD49d<sup>-</sup> CD44<sup>+</sup>, but not the CD49d<sup>+</sup> CD44<sup>+</sup>, subset was expanded in the CD8.4 mouse, indicating that these subsets are not related (Fig 2E). Accordingly, CD122<sup>HI</sup> CD49d<sup>-</sup> CD44<sup>+</sup> T cells, but not CD122<sup>LOW</sup> CD49d<sup>+</sup> CD44<sup>+</sup> T cells, were more abundant in germ-free CD8.4 mouse than in germ-free CD8WT mouse (Figs 2F and G, and EV2B). Collectively, these data implied that CD122<sup>HI</sup> CD49d<sup>-</sup> memory T cells represent the CD8<sup>+</sup> VM T-cell population, which originates from naïve T cells with a relatively strong level of self-reactivity independently of foreign antigens.

#### Virtual memory T cells use distinct TCR repertoire than naïve T cells

Based on the previous data, generation of VM T cells can be understood as a fate decision checkpoint of individual naïve T cells (staying naïve vs. becoming VM), where the decision is based on the level of self-reactivity of the T cell's TCR. This hypothesis predicts that naïve and VM T-cell compartments should contain different T-cell clones with distinct TCR repertoires. We analyzed the TCR repertoires by using a V $\beta$ 5 transgenic mouse with fixed TCR $\beta$  from the OT-I TCR (Fink et al, 1992). The advantage of this mouse is that it generates a polyclonal population of T cells, but the variability between the clones is limited to TCR $\alpha$  chains. Moreover, pairing of TCR $\alpha$  and TCR $\beta$  upon repertoire analyses is not an issue in this model. Last, but not least, this mouse has a relatively high frequency of oligoclonal T cells that recognize the ovalbumin antigen (Zehn & Bevan, 2006).

Unimmunized V $\beta$ 5 mice have a frequency of memory CD8<sup>+</sup> T cells around 10–15% which is comparable to wild-type mice (Fig 3A). When we analyzed the frequency of VM vs. naïve T cells among particular T-cell subsets defined by the expression of particular TCRV $\alpha$  segments, we observed that TCRV $\alpha$ 3.2<sup>+</sup> T cells are comparable to the overall population, TCRV $\alpha$ 2<sup>+</sup> T cells are slightly enriched for the VM T cells, and TCRV $\alpha$ 8.3<sup>+</sup> T cells have lower frequency of VM T cells than the overall population (Fig 3A). These data suggested that naïve and VM T cells might have distinct TCR repertoires. However, the differences between the subsets were only minor, most likely because particular TCRV $\alpha$  subsets had still significant intrinsic diversity. To further reduce clonality in our groups, we gated on K<sup>b</sup>-OVA-specific TCRV $\alpha$ 3.2<sup>+</sup>, TCRV $\alpha$ 2<sup>+</sup>, and TCRV $\alpha$ 8.3<sup>+</sup> T cells (Fig 3B). Interestingly, around 50% of OVA-specific TCRV $\alpha$ 2<sup>+</sup> clones exhibited VM phenotype, whereas vast majority of OVA-specific TCRV $\alpha$ 8.3<sup>+</sup> T cells were naïve and OVA-specific TCRV $\alpha$ 3.2<sup>+</sup> T cells had intermediate frequency of VM T cells in peripheral LN, mesenteric LN as well as in the spleen (Fig 3B and C). Accordingly, the frequency of TCRV $\alpha$ 2<sup>+</sup> T cells is almost 10-fold higher in VM than in naïve OVA-specific T-cell population, whereas the frequency of TCRV $\alpha$ 8.3<sup>+</sup> T cells is slightly lower in VM than in naïve OVA-specific T cells (Fig EV3A). Similar differences between total and OVA-specific TCRV $\alpha$ 3.2<sup>+</sup>, TCRV $\alpha$ 2<sup>+</sup>, and TCRV $\alpha$ 8.3<sup>+</sup> CD8<sup>+</sup> T cell subsets were observed in germ-free V $\beta$ 5 mice (Fig 3D and E), confirming the VM identity of memory-phenotype T cells in the V $\beta$ 5 mice. In addition, OVA-specific TCRV $\alpha$ 2<sup>+</sup> had higher levels of CD5 than TCRV $\alpha$ 8.3<sup>+</sup> (Fig EV3B and C), suggesting that OVA-specific TCRV $\alpha$ 2<sup>+</sup> clones are on average more self-reactive than TCRV $\alpha$ 8.3<sup>+</sup> clones. This explains why more OVA-specific TCRV $\alpha$ 2<sup>+</sup> T cells than TCRV $\alpha$ 8.3<sup>+</sup> T cells acquire the VM phenotype in V $\beta$ 5 mice.

Based on the analysis of particular TCRV $\alpha$  subsets, we hypothesized that naïve and VM T cells would contain different TCR clonotypes. We cloned and sequenced genes encoding for TCR $\alpha$  chains from OVA-reactive CD8<sup>+</sup> VM and naïve T-cell subsets from germ-free V $\beta$ 5 mice using primers specific for TRAV14 (TCRV $\alpha$ 2) and TRAV12 (TCRV $\alpha$ 8) TCR genes (Table EV1). The distribution of the clonotypes as well as TRAJ usage was significantly different between VM and naïve subsets (Figs 3F and EV3D). We observed essentially two types of clonotypes that were captured in more than 1 experiment (Fig 3F). One type of clonotypes, called "VM clones",



**Figure 2. CD8-Lck coupling is a limiting factor for the size of the virtual memory T-cell compartment.**

A, B Percentages of naïve ( $CD44^- CD62L^+$ ), central memory ( $CD44^+ CD62L^+$ ), and effector/effector memory ( $CD44^+ CD62L^-$ ) (A) and Eomes $^+$  Tbet $^+$  (B)  $CD8^+$  LN T cells isolated from  $CD8^{WT}$  and  $CD8.4$  mice were determined by flow cytometry. Representative experiments out of seven (A) or five (B) in total.  
 C–F LN cells and splenocytes were isolated from germ-free polyclonal  $CD8^{WT}$ ,  $CD8.4$ , and heterozygous  $CD8^{WT/8.4}$  mice and  $CD8^+$  T cells were analyzed by flow cytometry. (C) Percentage of  $CD44^+$  T cells among  $CD8^+$  LN cells and splenocytes. Mean  $\pm$  SEM,  $n = 9$ –14 mice per group from four independent experiments. (D) Percentage of Tbet $^+$  Eomes $^+$  double-positive T cells. Mean  $\pm$  SEM,  $n = 7$ –12 mice per group from three independent experiments. (E) Percentage of  $CD44^+$   $CD49d^-$  VM and  $CD44^+$   $CD49d^+$  true memory T cells in the spleen. A representative experiment out of four in total. (F) Absolute numbers of  $CD8^+$   $CD44^+$   $CD49d^-$  VM and  $CD8^+$   $CD44^+$   $CD49d^+$  true memory T cells in LN and the spleen were quantified. Mean  $\pm$  SEM,  $n = 9$ –14 mice from four independent experiments.  
 G Percentage of  $CD122^{HI}$   $CD49d^-$  VM and  $CD122^{LOW}$   $CD49d^+$  true CM cells among  $CD8^+$   $CD44^+$   $CD62L^+$  CM T cells isolated from LN. A representative experiment out of three in total.

Data information: Statistical significance was determined using two-tailed Mann–Whitney test. Source data are available online for this figure.

was enriched among VM T cells and was also present in naïve T cells. The other type, “naïve clones”, was almost exclusively detected in naïve T cells. These data demonstrate that naïve and VM T-cell population contain different T-cell clones.

To directly investigate whether TCR is the main factor that determines whether a particular T cell has the potential to differentiate into VM T cells, we established a protocol to generate monoclonal T-cell populations using transduction of a particular TCR $\alpha$ -encoding gene in a retrogenic vector into immortalized hematopoietic stem cells (Ruedl *et al.*, 2008). We transduced immortalized  $V\beta 5$  Rag2 $^{-/-}$  hematopoietic stem cells with expression vectors encoding for two VM TCR $\alpha$  clones (V14-C1 and V14-C2), three naïve TCR $\alpha$  clones (V14-C6, V14-C7, and V14-C17), or OT-I TCR $\alpha$  as a control (Fig EV3E). At least 8 weeks after the transplantation of the progenitors into a Ly5.1 recipient, we analyzed the cell fate of the donor monoclonal T-cell populations. T cells expressing VM TCR clones formed a significant VM T-cell population, whereas T cells expressing naïve TCR clones formed a homogenous naïve population (Figs 3G and EV3F). These data demonstrate that the virtual

memory T cells are formed only from certain T-cell clones and that the TCR sequence determines whether a T cell differentiates into a VM T cell or stays naïve.

In a next step, we addressed whether “VM clones” are more self-reactive than “naïve clones”. We compared levels of CD5, a commonly used reporter for self-reactivity, on naïve ( $CD44^-$ ) populations of retrogenic monoclonal T cells. “VM clones” expressed significantly higher CD5 levels than “naïve clones”, indicating that “VM clones” are indeed T cells with a relatively high level of self-reactivity (Figs 3H and EV3G). Interestingly, retrogenic OT-I T cells represented an intermediate VM population, which corresponds to their level of self-reactivity (Figs 1H, 3G, and EV3F and G). Moreover, the relative size of retrogenic OT-I VM population well corresponded to the frequency of VM T cells in conventional transgenic OT-I TCR mice (Fig 1E and H), indicating that the protocol for generation of retrogenic monoclonal T cells itself does not have a strong effect on VM formation. Overall, these results document that only relatively highly self-reactive clones form VM T cells.



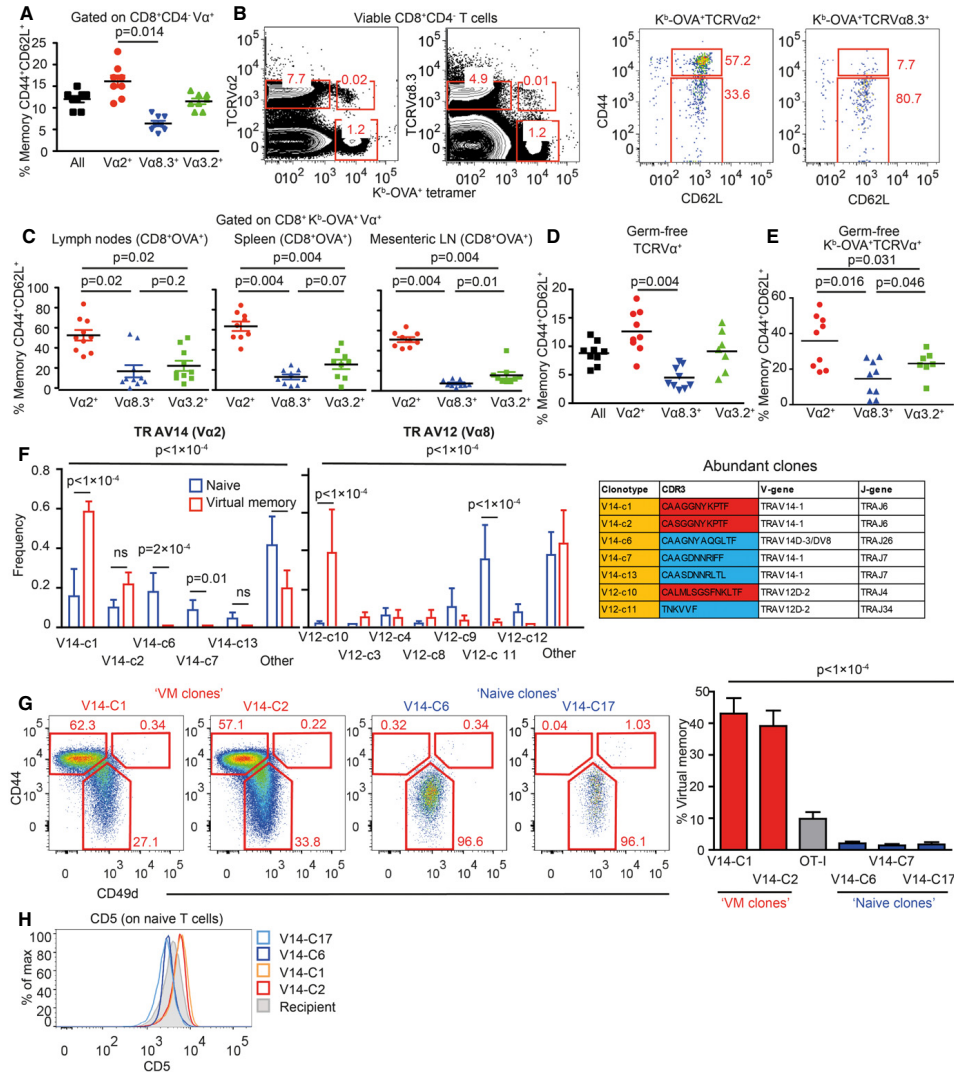


Figure 3.

**Virtual memory T cells represent an intermediate stage between naïve and memory T cells**

The relationship of the differentiation programs of naïve, VM, and true CM T cells is unclear. So far, CD49d and, to a lesser extent, CD122 were the only known markers discriminating between true

CM memory and VM T cells (Haluszczak et al, 2009; Chiu et al, 2013; Sosinowski et al, 2013; White et al, 2016). To compare their gene expression profiles, we performed deep RNA sequencing of the transcripts from sorted CD8<sup>+</sup> naïve (CD44<sup>-</sup> CD62L<sup>+</sup>) and VM (CD44<sup>+</sup> CD62L<sup>-</sup> CD49d<sup>-</sup>) T cells isolated from germ-free animals and from true antigen-specific CM T cells (TM) (K<sup>b</sup>-OVA<sup>+</sup> CD44<sup>+</sup>

**Figure 3. Virtual memory and naïve T cells use different TCR repertoires.**

- A** LN cells isolated from Vβ5 mice were stained for CD8, CD4, CD44, CD62L, and Vα2 or Vα8.3 or Vα3.2. CD8<sup>+</sup> T cells were gated as CD8<sup>+</sup> CD4<sup>-</sup> and then the percentage of CD44<sup>+</sup> CD62L<sup>+</sup> memory T cells among CD8<sup>+</sup> Vα2<sup>+</sup> or CD8<sup>+</sup> Vα8.3<sup>+</sup> or CD8<sup>+</sup> Vα3.2<sup>+</sup> T cells was determined by flow cytometry. Mean, *n* = 8 mice from eight independent experiments.
- B, C** Cells isolated from peripheral LN (B, C), mesenteric LN (C), and the spleen (C) were stained as in (A) with the addition of OVA tetramer. The OVA-reactive Vα-specific CD8<sup>+</sup> T cells were gated and the percentage of CD44<sup>+</sup> CD62L<sup>+</sup> memory T cells was determined by flow cytometry. *n* = 9–10 mice from five independent experiments.
- D** The same experiment as in (A) was performed using germ-free Vβ5 mice. Mean, *n* = 7–9 mice from four independent experiments.
- E** The same experiment as in (B, C) was performed using a mixture of T cells isolated from LNs and the spleen from germ-free Vβ5 mice. Mean, *n* = 7–9 from 2 to 3 independent experiments.
- F** RNA was isolated from memory (CD44<sup>+</sup>CD62L<sup>+</sup>) and (CD44<sup>+</sup>CD62L<sup>+</sup>) K<sup>b</sup>-OVA\* 4mer<sup>+</sup> T cells sorted from LNs and the spleen of germ-free Vβ5 mice. TCRα encoding genes using either TRAV12 (corresponding to Vα8) or TRAV14 (corresponding to Vα2) were cloned and sequenced. 12–20 clones were sequenced in each group/experiment. Clonotypes identified in at least two experiments are shown. Mean frequency + SEM, *n* = 4 independent experiments. Statistical significance was determined by chi-square test (global test) and paired two-tailed t-tests as a post-test (individual clones). CDR3 sequences of clonotypes enriched in naïve or VM compartments are shown in the table.
- G, H** Retroviral vectors encoding selected TCRα clones were transduced into immortalized Rag2<sup>-/-</sup> Vβ5 bone marrow stem cells. These cells were transplanted into an irradiated Iy5.1 recipient. (G) At least 8 weeks after the transplantation, frequency of virtual memory T cells among LN donor T cells (CD45.2<sup>+</sup> CD45.1<sup>-</sup> GFP<sup>+</sup>) was analyzed. Mean + SEM, *n* = 10–21 mice from 2 to 7 independent experiments. Statistical significance was tested using Kruskal–Wallis test. (H) CD5 levels on naïve monoclonal T cells were detected by flow cytometry. Representative mice out of 9–14 in total from two to four independent experiments.
- Data information: (A, C–E) Statistical significance was determined by two-tailed Wilcoxon signed-rank test. Source data are available online for this figure.

CD62L<sup>+</sup>), generated by infecting Vβ5 mice with Lm expressing OVA (Lm-OVA). The data showed that naïve, VM, and TM T cells represent three distinct T-cell populations (Fig EV4A and B). We identified genes differently expressed in VM T cells in comparison with naïve or TM T cells (Tables EV2–EV5). Based on previously published data (Kaech *et al*, 2002; Luckey *et al*, 2006; Wherry *et al*, 2007), we established lists of memory signature and naïve signature genes. As expected, memory signature genes were enriched in TM T cells and naïve signature genes were enriched in naïve T cells (Figs 4A and EV4C). Interestingly, VM T cells exhibited an intermediate gene expression profile (Figs 4A and EV4C). Pairwise rotation gene set tests revealed the hierarchy in the enrichment for memory signature genes and for naïve signature genes as TM > VM > naïve, and naïve > VM > TM, respectively (Fig 4B). VM T cells also showed an intermediate expression of cytokine and chemokine encoding genes (Figs 4C and EV4D). The transcription of genes encoding for cytokine and chemokine receptors in VM T cells seemed to be also somewhere half-way between naïve and true CM T cells (Fig EV4E and F).

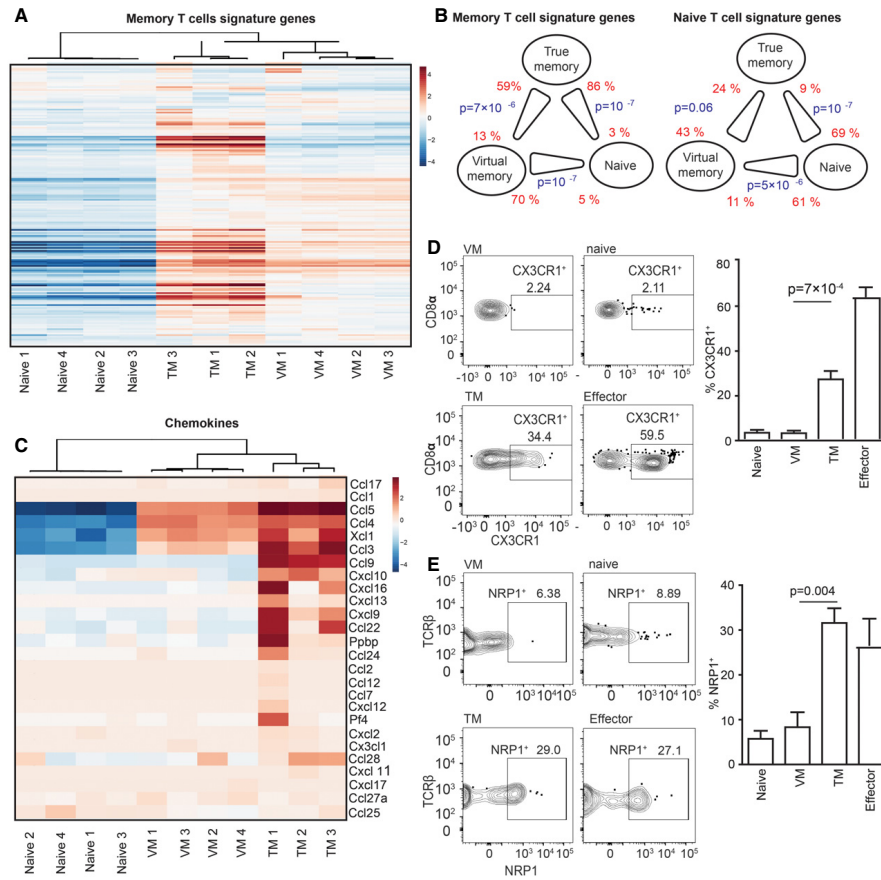
We further investigated selected differentially expressed genes between VM and true CM cells on a protein level. RNA encoding for CX3CR1 and NRP1 showed enrichment in TM vs. VM T cells. For this reason, we compared surface levels of CX3CR1 and NRP1 on naïve and VM T cells from unprimed mice and on TM and effector/effector memory T cells from Lm-OVA infected mouse during the memory phase (Fig 4D and E). In contrast to VM T cells, a significant percentage of effector and TM T cells expressed CX3CR1 and NRP1, confirming the transcriptomic data and suggesting that VM T cells can be characterized as CX3CR1 and NRP1 negative.

#### Differentiation into virtual memory T cells does not break self-tolerance

VM T cells provide better protection against Lm than naïve T cells and respond to proinflammatory cytokines IL-12 and IL-18 by producing IFNγ (Haluszczak *et al*, 2009; Lee *et al*, 2013; White *et al*, 2016). Moreover, VM T cells express higher levels of several killer lectin-like receptors than naïve T cells (Table EV4 and White *et al*,

2016). The combination of a hyperresponsive differentiation state with the expression of highly self-reactive TCRs suggests that VM CD8<sup>+</sup> T cells could be less self-tolerant than naïve T cells and might represent a risk for inducing autoimmunity. We used CD8WT OT-I T cells (mostly naïve) and CD8.4 OT-I T cells (mostly VM) for a functional comparison of naïve and VM T cells with the same TCR specificity. VM CD8.4 OT-I T cells, but not naïve OT-I T cells, rapidly produced IFNγ after the stimulation by PMA/ionomycin or cognate antigen (Fig 5A), supporting the idea of an autoimmune potential of VM T cells. We directly tested this hypothesis using an experimental model of autoimmune diabetes (King *et al*, 2012). We transferred CD8WT OT-I or CD8.4 OT-I T cells into RIP.OVA mice expressing OVA under the control of rat insulin promoter (Kurts *et al*, 1998) and primed them with Lm-OVA or Lm-Q4H7 (King *et al*, 2012). Q4H7 is an antigen that binds to the OT-I TCR with a low affinity and does not negatively select OT-I T cells in the thymus (Daniels *et al*, 2006; Stepanek *et al*, 2014). Thus, Q4H7 resembles a self-antigen that positively selected peripheral T cells might encounter at the periphery. Surprisingly, CD8.4 OT-I T cells were not more efficient in inducing the autoimmune diabetes than CD8WT OT-I T cells in any tested condition (Figs 5B and EV5A). Adoptively transferred naïve OT-I, CD8.4 OT-I, and even TM OT-I T cells did not promote clearance of Lm-Q4H7 in this experimental setup (relatively low number of injected CFUs, low antigen affinity; Fig EV5B), excluding the possibility that the bacterial burden differs between experimental groups.

To further analyze the functional responses of VM T cells, we stimulated CD8.4 OT-I and CD8WT OT-I T cells with dendritic cells loaded with OVA or suboptimal cognate antigens T4 or Q4H7 *ex vivo*. No significant difference in the upregulation of CD69 or CD25 between naïve and VM cells was observed in the case of high-affinity OVA stimulation. However, the responses to antigens with suboptimal affinity to the TCR differed between these two cell types. Interestingly, although CD8.4 OT-I T cells showed stronger CD69 upregulation than naïve T cells when stimulated with low antigen dose, when the antigen dose was high, the response of VM T cells was lower than that of naïve T cells (Fig 5C). Upregulation of CD25 was lower in CD8.4 OT-I T cells than in naïve T cells, when activated with the low-affinity antigens (Fig 5D).



**Figure 4. Virtual memory T cells represent an intermediate stage between naïve and true memory T cells.**

A–C Transcriptomes of naïve ( $n = 4$ ), VM ( $n = 4$ ), and TM ( $n = 3$ ) CD8<sup>+</sup> T cells were analyzed by deep RNA sequencing. (A) Enrichment of CD8<sup>+</sup> memory signature genes (as revealed by previous studies) in naïve, virtual memory, and true memory T cells. (B) Pairwise comparisons between naïve, VM, and TM CD8<sup>+</sup> cells for the overall enrichment of the memory signature and naïve signature gene sets by a method ROAST. The thick end of the connecting line between the populations indicates the population with the overall relative enrichment of the gene set, the percentage of the genes from the gene set that are more expressed in the indicated population ( $z\text{-score} > \sqrt{2}$ ) over the opposite population is indicated. (C) The relative enrichment of chemokine encoding transcripts in the samples is shown. D, E Surface staining for CX3CR1 (D) and NRP1 (E) was performed on naïve (gated as CD62L<sup>+</sup>CD44<sup>-</sup>CD49d<sup>low</sup>) and VM (CD62L<sup>+</sup>CD44<sup>+</sup>CD49d<sup>low</sup>) K<sup>b</sup>-OVA-4mer<sup>+</sup> CD8<sup>+</sup> T cells isolated from unprimed Vβ5 mouse and on true CM memory (gated as CD62L<sup>+</sup>CD44<sup>+</sup>CD49d<sup>high</sup>) and effector/effector memory (CD62L<sup>+</sup>CD44<sup>+</sup>CD49d<sup>high</sup>) K<sup>b</sup>-OVA-4mer<sup>+</sup> CD8<sup>+</sup> T cells isolated from Vβ5 mouse 30–45 days after Lm-OVA infection. A representative experiment out of five (D) or four (E) in total is shown. Mean percentage + SEM of CX3CR1<sup>+</sup> and NRP1<sup>+</sup> cells within the particular population is shown. (D)  $n = 10$  immunized mice and five unprimed mice from five independent experiments. (E)  $n = 8$  immunized mice and four unprimed mice from four independent experiments. Statistical analysis was performed by two-tailed Mann–Whitney test.

Source data are available online for this figure.

Next, we examined antigenic responses of naïve and VM T cells *in vivo*. CD8WT and CD8.4 OT-I T cells show comparable expansion when primed by Lm-OVA or Lm-Q4H7 (Fig EV5C). However, CD8.4

OT-I formed significantly less memory precursors (IL-7R<sup>+</sup>KLRG1<sup>-</sup>), more IL-7R<sup>+</sup>KLRG1<sup>+</sup> double-positive cells, and slightly more short-lived effector cells (IL-7R<sup>-</sup>KLRG1<sup>+</sup>) than CD8WT OT-I T cells upon

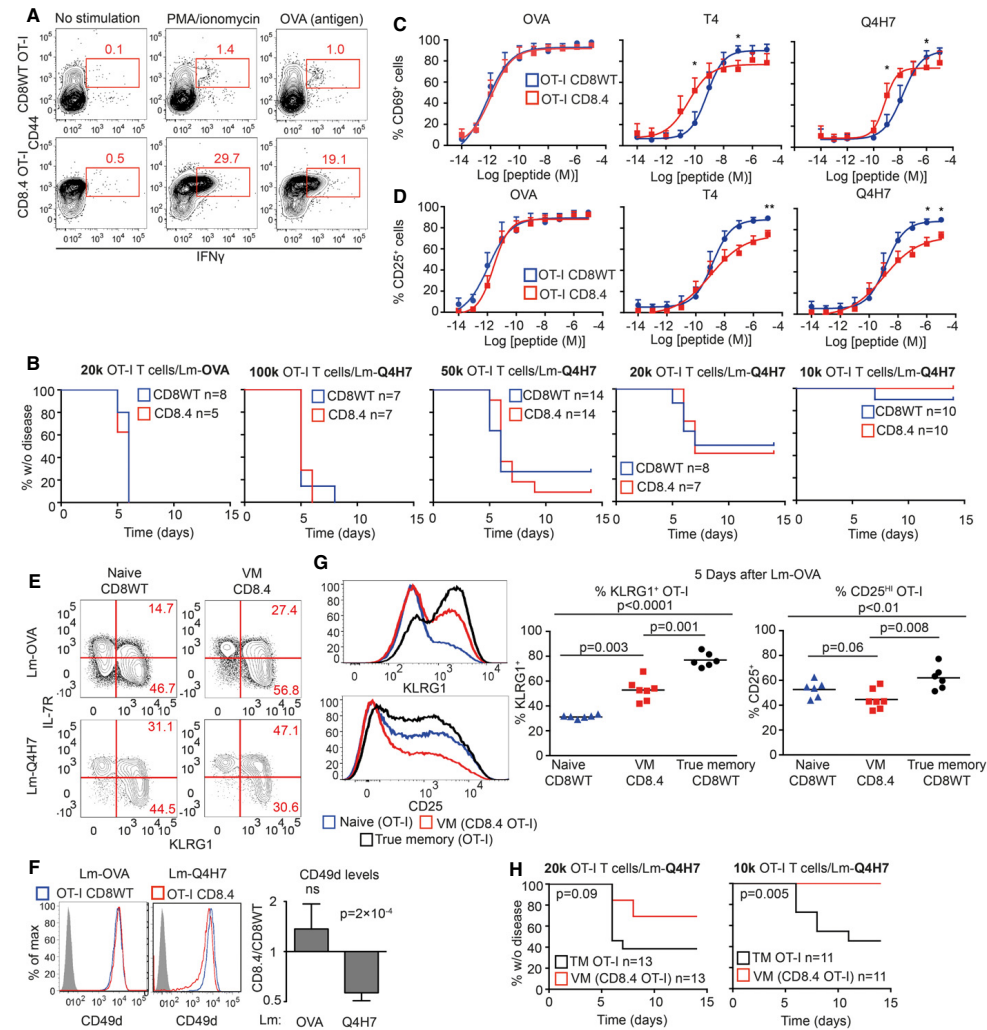


Figure 5.

priming with Lm-OVA (Figs 5E and EV5C). Interestingly, upon priming with low-affinity Lm-Q4H7, VM T cells formed less short-lived effector cells and more IL-7R<sup>+</sup> KLRG1<sup>+</sup> double-positive cells (Figs 5E and EV5C). Moreover, CD8.4 OT-I T cells did not upregulate CD49d (a subunit of VLA-4) to the same extent as CD8WT OT-I upon immunization with Lm-Q4H7 (Fig 5F). Collectively, VM T cells exhibited several signs of hyporesponsiveness in comparison with naïve T cells upon low-affinity antigenic stimulation: lower

upregulation of CD25 *in vitro*, lower frequency of short-lived effector cells, and lower CD49d upregulation.

Subsequently, we compared responses of VM CD8.4 T cells to naïve and true memory OT-I T cells *in vivo*. True memory showed stronger upregulation of KLRG1 and CD25 than VM T cells upon Lm-OVA challenge (Fig 5G). Importantly, true memory OT-I T cells were more potent in inducing the autoimmune diabetes in our RIP.OVA model (Figs 5H and EV5D). Collectively, these data

**Figure 5. Virtual memory T cells are as self-tolerant as naïve T cells.**

- A LN cells isolated from CD8WT OT-I and CD8.4 OT-I mice were stimulated with PMA and ionomycin or OVA peptide in the presence of BD GolgiStop for 5 h and the production of IFN $\gamma$  was analyzed by flow cytometry (gated as CD8 $^+$ ). A representative experiment out of four in total.
- B Indicated number of CD8WT OT-I or CD8.4 OT-I T cells were adoptively transferred into RIP.OVA hosts, which were infected with Lm-OVA or -Q4H7 1 day later. The glucose in the urine was monitored for 14 days. The percentage of non-diabetic mice in time is shown. Differences between OT-I and CD8.4 were not significant by log-rank test.  $n = 5-11$  (indicated) mice per group in 3-6 independent experiments.
- C, D CD8WT OT-I or CD8.4 OT-I LN T cells were stimulated *ex vivo* with dendritic cells loaded with varying concentrations of OVA, Q4R7, Q4H7 peptides overnight and the expression of CD69 (C) and CD25 (D) on CD8 $^+$  T cells was analyzed. Mean + SEM.  $n = 3-5$  independent experiments. Statistical significance was determined paired two-tailed Student's *t*-test (C, D). \* $P < 0.05$ , \*\* $P < 0.01$ .
- E, F CD8WT OT-I or CD8.4 OT-I LN T cells were adoptively transferred to polyclonal Ly5.1 host mice, which were infected 1 day later with transgenic Lm-OVA or -Q4H7. Six days after the infection, splenocytes from the hosts were isolated and analyzed for the expression of IL-7R, KLRG1 (E) or CD49d (F). (F) A representative experiment out of four (7-9 mice per group in total). (E)  $n = 7$  (Lm-OVA) or 9 (Lm-Q4H7) from four independent experiments. Statistical significance was determined using a one-value two-tailed *t*-test (for the ratio of CD49d MFI between the subsets). Normality of the data was tested using Shapiro-Wilk normality test (passing threshold  $P < 0.01$ ).
- G  $1 \times 10^4$  naïve CD8WT OT-I, VM CD8.4 OT-I, or true memory OT-I T cells loaded with 5  $\mu$ M CellTrace Violet were injected into Ly5.1 recipients followed by immunization with Lm-OVA 1 day later. Five days after the immunization, splenocytes were isolated and donor cells were examined for the expression of KLRG1 and CD25 by flow cytometry.  $n = 6$  from three independent experiments. Statistical significance was performed by Kruskal-Wallis test, and selected pairs of groups were compared by Mann-Whitney test.
- H Indicated number of CD8.4 OT-I or true memory OT-I T cells were adoptively transferred into RIP.OVA hosts, which were infected with Lm-Q4H7 1 day later. The glucose in the urine was monitored for 14 days. The percentage of non-diabetic mice in time is shown. Statistical significance was calculated by log-rank test.  $n = 11$  ( $1 \times 10^4$  transferred cells) or 13 ( $2 \times 10^4$  transferred cells) mice per group in four independent experiments.

Source data are available online for this figure.

suggest that virtual memory T cells are less efficient in their responses to the antigen *in vivo* and in inducing the autoimmune tissue pathology than true memory T cells.

We wondered whether CD8.4 OT-I T cells do respond to endogenous self-antigens Catnb and Mapk8 that were previously proposed as positive selecting antigens for OT-I T cells (Santori *et al*, 2002). In agreement with previous reports (Salmond *et al*, 2014; Oberle *et al*, 2016), we could not detect a substantial response of peripheral OT-I T cells to these antigens *in vitro* using antigen-loaded dendritic cells and *in vivo* using Lm-Catnb (Fig EV5E and F). CD8.4 OT-I T cells showed no significant response to these self-peptides as well (Fig EV5E and F). Although we could see that Lm infection induced proliferation of VM CD8.4 T cells (probably via cytokines), expression of the positive selecting self-antigen Catnb in the *Listeria* did not enhance this response at all (Fig EV5F). These experiments suggest that VM T cells are tolerant to self-antigens that have previously triggered their conversion to VM T cells.

**Retrogenic T cells as a model for functional differences between naïve and VM T cells**

To complement our data from CD8.4 OT-I VM model, we used sorted naïve and VM T cells from the OVA-specific clones V14-C1 and V14-C2 (Fig 3F-H). The advantage of this approach is that both naïve and VM express the same TCR and CD8 coreceptor and any differences between these populations can be attributed solely to their different developmental programs. We adoptively transferred these cells into RIP.OVA mice followed by infection with Lm-OVA. Naïve T cells were more efficient in inducing the autoimmune diabetes than VM T cells in case of both clones, but only the clone V14-C1 showed a statistically significant difference (Fig 6A). When we adoptively transferred naïve or VM T cells expressing V14-C1 or V14-C2 TCRs into Ly5.1 recipients followed by immunization with dendritic cells loaded with OVA or lower affinity antigen Q4R7, we observed that VM clones showed significantly lower level of upregulation of CD49d, a subunit of VLA4 important for tissue infiltration (Fig 6B). These observations were in agreement with the results

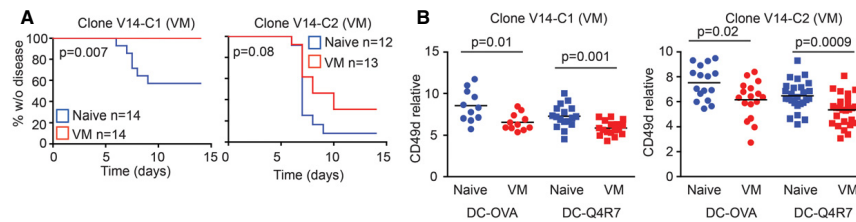
obtained with the CD8.4 OT-I model of monoclonal VM T cells, demonstrating that VM T cells are not inherently less self-tolerant than naïve T cells.

Although others and we showed that VM T cells elicit stronger responses than naïve T cells in some assays (Fig 5A and Lee *et al*, 2013), they do not show a stronger potency than naïve T cells to induce autoimmune pathology in our diabetic model. Most likely VM T cells acquire mechanisms to suppress their responses to antigens, infiltration of the tissue, and/or their effector functions. One such mechanism, contributing to the self-tolerance of VM T cells, can be lower expression of CD49d and CD25 upon activation. Collectively, these data establish that relatively strongly self-reactive T-cell clones differentiate into VM T cells and trigger a specific developmental program that enables them to efficiently respond to infection, but does not increase their autoimmune potential (Fig 7).

**Discussion**

We observed that CD8-Lck coupling frequency regulates intensity of TCR homeostatic signals. For the first time, we showed that the intrinsic sensitivity of the TCR signaling machinery sets the frequency of VM CD8 $^+$  T cells. We also showed that only relatively strongly self-reactive T-cell clones have the potential to form VM T cells. We identified the gene expression profile of VM T cells and showed that they represent an intermediate stage between naïve and true CM T cells. Although the combination of relatively strong self-reactivity and acquisition of the partial memory program could represent a potential risk for autoimmunity, we observed that VM T cells are not more potent than naïve T cells in a model of experimental type 1 diabetes.

It is well established that some memory-phenotype T cells respond to an antigen, and they have not been previously exposed to (Haluszczak *et al*, 2009; Lee *et al*, 2013; Sosinowski *et al*, 2013; Su *et al*, 2013; White *et al*, 2017). Some researchers call these cells as VM T cells and propose that they were generated in the absence of a foreign antigenic stimulation (Haluszczak *et al*, 2009; White

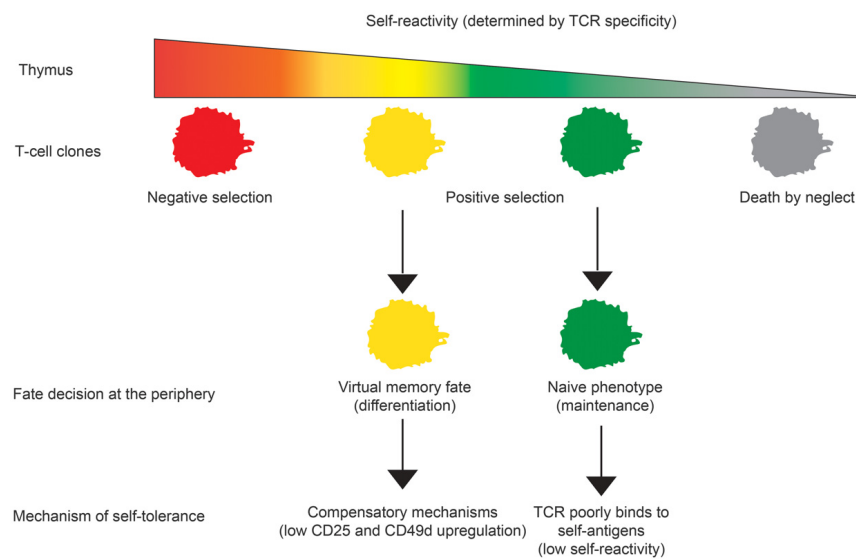


**Figure 6. Comparison of naïve and VM subsets generated from retrogenic T-cell clones.**

**A**  $5 \times 10^3$  FACS-sorted naïve (CD44<sup>+</sup>) or VM (CD44<sup>+</sup>) T cells from V14-C1 or V14-C2 T cells generated via bone marrow transfer (Fig EV3E) were adoptively transferred into RIP.OVA mice followed by immunization with Lm-OVA 1 day later. Glucose concentration in the urine was monitored for 14 days. Statistical significance was tested using log-rank test.  $n = 12-14$  mice per group in 4-5 independent experiments.

**B** FACS-sorted naïve (CD44<sup>+</sup>) or VM (CD44<sup>+</sup>) T cells from V14-C1 or V14-C2 T cells generated via bone marrow transfer (Fig EV3E) were adoptively transferred into RIP.OVA mice followed by immunization with OVA- or Q4R7-loaded bone marrow-derived dendritic cells. The number of adoptively transferred T cells was  $1 \times 10^3$  and  $3 \times 10^3$  for OVA- and Q4R7-loaded dendritic cells, respectively.  $n = 11-27$  mice per group in 5-6 independent experiments. Mean is indicated. Statistical significance was tested using Mann-Whitney test.

Source data are available online for this figure.



**Figure 7. Schematic representation of the role of self-reactivity in major cell fate decisions of conventional CD8<sup>+</sup> T cells.**

Our results establish a novel T-cell fate decision checkpoint, differentiation of positively selected T-cell clone with a relatively high level of self-reactivity into virtual memory T cells.

*et al.*, 2017). The main argument supporting this hypothesis is that germ-free mice, with low levels of foreign antigenic exposure, contain comparable levels of CM-phenotype T cells as control mice (Haluszczak *et al.*, 2009). However, in mice with normal microbiota, which were used for the subsequent characterization of VM T cells, it is difficult to exclude the existence of cross-reactive memory T

cells that were previously exposed to another foreign antigen (Su *et al.*, 2013). Importantly, we show that CD8.4 knock-in mice with enhanced homeostatic TCR signaling exhibit larger VM compartment than CD8WT T cells in SPF and germ-free conditions. We confirmed that VM T cells have lower expression of CD49d than antigen-experienced cells using germ-free mice and confirmed that

antigen-inexperienced VM T cells can be defined as CD49<sup>+</sup>CD122<sup>hi</sup> T cells. Altogether these data established that the strength of homeostatic signals provided to T cells is a major factor leading to formation of VM compartment independently of stimulation with cognate foreign antigens.

It has been observed that IL-15 availability is a limiting factor regulating the size of the VM subset (Sosinowski *et al*, 2013; White *et al*, 2016). In this study, we showed that the intrinsic sensitivity of the TCR signaling machinery (specifically the CD8-Lck coupling frequency) is another major factor that sets the frequency of VM CD8<sup>+</sup> T cells in the secondary lymphoid organs. It has been suggested that the level of CD5, a marker of self-reactivity, is linked with the T-cell ability to form VM T cells (White *et al*, 2016). We investigated individual T-cell clones using transgenic cells with normal and hypersensitive TCR signaling machinery, comparing TCR repertoires of naïve and VM T cells, and analyzing retrogenic monoclonal T-cell populations. These complementary approaches revealed that VM T-cell formation absolutely depends on the level of self-reactivity of a particular T cell and exhibits a threshold behavior. Relatively highly self-reactive T cell clones frequently differentiate into VM T cells (~40–50%), whereas weakly self-reactive T cells completely lack this property. This finding characterizes the formation of VM T cells as a previously unappreciated T-cell fate decision check point, where the intensity of homeostatic TCR signals is the critical decisive factor. Our data also explain a previous observation that VM T cells are formed exclusively from T cells expressing endogenous recombinant TCR chains in OT-1 Rag<sup>+</sup> mice during aging (Renkema *et al*, 2014). Some of the T-cell clones that replaced the OT-1 TCR with a variable endogenous one are probably more self-reactive than OT-1 T cells, which drives their differentiation in VM T cells.

The functionality of a T-cell subset is determined by its gene expression profile. Whereas it is clear that VM T cells substantially differ from naïve T cells (Haluszczak *et al*, 2009; Lee *et al*, 2013; Sosinowski *et al*, 2013; White *et al*, 2016), the CD49d and CD122 were the only markers that can distinguish VM T cells from true memory (TM) T cells. In this study, we characterized gene expression of VM T cells and compared it to naïve T cells from germ-free mice and foreign antigen-specific TM T cells. Analysis focusing on previously established naïve and memory T-cell signature genes revealed that VM T cells have an intermediate gene expression profile between naïve and TM T cells. Accordingly, expression of chemokines and cytokines was generally lower in VM T cells than in TM T cells. These data suggest that VM T cells trigger a partial memory program. Alternatively, TM CD8<sup>+</sup> T cells might represent a heterogeneous population of two or more subsets with different degrees of similarity to VM T cells, as suggested by heterogeneous expression of CX3CR1 and NRP1, two genes that showed a large difference between TM and VM T cells. Indeed, CX3CR1 has been proposed as a marker that discriminates different subsets of memory T cells (Bottcher *et al*, 2015; Gerlach *et al*, 2016). Single-cell gene expression profiling would show whether immune responses to foreign antigens generate any TM T cells identical to VM T cells.

VM T cells share some phenotypic traits with stem-like memory (SCM) T cells, including higher expression of CD122, CXCR3, and dependency on IL-15 (Zhang *et al*, 2005). However, unlike VM cells, SCM T cells are derived from CD44<sup>low</sup> population and human SCM

T-cell counterparts are derived from the CD45RA<sup>+</sup> population (Gattinoni *et al*, 2011). Furthermore, SCM T cells express Sca-1 stemness marker which is not upregulated in the VM T cells as revealed by our RNAseq data. Thus, VM and SCM T cells represent two distinguishable subsets of CD8<sup>+</sup> T cells. However, because SCM T cells give rise to central memory, effector memory, and effector CD8<sup>+</sup> T cells (Gattinoni *et al*, 2011), we cannot exclude that VM T-cell population preferentially arise from SCM T cells.

VM T cells were shown to surpass naïve T cells in their response to inflammatory cytokines IL-12 and IL-18 (Haluszczak *et al*, 2009), in the rapid generation of short-lived effectors (Lee *et al*, 2013), rapid IFN $\gamma$  production, and in the protection against Lm both in antigen-specific (Lee *et al*, 2013) and in by-stander manners (Wu *et al*, 2010). We demonstrated that VM T cells develop from relatively strongly self-reactive T-cell clone. Both the hyperresponsiveness and self-reactivity of VM T cells might potentially enhance their capacity to break self-tolerance. We addressed the potency of VM T cells to induce experimental autoimmune pathology by using two monoclonal models for comparing naïve and VM T cells with the same TCR specificity. We observed that VM T cells were not more efficient than naïve T cells in inducing the experimental autoimmune diabetes on a per cell basis. This can be at least partially explained by the fact that VM T cells show lower upregulation of CD25 and VLA-4 than naïve T cells when activated with a suboptimal antigen. VLA-4 has been previously shown to be essential for the induction of the tissue pathology in the mouse experimental model of type 1 diabetes (King *et al*, 2012). We propose that VM T cells surpass naïve T cells in some kind of responses to promote rapid immunity to pathogens (Lee *et al*, 2013; White *et al*, 2016), but they also develop compensatory mechanisms that make these cells self-tolerant to an extent comparable to naïve T cells. We used an experimental model of autoimmune diabetes, a prototypic autoimmune pathology that involves self-reactive CD8<sup>+</sup> T cells. The important aspect of our model is that the adoptively transferred neoself-reactive T cells developed in the absence of the neoself antigen. We cannot exclude the possibility that VM T cells represent a major risk in other types of autoimmune diseases/conditions.

Based on pilot studies in the field (Pihlgren *et al*, 1996; Curtsinger *et al*, 1998; London *et al*, 2000), it was generally accepted that one feature of immunological memory is that a memory T cell elicits a faster and stronger response to cognate antigens than a naïve T cell. However, recent evidence showed that, at least under certain conditions, the response of naïve T cells to an antigen is stronger than the response of memory T cells (Knudson *et al*, 2013; Mehlhop-Williams & Bevan, 2014; Cho *et al*, 2016). We showed that true memory T cells surpass virtual memory T cells in the upregulation of KLRG1, CD25, and in their potency to induce experimental autoimmune pathology. These data correspond to a previous study showing stronger responses of TM T cells in comparison with lymphopenia-induced memory T cells (Cheung *et al*, 2009), suggesting that virtual memory and lymphopenia-induced memory T cells might have similar functions. The physiological role of VM T cells needs to be further investigated, but it seems plausible that VM T cells have unique type of responses to pathogens and thus contribute to functional diversity of T-cell immunity, which might be required for efficient immune protection.

Recently, it has been proposed that human innate Eomes<sup>+</sup> KIR/NKG2A<sup>+</sup> CD8<sup>+</sup> T cells (Jacomet *et al.*, 2015) represent counterparts of murine VM T cells, although expression of some markers including CD27 and CD5 substantially differed between these two subsets (White *et al.*, 2016). It would be interesting to elucidate whether the human Eomes<sup>+</sup> KIR/NKG2A<sup>+</sup> CD8<sup>+</sup> subset shows similar gene expression pattern as mouse VM T cells, whether they originate from relatively highly self-reactive clones, and whether these cells acquire tolerance mechanisms as murine VM CD8<sup>+</sup> T cells do.

## Materials Methods

### Antibodies and reagents

Antibodies to following antigens were used for flow cytometry: CD69 (clone H1.2F3), CD11a (LFA-1) (clone M17/4), CD25 (PC61), CD3 (145-2C11), IFN $\gamma$  (XMG1.2), TCR $\beta$  (H57-597), TCR V $\alpha$ 2 (B20.1), TCR V $\alpha$ 8.3 (B21.14), TCR V $\alpha$ 3.2 (R3-16), CD49d (R1-2), CD5 (53-7.3) (all BD Biosciences), Tbet (4B10), Eomes (Dan11mag), CD8 $\alpha$  (53-6.7), CD8 $\beta$  (H35-17.2), CD127 (A7R34) (all eBioscience) CD44 (IM7), CD4 (RM-45), CD62L (MEL-14), CD122 (TM-beta1), KLRG1 (2F1), PD-1 (RMP1-30), CD19 (6D5) (all Biolegend), pErk1/2 (D13.14.4E, Cell Signaling). The antibodies were conjugated with various fluorescent dyes or with biotin by manufacturers. K<sup>b</sup>-OVA PE tetramer was prepared as described previously (Stepanek *et al.*, 2014). Peptides OVA<sub>257-264</sub> (SIINFEKL), Q4R7 (SIIRFERL), Q4H7 (SIIRFEHL), NP68 (ASNENMDAM), NP372E (ASNENMEAM), Mapk8<sub>267-274</sub> (AGYSFEKL), and Catnb<sub>329-336</sub> (RTYTYEKL) were purchased from Eurogentec or Peptides&Elephants. Proliferation dye CellTrace Violet was purchased from ThermoFisher Scientific (C34557).

### Flow cytometry and cell counting

For the surface staining, cells were incubated with diluted antibodies in PBS/0.5% gelatin or PBS/2% goat serum on ice. LIVE/DEAD near-IR dye (Life Technologies) or Hoechst 33258 (Life Technologies) was used for discrimination of live and dead cells. For the intracellular staining, cells were fixed and permeabilized using Foxp3/Transcription Factor Staining Buffer Set (eBioscience, 00-5523-00). For some experiments, enrichment of CD8<sup>+</sup> T cells was performed using magnetic bead separation kits EasySep (STEMCELL Technologies) or Dynabeads (Thermo Fisher Scientific) according to manufacturer's instructions prior to the analysis or sorting by flow cytometry. Cells were counted using Z2 Coulter Counter (Beckman) or using AccuCheck counting beads (Thermo Fisher Scientific) and a flow cytometer. Flow cytometry was carried out with a FACSCantoII, LSRII, or a LSRFortessa (BD Bioscience). Cell sorting was performed using a FACSARIA III or Influx (BD Bioscience). Data were analyzed using FlowJo software (TreeStar).

### Experimental animals

All mice were 5–12 weeks old and had C57Bl/6j background. RIP.OVA (Kurts *et al.*, 1998), OT-I Rag2<sup>-/-</sup> (Palmer *et al.*, 2016), CD8.4, F5 Rag1<sup>-/-</sup> (Erman *et al.*, 2006), and V $\beta$ 5 (Fink *et al.*, 1992)

strains were described previously. Mice were bred in our facilities (SPF mice: University Hospital Basel and Institute of Molecular Genetics; germ-free mice: University of Bern, Switzerland) in accordance with Cantonal and Federal laws of Switzerland and the Czech Republic. Animal protocols were approved by the Cantonal Veterinary Office of Basel-Stadt, Switzerland, and Czech Academy of Sciences, Czech Republic. Transfer into germ-free conditions was performed using time-mating followed by transferring 2-cell embryos into germ-free foster mothers.

Males and females were used for the experiments. Age- and sex-matched pairs of animals were used in the experimental groups. If possible, littermates were equally divided into the experimental groups. The randomization for adoptive transfer experiments was done by assigning the experimental conditions to recipient mouse ID numbers by an experimenter who had no prior contact with the mice. Other experiments were not randomized. The experiments were not blinded since no subjective scoring method was used.

### RNA sequencing

RNA was isolated using Trizol (Thermo Fisher Scientific) followed by in-column DNase treatment using RNA clean & concentrator kit (Zymo Research). The library preparation and RNA sequencing by HiSeq2500 (HiSeq SBS Kit v4, Illumina) were performed by the Genomic Facility of D-BSSE ETH Zurich in Basel. Obtained single-end RNAseq reads were mapped to the mouse genome assembly, version mm9, with RNA-STAR (Dobin *et al.*, 2013), with default parameters except for allowing only unique hits to genome (outFilterMultimapNmax = 1) and filtering reads without evidence in spliced junction table (outFilterType = "BySJout"). All subsequent gene expression data analysis was done within the R software (R Foundation for Statistical Computing, Vienna, Austria). Raw reads and mapping quality were assessed by the qQCreport function from the R/Bioconductor software package QuasR (version 1.12.0; Gaidatzis *et al.*, 2015). Using RefSeq mRNA coordinates from UCSC (genome.ucsc.edu, downloaded in July 2013) and the qCount function from QuasR package, we quantified gene expression as the number of reads that started within any annotated exon of a gene. The differentially expressed genes were identified using the edgeR package (version 3.14.0; Robinson *et al.*, 2010). We generated lists of naïve and memory signature genes based on previously published studies [gene sets M3022, M5832, M3039 for memory, and M3020, M5831, M3038 for naïve T cells in the Molecular Signature Databases (Kaech *et al.*, 2002; Subramanian *et al.*, 2005; Luckey *et al.*, 2006; Wherry *et al.*, 2007)]. In our memory and naïve signature gene lists, we included only genes that were listed at least in two out of the above-mentioned three respective gene sets. For the global comparison of the expression of the signature genes in naïve, VM, and true CM T cells, we used self-contained gene set enrichment test called Roast, which is available in edgeR package (Wu *et al.*, 2010).

### DNA cloning and production and viruses

RNA was isolated using Trizol reagent (Thermo Fisher Scientific) and RNA clean & concentrator kit (Zymoresearch, R1013). Reverse transcription was performed using RevertAid (Thermo Fisher Scientific) according to the manufacturer's instructions. TCR sequences



were amplified using cDNA from sorted T cells by PCR using Phusion polymerase (New England Biolabs) and following primers: TRACrev (EcoRI) 5'-TCAGACggaattcTCAACTGGACCACAGCCTCA, TRAV14for (XhoI) 5' GTAGTctcgagATGGACAAGATCTTGACA GCA, TRAV12for (XhoI) 5' GTAGTctcgagATGCGTCTGDCACCTG CTC and ligated into pBlueScript vector using T4 ligase (New England Biolabs) and sequenced by Sanger sequencing using T7 primer 5' TAATACGACTCACTATAGGG. Selected clones were cloned into MSCV-GFP vector via EcoRI and XhoI (New England Biolabs).

Coding sequence of SCF, IL-3 and IL-6 was obtained from bone marrow cDNA with Phusion polymerase using these primers: SCFfor 5'-TTGGATCCGCCACCATGAAGAAGACAAAACCTGGATT ATC, SCFrev 5'-AACTCGAGTTACACCTCTTGAATTTCTCTCTTTC, IL-3for 5'-TTGAATTCGCCACCATTGTTCTGCCAGCTCTACCACCAG, IL3rev 5'-AACTCGAGTTAACATTCACCGTTCCACGGTTAGG, IL-6 for 5'-TTGAATTCGCCACCATGAAGTTCTCTCTGCAAGAGACTT, IL6 rev 5' AACTCGAGCTAGGTTTCCGAGTAGATCTCAAAGTG. cDNA was cloned into pXJ41 expression vector using BamHI or EcoRI and XhoI restriction sites and sequenced. Cytokines were produced in HEK293 cells transfected with pXJ41 using polyethylenimine (PEI) transfection in ratio 2.5 µl PEI to 1 µg DNA. Supernatant was harvested 3 days after transfection. Titration against commercial recombinant cytokines of known concentration and their effect on BM cell proliferation *in vitro* was used to determine biological activity of cytokines in supernatant. Dilution of supernatant corresponding to concentration of 100 ng/ml SCF, 20 ng/ml IL-3 and 10 ng/ml IL-6 was used for cultivation of immortalized bone marrow cells.

Retroviral MSCV and pMYs particles were generated by transfection of the vectors into Platinum-E cells (Cell Biolabs) by PEI as described above.

#### Ex vivo activation assay

For the analysis of IFN $\gamma$  production, T cells ( $1 \times 10^6$ /ml in RPMI/10% FCS) were stimulated with 10 ng/ml PMA and 1.5 µM ionomycin or 1 µM OVA peptide in the presence of BD Golgi Stop for 5 h. For the CD69 and CD25 upregulation assay, dendritic cells differentiated from fresh or immortalized bone marrow stem cells were pulsed with indicated concentration of indicated peptides, mixed with T cells isolated from LNs in a 1:2 ratio, and analyzed after ~16 h of coculture as described previously (Palmer *et al*, 2016).

#### Bone marrow chimeras

Bone marrow cells were isolated from long bones of indicated mouse strains and lymphocytes were depleted using biotinylated antibodies to CD3 and CD19 and Dynabeads biotin binder kit (Thermo Fisher Scientific). In total,  $6 \times 10^6$  cells (always a 1:1 mixture from two different donor strains) in 200 µl of PBS were injected into irradiated (300 cGy) Rag2 $^{-/-}$  host mice *i.v.* The mice were analyzed 8 weeks after the transfer.

#### Monoclonal retrogenic T cells

Generation of immortalized bone marrow was described previously (Ruedl *et al*, 2008). Briefly, V $\beta$ 5 Rag2 $^{-/-}$  mice were treated with

100 mg/kg 5-fluorouracil and bone marrow cells were harvested 5 days later. Cells were cultivated in complete IMDM (10% FCS) supplemented with SCF, IL-3, and IL-6. After 2 days, proliferating cells were virally transduced with a fusion construct NUP98-HOXB4 in a retroviral vector pMYs. Viral infections were performed in the presence of 10 µg/ml polybrene by centrifugation (90 min, 1,250 g, 30°C). The transduced cells were selected for 2 days in puromycin (1 µg/ml). Selected immortalized cells were subsequently virally transduced with MSCV vector containing sTCR $\alpha$ -encoding gene and GFP as a selection marker. Two days after the transduction, GFP $^{+}$  was FACS-sorted and transplanted into irradiated (7 Gy) congenic Ly5.1 recipients. At least 8 weeks after the transplantation, the recipient mice were sacrificed and donor LN T cells were used for cell fate analysis by flow cytometry or for adoptive transfers.

#### In vivo activation and a model for autoimmune diabetes

Indicated numbers of T cells were adoptively transferred into a host mouse *i.v.* On a following day, the host mice were immunized with indicated peptide (50 µg) and LPS (25 µg) in 200 µl of PBS *i.p.* or with 5,000 CFU of Lm. Lm strains expressing OVA, Q4R7, and Q4H7 have been described previously (King *et al*, 2012; Oberle *et al*, 2016). Lm expressing NP68 was produced by adding the ASNENMDAM epitope to ovalbumin encoding gene and introduced to Lm as previously described (Zehn *et al*, 2009). Dendritic cells for *in vivo* experiments were generated from full bone marrow isolated from long bones of 6- to 10-week-old mice. Cells were cultured for 10 days in complete Iscove's modified Dulbecco's medium (10% FCS) conditioned with 2% GM-CSF supernatant (Lutz cells). Medium was refreshed for new on day 4 and 7. Differentiated DCs were pulsed with corresponding peptide ( $10^{-7}$  M) in the presence of LPS (100 ng/ml) for 3 h and  $1 \times 10^6$  antigen-loaded DCs were used for *i.v.* immunization. In the experimental model of autoimmunity, we monitored glucose in the urine of RIP.OVA mice on a daily basis using test strips (Diabur-Test 5000, Roche or GLUKOPHAN, Erba Lachema, Czech Republic). The animal was considered to suffer from lethal autoimmunity when the concentration of glucose in the urine reached  $\geq 1,000$  mg/dl. We also measured blood glucose by contour blood glucose meter (Bayer) on day 7 post-infection. In the diabetic experiments, mice that died before the end of the monitored period (14 days) and before they reached 1,000 mg/dl glucose levels in the urine were excluded. Only one mouse in total was excluded based on this pre-established criterium.

#### Generation of true memory T cells

True memory T cells were generated by infecting V $\beta$ 5 mice with 5,000 CFU of Lm-OVA. After 60–90 days (for RNAseq) or 30–50 days (for FACS staining), CD8 $^{+}$  Kb-OVA tetramer $^{+}$  CD49d $^{+}$  CD44 $^{+}$  CD62L $^{+}$  from LNs and the spleen were sorted (or gated). TM OT-I T cells were generated by adoptive transfer of  $1 \times 10^6$  T cells from OT-I Rag2 $^{-/-}$  mouse into Ly5.1 recipient and subsequent infection with 5,000 CFU of Lm-OVA. At least 30 days after infection, CD8 $^{+}$  Ly5.2 $^{+}$  cells from LNs and the spleen were sorted and adoptively transferred into recipient mice.

**Listeria clearance**

FACS-sorted  $1 \times 10^4$  naïve CD8<sup>WT</sup> OT-I, CD8.4 OT-I (VM), sorted true memory OT-I T cells, or no T cells were adoptively transferred into Ly5.1 C57Bl/6j mice followed by infection with 5,000 CFU Lm-Q4H7. The recipient mice were sacrificed on day 3 and 5 post-infection, and the spleen was homogenized and lysed in PBS with 0.1% Tergitol (Sigma-Aldrich). 1/20 of splenic lysate was plated onto brain–heart infusion agar (BHI, Sigma-Aldrich) plates with 200 µg/ml streptomycin and incubated at 37°C. The resulting number of colonies was quantified the following day.

**Statistics**

Statistical analysis was carried out using Prism (V5.04, GraphPad Software) or MS Excel. The statistical tests are indicated for each experiment. Whenever possible, we used nonparametric statistical tests. In one case, we use one-value *t*-test after the data passed Shapiro–Wilk normality test. In the *ex vivo* activation assays, we used paired Student's *t*-test (pairs = individual experiments). In this case, we tested the normality of differences using Shapiro–Wilk test, using pooled differences from two highest concentrations of peptides for each condition (because of too few data points for each peptide concentration). For comparing the abundance of individual TCR clones in different subsets, we use paired *t*-test as a post-test after using global chi-square test. Because of the very low  $n = 3$ , we could not test the normality of differences. All statistical tests were two-tailed.

**Data availability**

The data RNAseq data are deposited in the GEO database (GSE90522).

**Expanded View** for this article is available online.

**Acknowledgements**

We thank Prof. Alfred Signer for providing us with CD8.4 mice. We thank Ladislav Cupak, Barbara Hausmann, and Rosmarie Lang for their technical assistance and genotyping of mice. We thank Zdenek Cimburek and Matyas Sima for cell sorting. We thank Prof. Ed Palmer for his multidisciplinary support to the project. This project was supported by the Swiss National Science Foundation (Promys, IZ1120\_166538), the Czech Science Foundation (GJ16-09208Y) to OS, ERC Starting Grant (ProtecTC) to DZ, and the Institute of Molecular Genetics (RVO 68378050). The animal facility of the IMG is a part of the Czech Centre for Phenogenomics and the work there was supported in part by following grants: LM2015040, OP RDI CZ.1.05/2.1.00/19.0395, OP RDI BIOCEV CZ.1.05/1.1.00/02.0109 provided by the Czech Ministry of Education, Youth, and Sports and the European Regional Development Fund. The Group of Adaptive Immunity at the Institute of Molecular Genetics in Prague is supported by an EMBO Installation grant. AM, VH, and MP are students of the Faculty of Science, Charles University, Prague.

**Author contributions**

AD, AM, DM, MH, and OS planned, performed, and analyzed experiments. VH and MP performed and analyzed experiments. PD analyzed experiments. RI did the bioinformatic analysis of the RNA sequencing data. SO and DZ prepared transgenic Lm strains and provided Vβ5 mice. KDM

established and managed the germ-free strains. OS conceived the study. OS, AD, AM, and PD wrote the manuscript. All authors commented on the manuscript.

**Conflict of interest**

The authors declare that they have no conflict of interest.

**References**

- Akue AD, Lee JY, Jameson SC (2012) Derivation and maintenance of virtual memory CD8 T cells. *J Immunol* 188: 2516–2523
- Botcher JP, Beyer M, Meissner F, Abdullah Z, Sander J, Hochst B, Eickhoff S, Rieckmann JC, Russo C, Bauer T, Flecken T, Giesen D, Engel D, Jung S, Busch DH, Protzer U, Thimme R, Mann M, Kurts C, Schultze JL et al (2015) Functional classification of memory CD8(+) T cells by CX3CR1 expression. *Nat Commun* 6: 8306
- Cheung KP, Yang E, Goldrath AW (2009) Memory-like CD8<sup>+</sup> T cells generated during homeostatic proliferation defer to antigen-experienced memory cells. *J Immunol* 183: 3364–3372
- Chiu BC, Martin BE, Stolberg VR, Chensue SW (2013) Cutting edge: central memory CD8 T cells in aged mice are virtual memory cells. *J Immunol* 191: 5793–5796
- Cho JH, Kim HO, Ju YJ, Kye YC, Lee GW, Lee SW, Yun CH, Bottini N, Webster K, Goodnow CC, Surh CD, King C, Sprent J (2016) CD45-mediated control of TCR tuning in naïve and memory CD8<sup>+</sup> T cells. *Nat Commun* 7: 13373
- Chu T, Tyznik AJ, Roepke S, Berkley AM, Woodward-Davis A, Pattacini L, Bevan MJ, Zehn D, Pricl M (2013) Bystander-activated memory CD8 T cells control early pathogen load in an innate-like, NKG2D-dependent manner. *Cell Rep* 3: 701–708
- Curtsinger JM, Lins DC, Mescher MF (1998) CD8(+) memory T cells (CD44<sup>high</sup>, Ly-6C<sup>+</sup>) are more sensitive than naïve cells (CD44<sup>low</sup>), Ly-6C<sup>-</sup>) to TCR/CD8 signaling in response to antigen. *J Immunol* 160: 3236–3243
- Daniels MA, Teixeira E, Gill J, Hausmann B, Roubaty D, Holmberg K, Werlen G, Hollander GA, Gascoigne NRJ, Palmer E (2006) Thymic selection threshold defined by compartmentalization of Ras/MAPK signalling. *Nature* 444: 724–729
- Decman V, Laidlaw BJ, Doering TA, Leng J, Ertl HC, Goldstein DR, Wherry EJ (2012) Defective CD8 T cell responses in aged mice are due to quantitative and qualitative changes in virus-specific precursors. *J Immunol* 188: 1933–1941
- Dobin A, Davis CA, Schlesinger F, Drenkow J, Zaleski C, Jha S, Batut P, Chaisson M, Gingeras TR (2013) STAR: ultrafast universal RNA-seq aligner. *Bioinformatics* 29: 15–21
- Erman B, Alag AS, Dahle O, van Laethem F, Sarafova SD, Guinter TI, Sharrow SO, Grinberg A, Love PE, Singer A (2006) Coreceptor signal strength regulates positive selection but does not determine CD4/CD8 lineage choice in a physiologic *in vivo* model. *J Immunol* 177: 6613–6625
- Fink PJ, Swan K, Turk G, Moore MW, Carbone FR (1992) Both intrathymic and peripheral selection modulate the differential expression of V-Beta-5 among Cd4<sup>+</sup> and Cd8<sup>+</sup> T-Cells. *J Exp Med* 176: 1733–1738
- Gaidatzis D, Lerch A, Hahne F, Stadler MB (2015) QuasR: quantification and annotation of short reads in R. *Bioinformatics* 31: 1130–1132
- Gattinoni L, Lugli E, Ji Y, Pos Z, Paulos CM, Quigley MF, Almeida JR, Gostick E, Yu ZY, Carpenito C, Wang E, Douek DC, Price DA, June CH, Marincola FM, Roederer M, Restifo NP (2011) A human memory T cell subset with stem cell-like properties. *Nat Med* 17: 1290–1297

- Ge Q, Bai A, Jones B, Eisen HN, Chen J (2004) Competition for self-peptide-MHC complexes and cytokines between naive and memory CD8<sup>+</sup> T cells expressing the same or different T cell receptors. *Proc Natl Acad Sci USA* 101: 3041–3046
- Gerlach C, Moseman EA, Loughhead SM, Alvarez D, Zwijnenburg AJ, Waanders L, Garg R, de la Torre JC, von Andrian UH (2016) The chemokine receptor CX3CR1 defines three antigen-experienced CD8 T cell subsets with distinct roles in immune surveillance and homeostasis. *Immunity* 45: 1270–1284
- Graef P, Buchholz VR, Stemmerger C, Flossdorf M, Henkel L, Schiemann M, Drexler I, Hofer T, Riddell SR, Busch DH (2014) Serial transfer of single-cell-derived immunocompetence reveals stemness of CD8(+) central memory T cells. *Immunity* 41: 116–126
- Haluszczak C, Akue AD, Hamilton SE, Johnson LD, Pujanauskis L, Teodorovic L, Jameson SC, Kedl RM (2009) The antigen-specific CD8<sup>+</sup> T cell repertoire in unimmunized mice includes memory phenotype cells bearing markers of homeostatic expansion. *J Exp Med* 206: 435–448
- Hogan T, Shuvaev A, Commenges D, Yates A, Callard R, Thiebaut R, Seddon B (2013) Clonally diverse T cell homeostasis is maintained by a common program of cell-cycle control. *J Immunol* 190: 3985–3993
- Jacomot F, Cayssials E, Basbous S, Levescot A, Piccirilli N, Desmier D, Robin A, Barra A, Giraud C, Guilhot F, Roy L, Herbelin A, Gombert JM (2015) Evidence for eomesodermin-expressing innate-like CD8(+) KIR/NKG2A(+) T cells in human adults and cord blood samples. *Eur J Immunol* 45: 1926–1933
- Kaech SM, Hemby S, Kersh E, Ahmed R (2002) Molecular and functional profiling of memory CD8 T cell differentiation. *Cell* 111: 837–851
- Kimura MY, Pobeziński LA, Guinter TI, Thomas J, Adams A, Park JH, Tai XG, Singer A (2013) IL-7 signaling must be intermittent, not continuous, during CD8(+) T cell homeostasis to promote cell survival instead of cell death. *Nat Immunol* 14: 143–151
- King CG, Koehli S, Hausmann B, Schmalzer M, Zehn D, Palmer E (2012) T cell affinity regulates asymmetric division, effector cell differentiation, and tissue pathology. *Immunity* 37: 709–720
- Knudson KM, Goplen NP, Cunningham CA, Daniels MA, Teixeira E (2013) Low-affinity T cells are programmed to maintain normal primary responses but are impaired in their recall to low-affinity ligands. *Cell Rep* 4: 554–565
- Kurts C, Miller JFAP, Subramaniam RM, Carbone FR, Heath WR (1998) Major histocompatibility complex class I-restricted cross-presentation is biased towards high dose antigens and those released during cellular destruction. *J Exp Med* 188: 409–414
- Kurzweil V, LaRoche A, Oliver PM (2014) Increased peripheral IL-4 leads to an expanded virtual memory CD8<sup>+</sup> population. *J Immunol* 192: 5643–5651
- Lee JY, Hamilton SE, Akue AD, Hogquist KA, Jameson SC (2013) Virtual memory CD8 T cells display unique functional properties. *Proc Natl Acad Sci USA* 110: 13498–13503
- London CA, Lodge MP, Abbas AK (2000) Functional responses and costimulator dependence of memory CD4(+) T cells. *J Immunol* 164: 265–272
- Luckey CJ, Bhattacharya D, Goldrath AW, Weissman IL, Benoist C, Mathis D (2006) Memory T and memory B cells share a transcriptional program of self-renewal with long-term hematopoietic stem cells. *Proc Natl Acad Sci USA* 103: 3304–3309
- Mehlhop-Williams ER, Bevan MJ (2014) Memory CD8<sup>+</sup> T cells exhibit increased antigen threshold requirements for recall proliferation. *J Exp Med* 211: 345–356
- Oberle SG, Hanna-El-Daher L, Chennupati V, Enouz S, Scherer S, Prlc M, Zehn D (2016) A minimum epitope overlap between infections strongly narrows the emerging T cell repertoire. *Cell Rep* 17: 627–635
- Palmer E, Drobek A, Stepanek O (2016) Opposing effects of actin signaling and LFA-1 on establishing the affinity threshold for inducing effector T-cell responses in mice. *Eur J Immunol* 46: 1887–1901
- Park JH, Adoro S, Lucas PJ, Sarafova SD, Alag AS, Doan LL, Erman B, Liu X, Ellmeier W, Bosselut R, Feigenbaum L, Singer A (2007) Coreceptor tuning: cytokine signals transcriptionally tailor CD8 coreceptor expression to the self-specificity of the TCR. *Nat Immunol* 8: 1049–1059
- Pihlgren M, Dubois PM, Tomkowiak M, Sjogren T, Marvel J (1996) Resting memory CD8(+) T cells are hyperreactive to antigenic challenge *in vitro*. *J Exp Med* 184: 2141–2151
- Renkema KR, Li G, Wu A, Smithey MJ, Nikolich-Zugich J (2014) Two separate defects affecting true naive or virtual memory T cell precursors combine to reduce naive T cell responses with aging. *J Immunol* 192: 151–159
- Robinson MD, McCarthy DJ, Smyth GK (2010) edgeR: a Bioconductor package for differential expression analysis of digital gene expression data. *Bioinformatics* 26: 139–140
- Ruedl C, Khameneh HJ, Karjalainen K (2008) Manipulation of immune system via immortal bone marrow stem cells. *Int Immunol* 20: 1211–1218
- Salmond RJ, Brownlie RJ, Morrison VL, Zamoyka R (2014) The tyrosine phosphatase PTPN22 discriminates weak self peptides from strong agonist TCR signals. *Nat Immunol* 15: 875–883
- Santori FR, Kieper WC, Brown SM, Lu Y, Neubert TA, Johnson KL, Naylor S, Vukmanovic S, Hogquist KA, Jameson SC (2002) Rare, structurally homologous self-peptides promote thymocyte positive selection. *Immunity* 17: 131–142
- Shotton DM, Attaran A (1998) Variant antigenic peptide promotes cytotoxic T lymphocyte adhesion to target cells without cytotoxicity. *Proc Natl Acad Sci USA* 95: 15571–15576
- Sosinowski T, White JT, Cross EW, Haluszczak C, Marrack P, Gapin L, Kedl RM (2013) CD8alpha<sup>+</sup> dendritic cell trans presentation of IL-15 to naive CD8<sup>+</sup> T cells produces antigen-inexperienced T cells in the periphery with memory phenotype and function. *J Immunol* 190: 1936–1947
- Stepanek O, Prabhakar AS, Osswald C, King CG, Bulek A, Naeher D, Beauflis-Hugot M, Abanto ML, Galati V, Hausmann B, Lang R, Cole DK, Huseby ES, Sewell AK, Chakraborty AK, Palmer E (2014) Coreceptor scanning by the T cell receptor provides a mechanism for T cell tolerance. *Cell* 159: 333–345
- Su LF, Kidd BA, Han A, Kotzin JJ, Davis MM (2013) Virus-specific CD4(+) memory-phenotype T cells are abundant in unexposed adults. *Immunity* 38: 373–383
- Subramaniam A, Tamayo P, Mootha VK, Mukherjee S, Ebert BL, Gillette MA, Paulovich A, Pomeroy SL, Golub TR, Lander ES, Mesirov JP (2005) Gene set enrichment analysis: a knowledge-based approach for interpreting genome-wide expression profiles. *Proc Natl Acad Sci USA* 102: 15545–15550
- Tripathi P, Morris SC, Perkins C, Sholl A, Finkelman FD, Hildeman DA (2016) IL-4 and IL-15 promotion of virtual memory CD8<sup>+</sup> T cells is determined by genetic background. *Eur J Immunol* 46: 2333–2339
- Wherry EJ, Ha SJ, Kaech SM, Haining WN, Sarkar S, Kalia V, Subramaniam S, Blattman JN, Barber DL, Ahmed R (2007) Molecular signature of CD8<sup>+</sup> T cell exhaustion during chronic viral infection. *Immunity* 27: 670–684
- White JT, Cross EW, Burchill MA, Danhorn T, McCarter MD, Rosen HR, O'Connor B, Kedl RM (2016) Virtual memory T cells develop and mediate bystander protective immunity in an IL-15-dependent manner. *Nat Commun* 7: 11291
- White JT, Cross EW, Kedl RM (2017) Antigen-inexperienced memory CD8<sup>+</sup> T cells: where they come from and why we need them. *Nat Rev Immunol* 17: 391–400

Wu D, Lim E, Vaillant F, Asselin-Labat ML, Visvader JE, Smyth GK (2010) RQAST: rotation gene set tests for complex microarray experiments. *Bioinformatics* 26: 2176–2182

Zehn D, Bevan MJ (2006) T cells with low avidity for a tissue-restricted antigen routinely evade central and peripheral tolerance and cause autoimmunity. *Immunity* 25: 261–270

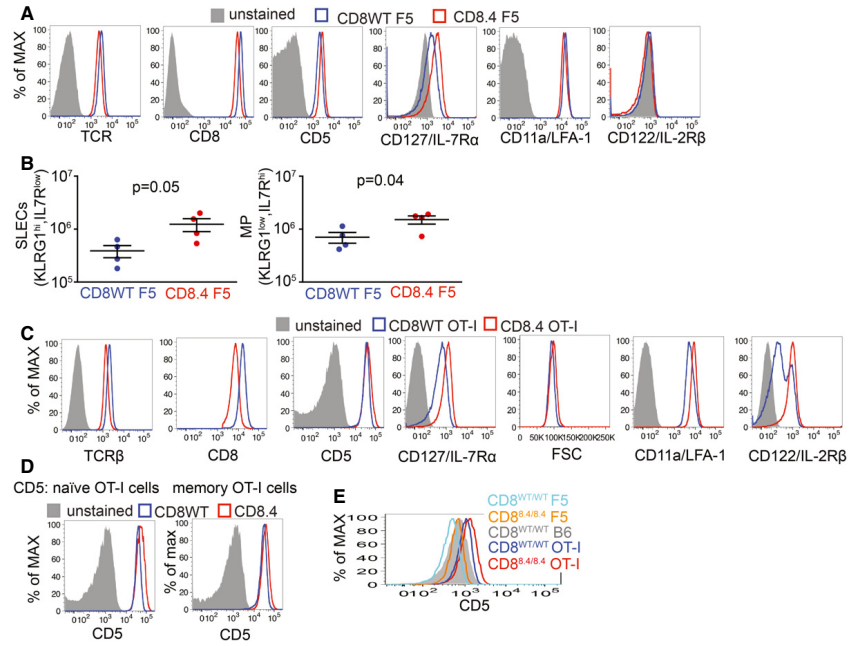
Zehn D, Lee SY, Bevan MJ (2009) Complete but curtailed T-cell response to very low-affinity antigen. *Nature* 458: 211–214

Zhang Y, Joe G, Hexner E, Zhu J, Emerson SG (2005) Host-reactive CD8(+) memory stem cells in graft-versus-host disease. *Nat Med* 11: 1299–1305



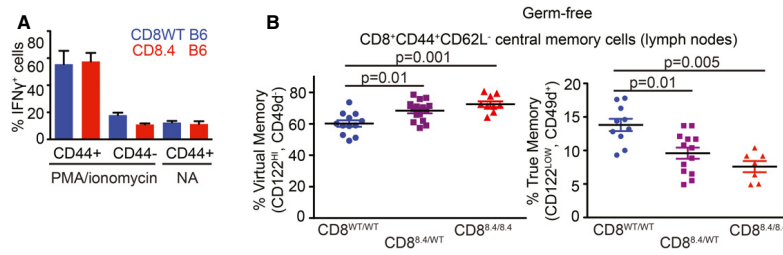
**License:** This is an open access article under the terms of the Creative Commons Attribution License, which permits use, distribution and reproduction in any medium, provided the original work is properly cited.

## Expanded View Figures



**Figure EV1.** Analysis of CD8WT and CD8.4 monoclonal T cells, related to Fig 1.

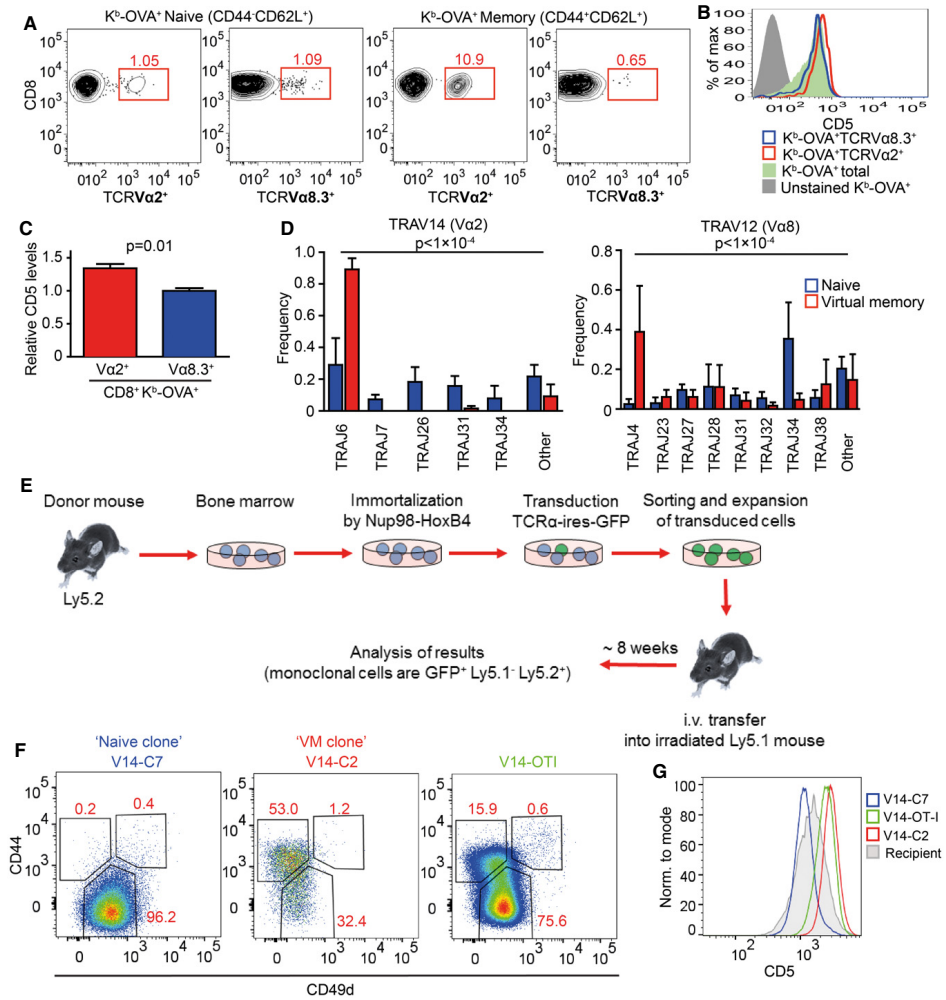
- A Expression of indicated surface markers on CD8WT F5 and CD8.4 F5 LN T cell was analyzed by flow cytometry. A representative experiment out of four in total.
- B CD8WT F5 and CD8.4 F5 T cells primed by Lm-NP68 (Fig 1D) were examined by flow cytometry. Absolute numbers of KLRG1<sup>+</sup> IL-7R<sup>low</sup> short-lived effector cells and KLRG1<sup>+</sup> IL-7R<sup>hi</sup> memory precursors were determined. Mean  $\pm$  SEM.  $n = 4$  mice per group from two independent experiments. Statistical significance was determined by two-tailed t-test. The data do not seem to be strongly deviated from the normal distribution and seem to have equal variance. However, because of the low  $n$ , we could not test the normality/equal variance rigorously.
- C Expression of indicated markers on CD8WT OT-I and CD8.4 OT-I LN T cell and their size estimated by FSC signal was analyzed by flow cytometry. A representative experiment out of 10 in total.
- D Expression of CD5 on CD44<sup>+</sup> (naive) and CD44<sup>+</sup> (memory subsets) of CD8WT OT-I and CD8.4 OT-I LN T cells was analyzed by flow cytometry. A representative experiment out of three in total.
- E Expression of CD5 on T cells isolated from LN of indicated mouse strains by flow cytometry. A representative experiment out of two in total.



**Figure EV2. Analysis of CD8WT and CD8.4 polyclonal T cells, related to Fig 2.**

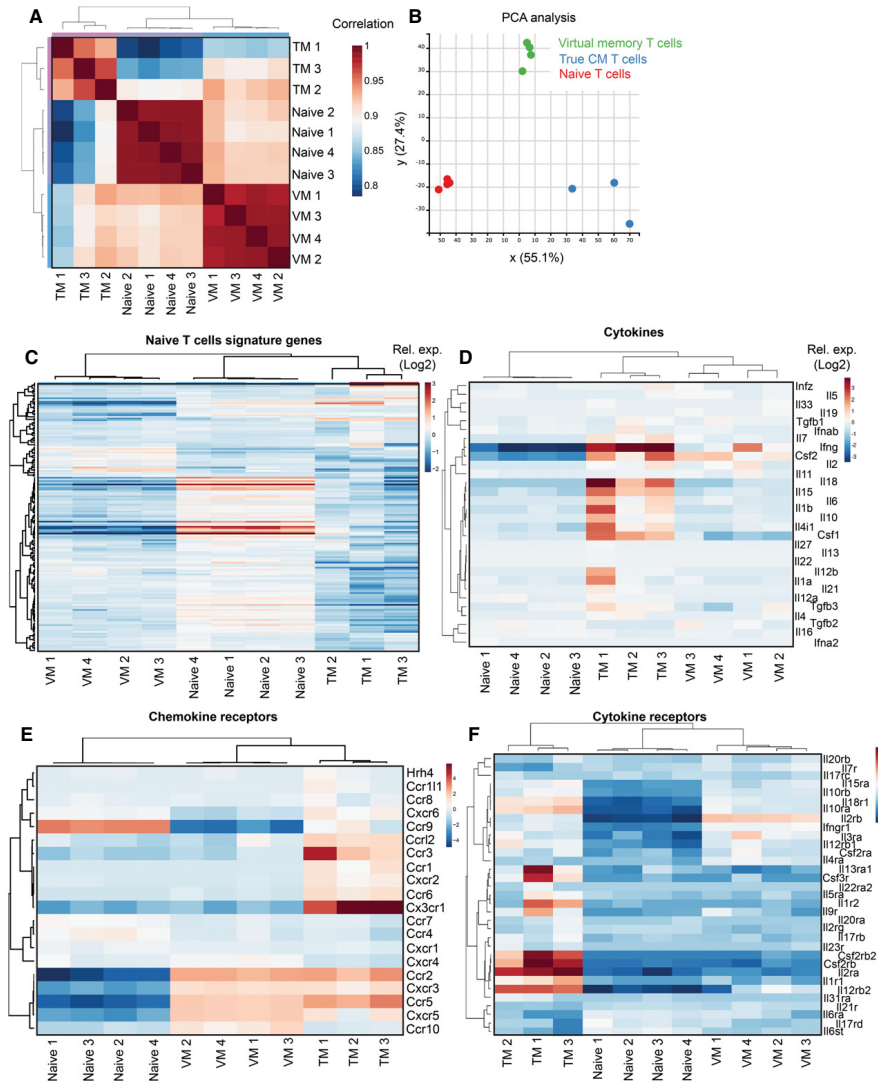
A LN cells isolated from polyclonal CD8WT and CD8.4 mice were stimulated with 10 ng/ml PMA and 1.5  $\mu$ M ionomycin or left untreated for 5 h in the presence of BD Golgi Stop and the percentage of IFN $\gamma$ -producing cells was determined by flow cytometry. The cells were gated as CD8<sup>+</sup> and further divided into CD44<sup>+</sup> and CD44<sup>-</sup> populations. Mean  $\pm$  SEM. *n* = 4 independent experiments.

B Quantification of the frequency of CD122<sup>hi</sup> CD49d<sup>+</sup> VM and CD122<sup>low</sup> CD49d<sup>+</sup> true memory cells among CD8<sup>+</sup> CD44<sup>+</sup> CD62L<sup>+</sup> CM T cells isolated from LN is shown. Mean, *n* = 9–15 mice per group from four independent experiments. Statistical significance was determined using two-tailed Mann–Whitney test.



**Figure EV3. Differences in TCR repertoires between naïve and VM T cells, related to Fig 3.**

- A Alternative gating strategy for the same samples as shown in Fig 3B–D (T cells from Vβ5 mice). A representative experiment out of eight in total.
- B, C The expression of CD5 on CD8<sup>+</sup> K<sup>O</sup>-OVA-4mer<sup>+</sup> CD8<sup>+</sup> Va2<sup>+</sup> or Va8.3<sup>+</sup> cells or total CD8<sup>+</sup> K<sup>O</sup>-OVA-4mer<sup>+</sup> isolated from LN and the spleen was determined by flow cytometry. Relative MFI CD5 levels were quantified (CD5 levels on CD8<sup>+</sup> K<sup>O</sup>-OVA-4mer<sup>+</sup> Va8.3<sup>+</sup> were arbitrarily set as 1). Mean + SD, n = 3 independent experiments. Statistical significance was determined using two-tailed one-value t-test.
- D TCRα sequences from Fig 3F were analyzed for TRAJ usage. Means + SEM. n = 4 independent experiments. Statistical significance was determined by chi-square test.
- E Schematic representation of the generation and analysis of retrogenic monoclonal T-cell subsets.
- F Frequency of VM T cells among monoclonal populations expressing TCR clones V14-C2, V14-C7, and OT-I generated as in Fig 3G.
- G CD5 levels on naïve monoclonal T cells expressing V14-C2, V14-C7, and OT-I. Representative mice out of 9–14 in total from two to four independent experiments.



**Figure EV4. Gene expression analysis of naive, VM, and TM T cells, related to Fig 4.**

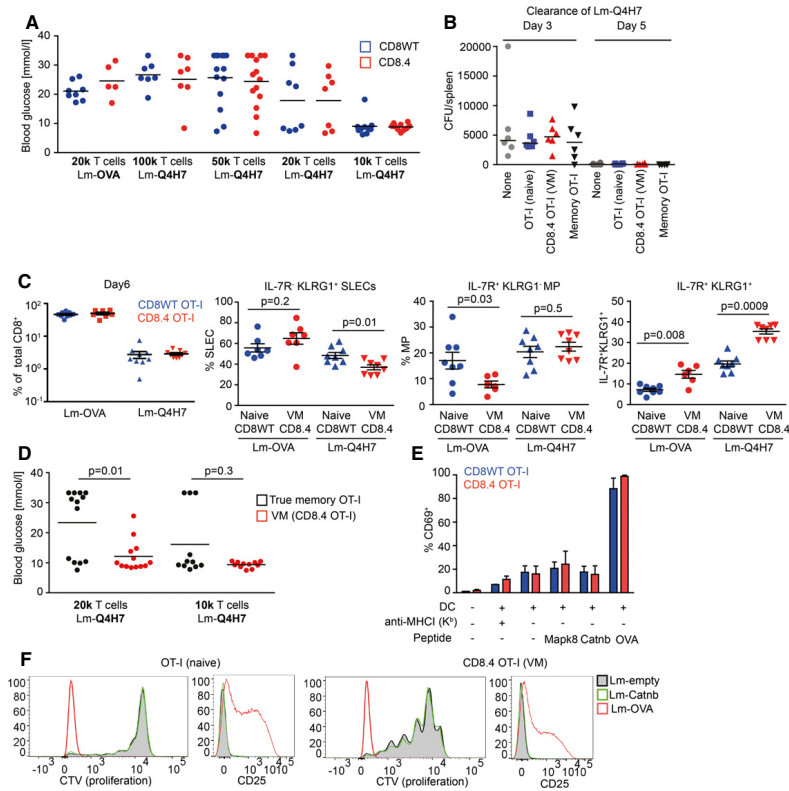
Transcriptomes of naive ( $n = 4$ ), VM ( $n = 4$ ), and TM ( $n = 3$ ) CD8<sup>+</sup> T cells were analyzed by deep RNA sequencing.

A Correlation of the gene expression between individual samples.

B PCA analysis between the samples.

C-F Enrichment of CD8<sup>+</sup> naive signature genes (as revealed by previous studies) (C), cytokine encoding genes (D), chemokine receptor encoding genes (E), and cytokine receptor encoding genes (F) in naive, VM, and true CM T cells.





**Figure EV5. Functional characterization of naïve, VM, and TM T cells, related to Fig 5.**


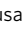


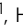



- A** Indicated number of CD8WT OT-I or CD8.4 OT-I T cells were adoptively transferred into RIP-OVA hosts, which were infected with Lm-OVA or -Q4H7 1 day later. Blood glucose was measured 7 days after the infection.  $n = 5-11$  mice per group in 3-6 independent experiments. These are the same experiments as in Fig 5A. Mean is indicated.
- B** FACS-sorted  $1 \times 10^4$  naïve CD8WT OT-I, CD8.4 OT-I (VM), sorted true memory OT-I T cells or no T cells were adoptively transferred into Ly5.1 C57Bl/6 mice followed by infection with 5,000 CFU Lm-Q4H7. Total Lm-Q4H7 CFU counts in the spleen were quantified on day 3 and day 5 post-infection.  $n = 6$  mice in two independent experiments.
- C** Quantification of the experiment shown in Fig 5E and F. Percentage of donor OT-I and CD8.4 OT-I T cells among all CD8<sup>+</sup> T cells is shown. Percentage of short-lived effector cells (IL-7R<sup>+</sup> KLRG1<sup>+</sup>), memory precursors (IL-7R<sup>+</sup> KLRG1<sup>-</sup>), and double-positive cells IL-7R<sup>+</sup> KLRG1<sup>+</sup> among the donor cells are shown. Statistical significance was calculated using Mann-Whitney test.  $n = 7$  (CD8.4 OT-I + Lm-OVA) or 9 (the other three experimental conditions) in four independent experiments.
- D** Indicated number of CD8.4 OT-I or true memory OT-I T cells were adoptively transferred into RIP-OVA hosts, which were infected with Lm-Q4H7 1 day later. The glucose in the blood was measured on day 7 post-infection. Statistical significance was calculated using Mann-Whitney test  $n = 11$  ( $1 \times 10^4$  transferred cells) or 13 ( $2 \times 10^4$  transferred cells) mice per group in four independent experiments. These are the same experiments as in Fig 5H.
- E** OT-I or CD8.4 OT-I was cocultured with bone marrow dendritic cells that were pre-loaded or not with 10  $\mu$ M putative endogenous positive selecting peptides for OT-I T cells (Mapk8, AGYSFEK1; Cantb, RTYTYEK1) or with 0.1  $\mu$ M OVA peptide. Blocking of the MHC-I by adding anti-H2-K<sup>b</sup> antibody (clone Y3, 10  $\mu$ g/ml) was used as a negative control. Percentage of CD69<sup>+</sup> T cells in the overnight stimulation was quantified by flow cytometry. Mean  $\pm$  SEM.  $n = 2$  (MHC-I blocking) or 3 (all the other experimental conditions) independent experiments.
- F** CellTrace violet-loaded OT-I or CD8.4 OT-I T cells were adoptively transferred into Ly5.1 C57Bl/6 donors followed by infection with Lm-OVA ( $1 \times 10^4$  transferred cells), Lm-Catnb, or empty Lm (both  $1 \times 10^3$  transferred cells) 1 day later. Expression of activation marker CD25 and dilution of the proliferation dye in donor cells was examined on day 5 post-infection. Representative mice out of seven in total from three independent experiments are shown. The cells from the Lm-OVA infected mice are the same as used for the analysis in Fig 5C.



## **Attachment 4**

The Order and Logic of CD4 versus CD8  
Lineage Choice and Differentiation in Mouse  
Thymus

# The order and logic of CD4 versus CD8 lineage choice and differentiation in mouse thymus

Mohammad M. Karimi <sup>1,5</sup>, Ya Guo<sup>1,6</sup>, Xiaokai Cui<sup>1</sup>, Husayn A. Pallikonda <sup>1</sup>, Veronika Horková <sup>2</sup>, Yi-Fang Wang<sup>1</sup>, Sara Ruiz Gil<sup>3</sup>, Gustavo Rodriguez-Esteban<sup>3</sup>, Irene Robles-Rebollo<sup>1</sup>, Ludovica Bruno<sup>1</sup>, Radina Georgieva<sup>1</sup>, Bhavik Patel<sup>1</sup>, James Elliott<sup>1</sup>, Marian H. Dore<sup>1</sup>, Danielle Dauphars<sup>4</sup>, Michael S. Krangel<sup>4</sup>, Boris Lenhard <sup>1</sup>, Holger Heyn <sup>3</sup>, Amanda G. Fisher <sup>1</sup>, Ondřej Štěpánek <sup>2</sup> & Matthias Merkenschlager <sup>1</sup>✉

CD4 and CD8 mark helper and cytotoxic T cell lineages, respectively, and serve as coreceptors for MHC-restricted TCR recognition. How coreceptor expression is matched with TCR specificity is central to understanding CD4/CD8 lineage choice, but visualising coreceptor gene activity in individual selection intermediates has been technically challenging. It therefore remains unclear whether the sequence of coreceptor gene expression in selection intermediates follows a stereotypic pattern, or is responsive to signaling. Here we use single cell RNA sequencing (scRNA-seq) to classify mouse thymocyte selection intermediates by coreceptor gene expression. In the unperturbed thymus,  $Cd4^+Cd8a^-$  selection intermediates appear before  $Cd4^+Cd8a^+$  selection intermediates, but the timing of these subsets is flexible according to the strength of TCR signals. Our data show that selection intermediates discriminate MHC class prior to the loss of coreceptor expression and suggest a model where signal strength informs the timing of coreceptor gene activity and ultimately CD4/CD8 lineage choice.

<sup>1</sup>MRC London Institute of Medical Sciences, Institute of Clinical Sciences, Faculty of Medicine, Imperial College London, London, UK. <sup>2</sup>Laboratory of Adaptive Immunity, Institute of Molecular Genetics of the Czech Academy of Sciences, Prague, Czech Republic. <sup>3</sup>CNAG-CRG, Centre for Genomic Regulation (CRG), The Barcelona Institute of Science and Technology (BIST), Barcelona, Spain. <sup>4</sup>Department of Immunology, Duke University Medical Center, Durham, NC, USA. <sup>5</sup>Present address: Comprehensive Cancer Centre, School of Cancer & Pharmaceutical Sciences, Faculty of Life Sciences & Medicine, King's College London, London, UK. <sup>6</sup>Present address: School of Life Sciences and Biotechnology, Shanghai Jiao Tong University, Shanghai, China. ✉email: [matthias.merkenschlager@lms.mrc.ac.uk](mailto:matthias.merkenschlager@lms.mrc.ac.uk)

**C**D4 helper T cells and CD8 cytotoxic T cells are the two principal T cell lineages in the mammalian immune system. Although distinct in phenotype and function, CD4 and CD8 T cells arise in the thymus from bi-potential, CD4<sup>+</sup> CD8<sup>+</sup> double-positive (DP) progenitors. CD4/CD8 lineage choice is critical for the generation and selection of the T cell receptor (TCR) repertoire, and represents one of the most intensely studied and enigmatic examples of a binary lineage decision. TCR rearrangement is fundamentally stochastic, and the functional properties of the newly generated TCR repertoire are established empirically during positive and negative selection. CD4 and CD8 act as coreceptors for TCR recognition restricted by major histocompatibility complex (MHC) class II or class I, respectively. Competing models have been proposed for how coreceptor expression is matched with TCR specificity, and differ with respect to the mode of lineage branching and the role of TCR signal strength in MHC class discrimination. One class of models envisage symmetric branching of the CD4 and CD8 lineages where lineage choice is either instructive<sup>1</sup> or stochastic<sup>2,3</sup>. Alternatively, kinetic signalling models posit that CD4/CD8 lineage choice occurs in a series of sequential steps whereby TCR-signalled thymocytes initially downregulate *Cd8* to audition for the CD4 lineage, and switch coreceptor expression from *Cd4<sup>+</sup>Cd8<sup>-</sup>* to *Cd4<sup>+</sup>Cd8<sup>+</sup>* only if they experience a loss of CD8-dependent TCR signalling<sup>4–8</sup>. MHC class discrimination by signal strength is critical in instructive models<sup>1</sup>, but entirely dispensable in stochastic/selective models of CD4/CD8 lineage choice<sup>2,3</sup>. Proposals of CD4/CD8 lineage choice driven by signal strength and duration<sup>9–14</sup> have been largely superseded by the idea that MHC class discrimination is based solely on signal continuity during sequential expression of coreceptors<sup>4,6,7,15,16</sup>.

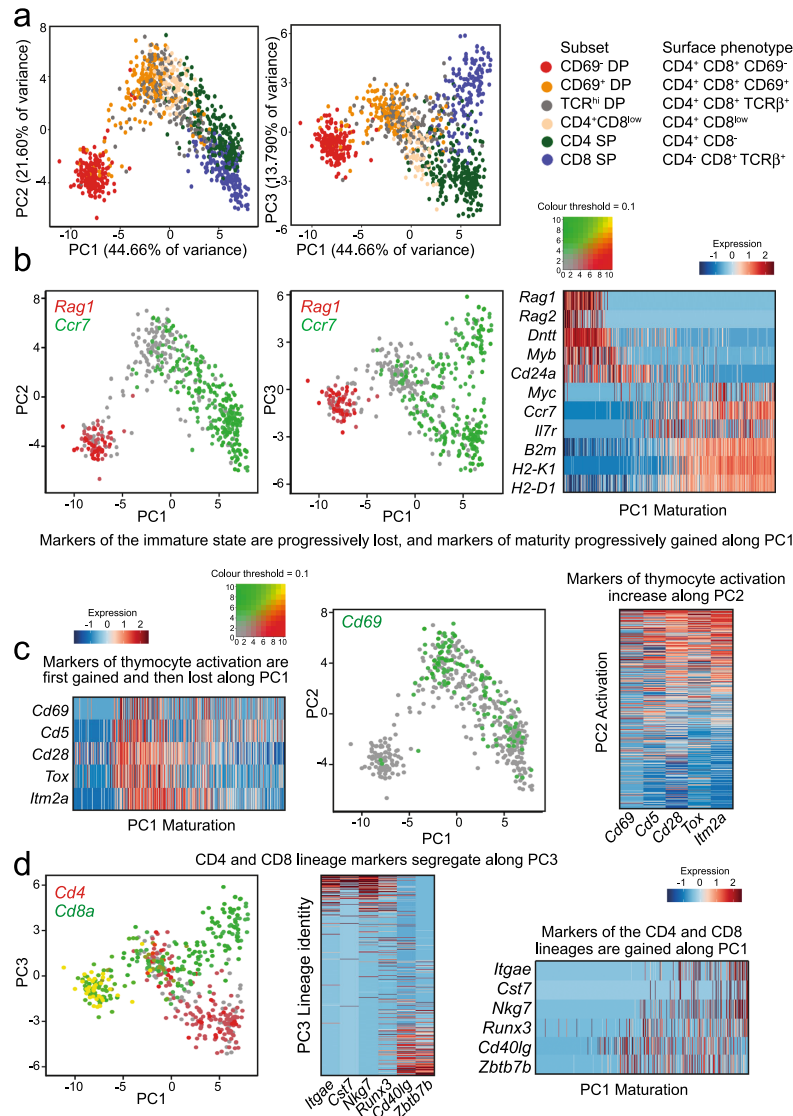
Lineage commitment occurs at the level of individual progenitor cells, and is therefore inherently difficult to study at the population level. The expression of *Cd4* and *Cd8* coreceptor genes by individual selection intermediates is central to understanding CD4/CD8 lineage choice, but has never been observed directly. Previous single-cell RNA-seq studies of the thymus have largely ignored cells in transition from bipotential progenitors to the CD4 SP or the CD8 SP stages<sup>17–19</sup>, in part because such selection intermediates are rare and make up only a few percent of cells in the thymus. High throughput scRNA-seq approaches may profile gene expression by large numbers of cells lack often the depth required to unambiguously assign *Cd4* and/or *Cd8* expression to individual selection intermediates, while scRNA-seq approaches that deliver sufficient depth have limited throughput.

Here we address this challenge by prospective isolation of selection intermediates combined with scRNA-seq of full length transcripts. This approach provides a direct view of *Cd4* and *Cd8a* coreceptor gene activity in individual selection intermediates within a framework of maturation, activation and lineage specification during CD4/CD8 lineage choice. The resulting data are broadly in line with models of sequential lineage determination by kinetic signalling, albeit with substantial refinements and modifications. In the unperturbed thymus, the order of coreceptor gene expression states is *Cd4<sup>+</sup>Cd8a<sup>+</sup>* followed by *Cd4<sup>+</sup>Cd8a<sup>-</sup>* and later by *Cd4<sup>-</sup>Cd8a<sup>+</sup>*, providing direct support for sequential coreceptor gene expression during CD4/CD8 lineage choice. Interestingly, however, perturbation experiments reveal that selection intermediates discriminate between MHC classes prior to the loss of *Cd4* or *Cd8* coreceptor expression, and accelerate their transition to the *Cd4<sup>-</sup>Cd8a<sup>+</sup>* state in response to weaker TCR signals in the absence of MHC class II. These findings suggest a model that links signal strength and the timing of coreceptor gene expression.

## Results

**scRNA-seq of CD4 CD8 lineage choice and differentiation.** We performed scRNA-seq of normal thymocytes from unmanipulated adult mice at steady-state. To address patterns of coreceptor gene activity and associated gene expression programs, we opted for deep sequencing of full-length transcripts by SMART-seq. This approach identifies thousands of transcripts per cell at sufficient depth to reliably call coreceptor expression by individual selection intermediates (see below). To capture sufficient numbers of selection intermediates, we isolated single cells representing thymocytes before (CD69<sup>-</sup> DP), during (CD69<sup>+</sup> DP, TCRβ<sup>hi</sup> DP, CD4<sup>+</sup> CD8<sup>low</sup>), and after lineage choice and differentiation (CD4 SP, TCRβ<sup>hi</sup> CD8 SP) from wild-type C57BL/6 mice (Supplementary Fig. 1). Full-length single-cell RNA-seq libraries were prepared and sequenced, identifying thousands of transcripts per cell (Supplementary Table 1, see Methods). We identified highly variable genes (Supplementary Data 1) and removed *Cd4*, *Cd8a/b1* for later use in the classification of selection intermediates (see below). Principal component analysis (PCA) showed that PC1, PC2 and PC3 accounted for 44.66%, 21.60% and 13.79% of differential gene expression among the first five PCs (Fig. 1a). The first principal component, PC1, positioned sorted thymocyte subsets in order of maturity: pre-selection thymocytes (CD69<sup>-</sup> DP, red) on the left, CD4 SP (green) and CD8 SP (blue) on the right. Selection intermediates (CD69<sup>+</sup> DP, orange, TCRβ<sup>hi</sup> DP, grey, and CD4<sup>+</sup> CD8<sup>low</sup>, yellow) were in the centre of PC1 (Fig. 1a). The observed patterns were highly reproducible between replicates (Supplementary Fig. 2).

**scRNA-seq captures maturation, activation and lineage identity as the first three principal components of CD4/CD8 lineage choice and differentiation.** To validate the approach, we examined differentially expressed genes with well-defined expression patterns during CD4/CD8 lineage choice and differentiation (Supplementary Fig. 3a and Supplementary Data 2). *Rag1* and *Dnnt1* are active in pre-selection DPs where they contribute to the somatic rearrangement of the *Tcrα/d* locus. scRNA-seq found highly correlated *Rag1* and *Dnnt1* expression in individual cells ( $R = 0.75$ ,  $P < 2.2e-16$ ; Supplementary Fig. 3b). The expression of genes that are highly active in pre-selection DP thymocytes (e.g. *Rag1*, *Dnnt1*, *Cd24a*) progressively decreased along PC1 (Fig. 1b). The expression of genes associated with thymocyte maturation such as *Ccr7*, *Il7r* *B2m* and the MHC class I genes *H2-D1* and *H2-K1* progressively increased along PC1 (Fig. 1c). *Rag1* and *Dnnt1* are silenced by TCR signals, and their expression is superseded by activation markers such as *Cd69*. *Rag1* and *Cd69* were anti-correlated in individual cells by scRNA-seq ( $R = -0.27$ ,  $P = 1.7e-09$ , Supplementary Fig. 3c). Maturation markers such as *Ccr7* and *Il7r* were positively correlated in individual cells ( $R = 0.38$ ,  $P < 2.2e-16$ , Supplementary Fig. 3d). Genes that showed non-linear behaviour during thymocyte differentiation featured strongly in the second principal component, PC2, which reflects the transient induction and repression of genes by TCR signalling such as *Cd69*, *Cd5*, *Tox*, *Cd28* and *Itim2a* (Fig. 1c). *Cd4* and *Cd8a* were co-expressed in pre-selection DP but mutually exclusive in CD4 and CD8 SP (Supplementary Fig. 3e). *Cd4*, *Cd8a* and other markers of the CD4 and CD8 lineages segregated in the third principal component PC3, which showed a branched trajectory from the pre-selection DP stage (CD69<sup>-</sup> DP) through intermediate CD69<sup>+</sup> DP and CD4<sup>+</sup> CD8<sup>low</sup> stages towards CD4 and CD8 single-positive populations (Fig. 1d). Although maturation, activation and lineage identity are recognised as central components of lineage choice and differentiation in the thymus, our analysis quantifies the relative contribution of each (maturation, activation and lineage identity) to

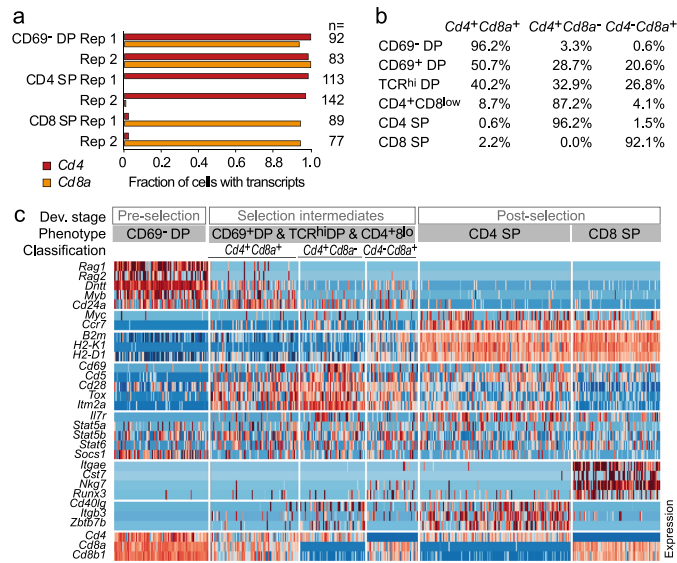


the overall variance of gene expression, and shows that scRNA-seq data alone are sufficient to derive a coherent framework for CD4/CD8 lineage choice and differentiation.

To challenge the interpretation of PC1 as maturation, PC2 as activation and PC3 as CD4/CD8 lineage identity, we identified genes associated with thymocyte maturation, activation and CD4/CD8 lineage choice derived from population RNA-seq for use as an external reference. We defined activation genes as genes that

were transiently up- or downregulated between the CD69<sup>-</sup> DP stage and the CD4 and CD8 SP stages of differentiation ( $P < 0.05$ ,  $n = 524$ ), and CD4 and CD8 lineage genes as genes that were differentially expressed between CD69<sup>-</sup> CD4SP and TCR<sup>hi</sup> CD8SP ( $P < 0.05$ ,  $n = 344$ ; Supplementary Data 3). We then calculated the enrichment of activation genes and lineage genes. PC1 was not enriched for activation ( $P = 0.327$ , Fisher Exact test, top 1000 highly correlated genes with PC1) and moderately

**Fig. 1 scRNA-seq captures maturation, activation and lineage identity as principal components of CD4/CD8 lineage choice and differentiation.** **a** Highly variable genes in the scRNA-seq data were identified and principal component analysis (PCA) was performed, excluding *Cd4*, *Cd8a* and *Cd8b1*. PC1 versus PC2 (left) and PC1 versus PC3 (right) are shown, and the percentage of variance explained by each PC is indicated as a percentage of the first five PCs. PC4 and PC5 explained 11.45% and 8.50% of variance within the first five PCs and 5.82% and 4.32% of total variance, respectively. Sorted subsets are coloured as indicated in the key. Cell numbers are shown in Supplementary Table 2. Source data are provided as a Source Data file. **b** PC1 reflects progressive thymocyte maturation. A two-colour dot plot projected onto a map of PC1 versus PC2 shows expression of *Rag1*(red), which was confined to pre-selection thymocytes, and *Ccr7*, which was acquired during maturation. A heat map of key thymocyte maturation genes (right) shows how markers of immature thymocytes are progressively lost along PC1 and markers of mature thymocytes are progressively gained along PC1. Source data are provided as a Source Data file. **c** PC2 reflects transient thymocyte activation. Expression of the activation marker *Cd69* (green) projected onto a map of PC1 versus PC2. Heat maps of key thymocyte activation genes (right) show how markers of thymocyte activation are progressively gained along PC2. The same markers show non-linear behaviour along PC1, as they are first gained and then lost during thymocyte maturation. Source data are provided as a Source Data file. **d** PC3 reflects CD4/CD8 lineage identity. Expression of *Cd4* (red) and *Cd8a* (green), as a two-colour dot plot projected onto a map of PC1 versus PC3. A heat map of CD4- and CD8 lineage-specific genes (right) shows how PC3 segregates markers of the CD4 and CD8 lineages. Source data are provided as a Source Data file.



**Fig. 2 scRNA-seq reliably detects the coreceptor transcripts *Cd4* and *Cd8a*.** **a** scRNA-seq detection frequencies of *Cd4* (red) and *Cd8a* (orange) in sorted CD69<sup>-</sup> DP, CD4 SP and CD8 SP wild-type thymocytes. Bars of the same colour represent independent biological replicates. Cell numbers are listed in Supplementary Table 2. Source data are provided as a Source Data file. **b** Representation of *Cd4*<sup>+</sup>*Cd8a*<sup>+</sup>, *Cd4*<sup>+</sup>*Cd8a*<sup>-</sup> and *Cd4*<sup>-</sup>*Cd8a*<sup>+</sup> coreceptor gene expression patterns in by CD69<sup>-</sup> DP, CD69<sup>+</sup> DP, TCR<sup>hi</sup> DP, CD4<sup>+</sup>CD8<sup>low</sup>, CD4 SP and CD8 SP wild-type thymocytes. **c** Cells (columns) are grouped by developmental stage (pre-selection, selection intermediates and post-selection) and cell surface phenotype. CD69<sup>-</sup> DP represent pre-selection thymocytes, pooled CD69<sup>+</sup> DP, TCR<sup>hi</sup> DP and CD4<sup>+</sup>CD8<sup>low</sup> represent selection intermediates, CD4 SP, TCR<sup>hi</sup> CD8 SP represent post-selection thymocytes. Selection intermediates are classified into *Cd4*<sup>+</sup>*Cd8a*<sup>+</sup>, *Cd4*<sup>+</sup>*Cd8a*<sup>-</sup> and *Cd4*<sup>-</sup>*Cd8a*<sup>+</sup> based on scRNA-seq detection of *Cd4* and *Cd8a*. The data shown are for replicate 2. See Supplementary Table 7 for cell numbers.

enriched for CD4/CD8 lineage ( $P = 3.00e-06$ , Fisher Exact test, top 1000 highly correlated genes with PC1). PC2 was strongly enriched for activation ( $P = 2.22e-12$ , Fisher Exact test, top 1000 highly correlated genes with PC2), and only weakly for CD4/CD8 lineage ( $P = 0.0021$ , Fisher Exact test, top 1000 highly correlated genes with PC3). Finally, PC3 was strongly enriched for CD4/CD8 lineage ( $P = 1.15e-9$ , Fisher Exact test, top 1000 highly correlated genes with PC3), and only weakly for activation ( $P = 0.0055$ , Fisher Exact test, top 1000 highly correlated genes with PC3). This analysis validated that PC2 and PC3 reflect activation, and CD4/CD8 lineage identity, respectively.

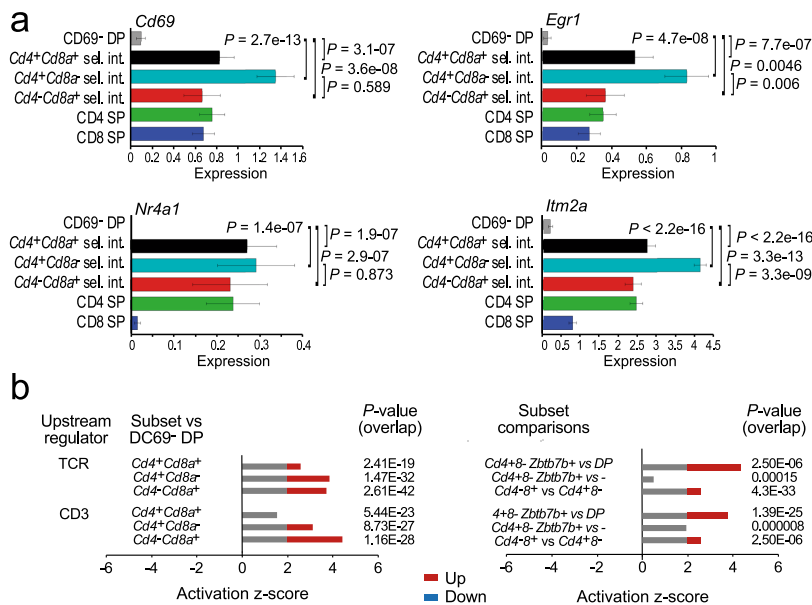
**Classification of selection intermediates by *Cd4* and *Cd8a* coreceptor gene expression.** We next examined the ability of scRNA-seq to reliably detect coreceptor transcripts in pre- and post-selection thymocytes. scRNA-seq found expression of both *Cd4* and *Cd8a* (*Cd4* and *Cd8a*) in 93.5% (93.5% *Cd4*<sup>+</sup> *Cd8a*<sup>+</sup>, replicate 1) and 98.8% (98.8% *Cd4*<sup>+</sup> *Cd8a*<sup>+</sup>, replicate 2) of individual pre-selection DP thymocytes. scRNA-seq detected *Cd4* but not *Cd8a* in 98.6% (98.6% *Cd4*<sup>+</sup> *Cd8a*<sup>-</sup>, replicate 1) and 96.2% (96.2% *Cd4*<sup>+</sup> *Cd8a*<sup>-</sup>, replicate 2) of CD4 SP and *Cd8a* but not *Cd4* in 92.1% of CD8 SP (92.1% *Cd4*<sup>-</sup> *Cd8a*<sup>+</sup>, replicates 1 and 2, Fig. 2a). These data indicate that scRNA-seq detects

appropriate constellations of coreceptor transcripts in the vast majority of pre- and post-selection thymocytes, and can therefore be used to classify selection intermediates into  $Cd4^+ Cd8a^+$ ,  $Cd4^+ Cd8a^-$ , and  $Cd4^- Cd8a^+$  (Fig. 2b). This allowed us to identify transcriptional programs of individual selection intermediates of defined coreceptor status (Fig. 2c, see Supplementary Data 4 for an analysis of differential gene expression between selection intermediates classified by coreceptor status and Supplementary Fig. 4 for a heatmap of gene expression by individual selection intermediates in MHC class II<sup>-/-</sup> thymus).

**Expression of TCR and cytokine signalling genes by selection intermediates of defined coreceptor expression status.** Kinetic signalling models predict that selection intermediates that terminate  $Cd8$  expression react to a loss of CD8-dependent TCR signalling by increased responsiveness to cytokines, which results in the expression of *Runx3* and the reversal of coreceptor gene expression<sup>4</sup>. In contrast to models where the differentiation of selection intermediates towards the CD8 lineage following CD4 to CD8 coreceptor reversal is exclusively driven by cytokine signals<sup>20</sup>, the expression of TCR-driven activation genes such as *Cd69*, *Egr1*, *Nr4a1* and *Itm2a* was significantly higher in  $Cd4^+ Cd8a^+$ ,  $Cd4^+ Cd8a^-$  and  $Cd4^- Cd8a^+$  selection intermediates than in pre-selection DP (Fig. 3a).  $Cd4^- Cd8a^+$  selection intermediates expressed slightly less *Cd69*, *Egr1* and *Itm2a*, (but not *Nr4a1*) than  $Cd4^+ Cd8a^-$  selection intermediates, but differences in TCR signalling gene expression between subsets of selection

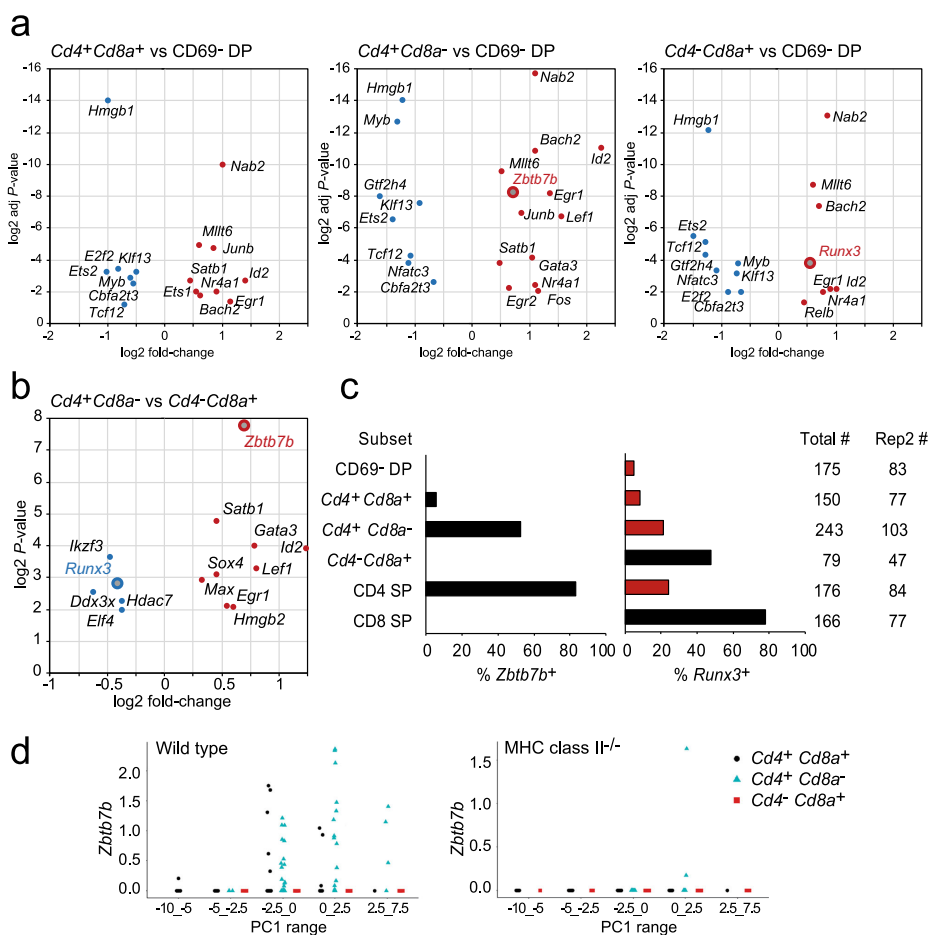
intermediates were minor compared to the highly significant changes from pre-selection DP to selection intermediates (Fig. 3a). IPA pathway analysis indicated significant activation of pathways downstream of the TCR and of CD3 in both  $Cd4^+ Cd8a^-$  and  $Cd4^- Cd8a^+$  selection intermediates (Fig. 3b, left), again with minor differences between  $Cd4^-$  and  $Cd8a^-$ -defined subsets of selection intermediates (Fig. 3b, right). Together, these data indicate active TCR signalling in both  $Cd4^+ Cd8a^-$  and  $Cd4^- Cd8a^+$  selection intermediates.

Expression of the *Il7r* gene was significantly elevated in  $Cd4^+ Cd8a^+$ ,  $Cd4^+ Cd8a^-$  and  $Cd4^- Cd8a^+$  selection intermediates compared to pre-selection DP (Supplementary Fig. 5a). Conversely, expression of *Socs1*, the gene encoding the suppressor of cytokine signalling SOCS1, was significantly reduced in  $Cd4^+ Cd8a^-$  and  $Cd4^- Cd8a^+$  selection intermediates compared to pre-selection DP (Supplementary Fig. 5a). The expression of *Gimap* genes, which are targets of IL7R signalling, was also significantly elevated in  $Cd4^+ Cd8a^+$ ,  $Cd4^+ Cd8a^-$  and  $Cd4^- Cd8a^+$  selection intermediates compared to pre-selection DP (Supplementary Fig. 5a). Members of the JAK and STAT families and a range of cytokines showed evidence for activation (Supplementary Fig. 5b), and so did TGFβ/SMAD and IFNγ, which are among the cytokines that can support the differentiation and/or survival of CD8 lineage thymocytes<sup>20</sup> (Supplementary Fig. 5b). Significant activation scores downstream of STATs and IFNγ in  $Cd4^- Cd8a^+$  selection intermediates and of JAKs, TGFβ/SMAD and other cytokines in both  $Cd4^+ Cd8a^-$  and  $Cd4^- Cd8a^+$  subsets suggest that cytokine signalling pathway activity is



**Fig. 3 Expression of TCR signalling genes by selection intermediates of defined coreceptor gene expression status.** **a** Expression of TCR activation genes *Cd69*, *Egr1*, *Nr4a1* and *Itm2a* by selection intermediates of the indicated coreceptor status. Means and standard errors are shown. P-values are derived by two-sided Wilcoxon rank-sum test. Cell numbers are listed in Supplementary Tables 2 and 3. Source data are provided as a Source Data file. **b** IPA analysis of pathway activity downstream of the TCR and of CD3. Activation z-scores above 2 and below -2 are considered significant. Selection intermediates versus CD69<sup>-</sup> DP is shown on the left. Where available, comparisons between subsets of selection intermediates are shown on the right. Source data are provided as a Source Data file.





**Fig. 4** Lineage-specific expression of *Zbtb7b* but not *Runx3*. **a** Differential expression of transcriptional regulators in *Cd4<sup>+</sup>Cd8a<sup>+</sup>* (left), *Cd4<sup>+</sup>Cd8a<sup>-</sup>* (middle) and *Cd4<sup>-</sup>Cd8a<sup>+</sup>* selection intermediates (right) compared to CD69<sup>-</sup> DP. Shown are log<sub>2</sub> fold-changes and adjusted *P*-values (two-sided Wilcoxon rank-sum test). *Zbtb7b* and *Runx3* are highlighted. Source data are provided as a Source Data file. **b** Differential expression of transcriptional regulators in *Cd4<sup>+</sup>Cd8a<sup>-</sup>* versus *Cd4<sup>-</sup>Cd8a<sup>+</sup>* selection intermediates. Shown are log<sub>2</sub> fold-changes and nominal *P*-values (two-sided Wilcoxon rank-sum test). *Zbtb7b* and *Runx3* are highlighted. Source data are provided as a Source Data file. **c** The frequency of *Zbtb7b* (left) and *Runx3* expression (right) in the indicated thymocyte subsets is shown for wild-type replicate 2. Black: 'lineage-appropriate' expression. Red: 'lineage-inappropriate' expression. Source data are provided as a Source Data file. **d** The expression of *Zbtb7b* by selection intermediates of the indicated coreceptor gene expression status for different PC1 ranges in wild type (left) and MHC class II<sup>-/-</sup> thymus (right). Source data are provided as a Source Data file.

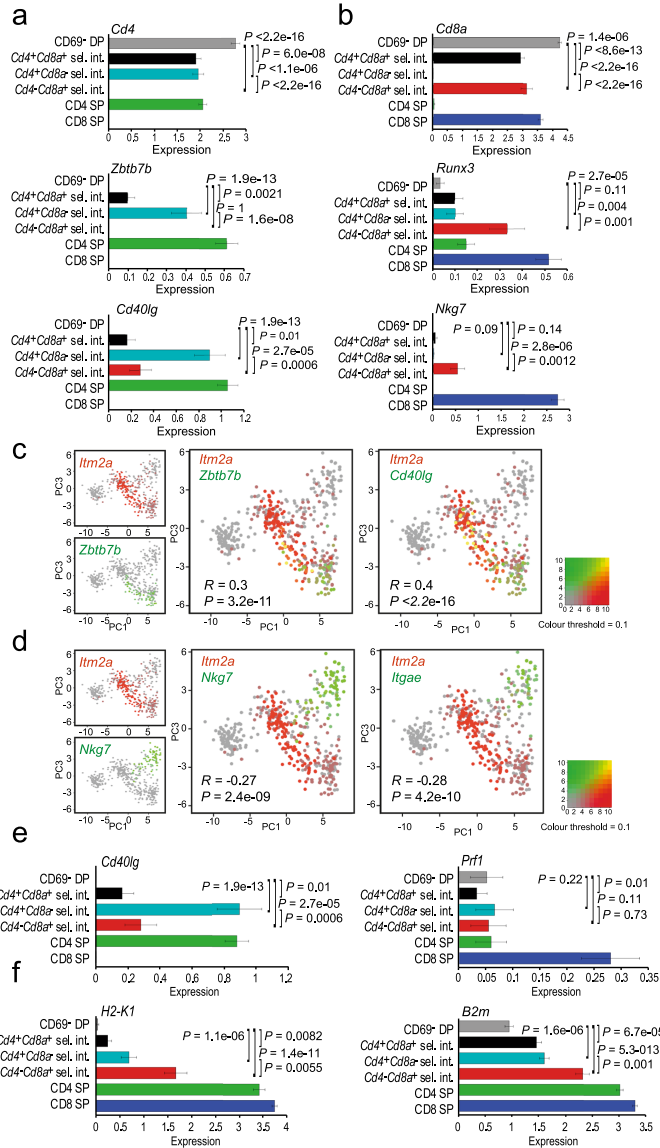
not restricted to *Cd4<sup>-</sup> Cd8a<sup>+</sup>* selection intermediates, and therefore not strictly linked to coreceptor reversal<sup>21–23</sup>.

**Lineage-specific expression of *Zbtb7b* but not *Runx3*.** The transcription factors *Zbtb7b* and *Runx3* are central to CD4 and CD8 lineage specification, respectively<sup>24–27</sup>. In wild-type selection intermediates, *Zbtb7b* was significantly upregulated in the *Cd4<sup>+</sup> Cd8a<sup>-</sup>* subset, while *Runx3* was significantly upregulated in the *Cd4<sup>-</sup> Cd8a<sup>+</sup>* subset of selection intermediates (Fig. 4a). Accordingly, *Zbtb7b* and *Runx3* were differentially expressed

between *Cd4<sup>+</sup> Cd8a<sup>-</sup>* versus *Cd4<sup>-</sup> Cd8a<sup>+</sup>* selection intermediates (Fig. 5b). *Zbtb7b* was expressed in *Cd4<sup>+</sup> Cd8a<sup>+</sup>* and *Cd4<sup>+</sup> Cd8a<sup>-</sup>* selection intermediates and CD4 SP thymocytes (Fig. 4c, d), but was completely absent from pre-selection DP, *Cd4<sup>-</sup> Cd8a<sup>+</sup>* selection intermediates, and CD8 SP thymocytes (Fig. 4c). *Zbtb7b* was almost completely absent from selection intermediates in MHC class II-deficient thymi (Fig. 4d), indicating that MHC class II was required for the expression of *Zbtb7b* by selection intermediates<sup>28</sup>. Hence, *Zbtb7b* expression was restricted to the CD4 lineage, and its induction required MHC class II, consistent with

its role as a CD4 lineage-specifying transcription factor<sup>24,25,28</sup>. In contrast, *Runx3* transcripts were detected not only in CD8 lineage cells, but also in CD4 SP, *Cd4<sup>+</sup> Cd8a<sup>+</sup>* and *Cd4<sup>+</sup> Cd8a<sup>-</sup>* selection intermediates (Fig. 4c). These *Runx3* transcripts originated predominantly from the distal *Runx3* promoter. *Runx3* expression in CD4 lineage cells (CD4 SP and *Cd4<sup>+</sup> Cd8a<sup>-</sup>* selection intermediates) was significantly more frequent (63/419) than *Zbtb7b*

expression in CD8 lineage cells (0/245 CD8 SP and *Cd4<sup>-</sup> Cd8a<sup>+</sup>* selection intermediates,  $P = 4.58e-14$ , two-sided Fisher's Exact test for count data). According to kinetic signalling models, the expression of *Runx3* is linked to coreceptor reversal from *Cd4<sup>+</sup> Cd8a<sup>-</sup>* to *Cd4<sup>-</sup> Cd8a<sup>+</sup>* and to CD8 lineage differentiation<sup>4</sup>. The presence of *Runx3* in *Cd4<sup>+</sup> Cd8a<sup>+</sup>* and *Cd4<sup>+</sup> Cd8a<sup>-</sup>* selection intermediates and CD4 SP thymocytes indicates that *Runx3*



**Fig. 5 CD4 and CD8 lineage characteristics are established at different times during CD4/CD8 lineage choice and differentiation.** **a** Expression of *Cd4*, *Zbtb7b* and *Cd40lg* by selection intermediates of the indicated coreceptor status. Means and standard errors are shown. *P*-values are derived by two-sided Wilcoxon rank-sum test. Cell numbers are listed in Supplementary Tables 2 and 3. Source data are provided as a Source Data file. **b** Expression of *Cd8a*, *Runx3* and *Nkg7* by selection intermediates of the indicated coreceptor status. Means and standard errors are shown. *P*-values are derived by two-sided Wilcoxon rank-sum test. Cell numbers are listed in Supplementary Tables 2 and 3. Source data are provided as a Source Data file. **c** Co-expression of the activation marker *Itm2a* with the CD4 lineage marker *Zbtb7b* and of *Cd40lg* ( $R = 0.30$ ,  $P = 3.2 \times 10^{-11}$  and  $R = 0.40$ ,  $P < 2.2 \times 10^{-16}$ , respectively). See Supplementary Fig. 6a for a depiction of the positive correlation between *Itm2a* and the CD4 lineage markers *Zbtb7b* and *Cd40lg*. Source data are provided as a Source Data file. **d** Lack of co-expression of the activation marker *Itm2a* with the CD8 lineage markers *Nkg7* and *Itgae* ( $R = -0.27$ ,  $P = 2.4 \times 10^{-9}$  and  $R = -0.28$ ,  $P = 4.2 \times 10^{-10}$ , respectively). See Supplementary Fig. 6b for a depiction of the negative correlation between *Itm2a* and the CD8 lineage markers *Nkg7* and *Itgae*. Source data are provided as a Source Data file. **e** Mean expression of *Cd40lg*, involved in T cell help, and the cytotoxic T cell marker *Prfl* in selection intermediates with distinct coreceptor gene expression. Means and standard errors are shown. *P*-values are derived by two-sided Wilcoxon rank-sum test. Cell numbers are listed in Supplementary Tables 2 and 3. Source data are provided as a Source Data file. **f** Mean expression of *H2-K1* and *B2m* in selection intermediates with distinct coreceptor gene expression. Means and standard errors are shown. *P*-values are derived by two-sided Wilcoxon rank-sum test. Cell numbers are listed in Supplementary Tables 2 and 3. Source data are provided as a Source Data file.

expression is not strictly lineage-specific, and that the induction of *Runx3* is not linked to coreceptor reversal.

#### CD4 and CD8 lineage characteristics are established at different times during CD4/CD8 lineage choice and differentiation.

Gene expression in  $Cd4^+ Cd8a^-$  and  $Cd4^- Cd8a^+$  subsets of selection intermediates showed a modest ( $R = 0.17$ ) but highly significant correlation with CD4 SP and CD8 SP populations, respectively (Supplementary Table 4) with overall coherence in the direction of regulation ( $P < 2.2 \times 10^{-16}$ , Asymptotic Linear-by-Linear Association Test).  $Cd4^+ Cd8a^-$  selection intermediates showed higher expression of the CD4 lineage marker *Zbtb7b* and of *Cd40lg* than  $Cd4^- Cd8a^+$  selection intermediates (Fig. 5a). By contrast,  $Cd4^- Cd8a^+$  selection intermediates showed higher expression of *Runx3* and the CD8 lineage marker *Nkg7* (Fig. 5b). These data indicate that  $Cd4^+ Cd8a^-$  selection intermediates have features of CD4 lineage cells, and  $Cd4^- Cd8a^+$  selection intermediates have features of CD8 lineage cells.

To address the temporal relationship between thymocyte activation and lineage specification, we examined the dynamics of CD4 and CD8 lineage marker gene expression at the single-cell level. We found that the CD4 lineage marker *Zbtb7b* and also *Cd40lg* were frequently expressed alongside activation markers, as illustrated by *Itm2a* (Fig. 5c). The expression of *Zbtb7b* and *Cd40lg* was positively correlated with *Itm2a* (Fig. 5c and Supplementary Fig. 6a). In contrast, CD8 lineage markers such as *Nkg7* and *Itgae* were upregulated largely after the expression of *Itm2a* had subsided, and the expression of *Nkg7* and *Itgae* was negatively correlated with *Itm2a* (Fig. 5d and Supplementary Fig. 6b). *Cd40lg* (CD154) is a mediator of T cell help<sup>29</sup>, and acquired by  $Cd4^+ Cd8a^-$  selection intermediates (Fig. 5e). Granzyme B (*Gzmb*) and perforin (*Prfl*) mediate cytotoxic T cell functions. While *Gzmb* expression is acquired by CD8 T cells post-thymically, *Prfl* expression was largely restricted to CD8 SP (Fig. 5e). The same was seen for *Itgae* (CD103), which forms a heterodimer that interacts with E-cadherin and facilitates cytotoxic functions<sup>30,31</sup>. Hence, the CD4 lineage characteristics examined here were acquired concomitantly with activation during CD4/CD8 lineage choice and differentiation, whereas CD8 lineage characteristics were acquired largely subsequent to activation. To ask how patterns of coreceptor expression relate to maturation state, we compared the expression of *H2-K1* and *B2m* between  $Cd4^+ Cd8a^-$  and  $Cd4^- Cd8a^+$  selection intermediates. *H2-K1* and *B2m* were more highly expressed in  $Cd4^- Cd8a^+$  than in  $Cd4^+ Cd8a^+$  or  $Cd4^+ Cd8a^-$  selection intermediates (Fig. 5f), suggesting that  $Cd4^- Cd8a^+$  selection intermediates are more mature than the  $Cd4^+ Cd8a^+$  or  $Cd4^+ Cd8a^-$  subsets.

#### Waves of coreceptor gene expression during CD4/CD8 lineage choice and differentiation.

To address the order and the timing of coreceptor gene activity patterns during CD4/CD8 lineage choice and differentiation, we projected the expression of *Cd4* and *Cd8a* onto the principal components PC1 versus PC2 (Fig. 6a), and PC1 versus PC3 (Fig. 6b). Visual inspection suggested that  $Cd4^+ Cd8a^-$  cells appear before  $Cd4^- Cd8a^+$  cells along the maturation axis PC1. This was supported by average Euclidian distances between subsets of selection intermediates and SP thymocytes (PC1 and PC3:  $Cd4^+ Cd8a^-$  selection intermediates: 6.08 to CD4 SP, 6.93 to CD8 SP;  $Cd4^- Cd8a^+$  selection intermediates: 5.43 to CD4 and CD8 SP). To formally evaluate the order of  $Cd4^+ Cd8a^+$ ,  $Cd4^+ Cd8a^-$  and  $Cd4^- Cd8a^+$  selection intermediates, we plotted their frequencies and compared their position along the PC1 trajectory with that of pre-selection DP (CD69<sup>-</sup> DP), CD4 SP and CD8 SP thymocytes (Fig. 6c). We found that early peaks of  $Cd4^+ Cd8a^+$  and  $Cd4^+ Cd8a^-$  selection intermediates were followed by a later peak of  $Cd4^- Cd8a^+$  selection intermediates (Fig. 6d,  $P = 1.35 \times 10^{-14}$ , one-sided Kolmogorov–Smirnov test, Supplementary Fig. 7).

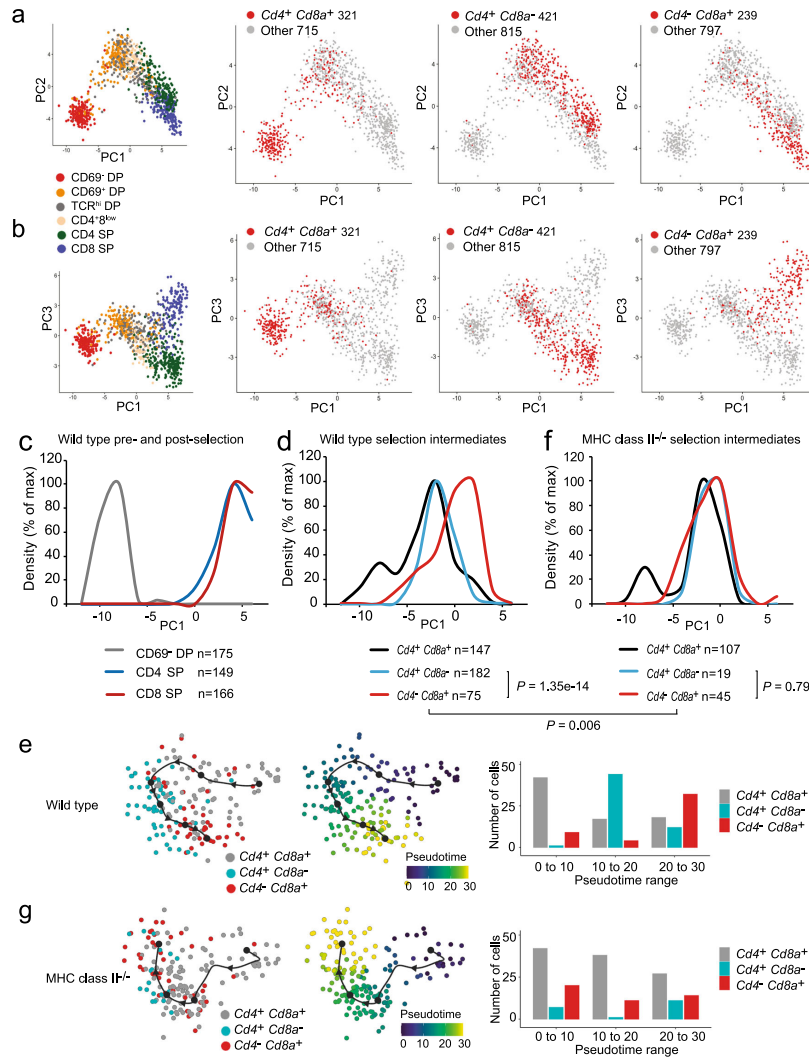
As a complementary approach to gauge the order of coreceptor activity patterns, we examined trajectories identified by the Slingshot algorithm<sup>32</sup> (Fig. 6e, left). Quantification of selection intermediates along pseudotime (Fig. 6e, middle) supported the conclusion that  $Cd4^+ Cd8a^-$  selection intermediates precede  $Cd4^- Cd8a^+$  selection intermediates (Fig. 6e, right,  $P = 1.18 \times 10^{-08}$ , one-sided Kolmogorov–Smirnov test).

If this order reflects an inherent program of coreceptor gene expression in TCR-signalled thymocytes with fixed timing, the same sequence of events would ensue even in a setting where all TCR signals are triggered by engagement of MHC class I. Selection intermediates in MHC class II-deficient thymi provide a simple test for this prediction. We therefore repeated the analysis described above with thymocytes from MHC class II-deficient mice. Unexpectedly, we found that  $Cd4^+ Cd8^-$  and  $Cd4^- Cd8^+$  selection intermediates arose simultaneously along PC1 when TCR ligand availability was restricted to MHC class I (Fig. 6f,  $P = 0.79$ , one-sided Kolmogorov–Smirnov test). This conclusion was corroborated by trajectory analysis (Fig. 6g,  $P = 0.77$ , one-sided Kolmogorov–Smirnov test). These data suggest that the CD4 and CD8 lineages arise sequentially, but that the timing of this sequence is not hardwired.

**MHC class discrimination by selection intermediates.** Given that the timing of coreceptor gene expression patterns was determined by the availability of MHC class II, we next analysed the expression of TCR activation genes as a proxy for TCR signalling in wild-type and MHC class II-deficient selection intermediates. MHC class II<sup>-/-</sup>  $Cd4^+ Cd8a^+$  selection intermediates

showed significantly lower expression of *Cd69*, *Cd5* and other TCR activation genes than wild-type *Cd4<sup>+</sup>Cd8a<sup>+</sup>* selection intermediates (Fig. 7a and Supplementary Fig. 8). The expression of the inducible transcription factors *Nr4a1*, *Egr1* and *Nab2* (a repressor of EGR transcription factors) and the inducible signalling component *Mapk11* was also reduced in MHC class II<sup>-/-</sup> *Cd4<sup>+</sup>Cd8a<sup>+</sup>* selection intermediates (Fig. 7a). This indicates that *Cd4<sup>+</sup>Cd8a<sup>+</sup>* selection intermediates are capable of MHC class discrimination. Reduced expression of TCR-induced genes was also found in *Cd4<sup>+</sup>Cd8a<sup>+</sup>* selection intermediates that were phenotypically CD4<sup>+</sup>CD8<sup>+</sup> (Fig. 7b). This indicates that MHC class discrimination by selection intermediates was not

contingent on the loss of either CD4 or CD8 coreceptors. MHC class-dependent differences in TCR activation gene expression in *Cd4<sup>+</sup>Cd8a<sup>+</sup>* selection intermediates were followed by altered transcription factor and cytokine signalling gene expression at the *Cd4<sup>+</sup>Cd8a<sup>-</sup>* stage. MHC class II<sup>-/-</sup> *Cd4<sup>+</sup>Cd8a<sup>-</sup>* selection intermediates showed increased expression of the IL7R downstream gene *Gimap3*, increased expression of *Runx1*, and a trend towards increased expression of *Runx3* (Fig. 7c). *Runx* transcription factors are known regulators of *Cd4* and *Cd8a* expression<sup>26,27</sup>. Taken together with the finding that *Cd4<sup>+</sup>Cd8<sup>-</sup>* and *Cd4<sup>-</sup>Cd8<sup>+</sup>* selection intermediates appear simultaneously in the MHC class II<sup>-/-</sup> thymus, these data indicate that the strength



**Fig. 6 The temporal sequence of coreceptor gene expression by selection intermediates.** **a** PCA 1 versus 2. The inset (far left) shows all cells coloured by cell surface phenotype. Red dots show the position of cells that are  $Cd4^+Cd8a^+$  (left),  $Cd4^+Cd8a^-$  (centre) or  $Cd4^-Cd8a^+$  (right). Source data are provided as a Source Data file. **b** PCA 1 versus 3. The inset (far left) shows all cells coloured by cell surface phenotype. Red dots show the position of cells that are  $Cd4^+Cd8a^+$  (left),  $Cd4^+Cd8a^-$  (centre) or  $Cd4^-Cd8a^+$  (right). Source data are provided as a Source Data file. **c** The temporal sequence of pre- and post-selection wild-type thymocytes. The vertical axis shows the number of pre-selection DP, CD4 SP and CD8 SP expressed normalised to the maximal number of cells detected for each population. The number of cells in each cell population is indicated. Source data are provided as a Source Data file. **d** The temporal sequence of coreceptor gene expression by selection intermediates. The vertical axis shows the number of selection intermediates with the indicated coreceptor gene expression normalised to the maximal number of cells for each gene expression pattern. The number of selection intermediates with each coreceptor gene expression pattern is indicated. *P*-values: one-sided Kolmogorov-Smirnov test. See Supplementary Fig. 7 for individual biological replicates. Source data are provided as a Source Data file. **e** Slingshot trajectory of wild-type  $Cd4^+Cd8a^+$ ,  $Cd4^+Cd8a^-$ ,  $Cd4^-Cd8a^+$  selection intermediates based on PCA clustering (top), pseudotime analysis (middle) and quantification of coreceptor gene expression patterns along the pseudotime axis (bottom). *P*-values: one-sided Kolmogorov-Smirnov test. The alternative Slingshot clustering options, MDS and t-SNE, gave equivalent results. **f** The order of coreceptor gene expression patterns is not invariant. The position of MHC class II<sup>-/-</sup> selection intermediates  $Cd4^+Cd8a^+$ ,  $Cd4^+Cd8a^-$ ,  $Cd4^-Cd8a^+$  along PC1. Note the difference between wild-type (**d**) and MHC class II<sup>-/-</sup> (**f**). *P*-values: one-sided Kolmogorov-Smirnov test. Source data are provided as a Source Data file. **g** Slingshot trajectory of MHC class II<sup>-/-</sup>  $Cd4^+Cd8a^+$ ,  $Cd4^+Cd8a^-$ ,  $Cd4^-Cd8a^+$  selection intermediates based on PCA clustering (top), pseudotime analysis (middle) and quantification of coreceptor gene expression patterns along the pseudotime axis (bottom). *P*-values: one-sided Kolmogorov-Smirnov test. The alternative Slingshot clustering options, MDS and t-SNE, gave equivalent results.

of TCR signals affects the time spent at the  $Cd4^+Cd8^-$  selection intermediate stage. Convergence of signal strength and the timing of coreceptor gene expression in selection intermediates unifies key aspects of quantitative and kinetic signalling models<sup>4,13</sup> (summarised in Fig. 7d discussed below).

**Signal strength has the potential to subvert CD4/CD8 lineage choice.** Current kinetic signalling models posit that CD4/CD8 lineage choice is determined exclusively by signal continuity in the face of sequential expression of CD4 and CD8 coreceptors, and not by MHC class discrimination based on signal strength<sup>4,6,7,15,16</sup>. This view was supported by re-engineering of *Cd8a* to encode the stronger signalling cytoplasmic tail of CD4 (CD8.4; ref. 16). Greater signal strength increased the number of preselection thymocytes recruited into the selection process and the efficiency of positive selection, but not CD4/CD8 lineage choice in MHC class II-deficient thymocytes or in mice transgenic for the MHC class I-restricted F5 TCR (refs. 16,33). To further explore whether signal strength can affect lineage choice, we examined the fate of thymocytes we opted for the MHC class I-restricted OT-I TCR because this TCR drives a prominent subset of  $CD4^+CD8^{low}$  selection intermediates in the presence of wild-type CD8, and our previous studies had shown that CD8.4 enhances TCR-proximal signalling in OT-I transgenic thymocytes while retaining the requirement for MHC class I in positive selection<sup>33</sup>. We examined the generation of CD4 lineage cells in CD8.4 *Rag2*<sup>-/-</sup> OT-I TCR transgenic mice and found substantial numbers of CD4 SP thymocytes (Supplementary Fig. 9a) and CD4 lymph node T cells (Supplementary Fig. 9b), indicating that signal strength can undermine lineage choice.

## Discussion

A major obstacle to understanding CD4/CD8 lineage choice and differentiation has been that the expression of *Cd4* and *Cd8* coreceptor genes is not directly visible, and that the cell surface phenotype of selection intermediates does not reliably indicate coreceptor gene expression<sup>34</sup>. scRNA-seq identified *Cd4* and *Cd8a* coreceptor gene transcripts in the great majority of pre- and post-selection thymocytes, indicating very low dropout rates for the coreceptor genes *Cd4* and *Cd8a* in our scRNA-seq. The detection of coreceptor transcripts was therefore a strong indicator for the activity of coreceptor genes in individual cells, and allowed the classification of selection intermediates based on coreceptor gene expression. When combined with the position of individual selection intermediates within the framework of

maturation, activation and lineage specification, this provided a direct view of the temporal order of coreceptor gene activity and the associated gene expression programs.

In the unperturbed thymus,  $Cd4^-Cd8^+$  selection intermediates appeared significantly later than  $Cd4^+Cd8^-$  selection intermediates. Interestingly, the order and the timing of coreceptor gene expression by selection intermediates was not hardwired, as  $Cd4^+Cd8^-$  and  $Cd4^-Cd8^+$  subsets arose simultaneously when TCR ligand availability was restricted to MHC class I.

The expression of *Zbtb7b* was initiated relatively early in  $Cd4^+Cd8a^-$  selection intermediates, at a time when selection intermediates still showed abundant expression of activation markers. *Zbtb7b* expression was absolutely dependent on MHC class II and highly CD4 lineage-specific. In contrast, *Runx3* was expressed in a substantial fraction of non-CD8 lineage cells. This indicates that *Runx3* is not strictly a CD8 lineage marker, and that *Runx3* expression is not directly linked to coreceptor reversal.

$Cd4^+Cd8^-$  and  $Cd4^-Cd8^+$  selection intermediates expressed TCR signalling-induced activation markers at significantly higher levels than pre-selection DP thymocytes. This suggests that TCR signalling continues in  $Cd4^-Cd8^+$  selection intermediates, even though cytokine signalling is necessary for CD8 lineage differentiation and/or survival<sup>20</sup>. These data disagree with predictions by kinetic signalling models that termination of TCR signalling is essential for CD8 lineage commitment<sup>20</sup> and instead support the view that continued TCR engagement and downstream signalling contribute to CD8 lineage differentiation<sup>35–37</sup>.

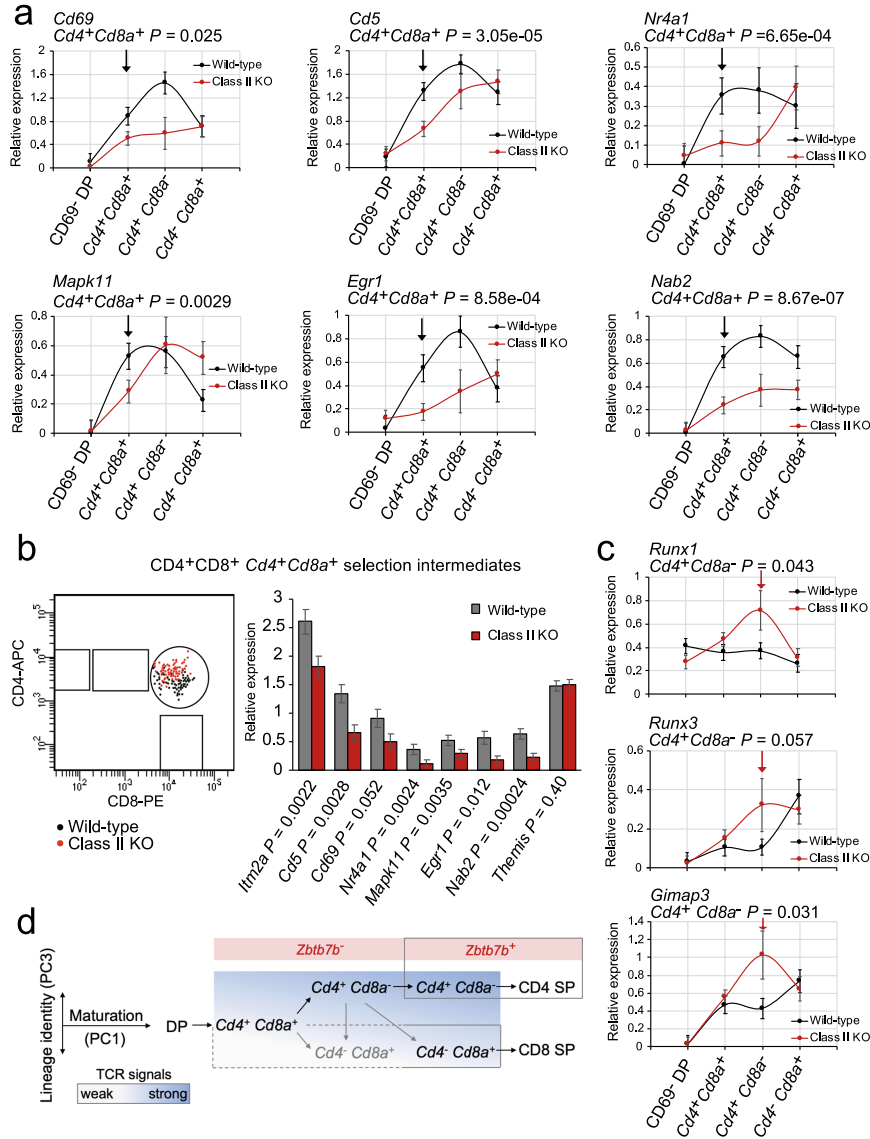
Early acquisition of CD4 lineage markers and mediators of helper T cell function contrasted with late acquisition of CD8 lineage markers and mediators of CTL function. We did not find co-expression of markers for both the CD4 and the CD8 cell lineage by selection intermediates other than *Cd4* and *Cd8a*. An interesting interpretation is that CD4 and CD8 lineage programs do not interfere with each other because they are implemented at different times during differentiation.

The expression of TCR activation genes was reduced when class II was absent, even in  $Cd4^+Cd8a^-$  selection intermediates that still expressed both CD4 and CD8 on the cell surface. Hence, selection intermediates discriminate between MHC class I and -II, and this discrimination does not require the loss of coreceptor proteins or RNA. The absence of MHC class II also changed the timing of coreceptor gene expression by selection intermediates. We suggest a model that links signal strength and the timing of coreceptor gene expression in selection intermediates. In this scenario, the strength of TCR signals affects the time spent at the  $Cd4^+Cd8^-$  selection intermediate stage (Fig. 7d). This model

links MHC class discrimination to coreceptor gene expression where  $Cd4^+Cd8a^+$  selection intermediates can distinguish between MHC classes before—and perhaps without—down-regulation of  $Cd8$  expression. Cytokine signals are implicated in the expression of *Runx3*, which acts to repress *Cd4* and to activate *Cd8a* (refs. 26,27). MHC class II<sup>-/-</sup> selection intermediates showed a notable trend for increased expression of the IL7R downstream gene *Gimap3* as well as *Runx1* and *Runx3* as

potential mediators of coreceptor switching from  $Cd4^+Cd8a^-$  to  $Cd4^-Cd8a^+$  (refs. 4,20,22).

The ability of thymocytes to discriminate between MHC classes based on signal strength was a cornerstone of instructive models for CD4/CD8 lineage choice<sup>1</sup>, and an important feature of proposals that lineage choice is based on signal strength and duration<sup>9–12</sup>. Lineage choice by signal strength subsequently fell out of favour, largely because experiments with chimeric coreceptors



**Fig. 7 MHC class discrimination and *Cd4 Cd8a* coreceptor gene expression in selection intermediates.** **a** Expression of TCR activation genes in CD69<sup>+</sup> DP thymocytes and selection intermediates of the indicated coreceptor status in wild-type (black) and MHC class II-deficient thymi (red). Means and standard errors are shown. *P*-values (one-sided Wilcoxon rank-sum test) are for *Cd4<sup>+</sup>Cd8a<sup>+</sup>* selection intermediates. Cell numbers are listed in Supplementary Tables 2 and 3. Source data are provided as a Source Data file. **b** Expression of cell surface CD4 and CD8 (left) and activation markers, transcription factors and signalling components (right) by CD69<sup>+</sup>DP and TCR<sup>hi</sup> DP selection intermediates that retain expression of both *Cd4* and *Cd8a* coreceptors at the RNA level (wild-type *n* = 73, MHC class II-deficient *n* = 77). This is shown to illustrate that not all selection-related genes showed differential expression between MHC class II-deficient and wild-type selection intermediates. Means and standard errors are shown. *P*-values: one-sided Wilcoxon rank-sum test. Source data are provided as a Source Data file. **c** Expression of *Runx1*, *Runx3* and *Gimap3* in CD69<sup>+</sup> DP thymocytes and selection intermediates of the indicated coreceptor status in wild-type (black) and MHC class II-deficient thymi (red). Means and standard errors are shown. *P*-values (one-sided Wilcoxon rank-sum test) are for *Cd4<sup>+</sup>Cd8a<sup>-</sup>* selection intermediates. Cell numbers are listed in Supplementary Tables 2 and 3. Source data are provided as a Source Data file. **d** A working model that combines key aspects of signal strength and sequential coreceptor models by proposing that the signal strength is linked to the dynamics of coreceptor gene expression during CD4/CD8 lineage choice and differentiation. Boxed areas indicate dependence on MHC class II. The emergence of *Zbtb7b<sup>+</sup>Cd4<sup>+</sup>Cd8a<sup>-</sup>* selection intermediates requires MHC class II (top). The strength of TCR signals affects the time spent at the *Cd4<sup>+</sup>Cd8<sup>-</sup>* selection intermediate stage (darker blue indicates stronger signals, bottom). Grey arrows indicate possible transitions between coreceptor activity states that cannot be inferred directly from the data.

suggested that increased signal strength failed to subvert CD4/CD8 lineage choice<sup>4,16</sup>. Our own data show that the chimeric CD8.4 coreceptor diverts thymocytes expressing the MHC class I-restricted OT-I TCR differentiate to the CD4 lineage. We suggest that weaker TCR signals downstream of MHC class I engagement trigger accelerated transition to *Cd4<sup>+</sup>Cd8a<sup>+</sup>* coreceptor status and in this way minimise the risk of inappropriate lineage choice.

In summary, our single cell view of CD4/CD8 lineage choice and differentiation shows that selection intermediates discriminate MHC classes prior to the termination of *Cd4* or *CD8a* expression and adjust the timing of coreceptor gene expression accordingly. These findings bring together key aspects of quantitative signalling models where differences between TCR/CD4/MHC class II signals and TCR/CD8/MHC class I signals determine lineage choice and differentiation of DP thymocytes<sup>13,38–40</sup> and of kinetic signalling models where lineage choice is aided by a program of sequential expression of coreceptors<sup>4</sup>. Signal strength alone does not fully explain lineage choice<sup>4,6,7,9</sup> but contributes to correct lineage outcome, as indicated by mismatches between TCR specificity and lineage choice in settings where signal strength is perturbed (e.g. ref. <sup>15</sup>, this study). We suggest that such mismatches may be minimised by the strategy uncovered here, which is to link transitions between coreceptor gene activity to signal strength.

## Methods

**Flow cytometry and cell sorting.** Thymocyte cell suspensions were stained for 20 min at room temperature with CD4-APC, CD8a-PE, TCRb-BV421 and CD69-FITC (BD-Pharmingen). Single cells were sorted into 96-well plates containing lysis buffer using a FACSAria Fusion flow cytometer (BD Biosciences) and the gates depicted in Supplementary Fig. 1. Flow cytometry standard files were analysed with DIVA (BD Biosciences) and FlowJo v10 (TreeStar Inc) analysis software.

C57BL/6 (C57BL/6OlaHsd, Envigo, UK) and Mice lacking MHC class II expression<sup>41</sup> (JAX stock #003584) were maintained separately under specific pathogen-free conditions under Project Licences issued by the Home Office, UK. OT-I *Rag2<sup>-/-</sup>* and CD8.4 OT-I *Rag2<sup>-/-</sup>* mice<sup>32</sup> were maintained together at the Institute of Molecular Genetics of the Czech Academy of Sciences, Prague, in accordance with laws of the Czech Republic. Six-week-old male or female mice were killed by cervical dislocation, and thymocyte or lymph-node cell suspensions were stained with CD4-APC, TCRb-FITC, CD69-BV421 (Pharmingen) or CD4-Alexa Fluor 700, CD8a-PE or CD8a-BV421, TCRb-APC (Biolegend), and LIVE/DEAD NIR (ThermoFisher). Data acquisition was on a Cytek Aurora flow cytometer (Cytek Biosciences) and flow cytometry standard files were analysed with FlowJo v10 (TreeStar Inc) analysis software. Data were further analysed using GraphPad Prism v5.04 (GraphPad Software).

**scRNA-seq libraries and sequencing.** Wild-type replicate 1: Full-length single-cell RNA-seq libraries were prepared using the Smart-seq2 protocol<sup>42</sup> with minor modifications. Briefly, freshly harvested single cells were sorted into 96-well plates containing the lysis buffer (0.2% Triton-100, 1 U/μl RNase inhibitor). Reverse transcription was performed using SuperScript II (ThermoFisher Scientific) in the

presence of 1 μM oligo-dT30VN (IDT), 1 μM template-switching oligonucleotides (QIAGEN) and 1 M betaine. cDNA was amplified using the KAPA HiFi Hotstart ReadyMix (Kapa Biosystems) and IS PCR primer (IDT), with 25 cycles of amplification. Following purification with Agencourt Ampure XP beads (Beckmann Coulter), product size distribution and quantity were assessed on a Bioanalyzer using a High Sensitivity DNA Kit (Agilent Technologies). A total of 140 pg of the amplified cDNA was fragmented using Nextera XT (Illumina) and amplified with Nextera XT indexes (Illumina). Products of each well of the 96-well plate were pooled and purified twice with Agencourt Ampure XP beads (Beckmann Coulter). Final libraries were quantified and checked for fragment size distribution using a Bioanalyzer High Sensitivity DNA Kit (Agilent Technologies). Pooled sequencing of Nextera libraries was carried out using a HiSeq2000 (Illumina) to an average sequencing depth of 0.5 million reads per cell. Sequencing was carried out as paired-end (PE75) reads with library indexes corresponding to cell barcodes.

Wild-type replicate 2 and MHC class II<sup>-/-</sup>: Full-length single-cell RNA-seq libraries were prepared using the SMART-Seq v5 Ultra Low Input RNA (SMARTer) Kit for Sequencing (Takara Bio). All reactions were downscaled to one quarter of the original protocol and performed following thermal cycling manufacturer's conditions. Cells were sorted into 96-well plates containing 2.5 μl of the Reaction buffer (1x Lysis Buffer, RNase Inhibitor 1 U/μl). Reverse transcription was performed using 2.5 μl of the RT MasterMix (SMART-Seq v5 Ultra Low Input RNA Kit for Sequencing, Takara Bio). cDNA was amplified using 8 μl of the PCR MasterMix (SMART-Seq v5 Ultra Low Input RNA Kit for Sequencing, Takara Bio) with 25 cycles of amplification. Following purification with Agencourt Ampure XP beads (Beckmann Coulter), product size distribution and quantity were assessed on a Bioanalyzer using a High Sensitivity DNA Kit (Agilent Technologies). A total of 140 pg of the amplified cDNA was fragmented using Nextera XT (Illumina) and amplified with double indexed Nextera PCR primers (IDT). Products of each well of the 96-well plate were pooled and purified twice with Agencourt Ampure XP beads (Beckmann Coulter). Final libraries were quantified and checked for fragment size distribution using a Bioanalyzer High Sensitivity DNA Kit (Agilent Technologies). Pooled sequencing of Nextera libraries was carried out using a HiSeq4000 (Illumina) to an average sequencing depth of 0.5 million reads per cell. Sequencing was carried out as paired-end (PE75) reads with library indexes corresponding to cell barcodes.

**Data analysis.** Smart-seq2 and SMARTer sequencing data were aligned with TopHat2 version 2.1.1 (ref. <sup>43</sup>) that uses the bowtie2 version 2.3.4.3 for alignment<sup>44</sup>. We used the GRCm38 (mm10) mouse genome reference for alignment and gene annotation from UCSC. Read counts for genes were calculated using velocity version 0.17 (ref. <sup>45</sup>), for SMARTer sequencing data cells with total read counts <500,000 or >1,500,000 were excluded, and the cell-gene count matrix obtained was used for downstream analysis.

We performed Seurat v3 (ref. <sup>46</sup>) pre-processing (log-normalisation using variance stabilising transformation method), and identified highly variable (F-set) genes individually for each wild-type replicate (Supplementary Data 1). The highly variable genes from replicate 2 were selected and read counts from both replicates were piped to Seurat v3 standard integration workflow in order to generate integrated PCA for replicate 1 and replicate 2. We chose F-set from replicate 2 because replicate 2 scRNA-seq data were generated using the more sensitive SMARTer protocol compared to replicate 1 WT Smartseq2 data.

Using read counts for F-set genes, we applied Seurat v3 standard integration workflow for integrated analysis of replicate 1 WT Smartseq2 and replicate 2 WT/MHC class II<sup>-/-</sup> SMARTer datasets. The pipeline identified shared cell states that were present between replicate 1 and 2 by generating a batch-corrected expression matrix for F-set genes in all cells and enabling them to be jointly analysed. We then scaled the integrated data, ran PCA and visualised the results.

To find differentially expressed genes between sorted thymocyte subsets and between selection intermediates classified by coreceptor status, we applied Seurat v3 FindMarkers function on replicate 2 WT using two-sided Wilcoxon rank-sum test without cut-off threshold on log-fold-change. Heat maps were generated with Seurat v3 DoHeatmap function using log-normalisation values for candidate genes. FeaturePlot function with blend option was applied for visualisation of co-expression of gene pairs.

To find genes that changed along PC1, PC2 and PC3, we tested the null hypothesis of no change along PCs for each gene using the gam R package. Top 1000 genes by *P*-value were selected to create contingency tables with activation, differentiation and lineage-specific gene markers for Fisher Exact test.

Slingshot (ref. 32) was used for trajectory inference and pseudotime analysis of selection intermediates, based on a recent benchmark study of 57 trajectory inference methods<sup>47</sup>.

**Reporting summary.** Further information on research design is available in the Nature Research Reporting Summary linked to this article.

#### Data availability

scRNA-seq data have been deposited at GEO under accession number [GSE149207](https://www.ncbi.nlm.nih.gov/geo/query/acc.cgi?acc=GSE149207). Population RNA-seq data has been deposited at GEO under accession number [GSE154670](https://www.ncbi.nlm.nih.gov/geo/query/acc.cgi?acc=GSE154670). All other data are included in the supplemental information or available from the authors upon reasonable request. Source data are provided with this paper.

#### Code availability

Custom Rmd scripts used for generating figures are available from Github: <https://github.com/LMSBioinformatics/ScRNAseq-SMARTer-Analysis>.

Received: 14 June 2020; Accepted: 22 November 2020;

Published online: 04 January 2021

#### References

1. Robey, E. et al. Thymic selection in CD8 transgenic mice supports an instructive model for commitment to a CD4 or CD8 lineage. *Cell* **64**, 99–107 (1991).
2. Chan, H. S., Cosgrove, D., Waltzinger, C., Benoist, C. & Mathis, D. Another view of the selective model of thymocyte selection. *Cell* **73**, 225–236 (1993).
3. Davis, C. B. et al. Evidence for a stochastic mechanism in the differentiation of mature subsets of T lymphocytes. *Cell* **73**, 237–247 (1993).
4. Brugnera, E. et al. I. Coreceptor reversal in the thymus: signaled CD4+8+ thymocytes initially terminate CD8 transcription even when differentiating into CD8+ T cells. *Immunity* **13**, 59–71 (2000).
5. Liu, X. & Bosselut, R. Duration of TCR signaling controls CD4-CD8 lineage differentiation in vivo. *Nat. Immunol.* **5**, 280–288 (2004).
6. Singer, A. New perspectives on a developmental dilemma: the kinetic signaling model and the importance of signal duration for the CD4/CD8 lineage decision. *Curr. Opin. Immunol.* **14**, 207–215 (2002).
7. Singer, A., Adoro, S. & Park, J. H. Lineage fate and intense debate: myths, models and mechanisms of CD4- versus CD8-lineage choice. *Nat. Rev. Immunol.* **8**, 788–801 (2008).
8. Kimura, M. Y. et al. Timing and duration of MHC I positive selection signals are adjusted in the thymus to prevent lineage errors. *Nat. Immunol.* **17**, 1415–1423 (2016).
9. Germain, R. N. T-cell development and the CD4-CD8 lineage decision. *Nat. Rev. Immunol.* **2**, 309–322 (2002).
10. Matechak, E. O., Killeen, N., Hedrick, S. M. & Fowlkes, B. J. MHC class II-specific T cells can develop in the CD8 lineage when CD4 is absent. *Immunity* **4**, 337–347 (1996).
11. Hernández-Hoyos, G., Sohn, S. J., Rothenberg, E. V. & Alberola-Ila, J. Lck activity controls CD4/CD8 T cell lineage commitment. *Immunity* **12**, 313–322 (2000).
12. Zeidan, N., Damen, H., Roy, D. C. & Dave, V. P. Critical role for TCR signal strength and MHC specificity in ThPOK-induced CD4 helper lineage choice. *J. Immunol.* **202**, 3211–3225 (2019).
13. Itano, A. et al. The cytoplasmic domain of CD4 promotes the development of CD4 lineage T cells. *J. Exp. Med.* **183**, 731–741 (1996).
14. Yasutomo, K., Doyle, C., Miele, L., Fuchs, C. & Germain, R. N. The duration of antigen receptor signalling determines CD4+ versus CD8+ T-cell lineage fate. *Nature* **404**, 506–510 (2000).
15. Bosselut, R., Feigenbaum, L., Sharrow, S. O. & Singer, A. Strength of signaling by CD4 and CD8 coreceptor tails determines the number but not the lineage direction of positively selected thymocytes. *Immunity* **14**, 483–494 (2001).
16. Erman, B. et al. Coreceptor signal strength regulates positive selection but does not determine CD4/CD8 lineage choice in a physiologic in vivo model. *J. Immunol.* **177**, 6613–6625 (2006).
17. Satpathy, A. T. et al. Massively parallel single-cell chromatin landscapes of human immune cell development and intratumoral T cell exhaustion. *Nat. Biotechnol.* **37**, 925–936 (2019).
18. Park, J. E. et al. A cell atlas of human thymic development defines T cell repertoire formation. *Science* **367**, eaay3224 (2020).
19. Lavaert, M. et al. Integrated scRNA-Seq Identifies Human Postnatal Thymus Seeding Progenitors and Regulatory Dynamics of Differentiating Immature Thymocytes. *Immunity* **52**, 1088–1104 (2020).
20. Etzensperger, R. et al. Identification of lineage-specifying cytokines that signal all CD8+–cytotoxic-lineage-fate ‘decisions’ in the thymus. *Nat. Immunol.* **18**, 1218–1227 (2017).
21. Yu, Q., Erman, B., Bhandoola, A., Sharrow, S. O. & Singer, A. In vitro evidence that cytokine receptor signals are required for differentiation of double positive thymocytes into functionally mature CD8+ T cells. *J. Exp. Med.* **197**, 475–487 (2003).
22. Park, J. H. et al. Signaling by intrathymic cytokines, not T cell antigen receptors, specifies CD8 lineage choice and promotes the differentiation of cytotoxic-lineage T cells. *Nat. Immunol.* **11**, 257–264 (2010).
23. Katz, G. et al. T cell receptor stimulation impairs IL-7 receptor signaling by inducing expression of the microRNA miR-17 to target Janus kinase 1. *Sci. Signal.* **7**, ra83 (2014).
24. He, X., Park, K. & Kappes, D. J. The role of ThPOK in control of CD4/CD8 lineage commitment. *Annu. Rev. Immunol.* **28**, 295–320 (2010).
25. Sun, G. et al. The zinc finger protein cKrox directs CD4 lineage differentiation during intrathymic T cell positive selection. *Nat. Immunol.* **6**, 373–381 (2005).
26. Woolf, E. et al. Runx3 and Runx1 are required for CD8 T cell development during thymopoiesis. *Proc. Natl Acad. Sci. USA* **100**, 7731–7736 (2003).
27. Taniuchi, I. et al. Differential requirements for Runx proteins in CD4 repression and epigenetic silencing during T lymphocyte development. *Cell* **111**, 621–633 (2002).
28. Egawa, T. & Littman, D. R. ThPOK acts late in specification of the helper T cell lineage and suppresses Runx-mediated commitment to the cytotoxic T cell lineage. *Nat. Immunol.* **9**, 1131–1139 (2008).
29. Elgueta, R. et al. Molecular mechanism and function of CD40/CD40L engagement in the immune system. *Immunol. Rev.* **229**, 152–172 (2009).
30. Le Floch, A. et al. Minimal engagement of CD103 on cytotoxic T lymphocytes with an E-cadherin-Fc molecule triggers lytic granule polarization via a phospholipase Cgamma-dependent pathway. *Cancer Res.* **71**, 328–338 (2011).
31. Shields, B. D. et al. Loss of E-cadherin inhibits CD103 antitumor activity and reduces checkpoint blockade responsiveness in melanoma. *Cancer Res.* **79**, 1113–1123 (2019).
32. Street, K. et al. Slingshot: cell lineage and pseudotime inference for single-cell transcriptomics. *BMC Genom.* **19**, 477 (2018).
33. Stepanek, O. et al. Coreceptor scanning by the T cell receptor provides a mechanism for T cell tolerance. *Cell* **159**, 333–345 (2014).
34. Suzuki, H., Punt, J. A., Granger, L. G. & Singer, A. Asymmetric signaling requirements for thymocyte commitment to the CD4+ versus CD8+ T cell lineages: a new perspective on thymic commitment and selection. *Immunity* **2**, 413–425 (1995).
35. Kisielow, P. & Miasek, A. Positive selection of T cells: rescue from programmed cell death and differentiation require continual engagement of the T cell receptor. *J. Exp. Med.* **181**, 1975–1984 (1995).
36. Liu, X. et al. Restricting Zap70 expression to CD4+CD8+ thymocytes reveals a T cell receptor-dependent proofreading mechanism controlling the completion of positive selection. *J. Exp. Med.* **197**, 363–373 (2003).
37. Saini, M. et al. Regulation of Zap70 expression during thymocyte development enables temporal separation of CD4 and CD8 repertoire selection at different signaling thresholds. *Sci. Signal.* **3**, ra23 (2010).
38. Seong, R., Chamberlain, J. & Parnes, J. Signal for T-cell differentiation to a CD4 cell lineage is delivered by CD4 transmembrane region and/or cytoplasmic tail. *Nature* **356**, 718–720 (1992).
39. Gascoigne, N. R. & Palmer, E. Signaling in thymic selection. *Curr. Opin. Immunol.* **23**, 207–212 (2011).
40. Taniuchi, I. CD4 helper and CD8 cytotoxic T cell differentiation. *Annu. Rev. Immunol.* **36**, 579–601 (2018).
41. Madsen, L. et al. Mice lacking all conventional MHC class II genes. *Proc. Natl Acad. Sci. USA* **96**, 10338–10343 (1999).
42. Picelli, S. et al. Smart-seq2 for sensitive full-length transcriptome profiling in single cells. *Nature Methods* **10**, 1096–1098 (2013).
43. Kim, D. et al. TopHat2: accurate alignment of transcriptomes in the presence of insertions, deletions and gene fusions. *Genome Biol.* **14**, R36 (2013).
44. Langmead, B. & Salzberg, S. L. Fast gapped-read alignment with Bowtie 2. *Nat. Methods* **9**, 357–359 (2012).
45. La Manno, G. et al. RNA velocity of single cells. *Nature* **560**, 494–498 (2018).
46. Stuart, T. et al. Comprehensive integration of single-cell data. *Cell* **177**, 1888–1902 (2019).
47. Saels, W., Cannoodt, R., Todorov, H. & Saey, Y. A comparison of single-cell trajectory inference methods. *Nat. Biotechnol.* **37**, 547–554 (2019).



**Acknowledgements**

We thank Dr. B. Seddon (University College London) for discussion, Dr. J. Merkenchlagler (Rockefeller University) for critical reading of the manuscript, the referees for valuable suggestions, and Dr. G. Kassiotis (Crick Institute, London) for MHC class II<sup>-/-</sup> mice. Supported by the Medical Research Council, UK (B.L., A.G.F., M.M.), the Wellcome Trust (Investigator Award 099276/Z/12/Z to M.M.), the National Institutes of Health (NIH 1R35GM136284 to M.K.), and the Swiss National Science Foundation (SNSF Promys IZ11Z0\_166538 to O.S.).

**Author contributions**

Y.G., V.H., S.R.G., B.P., J.E., and M.M. carried out the experiments; M.M.K., X.C., H.A.P., V.H., Y.-F.W., G.R.-E., I.R.-R., R.G., M.H.D., D.D., M.S.K., O.S., and M.M. analysed and curated the data; M.M.K., V.H., G.R.E., I.R.-R., D.D., M.S.K., O.S. and M.M. visualised the data; M.M.K., L.B., M.S.K., B.L., H.H., A.G.F., O.S. and M.M. conceptualised the paper; M.M.K., V.H., O.S. and M.M. wrote the paper.

**Competing interests**

The authors declare no competing interests.

**Additional information**

**Supplementary information** is available for this paper at <https://doi.org/10.1038/s41467-020-20306-w>.

**Correspondence** and requests for materials should be addressed to M.M.

**Peer review information** *Nature Communications* thanks Ichiro Taniuchi and the other, anonymous, reviewer(s) for their contribution to the peer review of this work. Peer reviewer reports are available.

**Reprints and permission information** is available at <http://www.nature.com/reprints>

**Publisher's note** Springer Nature remains neutral with regard to jurisdictional claims in published maps and institutional affiliations.



**Open Access** This article is licensed under a Creative Commons Attribution 4.0 International License, which permits use, sharing, adaptation, distribution and reproduction in any medium or format, as long as you give appropriate credit to the original author(s) and the source, provide a link to the Creative Commons license, and indicate if changes were made. The images or other third party material in this article are included in the article's Creative Commons license, unless indicated otherwise in a credit line to the material. If material is not included in the article's Creative Commons license and your intended use is not permitted by statutory regulation or exceeds the permitted use, you will need to obtain permission directly from the copyright holder. To view a copy of this license, visit <http://creativecommons.org/licenses/by/4.0/>.

© The Author(s) 2021

**The order and logic of CD4 CD8 lineage choice and differentiation in mouse thymus**

Mohammad M Karimi<sup>1,5</sup>, Ya Guo<sup>1,6</sup>, Xiaokai Cui<sup>1</sup>, Husayn A Pallikonda<sup>1</sup>, Veronika Horková<sup>2</sup>, Yi-Fang Wang<sup>1</sup>, Sara Ruiz Gil<sup>3</sup>, Gustavo Rodriguez-Esteban<sup>3</sup>, Irene Robles-Rebollo<sup>1</sup>, Ludovica Bruno<sup>1</sup>, Radina Georgieva<sup>1</sup>, Bhavik Patel<sup>1</sup>, James Elliott<sup>1</sup>, Marian H Dore<sup>1</sup>, Danielle Dauphars<sup>4</sup>, Michael S. Krangel<sup>4</sup>, Boris Lenhard<sup>1</sup>, Holger Heyn<sup>3</sup>, Amanda G Fisher<sup>1</sup>, Ondřej Štěpánek<sup>2</sup>, Matthias Merkenschlager<sup>1\*</sup>

<sup>1</sup> MRC London Institute of Medical Sciences, Institute of Clinical Sciences, Faculty of Medicine, Imperial College London, London, UK

<sup>2</sup> Laboratory of Adaptive Immunity, Institute of Molecular Genetics of the Czech Academy of Sciences, Prague, Czech Republic

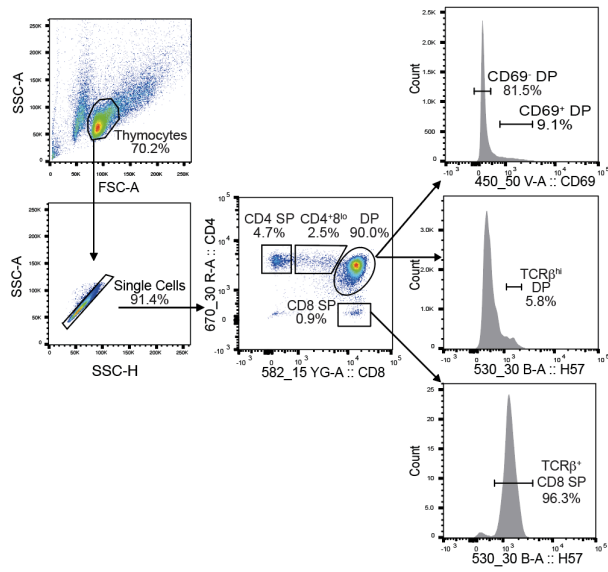
<sup>3</sup> CNAG-CRG, Centre for Genomic Regulation (CRG), The Barcelona Institute of Science and Technology (BIST), Barcelona, Spain

<sup>4</sup> Department of Immunology, Duke University Medical Center, Durham, NC, USA

<sup>5</sup> Present address: Comprehensive Cancer Centre, School of Cancer & Pharmaceutical Sciences, Faculty of Life Sciences & Medicine, King's College London, London, UK

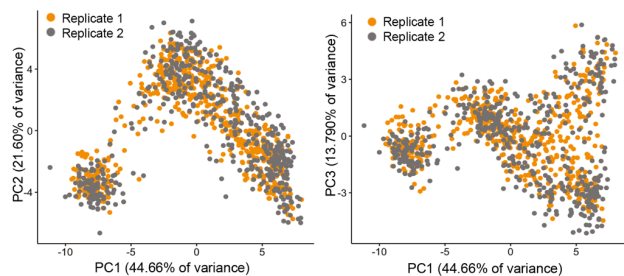
<sup>6</sup> Present address: School of Life Sciences and Biotechnology, Shanghai Jiao Tong University, Shanghai, China

Address correspondence to [matthias.merkenschlager@lms.mrc.ac.uk](mailto:matthias.merkenschlager@lms.mrc.ac.uk)



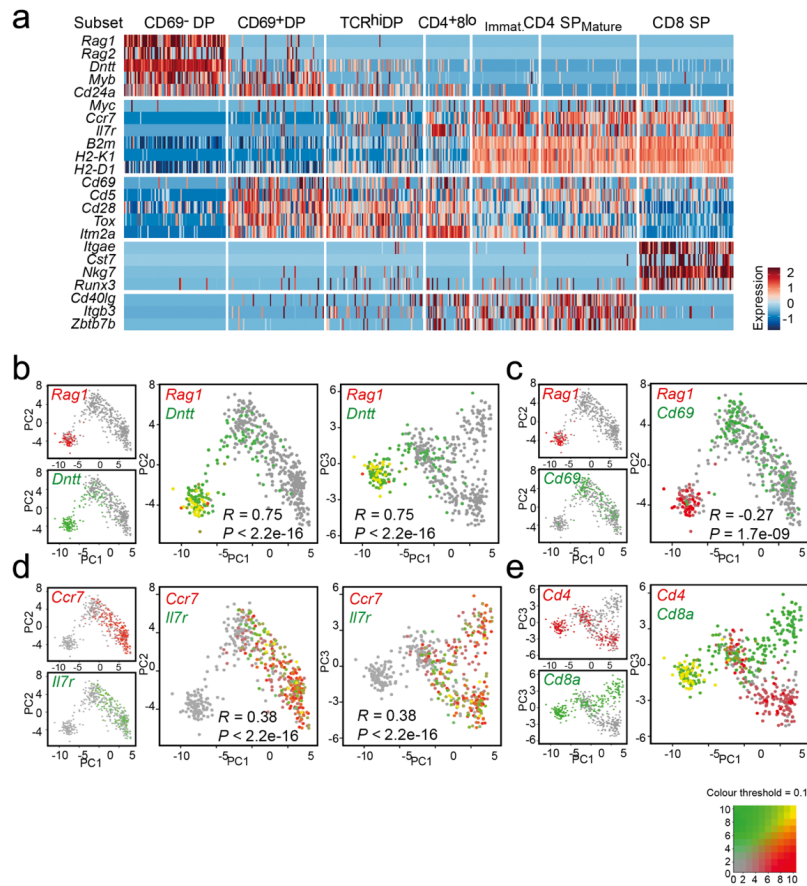
**Supplementary Figure 1. Isolation of thymocyte subsets.**

Plate layout was designed to represent each sorted population on each plate, enabling analysis of plates as technical replicates. Cells were sorted directly into lysis buffer and SMART-Seq2 libraries were prepared for sequencing of full length transcripts.



**Supplementary Figure 2. PCA analysis of scRNA-seq data - reproducibility between replicates**

PCA was performed as in Fig. 2a. Reproducibility between replicates is shown. Source data are provided as a Source Data file.



**Supplementary Figure 3. Key genes and correlations**

a) Heatmap of key genes. See Supplementary Data 2 for an analysis of differential gene expression between sorted thymocyte subsets.

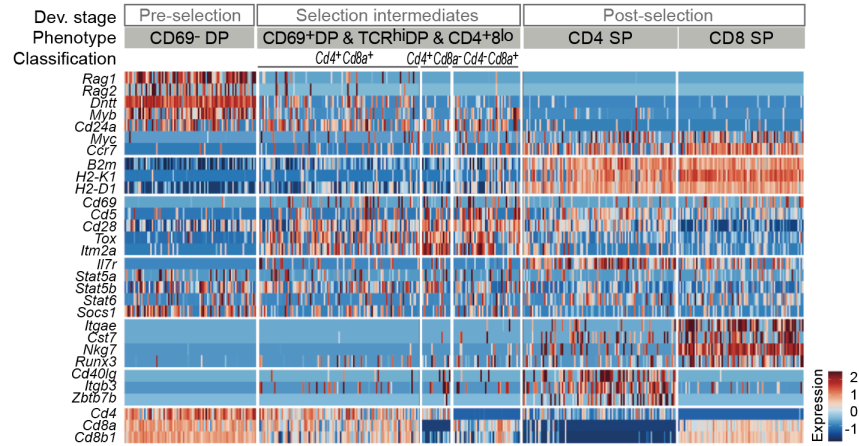
b) *Rag1* (red) and *Dnlt* (green) as two-colour dot plots projected onto maps of PC1 versus PC2 and -3. *Rag1* and *Dnlt* are expressed in pre-selection thymocytes and silenced by TCR signaling. Source data are provided as a Source Data file.

c) *Rag1* (red) and *Cd69* (green) as two-colour dot plots projected onto maps of PC1 versus PC2. *Rag1* is expressed in pre-selection thymocytes and *Cd69* is induced by TCR signaling. Source data are provided as a Source Data file.

d) *Ccr7* (red) and *Ii7r* (green) as two-colour dot plots projected onto maps of PC1 versus PC2 and -3. *Ccr7* and *Ii7r* expressed are induced during thymocyte maturation. Source data are provided as a Source Data file.

e) *Cd4* (red) and *Cd8a* (green) as two-colour dot plots projected onto maps of PC1 versus PC3. *Cd4* and *Cd8a* are co-expressed in pre-selection thymocytes, undergo expression changes in selection intermediates, and are expressed in a mutually exclusive pattern in CD4 SP and CD8 SP thymocytes. Source data are provided as a Source Data file.

MHC class II<sup>-/-</sup>

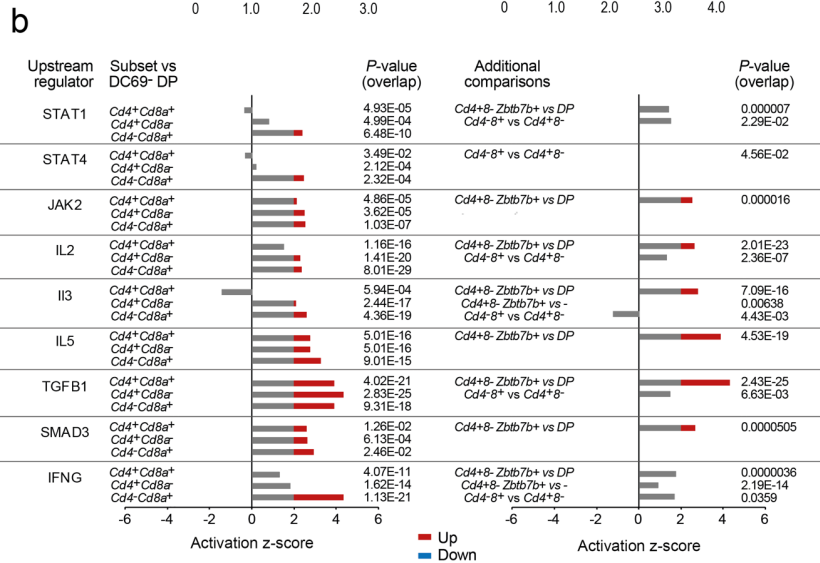
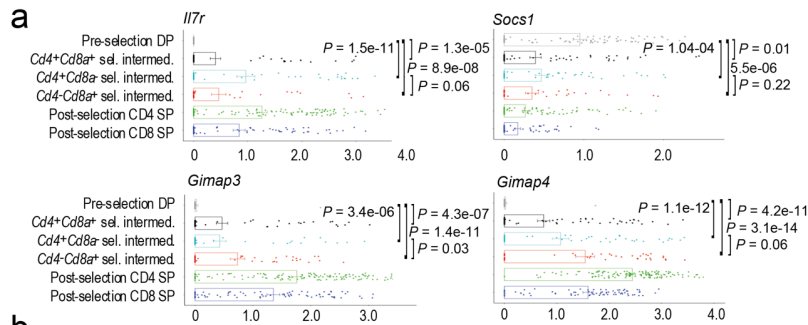


**Supplementary Figure 4: Overview of gene expression by individual selection intermediates in MHC class II<sup>-/-</sup> thymus.**

Cells (columns) were classified by *Cd4* and *Cd8a* coreceptor gene expression status, with pre- and post-selection thymocytes as comparators as in Fig. 3c. Cells are grouped by developmental stage (pre-selection, selection intermediates and post-selection) and cell surface phenotype. CD69<sup>-</sup> DP represent pre-selection thymocytes, pooled CD69<sup>+</sup> DP, TCR<sup>hi</sup> DP and CD4<sup>+</sup> CD8<sup>low</sup> represent selection intermediates, CD4 SP, TCR<sup>hi</sup> CD8 SP represent post-selection thymocytes. Selection intermediates are further classified into *Cd4<sup>+</sup>Cd8a<sup>+</sup>*, *Cd4<sup>+</sup>Cd8a<sup>-</sup>* and *Cd4<sup>-</sup>Cd8a<sup>+</sup>* based on scRNA-seq detection of *Cd4* and *Cd8a*.

MHC class II<sup>-/-</sup>

Subset	Surface phenotype	Number
CD69 <sup>-</sup> DP	CD4 <sup>+</sup> CD8 <sup>+</sup> CD69 <sup>-</sup>	88
CD69 <sup>+</sup> DP	CD4 <sup>+</sup> CD8 <sup>+</sup> CD69 <sup>+</sup>	58
TCR <sup>hi</sup> DP	CD4 <sup>+</sup> CD8 <sup>+</sup> TCR <sup>hi</sup>	68
CD4 <sup>+</sup> CD8 <sup>low</sup>	CD4 <sup>+</sup> CD8 <sup>low</sup>	59
CD4 SP	CD4 <sup>+</sup> CD8 <sup>-</sup>	102
CD8 SP	CD4 <sup>-</sup> CD8 <sup>+</sup> TCR <sup>hi</sup>	84

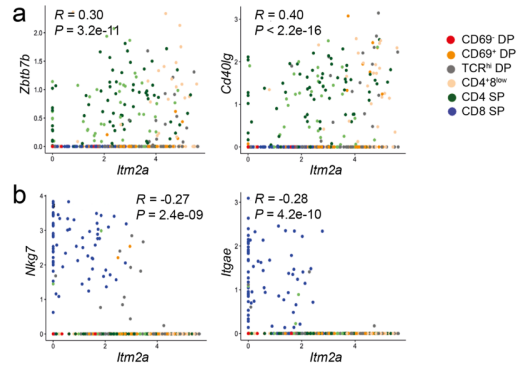


**Supplementary Figure 5. Expression of genes related to cytokine signaling by selection intermediates**

a) Expression of *Il7r*, *Socs1*, and the targets of IL7R signaling *Gimap3* and *Gmap4* by selection intermediates of the indicated coreceptor status. Means and standard errors are shown. *P*-values are derived by two-sided Wilcoxon rank-sum test. Cell numbers are listed in Supplementary Tables 2 and 3. Source data are provided as a Source Data file.

b) IPA analysis of pathway activity downstream of the indicated cytokines and cytokine signaling molecules. Activation z-scores above 2 and below -2 are considered significant. Selection intermediates versus CD69+ DP is shown on the left. Where available, comparisons between subsets of selection intermediates are shown on the right. Cell numbers are listed in Supplementary Tables 2 and 3. Source data are provided as a Source Data file.

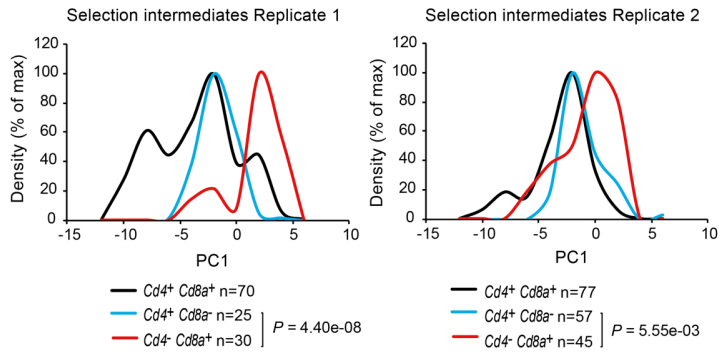




**Supplementary Figure 6. Expression of activation versus lineage markers**

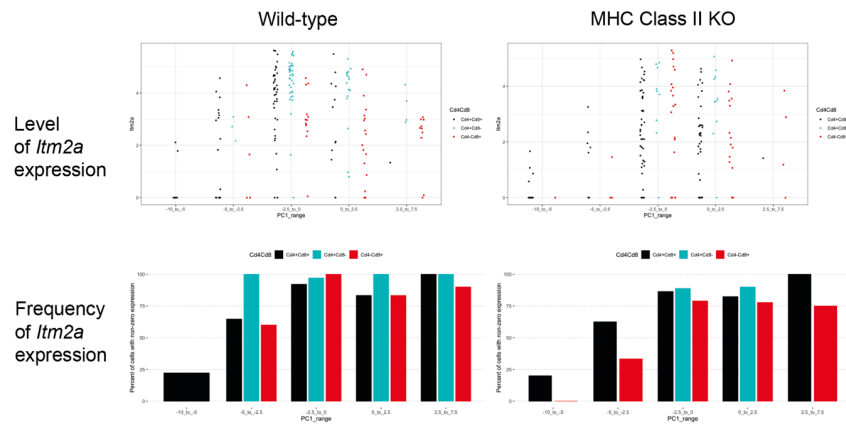
a) Positive correlation of the activation marker *Itm2a* with the CD4 lineage markers *Zbtb7b* and *Cd40lg* ( $R = 0.30$ ,  $P = 3.2e-11$  and  $R = 0.40$ ,  $P < 2.2e-16$ , respectively). Source data are provided as a Source Data file.

b) Negative correlation of the activation marker *Itm2a* with the CD8 lineage markers *Nkg7* and *Itgae* ( $R = -0.27$ ,  $P = 2.4e-09$  and  $R = -0.28$ ,  $P = 4.2e-10$ , respectively). Source data are provided as a Source Data file.



**Supplementary Figure 7. The order of coreceptor gene expression by wild-type selection intermediates in independent biological replicates.**

The vertical axis shows the number of selection intermediates with the indicated gene expression ( $Cd4^+ Cd8a^+$ ,  $Cd4^+ Cd8a^-$ ,  $Cd4^- Cd8a^+$ ) normalised to the maximal number of cells detected for each gene expression pattern in separate scRNA-seq replicates. The number of selection intermediates with each coreceptor gene expression pattern is indicated. *P*-values: one-sided Kolmogorov–Smirnov test. Source data are provided as a Source Data file.

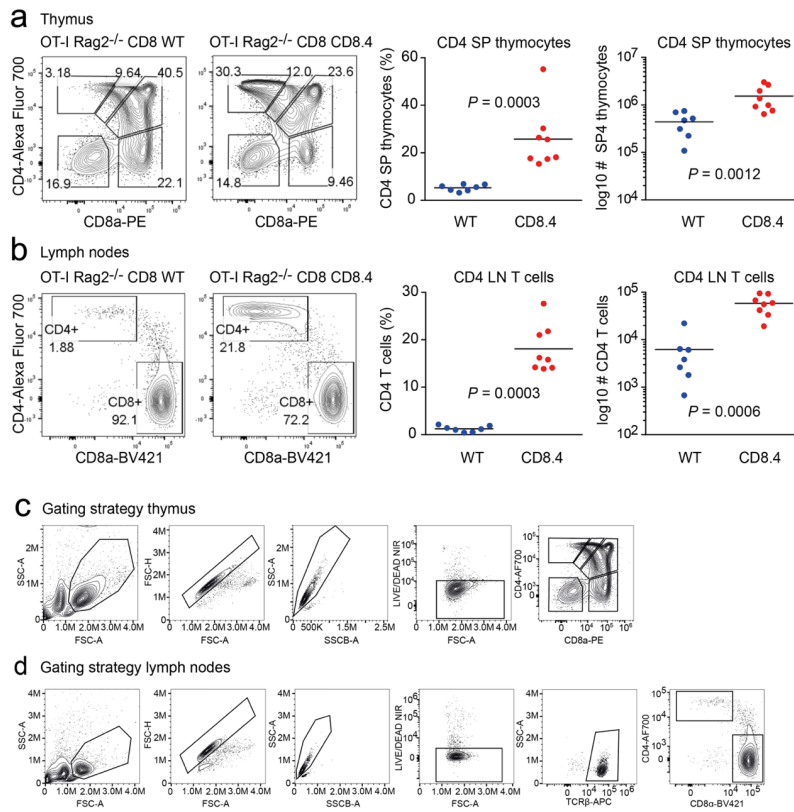


**Supplementary Figure 8. Activation marker expression by individual selection intermediates ordered along the maturation trajectory PC1.**

Top: The level of mRNA for the activation marker *Itm2a* is shown along the maturation trajectory PC1 for individual selection intermediates classified as  $Cd4^+ Cd8a^+$ ,  $Cd4^+ Cd8a^-$ , and  $Cd4^- Cd8a^+$  in wild-type (left) and MHC class II-deficient thymus (right).

Bottom: The frequency of cells containing mRNA for the activation marker *Itm2a* detected in subsets of selection intermediates classified as  $Cd4^+ Cd8a^+$ ,  $Cd4^+ Cd8a^-$ , and  $Cd4^- Cd8a^+$  in wild-type (left) and MHC class II-deficient thymus (right) is shown along the maturation trajectory PC1.

Source data are provided as a Source Data file.



**Supplementary Figure 9. Signal strength can undermine CD4/CD8 lineage choice.**

a) CD4 CD8 staining representative of OT-I-transgenic Rag2<sup>-/-</sup> thymocytes expressing wild-type Cd8a (left, n=4) or CD8.4 (right, n=5). Percentages and numbers of CD4 SP are shown. *P*-values were calculated by two-sided Mann-Whitney test in GraphPad Prism software. The gating strategy is shown in c). Source data are provided as a Source Data file.

b) CD4 CD8 staining representative of OT-I-transgenic Rag2<sup>-/-</sup> lymph node T cells expressing wild-type Cd8a (left, n=7) or CD8.4 (right, n=8). Percentages and numbers of CD4 T cells relative to total T cells are shown. *P*-values were calculated by two-sided Mann-Whitney test in GraphPad Prism software. The gating strategy is shown in d). Source data are provided as a Source Data file.

c) Gating strategy for thymocytes used in a).

d) Gating strategy for lymph node T cells used in b).

### Supplementary Tables

	Aver. transcripts/cell	Aver. reads/cell
Wild type repl. 1	1199.414	677142.7
Wild type repl. 2	2855.474	896571.1
MHC class II-/-	2843.217	839099.7

**Supplementary Table 1.** Number of transcripts and reads per cell

Subset	Surface phenotype	Rep1	Rep 2	Total
CD69 <sup>+</sup> DP	CD4 <sup>+</sup> CD8 <sup>+</sup> CD69 <sup>-</sup>	92	83	175
CD69 <sup>+</sup> DP	CD4 <sup>+</sup> CD8 <sup>+</sup> CD69 <sup>+</sup>	90	78	168
TCR <sup>hi</sup> DP	CD4 <sup>+</sup> CD8 <sup>+</sup> TCRβ <sup>+</sup>	96	79	175
CD4 <sup>+</sup> CD8 <sup>low</sup>	CD4 <sup>+</sup> CD8 <sup>low</sup>	71	36	107
CD4 SP	CD4 <sup>+</sup> CD8 <sup>-</sup>	113	142	255
CD8 SP	CD4 <sup>-</sup> CD8 <sup>+</sup> TCRβ <sup>+</sup>	89	77	166

**Supplementary Table 2.** The numbers of sorted subsets analysed.

	Rep1	Rep 2	Total
CD69- DP	92	83	175
<i>Cd4</i> <sup>+</sup> <i>Cd8a</i> <sup>+</sup> sel. int.	70	77	107
<i>Cd4</i> <sup>+</sup> <i>Cd8a</i> <sup>-</sup> sel. int.	125	57	182
<i>Cd4</i> <sup>-</sup> <i>Cd8a</i> <sup>+</sup> sel. int.	30	45	75
CD4 SP	113	132	245
CD8 SP	89	77	166

**Supplementary Table 3.** The numbers of wild-type *Cd4*<sup>+</sup>*Cd8a*<sup>+</sup>, *Cd4*<sup>+</sup>*Cd8a*<sup>-</sup> and *Cd4*<sup>-</sup>*Cd8a*<sup>+</sup> selection intermediates analysed.

		CD4SP/CD8SP		
		Up	N/C	Down
<i>Cd4</i> <sup>+</sup> <i>Cd8a</i> <sup>-</sup>	Up	22	44	3
<i>Cd4</i> <sup>-</sup> <i>Cd8a</i> <sup>+</sup>	N/C	326	9234	307
	Down	1	50	14

**Supplementary Table 4.** Gene expression in CD4 and CD8 SP versus *Cd4*<sup>+</sup>*Cd8a*<sup>-</sup> and *Cd4*<sup>-</sup>*Cd8a*<sup>+</sup> subsets of selection intermediates. Genes up or down in CD4 over CD8 SP (adj P < 0.05 in population RNA-seq) and log2 fold-change > 0.5 between *Cd4*<sup>+</sup>*Cd8a*<sup>-</sup> and *Cd4*<sup>-</sup>*Cd8a*<sup>+</sup> subsets of selection intermediates in scRNA-seq). N/C: No change. P < 2.2e-16, Z = 10.65. Asymptotic Linear-by-Linear Association Test. Data: Var2 (ordered) by Var1 (up < nc < down).



## **Attachment 5**

Lck Promotes Zap70-dependent LAT  
Phosphorylation by Bridging Zap70 to LAT

# Lck promotes Zap70-dependent LAT phosphorylation by bridging Zap70 to LAT

Wan-Lin Lo<sup>1</sup>, Neel H. Shah<sup>2</sup>, Nagib Ahsan<sup>3,4</sup>, Veronika Horkova<sup>5</sup>, Ondrej Stepanek<sup>5</sup>, Arthur R. Salomon<sup>6,7</sup>, John Kuriyan<sup>2,8</sup> and Arthur Weiss<sup>1,9\*</sup>

**T cell-antigen receptor (TCR) signaling requires the sequential activities of the kinases Lck and Zap70. Upon TCR stimulation, Lck phosphorylates the TCR, thus leading to the recruitment, phosphorylation, and activation of Zap70. Lck binds and stabilizes phospho-Zap70 by using its SH2 domain, and Zap70 phosphorylates the critical adaptors LAT and SLP76, which coordinate downstream signaling. It is unclear whether phosphorylation of these adaptors occurs through passive diffusion or active recruitment. We report the discovery of a conserved proline-rich motif in LAT that mediates efficient LAT phosphorylation. Lck associates with this motif via its SH3 domain, and with phospho-Zap70 via its SH2 domain, thereby acting as a molecular bridge that facilitates the colocalization of Zap70 and LAT. Elimination of this proline-rich motif compromises TCR signaling and T cell development. These results demonstrate the remarkable multifunctionality of Lck, wherein each of its domains has evolved to orchestrate a distinct step in TCR signaling.**

Signaling through the TCR is the defining event for proper thymocyte development and mature T cell homeostasis. TCR signaling is also critical for effective host responses to pathogens or tumors<sup>1–3</sup>. T cells interact with self-peptides bound to major-histocompatibility-complex proteins (self-pMHC) via their TCRs, throughout development and their lifespan, acquiring survival signals and avoiding autoreactivity. Simultaneously, T cells must be capable of responding to pathogen- or tumor-derived antigenic peptides bound to MHC molecules (pMHC) to mount rapid and appropriately protective responses. Although the molecular discrimination of self-pMHC from non-self-pMHC by the TCR plays a critical role in dictating these responses, recent engineered T cell therapies for cancer, which rely on artificial antigen-recognition domains fused with native intracellular signaling molecules, further underscore the importance of downstream TCR-proximal signaling events in controlling the specificity and sensitivity of T cell responses<sup>4</sup>.

Because the TCR has no intrinsic enzymatic activity, the tyrosine kinases Lck and Zap70 initiate TCR signaling. A pool of Lck, a Src family kinase, is active in T cells before pMHC recognition<sup>5</sup>. The level of Lck activity after TCR stimulation is controlled by multiple mechanisms<sup>6–10</sup>. For instance, the localization of Lck is regulated by its noncovalent association with the cytoplasmic segments of the CD4 and CD8 co-receptors. After engagement of the TCR with pMHC, the co-receptor coengagement localizes active Lck to the engaged TCR<sup>7</sup>. There, Lck phosphorylates the paired tyrosines of the immunoreceptor tyrosine-based activation motifs (ITAMs) in the invariant CD3 and  $\zeta$ -chains of the TCR complex<sup>8</sup>. If both tyrosines of an ITAM are phosphorylated, they form a high-affinity docking site for the tandem SH2 domains of Zap70 (refs<sup>10,11</sup>). Binding to the ITAMs partially relieves Zap70 autoinhibition. For

its full activation, Zap70 must also be phosphorylated by Lck to relieve its autoinhibition and to activate its catalytic activity, because Zap70 cannot be activated by transautophosphorylation<sup>12–14</sup>.

Thus, recruitment and activation of Zap70 are absolutely reliant on Lck catalytic activity<sup>14</sup>. Moreover, the binding of the Lck SH2 domain to phospho-Y319 in interdomain B of Zap70 may sustain Lck localization, its open active conformation, and the catalytic activities of both kinases, thereby providing positive feedback<sup>6,15,16</sup>. However, despite their colocalization, the two kinases have mutually exclusive preferences for their substrates<sup>14,17</sup>. Lck cannot phosphorylate the substrates of Zap70, namely the adaptors LAT and SLP76. Zap70 phosphorylates LAT and SLP76 on multiple tyrosines, thereby forming effective signaling complexes. LAT has four major tyrosine-phosphorylation sites that serve as docking sites for the SH2 domains of downstream signaling effectors. The assembly of LAT-based signalosomes is essential to amplify TCR-induced signals that result in calcium mobilization, mitogen-activated protein-kinase activation, and actin polymerization<sup>18</sup>.

Although many mechanisms prevent premature and inappropriate LAT phosphorylation, T cells must ensure rapid and specific LAT phosphorylation after agonist-pMHC stimulation of the TCR<sup>18</sup>. However, the prompt and specific phosphorylation of LAT after agonist-pMHC stimulation of the TCR presents a hurdle, considering that LAT is not known to directly associate with the TCR, where Zap70 is localized. Stimulated and activated Zap70 has been suggested to be induced to dissociate and diffuse away from the engaged TCR before the activated kinase encounters LAT<sup>19</sup>. However, such a mechanism could potentially decouple Zap70 activity from the TCR-recognition event and lead to inappropriate downstream signaling and amplification or premature termination of Zap70 activity via phosphatases or ubiquitin ligases<sup>20,21</sup>. Thus, the

<sup>1</sup>Division of Rheumatology, Rosalind Russell and Ephraim P. Engleman Arthritis Research Center, Department of Medicine, University of California, San Francisco, San Francisco, CA, USA. <sup>2</sup>Departments of Molecular and Cell Biology, University of California, Berkeley, Berkeley, CA, USA. <sup>3</sup>Division of Biology and Medicine, Alpert Medical School, Brown University, Providence, RI, USA. <sup>4</sup>Center for Cancer Research Development, Proteomics Core Facility, Rhode Island Hospital, Providence, RI, USA. <sup>5</sup>Institute of Molecular Genetics of the Czech Academy of Sciences, Prague, Czech Republic. <sup>6</sup>Department of Chemistry, Brown University, Providence, RI, USA. <sup>7</sup>Department of Molecular Biology, Cell Biology, and Biochemistry, Brown University, Providence, RI, USA. <sup>8</sup>The Howard Hughes Medical Institute, University of California, Berkeley, Berkeley, CA, USA. <sup>9</sup>The Howard Hughes Medical Institute, University of California, San Francisco, San Francisco, CA, USA. \*e-mail: [art.weiss@ucsf.edu](mailto:art.weiss@ucsf.edu)



question is raised of how Zap70 catalytic-effector function is appropriately coupled to TCR recognition.

Here, we report that Lck uses each of its functional domains to ensure that the agonist-pMHC-engaged TCR triggers efficient signal transduction leading to LAT phosphorylation. Our model suggests that Lck uses its SH2 domain to interact with TCR-bound Zap70 molecules that it has phosphorylated and activated, and its SH3 domain subsequently links Zap70 to its substrate, LAT, thus facilitating efficient TCR signal transduction. In LAT, we identified a proline-rich motif that is highly conserved across mammalian species and specifically interacts with the SH3 domain of Lck and consequently enhances LAT's phosphorylation by Zap70. Mutation of this proline-rich motif in LAT impeded TCR signal transduction and resulted in a significant decrease in thymocyte development. Our findings provide new insights into how efficient signal transduction by the TCR is coupled to the recognition of a bona fide agonist pMHC.

### Results

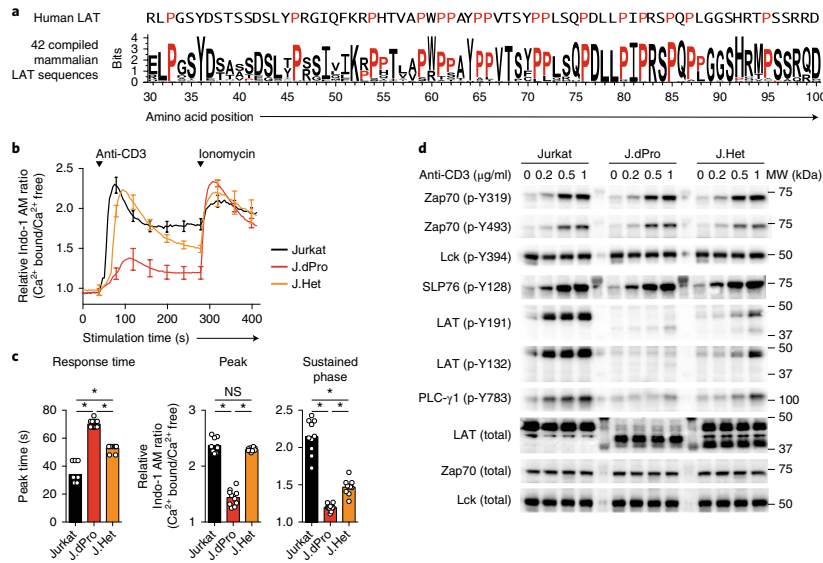
**LAT's proline-rich region is important for TCR signaling.** To understand how Zap70's catalytic-effector function mediates efficient LAT phosphorylation in response to TCR recognition, we compared the amino acid sequences of LAT from 42 mammals and identified an evolutionarily conserved amino acid sequence in the N-terminal membrane-proximal cytoplasmic segments of mammalian LAT molecules (Fig. 1a, Supplementary Fig. 1a and Supplementary Table 1). These sequences revealed a strikingly high degree of conservation, especially in the distribution and positioning of proline residues. The disproportionate presence of proline residues in LAT was also evident after we quantified the frequency of each amino acid in human LAT relative to other proteins (Supplementary Fig. 1b–d). Notably, no structural or functional properties of this proline-rich region of LAT have been reported in previous studies.

To explore the potential functional importance of this conserved sequence in LAT, we used CRISPR-Cas9 to generate mutants lacking the membrane-proximal segment in the *LAT* genomic locus, by using the Jurkat human T cell leukemic line, which is frequently used for TCR signaling studies. In one such mutant line, J.dPro, the resulting indels cause deletion of the proline-region-encoding sequences in both alleles (Supplementary Fig. 2a,b). The deletion of this proline-enriched segment did not interfere with the expression of LAT protein (Supplementary Fig. 2a and Fig. 1). J.dPro exhibited a delayed and markedly diminished cytoplasmic calcium increase in response to anti-CD3 stimulation (Fig. 1b,c). The calcium response was also affected, albeit much more moderately, in a heterozygous Jurkat variant clone (hereafter denoted J.Het), which contained only one allele of a nearly identical internal deletion of *LAT* (Fig. 1b,c and Supplementary Fig. 2b). Immunoblot analysis further revealed TCR-signaling defects in J.dPro mutant cells (Fig. 1d). The phosphorylation of LAT, as assessed on either Y132 or Y191, was markedly impaired in J.dPro cells. Presumably, as a consequence of its recruitment to phospho-Y132 LAT, the phosphorylation of the phospholipase PLC- $\gamma$ 1 was likewise diminished and markedly delayed, in agreement with the defective calcium responses observed. As expected, the CD3-mediated signaling events upstream of LAT remained intact, as evidenced by anti-CD3 stimulation of the mutant J.dPro cells inducing tyrosine phosphorylation of the Zap70 activation loop (phospho-Y493) and phosphorylation of SLP76. These results suggest that this evolutionarily conserved proline-enriched membrane-proximal region of LAT is critical for productive TCR signaling through LAT.

**The PIPRSP motif in LAT facilitates LAT phosphorylation.** The enrichment of prolines in the deleted segments of LAT suggested functional importance but may be explained by two hypotheses.

First, perhaps through yet-unknown structural properties of LAT, the proline-enriched segment in LAT may provide a minimal distance from the plasma membrane necessary for TCR-induced phosphorylation of its more C-terminal tyrosines. Alternatively, proline-enriched peptides may have important roles in intracellular signaling through their ability to interact in a sequence-specific context, for instance with SH3 domains<sup>22</sup>. Thus, the proline-rich region in LAT may interact with an SH3-containing protein that facilitates the ability of LAT to interact with Zap70, to relocate to engaged TCR complexes, or to assemble LAT clusters that might promote LAT phosphorylation. To distinguish among these possibilities, we explored the Eukaryotic Linear Motif resource to identify potential functional SH3-domain-binding sites in the membrane-proximal segment of LAT<sup>23</sup>. There were three potential proline-rich motifs in LAT predicted to interact with SH3 domains (Fig. 2a). Using CRISPR-Cas9, we generated a LAT-deficient Jurkat clone (J.LAT; Supplementary Fig. 2c,d) and reconstituted these cells with cDNAs encoding wild-type LAT or mutant LATs in which these three proline-enriched motifs had proline-to-alanine substitutions (Fig. 2a). Alanine mutations at the most evolutionarily conserved C-terminal PIPRSP motif markedly abrogated the ability to reconstitute a substantial calcium increase after anti-CD3 stimulation (Fig. 2b,c). Cells expressing the mutant AIARSA motif exhibited impaired TCR-induced phosphorylation of LAT at both Y132 and Y191 residues and diminished phosphorylation of PLC- $\gamma$ 1, whereas the other more N-terminal mutant motifs (AWAA or AAYAA) did not substantially impair the tyrosine phosphorylation of these signaling proteins (Fig. 2d). The AIARSA mutation consistently impaired TCR-induced phosphorylation of LAT and PLC- $\gamma$ 1 over a wide range of titrated CD3 stimuli (Supplementary Fig. 3a). Interestingly, in time-course experiments, the responses of cells expressing the AIARSA mutant motif eventually caught up to the responses observed with wild-type LAT (Supplementary Fig. 3b). Because these site-directed-mutagenesis experiments preserved the length of mutant LAT, the PIPRSP motif in LAT is likely to interact with other signaling molecules and promote LAT phosphorylation, thus precluding the possibility that the proline-rich region might function only as a structural spacer.

**Thymic selection signals require the PIPRSP motif in LAT.** To further examine the functional importance of the PIPRSP motif in LAT, we used a mouse model to explore whether primary mouse T lineage cells also rely on the PIPRSP-motif-containing LAT for pre-TCR and TCR signal transduction during thymocyte development. During thymic development, immature thymocytes require pre-TCR and TCR signals of appropriate strength to pass beta selection (mediated by the pre-TCR) and positive/negative selection (mediated by the mature TCR)<sup>24,25</sup>. LAT-deficient mice exhibit a severe developmental block at the beta-selection stage, which results from the inability of immature CD4<sup>+</sup>CD8<sup>-</sup> double-negative (DN) thymocytes that express the pre-TCR to transmit signals necessary for downstream translational and transcriptional programs required for proliferation and differentiation<sup>26,27</sup>. Thus, LAT-deficient mice provided a useful model to evaluate the functional ability of a PIPRSP-motif-mutant *LAT* in vivo to restore LAT function during development. We transduced CD45.2<sup>+</sup>Sca-1<sup>+</sup>c-Kit<sup>+</sup> LAT-deficient hematopoietic stem cells with lentiviruses expressing either wild-type LAT-P2A-mCherry or the mutant AIARSA LAT-P2A-mCherry. The mCherry was produced through the self-cleaving P2A peptide downstream of LAT, thus allowing us to identify cells expressing wild-type or mutant LAT (Fig. 3a). The comparable mean fluorescence intensities of mCherry expression, together with the results of our studies of this mutant in the Jurkat line (Supplementary Fig. 3), suggested that the expression of the wild-type and AIARSA LAT was similar (Fig. 3a). After 6–8 weeks, the expression of wild-type LAT successfully rescued the LAT-deficient thymocytes from the

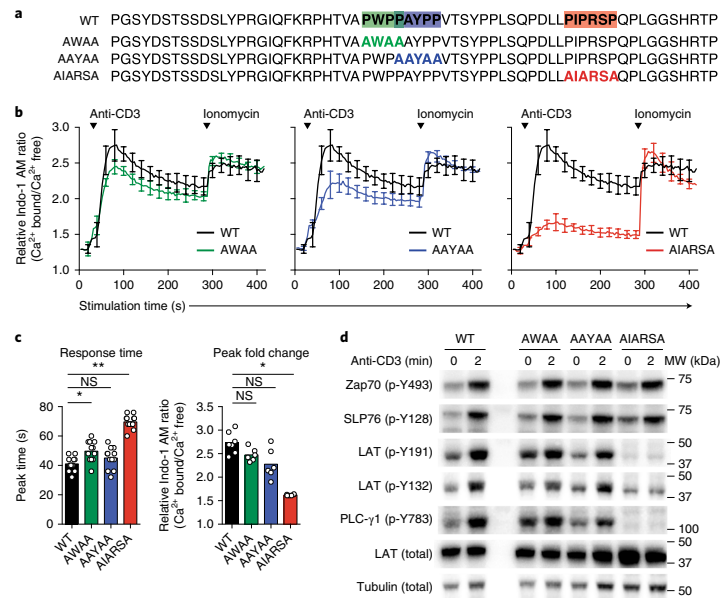


**Fig. 1 | A conserved proline-rich region in the membrane-proximal region of LAT is important for TCR signaling.** **a**, Sequence conservation, depicted in the membrane-proximal region of LAT in 42 mammalian species. The amino acid position is numbered on the basis of human LAT isoform 2, whose sequence is shown above the sequence logo. Proline residues are indicated in red. **b, c**, Intracellular free-calcium changes, expressed as the relative calcium-sensitive-fluorescence ratio of Jurkat and CRISPR-Cas9-generated Jurkat variants (J.dPro and J.Het) lacking the proline-enriched region, in response to anti-CD3 stimulation (0.5  $\mu\text{g/ml}$ ), as assessed with the calcium-indicator dye Indo-1 AM. **b**, Representative calcium-sensitive-fluorescence ratios in the indicated cells over time. Data are normalized to the basal calcium-sensitive ratio in unstimulated Jurkat cells at  $t=0$  (mean  $\pm$  s.d.).  $n=3$  technical replicates. Data are representative of at least two experiments. **c**, Quantification of the time required for Jurkat, J.dPro, or J.Het cells treated with anti-CD3 to reach the maximal Indo-1 AM ratio (left), or the magnitude of change in the Indo-1 AM ratio at the peak or the sustained phase from 200 s to 284 s (right). Each symbol represents an individual technical-replicate sample. Data are representative of duplicate samples in five independent experiments ( $n=10$ , mean  $\pm$  s.d.). \* $P < 0.0001$ ; NS, not significant; two-tailed Mann-Whitney test. **d**, Immunoblot analysis of phosphorylation of total TCR-proximal signaling molecules in Jurkat, J.dPro, or J.Het cells that were left unstimulated or were stimulated with anti-CD3 (concentrations indicated above blots) for 1.5 min. Data are representative of at least four independent experiments. Lanes separating cell-lysate samples contain mobility-marker proteins. MW, molecular weight.

LAT-deficient developmental block (Fig. 3b), whereas untransduced donor hematopoietic stem cells (mCherry-negative cells) remained blocked at the DN stage (data not shown). Thymocytes expressing wild-type LAT completed beta and positive selection, and matured into single-positive CD4<sup>+</sup> or CD8<sup>+</sup> (CD4SP or CD8SP) thymocytes (Fig. 3b–d and Supplementary Fig. 4a). In marked contrast, the expression of the mutant AIARSA LAT allowed only some DN immature thymocytes to pass beta selection and become DP cells, albeit inefficiently, thus resulting in relative accumulation of DN cells. Analysis of AIARSA-expressing DN subpopulations revealed a significant decrease in the DN4 stage and a concomitant increase in the DN3 stage, thus suggesting a partial block in the DN3-to-DN4 transition in which beta selection takes place (Fig. 3e,f and Supplementary Fig. 4b). The lack of the proline-rich motif in LAT also decreased positive selection, as evidenced by a significant twofold decrease in the CD4SP thymocyte population and a similar loss in CD24<sup>+</sup>TCR<sup>+</sup> mature CD8SP populations (Fig. 3b–d). During the positive-selection process, immature thymocytes upregulate expression of TCR and CD69, becoming TCR<sup>hi</sup> and CD69<sup>+</sup>. In cells expressing the AIARSA-mutant LAT, an approximate threefold decrease in TCR<sup>hi</sup>CD69<sup>+</sup> DP cells was observed (Fig. 3g,h and Supplementary Fig. 4c).

When DP thymocytes were stimulated by cross-linking anti-CD3 monoclonal antibodies (mAbs), cells expressing the AIARSA LAT mutant exhibited a markedly reduced calcium response (Fig. 4a) and impaired induction of Erk phosphorylation (Fig. 4b). Expression of CD5 can also be used as a proxy for TCR signal strength during thymic development. Despite similar TCR surface expression, CD4SP and CD8SP cells expressing the AIARSA LAT mutant had substantially lower CD5 protein expression (Fig. 4c), thereby supporting the notion that the AIARSA LAT mutant transduces weaker downstream signals. Thus, the absence of the PIPRSP proline-rich motif of LAT in T cell lineage development in vivo.

In peripheral lymphoid tissues, we did not observe significant differences in the frequencies of CD4<sup>+</sup> or CD8<sup>+</sup> T cell populations in AIARSA versus wild-type LAT-expressing bone marrow chimeras (Supplementary Fig. 5a). However, the expression of AIARSA consistently resulted in lower CD5 expression in peripheral CD4<sup>+</sup> and CD8<sup>+</sup> T cells, as was seen in thymocytes, although to a lesser extent (Supplementary Fig. 5b). In AIARSA-LAT-expressing CD4<sup>+</sup> and CD8<sup>+</sup> T cells, compared with the wild-type LAT-expressing T

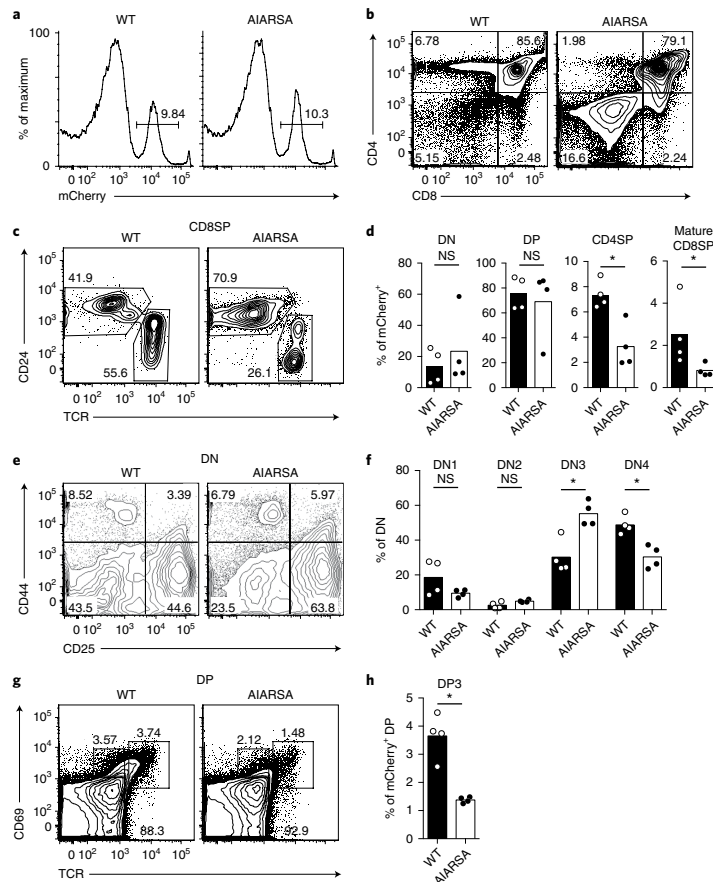


**Fig. 2 | A PIPRSP motif in LAT promotes the phosphorylation of LAT.** **a**, Location of three proline-rich motifs, PWPP, PAYPP, and PIPRSP, highlighted in green, blue, and red, respectively. Proline-to-alanine mutations in each of the motifs are shown below the wild-type (WT) sequences of human LAT. **b**, CRISPR-Cas9-generated LAT-deficient J.LAT cells were reconstituted with wild-type LAT or each proline-rich-motif-mutant LAT (AWAA, AAYAA, or AIARSA). Cells were loaded with Indo-1 AM and stimulated with 0.5  $\mu\text{g}/\text{ml}$  anti-CD3, and the changes in relative calcium-sensitive-fluorescence ratios over time for 400 s are shown (mean  $\pm$  s.d.;  $n=6$  technical replicates). Data are representative of five independent experiments with similar results. **c**, Left bar graph, analysis of response time to reach the peak (mean  $\pm$  s.d.;  $n=12$  technical replicates in five independent experiments). Experiments were done at least five times with similar results. \* $P=0.0029$  (exact value); \*\* $P<0.0001$ ; NS, not significant; two-tailed Mann-Whitney test. Right bar graph, quantification of the Indo-1 AM-ratio fold change at peak (mean  $\pm$  s.d.;  $n=7$  technical replicates in two experiments for wild type;  $n=6$  technical replicates in two experiments for AWAA, AAYAA, and AIARSA). Data are representative of at least five independent experiments. \* $P=0.0012$ ; NS, not significant; two-tailed Mann-Whitney test. **d**, Immunoblot analyses of J.LAT cells that were reconstituted with wild-type or mutant AWAA, AAYAA, or AIARSA LAT, and were left unstimulated or were treated with 0.5  $\mu\text{g}/\text{ml}$  anti-CD3 for 2 min. Data are representative of three experiments. Numbers to the right of cropped blots indicate the mobilities of molecular-mass-marker proteins (kDa). Tubulin, loading control.

cells, the CD44<sup>hi</sup>CD62L<sup>lo</sup> memory-like population was considerably enlarged (Supplementary Fig. 5c,d). The enlarged memory-like population may be a consequence of increased peripheral homeostatic proliferation in the AIARSA-LAT-expressing bone marrow chimeras. Thus, the mutations in the PIPRSP motif in LAT impaired thymic selection and led to fewer CD4SP and CD8SP cells developed in the thymus, and may have contributed to lymphopenia-induced T cell proliferation in the periphery.

**Lck associates with LAT in a PIPRSP-motif-dependent manner.** Our data demonstrate the importance of the PIPRSP motif in LAT in TCR signal transduction. The absence of the PIPRSP motif impaired the tyrosine phosphorylation of LAT itself and the activity of downstream signaling pathways important for T cell function and development. To explore the potential mechanism underlying this phenotype, we evaluated the role of the PIPRSP motif in mediating protein interactions with LAT. We stimulated the TCR on Jurkat cells expressing wild-type or AIARSA LAT proteins containing C-terminal Myc epitope tags, isolated LAT and its interacting proteins by immunoprecipitation, and used mass spectrometry to analyze the profiles of LAT-associated proteins. Mass spectrometry identified many proteins that were differentially

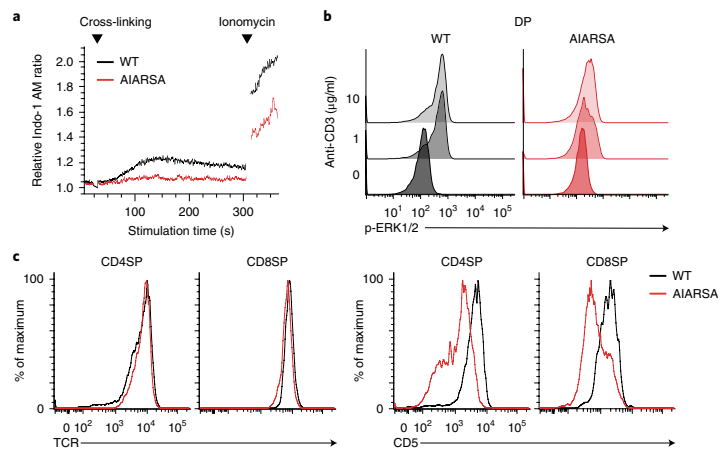
represented in wild-type and AIARSA LAT-associated interactomes (Supplementary Table 2). Unexpectedly, only ten of these proteins contained SH3 domains (Supplementary Table 3). Among these, Lck was noteworthy because of the abundance of its peptides and because it exhibited a differential capability of interacting with the proline-rich PIPRSP motif (Supplementary Fig. 6a). A previous study of the importance of the SH3 domain of Lck in downstream TCR signaling was of particular interest<sup>28</sup>. That study has shown that when a mutation at Trp97, which disrupts the function of the Lck SH3 domain, is introduced into mice, the mutation results in a significant decrease in beta selection and positive selection in thymocytes as well as reduced tyrosine phosphorylation of LAT, PLC- $\gamma$ 1, and Erk<sup>28</sup>. Consistent with our study, the phosphorylation of Zap70 and SLP76 was unperturbed<sup>28</sup>. These results are concordant with our findings with the AIARSA LAT mutant. Moreover, immunoblot analysis of LAT immunoprecipitates from TCR-stimulated cells further demonstrated that Lck inducibly associated with wild-type LAT to a greater degree than AIARISA-mutant LAT (Supplementary Fig. 6b). Together, our results suggested that Lck is an SH3-containing protein that interacts with LAT's PIPRSP motif and may mediate a functionally important interaction.



**Fig. 3 | Ectopic expression of LAT containing the PIPRSP-mutant motif AIARSA impairs thymocyte beta and positive selection in vivo.** Flow cytometric analysis of thymocytes from lethally irradiated bone marrow BoyJ (CD45.1<sup>+</sup>) chimeras reconstituted with CD45.2<sup>+</sup> LAT-deficient B6 hematopoietic stem cells transduced with lentiviruses expressing either wild-type LAT-P2A-mCherry (WT;  $n=4$  recipients) or mutant AIARSA LAT-P2A-mCherry (AIARSA;  $n=4$  recipients). Recipient mice were analyzed 6–8 weeks later. **a**, Representative mCherry expression of thymocytes, gated on CD45.2<sup>+</sup> cells. Numbers indicate percentages of mCherry<sup>+</sup> cells in each gate. **b**, Flow cytometric analysis of CD45.2<sup>+</sup> mCherry<sup>+</sup> thymocytes. Numbers in each quadrant indicate the percentage of cells in each. **c**, Flow cytometry analysis of CD24 versus TCR expression of CD45.2<sup>+</sup> mCherry<sup>+</sup> CD8SP thymocytes. **d**, Bar graphs representing the frequencies of DN, DP, CD4SP, and CD24-TCR<sup>+</sup> mature CD8SP thymocytes among CD45.2<sup>+</sup> mCherry<sup>+</sup> cells. Each symbol represents an individual mouse. Bars indicate the mean  $\pm$  s.d. ( $n=4$  independent animals in two independent experiments). \* $P=0.0286$ ; NS, not significant; two-tailed Mann-Whitney test. **e**, Flow cytometric analysis of DN1-to-DN4 cell development, on the basis of CD44 and CD25 expression, gated on CD45.2<sup>+</sup> mCherry<sup>+</sup> DN thymocytes. **f**, Frequency of DN1 (CD44<sup>+</sup>CD25<sup>-</sup>), DN2 (CD44<sup>+</sup>CD25<sup>+</sup>), DN3 (CD44<sup>-</sup>CD25<sup>+</sup>), and DN4 (CD44<sup>-</sup>CD25<sup>-</sup>) of CD45.2<sup>+</sup> mCherry<sup>+</sup> DN T cells in each quadrant of **e**. Bars indicate the mean  $\pm$  s.d. ( $n=4$  independent animals in two independent experiments). \* $P=0.0286$ ; NS, not significant; two-tailed Mann-Whitney test. **g**, Flow cytometric analysis of DP progression through thymic positive selection, on the basis of CD69 and TCR expression, gated on CD45.2<sup>+</sup> mCherry<sup>+</sup> DP thymocytes. **h**, Frequency of postselection DP3 (CD69<sup>+</sup>TCR<sup>hi</sup>) DP cells. Bars indicate the mean  $\pm$  s.d. ( $n=4$  independent animals in two independent experiments). \* $P=0.0286$ ; two-tailed Mann-Whitney test. All data are representative of two independent experiments with similar results.

**Lck bridges LAT and Zap70, thus enhancing LAT phosphorylation.** Given the concordance of our results with the AIARSA-mutant LAT and findings from previous studies on the inactivation

of the Lck SH3 domain, we hypothesized a mechanism to explain the role of the proline-rich PIPRSP motif in LAT for TCR signal transduction (Supplementary Fig. 6c). In our model, after TCR



**Fig. 4 | Mutation of the PIPRSP motif in LAT impedes TCR signal transduction of DP thymocytes. a**, Flow cytometric analysis of calcium-sensitive fluorescence changes in CD45.2<sup>+</sup>mCherry<sup>+</sup> DP T cells loaded with Indo-1 AM and stimulated with cross-linked anti-CD3 over time. **b**, Flow cytometric analysis of phosphorylated Erk in CD45.2<sup>+</sup>mCherry<sup>+</sup> DP thymocytes, in response to cross-linked anti-CD3 stimulation. **c**, Flow cytometric analysis of surface expression of the TCR (left) or CD5 (right) in CD45.2<sup>+</sup>mCherry<sup>+</sup> CD4SP or CD8SP thymocytes. Experiments were repeated independently twice with four independent animals and yielded similar results.

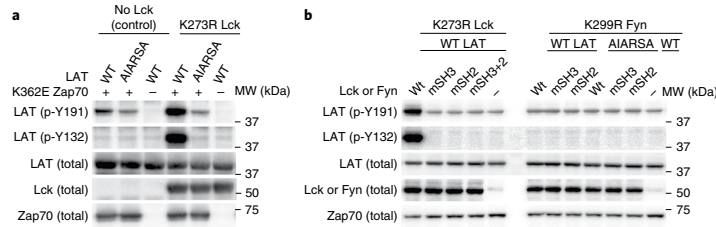
engagement, Lck may play multiple roles on the basis of both its catalytic and noncatalytic biochemical activities. First, in response to co-receptor-pMHC-TCR engagement, Lck has its well-established function as the protein tyrosine kinase that phosphorylates ITAM motifs in CD3 and  $\zeta$ -chains, and consequently leads to Zap70 recruitment. Second, it activates Zap70 by tyrosine phosphorylation. Third, Lck operates as a scaffold protein that stabilizes the active form of Zap70 through the previously described interaction between its SH2 domain with phospho-Y319 in Zap70, thereby also maintaining Lck in its open active conformation. Fourth, as described here, the SH3 domain of Lck binds the PIPRSP motif of LAT. Thus, through the latter two functions, Lck might act as a bridging molecule facilitating the interaction of Zap70 with LAT and promoting LAT phosphorylation.

To test this potential bridging function of Lck, we expressed Lck, LAT, and Zap70 in a heterologous cell system. Human embryonic kidney 293 (HEK293) cells, which do not express Lck, Zap70, or LAT, were used to study the mechanism of the putative interactions and functional consequences, i.e., LAT phosphorylation. To separate the dual roles of Lck, we used a kinase-inactive form of Lck (with the K273R mutation in the catalytic domain) that can function only as a scaffold protein (Supplementary Fig. 7a). We also took advantage of a recently identified mutation in Zap70, K362E, which disrupts autoinhibition and results in a weak activating effect of Zap70 catalytic activity (Supplementary Fig. 7a). To test our hypothesis, we expressed Lck<sup>K273R</sup> and Zap70<sup>K362E</sup> with either wild-type or mutant AIARSA LAT in HEK 293 cells, and examined the phosphorylation of two tyrosines on LAT: Y132 and Y191 (Supplementary Fig. 7b). We titrated the transfection ratio of Zap70 and LAT, and identified a dose range in which the weakly activated Zap70 displayed minimal phosphorylation of LAT. In the presence of the catalytically inactive Lck<sup>K273R</sup>, the phosphorylation of LAT Y132 and Y191 residues by Zap70<sup>K362E</sup> considerably increased (Fig. 5a). Notably, the increased phosphorylation of LAT was highly dependent on its PIPRSP motif, because the proline-to-alanine

mutations impaired the phosphorylation of LAT (Fig. 5a). In addition to the PIPRSP motif in LAT, the binding functions of both the SH3 and SH2 domains of catalytically inactive Lck were crucial for enhancing the phosphorylation of LAT (Fig. 5b). Inactivating point mutations in either the SH3 or the SH2 domain of catalytically inactive Lck diminished the phosphorylation of LAT. Thus, Lck's SH3 domain (which binds the PIPRSP proline-rich motif of LAT) and SH2 domain (which binds phospho-Y319 in interdomain B of Zap70 (ref. 15)) together potentially facilitate the formation of a transient LAT-Lck-Zap70 complex. Interestingly, the catalytically inactive Src family kinase Fyn<sup>K299R</sup>, also expressed in T cells, did not exhibit a similar enhancing effect on the phosphorylation of LAT (Fig. 5b). Although Fyn is structurally similar to Lck, having SH3 and SH2 domains, the binding specificities of these domains differ between Fyn and Lck<sup>29</sup>. Thus, the interaction between the SH3 domain of Lck and the PIPRSP motif of LAT exhibits a degree of specificity. These results support our hypothesis that after T cell stimulation, Lck's interaction with the PIPRSP motif of LAT may facilitate Zap70's phosphorylation of LAT.

#### The PIPRSP motif promotes localization of LAT to pMHC-TCR.

To explore the possibility that TCR stimulation by agonist pMHC might trigger the relocalization of LAT to engaged TCR complexes during antigen recognition, we took advantage of engineered Jurkat cells that express the mouse OT-I TCR and human CD8, and either do or do not express human Lck (J.OT-I.hCD8.Lck KO or J.OT-I.hCD8.Lck-FLAG, respectively). The coexpression of human CD8 facilitates the interaction of mouse OT-I TCR with mouse MHC I H-2K<sup>b</sup> (Supplementary Fig. 8a,b), with comparable affinity to that of mouse CD8 (ref. 30). We stimulated each of these cell lines with H-2K<sup>b</sup> OVA MHC class I tetramers and used anti- $\zeta$ -chain mAbs to immunoprecipitate proteins associated with engaged co-receptor-TCR complexes. First, the use of the Lck-deficient line demonstrated a requirement for Lck in inducible phosphorylation of the  $\zeta$ -chain and associated proteins. In cells expressing Lck, H-2K<sup>b</sup> OVA



**Fig. 5 | Interaction of the Lck SH3 domain and the LAT PIPRSP motif enhances Zap70-dependent phosphorylation of LAT.** A reconstituted system in HEK 293 cells was used to examine the regulation of LAT phosphorylation (additional data in Supplementary Fig. 7). Transient transfection of wild-type or AIARSA-mutant LAT, Zap70<sup>K362E</sup>, and/or Lck<sup>K273R</sup> or Fyn<sup>K299R</sup> were performed in HEK 293 cells as indicated. Data are representative of at least three independent experiments. **a**, Immunoblot analysis of LAT phosphorylated on Y132 and Y191 in HEK293 cells reconstituted with wild-type or AIARSA-mutant LAT, along with the presence of kinase-inactive Lck (K273R mutant) or control protein GFP, and weakly autoactivated Zap70 (K362E mutant). Data are representative of three experiments. **b**, Immunoblot analysis of phosphorylation of LAT in HEK 293 cells reconstituted with wild-type or AIARSA-mutant LAT, Zap70<sup>K362E</sup>, as well as Lck<sup>K273R</sup> or Fyn<sup>K299R</sup> with additional mutations in SH3 or SH2 domains, as indicated above the blots. Wt, kinase-inactive Lck or Fyn with functional SH3 and SH2 domains (Lck<sup>K273R</sup> or Fyn<sup>K299R</sup>); mSH3, mutant SH3 domain (Lck<sup>W97A K274R</sup> or Fyn<sup>W119A K299R</sup>); mSH2, mutant SH2 domain (Lck<sup>R154K K273R</sup> or Fyn<sup>R176A K299R</sup>); mSH3+2, mutant SH3 and SH2 domain (Lck<sup>W97A R154K K274R</sup>). Data are representative of three experiments.

tetramers induced signaling, as evidenced by  $\zeta$ -chain phosphorylation and the induction of interacting phosphoproteins (Fig. 6a). We observed TCR-stimulation-induced association of Zap70 and Lck with the  $\zeta$ -chain immunoprecipitates (Fig. 6a). Moreover, we detected an increase in phospho-LAT in these  $\zeta$ -chain immunoprecipitates. These data are consistent with LAT relocation to the stimulated TCR complexes, where activated Zap70 and Lck both are localized. With mouse OT-II CD4<sup>+</sup> T cells, we also observed similar results (Fig. 6b). Furthermore, we used CRISPR-Cas9 to generate LAT-deficient J.OT-I.hCD8.Lck-FLAG Jurkat variants and then reconstituted cells with either wild-type or AIARSA-mutant LAT. After H-2K<sup>b</sup> OVA tetramer stimulation followed by  $\zeta$ -chain immunoprecipitation, wild-type LAT, but not AIARSA LAT, associated with the  $\zeta$ -chain (Fig. 6c). These results are consistent with our working model in which the PIPRSP motif of LAT may contribute to relocalization of LAT to engaged TCR complexes.

## Discussion

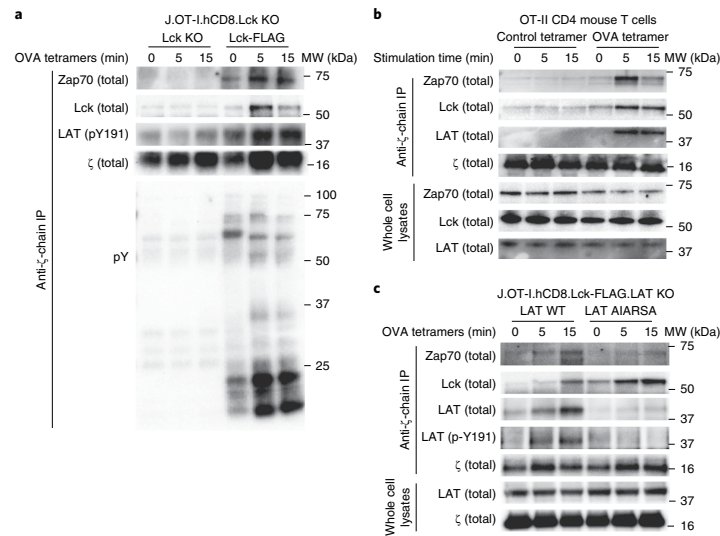
Our study revealed a mechanistic explanation for how Zap70 phosphorylates one of its key substrates, LAT. This process is mediated by an unanticipated scaffolding function of Lck, a kinase whose catalytic activity is critical to many events in the initiation of TCR signaling. In our model (Supplementary Fig. 6c), every structural feature of Lck is specifically accommodated in TCR's recognition of agonist pMHC. First, the acylation sites of Lck provide membrane anchorage. Second, the cysteine-rich motif within its unique domain allows for its linkage to CD4 or CD8 co-receptors. Third, the kinase domain promotes the phosphorylation of ITAMs and Zap70, thus leading to the eventual catalytic activation of Zap70. The Lck SH2 domain, which can interact with Y505 and consequently promote autoinhibition, can also bind phospho-Y319 in Zap70 and consequently maintain the open and active state of both Zap70 and Lck during TCR signaling. The Lck SH3 domain not only participates in its autoinhibition but, as shown here, also provides a unique link to the proline-rich motif in LAT, thereby recruiting activated Zap70 to LAT. Accommodating every structural feature of an SFK in a single cellular process is rare and suggests that Lck has uniquely evolved to serve these functions in TCR recognition and signaling. Because Lck is associated with co-receptors, which are involved in the recognition of pMHC, our model suggests that Zap70 and LAT are linked to TCR recognition of pMHC through Lck's ability to function both as a kinase and as a bridging scaffold that orchestrates efficient TCR signaling.

The segment of LAT that links its transmembrane segment to key tyrosines had no previously identified function. We found that the evolutionarily conserved segment contained one key functionally important proline-rich motif, PIPRSP. Mutation of this motif partially impeded TCR signaling and calcium responses. This PIPRSP motif supported efficient T cell development and function, as evidenced by bone marrow chimera studies. LAT is a major TCR signaling hub that coordinates many signaling effectors; thus, the role of the PIPRSP motif in facilitating LAT phosphorylation contributes to a pivotal event in TCR signal transduction.

The T cell developmental and functional deficiency resulting from the expression of proline-motif-mutant LAT was remarkably consistent with the results from a previously published study showing that an inactivating SH3-domain mutant of Lck (Lck<sup>W97A</sup>) impedes thymocyte development, as a result of partial blocks in beta and positive selection<sup>28</sup>. Although similar numbers of peripheral T cells were reported in Lck<sup>W97A</sup> mice and wild-type mice, the mutant cells were functionally impaired, as evidenced by diminished LAT and PLC1 phosphorylation<sup>31</sup>. These results are consistent with ours and support our proposed interaction between Lck and LAT during the initiation phase of TCR signal transduction. Notably, SLP76 was normally phosphorylated in both studies and may reflect the role of other adaptor proteins, such as CD6 (ref. 32).

Thymocytes reconstituted with AIARSA-mutant LAT exhibited an impaired ability to transition across pre-TCR and TCR developmental checkpoints. However, T cells in the periphery exhibited some evidence of accumulation of effector memory cells. This result may reflect the effects of an altered repertoire being inefficiently selected in the setting of impaired TCR signaling, which also mirror findings from previous work on dysfunctional LAT mutants, such as LAT<sup>Y136F</sup> knock-in mice<sup>33,34</sup>. T cells can use LAT-independent signaling pathways that promote the activation of Erk<sup>35–42</sup>, thus potentially explaining why the AIARSA mutant in LAT had less of an effect on the phosphorylation of Erk.

Signaling by the TCR critically depends on the integrated functions of the Lck and Zap70 kinases. The Zap70 kinase uses its tandem SH2 domains to be recruited to the phosphorylated ITAMs of the stimulated TCR. Protein-interaction domains of cytoplasmic tyrosine kinases were thought to be responsible for their substrate specificity by conferring their colocalization to substrates. Recent studies of Zap70 suggest that the kinase domain alone is sufficient for substrate specificity<sup>14</sup>. However, how activated Zap70, bound to the TCR, efficiently interacts with its substrate, LAT, had been



**Fig. 6 | TCR engagement triggers the association of LAT with TCR signaling complexes.** **a**, Lck-deficient J.Lck cells that were reconstituted with mouse OT-I TCR and human CD8, with or without FLAG-tagged human Lck. Cells were stimulated with H-2K<sup>b</sup> OVA tetramers (SIINFEKL) for the indicated times. Lysates were prepared and immunoprecipitated with anti- $\zeta$ -chain mAbs (clone 6B10). Immunoprecipitates (IP) were analyzed by immunoblotting and probed for Zap70, FLAG (Lck), phospho-LAT, and phosphotyrosine as indicated. Data are representative of three experiments. **b**, Mouse OT-II CD4 T cells were stained with H-2A<sup>b</sup> OVA tetramers or control tetramers on ice, and stimulated by warming at 37 °C for the indicated times. After lysis in NP-40, lysates were immunoprecipitated with anti- $\zeta$ -chain mAbs and analyzed by immunoblotting as in **a**. Data are representative of two experiments. **c**, LAT-deficient J.OT-I.hCD8.Lck-FLAG cells were reconstituted with wild-type or AIARSA LAT. Cells were stimulated, lysed, and immunoprecipitated with anti- $\zeta$ -chain mAbs as in **a**. Immunoprecipitates or whole cell lysates were analyzed by immunoblotting and probed for Zap70, FLAG (Lck), LAT, and phospho-LAT as indicated. Data are representative of four experiments.

unclear. Recent imaging studies have suggested that activated Zap70 is inducibly released from ITAM motifs<sup>19</sup>. A mobile but membrane-associated active pool of Zap70 may diffuse to and possibly phosphorylate distant LAT molecules, thereby allowing multiple Zap70 molecules that transiently interact with the stimulated TCR to amplify signaling. Although our study clearly indicates that the LAT proline-rich motif is important for the efficient phosphorylation of LAT by Zap70, we cannot exclude the possibility that a TCR-independent complex of Zap70 and Lck, or Lck and LAT, might also exist distal from the pMHC-bound TCR. However, the proposed release of Zap70 uncouples its function from TCR recognition of agonist pMHC and does not offer a means of protection from inactivation by cellular phosphatases or ubiquitin ligases after release from the TCR, thus raising concerns regarding how Zap70 would remain active. Moreover, our biochemical data with pMHC-tetramer stimulation suggested that LAT was recruited to the pMHC-stimulated TCR complex, which also contained Lck and Zap70. This result suggests that at least some LAT directly interacted with the stimulated TCR complex. Further work will be needed to assess the site at which Zap-70, Lck, and LAT form a functional signaling unit, and the stability as well as the longevity of these interactions. A recent report has also suggested that the potential interaction between Lck and LAT may fine-tune proximal TCR signaling<sup>43</sup>. Nonetheless, the evolutionarily conserved and functionally important proline-rich motif in LAT that we identified provides previously unappreciated insights into how components of the initially assembled TCR signaling machinery transduce information downstream via newly identified direct interactions.

## Methods

Methods, including statements of data availability and any associated accession codes and references, are available at <https://doi.org/10.1038/s41590-018-0131-1>.

Received: 17 January 2018; Accepted: 18 April 2018;

Published online: 18 June 2018

## References

- van der Merwe, P. A. & Dushek, O. Mechanisms for T cell receptor triggering. *Nat. Rev. Immunol.* **11**, 47–55 (2011).
- Chakraborty, A. K. & Weiss, A. Insights into the initiation of TCR signaling. *Nat. Immunol.* **15**, 798–807 (2014).
- Malissen, B. & Bongrand, P. Early T cell activation: integrating biochemical, structural, and biophysical cues. *Annu. Rev. Immunol.* **33**, 539–561 (2015).
- Hartmann, J., Schüsler-Lenz, M., Bondanza, A. & Buchholz, C. J. Clinical development of CAR T cells: challenges and opportunities in translating innovative treatment concepts. *EMBO Mol. Med.* **9**, 1183–1197 (2017).
- Nika, K. et al. Constitutively active Lck kinase in T cells drives antigen receptor signal transduction. *Immunity* **32**, 766–777 (2010).
- Thill, P. A., Weiss, A. & Chakraborty, A. K. Phosphorylation of a tyrosine residue on Zap70 by Lck and its subsequent binding via an SH2 domain may be a key gatekeeper of T cell receptor signaling in vivo. *Mol. Cell. Biol.* **36**, 2396–2402 (2016).
- Courtney, A. H. et al. A Phosphosite within the SH2 domain of Lck regulates its activation by CD45. *Mol. Cell* **67**, 498–511.e496 (2017).
- Stepanek, O. et al. Coreceptor scanning by the T cell receptor provides a mechanism for T cell tolerance. *Cell* **159**, 333–345 (2014).
- van Oers, N. S., Killeen, N. & Weiss, A. Lck regulates the tyrosine phosphorylation of the T cell receptor subunits and ZAP-70 in murine thymocytes. *J. Exp. Med.* **183**, 1053–1062 (1996).

10. Hatada, M. H. et al. Molecular basis for interaction of the protein tyrosine kinase ZAP-70 with the T-cell receptor. *Nature* **377**, 32–38 (1995).
11. Love, P. E. & Hayes, S. M. ITAM-mediated signaling by the T-cell antigen receptor. *Cold Spring Harb. Perspect. Biol.* **2**, a002485 (2010).
12. Deindl, S. et al. Structural basis for the inhibition of tyrosine kinase activity of ZAP-70. *Cell* **129**, 735–746 (2007).
13. Yan, Q. et al. Structural basis for activation of ZAP-70 by phosphorylation of the SH2-kinase linker. *Mol. Cell. Biol.* **33**, 2188–2201 (2013).
14. Shah, N. H. et al. An electrostatic selection mechanism controls sequential kinase signaling downstream of the T cell receptor. *eLife* **5**, e20105 (2016).
15. Pelosi, M. et al. Tyrosine 319 in the interdomain B of ZAP-70 is a binding site for the Src homology 2 domain of Lck. *J. Biol. Chem.* **274**, 14229–14237 (1999).
16. Wang, H. et al. ZAP-70: an essential kinase in T-cell signaling. *Cold Spring Harb. Perspect. Biol.* **2**, a002279 (2010).
17. Mukherjee, S. et al. Monovalent and multivalent ligation of the B cell receptor exhibit differential dependence upon Syk and Src family kinases. *Sci. Signal.* **6**, ra1 (2013).
18. Balagopal, L., Coussens, N. P., Sherman, E., Samelson, L. E. & Sommers, C. L. The LAT story: a tale of cooperativity, coordination, and choreography. *Cold Spring Harb. Perspect. Biol.* **2**, a005512 (2010).
19. Katz, Z. B., Novotná, L., Blount, A. & Lillemeier, B. F. A cycle of Zap70 kinase activation and release from the TCR amplifies and disperses antigenic stimuli. *Nat. Immunol.* **18**, 86–95 (2017).
20. Luis, B. S. & Carpino, N. Insights into the suppressor of T-cell receptor (TCR) signaling-1 (Sts-1)-mediated regulation of TCR signaling through the use of novel substrate-trapping Sts-1 phosphatase variants. *FEBS J.* **281**, 696–707 (2014).
21. Yang, M. et al. K33-linked polyubiquitination of Zap70 by Nrdp1 controls CD8<sup>+</sup> T cell activation. *Nat. Immunol.* **16**, 1253–1262 (2015).
22. Mayer, B. J. The discovery of modular binding domains: building blocks of cell signalling. *Nat. Rev. Mol. Cell Biol.* **16**, 691–698 (2015).
23. Dinkel, H. et al. ELM 2016: data update and new functionality of the eukaryotic linear motif resource. *Nucleic Acids Res.* **44**, D294–D300 (2016). D1.
24. Michie, A. M. & Zúñiga-Pflücker, J. C. Regulation of thymocyte differentiation: pre-TCR signals and beta-selection. *Semin. Immunol.* **14**, 311–323 (2002).
25. Moran, A. E. & Hogquist, K. A. T-cell receptor affinity in thymic development. *Immunology* **135**, 261–267 (2012).
26. Zhang, W. et al. Essential role of LAT in T cell development. *Immunity* **10**, 323–332 (1999).
27. Shen, S., Zhu, M., Lau, J., Chuck, M. & Zhang, W. The essential role of LAT in thymocyte development during transition from the double-positive to single-positive stage. *J. Immunol.* **182**, 5596–5604 (2009).
28. Rudd, M. L., Tua-Smith, A. & Straus, D. B. Lck SH3 domain function is required for T-cell receptor signals regulating thymocyte development. *Mol. Cell. Biol.* **26**, 7892–7900 (2006).
29. Palacios, E. H. & Weiss, A. Function of the Src-family kinases, Lck and Fyn, in T-cell development and activation. *Oncogene* **23**, 7990–8000 (2004).
30. Purbhoo, M. A. et al. The human CD8 coreceptor effects cytotoxic T cell activation and antigen sensitivity primarily by mediating complete phosphorylation of the T cell receptor zeta chain. *J. Biol. Chem.* **276**, 32786–32792 (2001).
31. McCoy, M. E., Finkelman, F. D. & Straus, D. B. Th2-specific immunity and function of peripheral T cells is regulated by the p56Lck Src homology 3 domain. *J. Immunol.* **185**, 3285–3294 (2010).
32. Paster, W. et al. A THEMIS:SHP1 complex promotes T-cell survival. *EMBO J.* **34**, 393–409 (2015).
33. Aguado, E. et al. Induction of T helper type 2 immunity by a point mutation in the LAT adaptor. *Science* **296**, 2036–2040 (2002).
34. Sommers, C. L. et al. A LAT mutation that inhibits T cell development yet induces lymphoproliferation. *Science* **296**, 2040–2043 (2002).
35. Miyaji, M. et al. Genetic evidence for the role of Erk activation in a lymphoproliferative disease of mice. *Proc. Natl. Acad. Sci. USA* **106**, 14502–14507 (2009).
36. Kortum, R. L. et al. A phospholipase C- $\gamma$ 1-independent, RasGRP1-ERK-dependent pathway drives lymphoproliferative disease in linker for activation of T cells-Y136F mutant mice. *J. Immunol.* **190**, 147–158 (2013).
37. Ravichandran, K. S. et al. Interaction of Shc with the zeta chain of the T cell receptor upon T cell activation. *Science* **262**, 902–905 (1993).
38. Ravichandran, K. S., Lorenz, U., Shoelson, S. E. & Burakoff, S. J. Interaction of Shc with Grb2 regulates association of Grb2 with mSOS. *Mol. Cell. Biol.* **15**, 593–600 (1995).
39. Ravichandran, K. S., Lorenz, U., Shoelson, S. E. & Burakoff, S. J. Interaction of Shc with Grb2 regulates the Grb2 association with mSOS. *Ann. NY Acad. Sci.* **766**, 202–203 (1995).
40. Zhou, M. M. et al. Structure and ligand recognition of the phosphotyrosine binding domain of Shc. *Nature* **378**, 584–592 (1995).
41. Ravichandran, K. S. et al. Evidence for a requirement for both phospholipid and phosphotyrosine binding via the Shc phosphotyrosine-binding domain in vivo. *Mol. Cell. Biol.* **17**, 5540–5549 (1997).
42. Pratt, J. C. et al. Requirement for Shc in TCR-mediated activation of a T cell hybridoma. *J. Immunol.* **163**, 2586–2591 (1999).
43. Arbulo-Echevarria, M. M. et al. A stretch of negatively charged amino acids of linker for activation of T-cell adaptor has a dual role in T-cell antigen receptor intracellular signaling. *Front. Immunol.* **9**, 115 (2018).

#### Acknowledgements

We thank L. Samelson and C. Sommers (NIH) for sharing the LAT-deficient mouse line; T. Kadlecik for generating the J.Lck mutant Jurkat cell clone; A. Roque for animal husbandry; W. Paster (Medical University Vienna) for sharing the CD8 expression vector; T. Brdicka (IMG, Prague) for sharing the Lck-encoding DNA sequence; the UCSF Parnassus Flow Cytometry Core for maintaining FACSaria instruments and services; the NIH Tetramer Core Facility for providing the H-2K<sup>b</sup> OVA tetramers and H-2A<sup>b</sup> OVA tetramers; and D. L. Donermeyer, B. B. Au-Yeung, H. Wang, and C. Morley for critical reading of the manuscript and providing comments. This work was supported by the Jane Coffin Childs Fund 61-1560 (to W.-L.L.); the Damon Runyon Cancer Research Foundation 2198-14 (to N.H.S.); the Czech Science Foundation GJ16-09208Y (to O.S.); the Howard Hughes Medical Institute (to A.W. and J.K.); NIH, NIAID P01 AI091580-06 (to A.W., J.K., and A.R.S.); R01 AI083636 and P30 GM110759 (to A.R.S.); and DRC Center Grant P30 DK063720 (UCSF Parnassus Flow Cytometry Core).

#### Author contributions

W.-L.L., N.H.S., and A.W. designed the experiments, W.-L.L., N.H.S., N.A., and V.H. conducted the experiments; W.-L.L., N.H.S., N.A., A.R.S., J.K., and A.W. analyzed data and provided intellectual input; V.H. and O.S. provided advice and reagents. W.-L.L., N.H.S., N.A., V.H., O.S., A.R.S., and A.W. wrote the manuscript.

#### Competing interests

The authors declare no competing interests.

#### Additional information

**Supplementary information** is available for this paper at <https://doi.org/10.1038/s41590-018-0131-1>.

**Reprints and permissions information** is available at [www.nature.com/reprints](http://www.nature.com/reprints).

**Correspondence and requests for materials** should be addressed to A.W.

**Publisher's note:** Springer Nature remains neutral with regard to jurisdictional claims in published maps and institutional affiliations.



## Methods

**Mice and cell lines.** The mice used in these studies were housed in the specific-pathogen-free facilities at the University of California, San Francisco, and were treated according to protocols that were approved by the UCSF Animal Care Ethics and Veterinary Committees, and are in accordance with NIH guidelines. The LAT-deficient mouse line (on a C57BL/6 background) was a gift from L. Samelson and C. Sommers (NIH). BoyJ (CD45.1) mice were obtained from Jackson Laboratories (B6.SJL-Ptpcr Pepcb/BoyJ). The human leukemic Jurkat T cell line, or Jurkat variants with LAT deficiency or knock-in mutations, were maintained in RPMI culture medium supplemented with 5% FBS and 2 mM glutamine. Cell lines that were reconstituted with wild-type LAT or various mutant LAT constructs were maintained in RPMI culture medium supplemented with 5% FBS, 2 mM glutamine, and 0.5 mg/ml of the aminoglycoside geneticin (G418). HEK293 cells were obtained from the ATCC and were maintained in DMEM supplemented with 10% FBS and 2 mM glutamine.

**Compilation and analysis of orthologous LAT sequences.** The mammalian LAT sequences used to generate Fig. 1 and Supplementary Fig. 1 were compiled through a series of protein-protein BLAST searches in the NCBI nonredundant protein database, as previously described<sup>4</sup>. A total of 42 mammalian LAT sequences were identified. Sequence logos were generated with the online tool WebLogo<sup>4</sup>.

**Generation of LAT-deficient or knock-in mutant Jurkat variants.** The Jurkat variants J.LAT (deficiency in LAT), J.dPro and J.Het (hemizygous or heterozygous mutant LAT lacking the membrane-proximal proline-rich region in LAT) were generated by transiently expressing Cas9, a guide sgRNA against the LAT proline-rich region and ssODN repair template, as previously described<sup>31</sup>. In brief, guide sgRNAs were cloned into the pU6-(BbsI)-CBh-Cas9-TZA-BFP vector (Addgene plasmid no. 64323) and electroporated into Jurkat T cells along with an ssODN repair template. Single cells were sorted into 96-well plates the next day. Successful knock-in-mutant clones were selected by screening with immunoblots probed for anti-C-terminal LAT (Santa Cruz Biotechnology, clone no. M19, cat. no. sc-5320), as shown in Supplementary Fig. 1. LAT-deficient clones (J.LAT) were also selected from the screen. Genomic DNA of J.LAT, J.dPro, and J.Het cells was purified and used as a template for genotyping. PCR products amplified from genomic DNA of J.Pro and J.Het were TOPO cloned into pCR2.1 vectors and prepared for sequencing. Additionally, cDNA products of J.dPro and J.Het cells were prepared, and LAT cDNA from J.Pro or J.Het cells was amplified by PCR, TOPO cloned, and sequenced. The oligonucleotides used in these studies were as follows: LAT sgRNA sense, 5'-CACCGCCATCTCCCGCGGGATTCTG A-3'; antisense, 5'-AAACTCAGAAATCCCGCGGGGAAGATGGC-3'; LAT ssODN HDR template, 5'-TCCTGGCTCACCAGCCCTCTCTTCCAGGCTCCTACGACTACCCA-TACGATGTTCCAGATTACGCTAGCACATCTCCAGATAGGTGAGTCCCGCCAGCATAGGCTGGCCTGAGCTGACTTGTCTCCCTCTCACCTCTCTTTGAAGCAACAGTGTGGCGACTACGAGAACGAGGGTGGCGTCTGGGATCCGAGGT-3'; LAT gDNA screen sense, 5'-AGGTGAGTGGAAACTGTGTG-3'; antisense, 5'-GCCTGGTGTGTATAGTCTGT-3'; LAT cDNA screen sense, 5'-GCTCTGCTGCTGCCATCC-3'; and antisense, 5'-AGTCTTAGCCGCTCCAGGAT-3'.

**Reconstituted LAT-deficient J.Lat cells with LAT mutants.** Reconstituted LAT-deficient (J.Lat) lines were generated by electroporation of J.Lat cells with a pEF vector to express WT LAT and AWA-1, AAYAA-1, and AIARSA-mutant LAT, and subsequent selection with 2 mM G418. Individual clones were single-cell sorted into 96-well plates and were later assessed for comparable CD3 expression by flow cytometry analysis and for comparable LAT expression by immunoblot analysis.

**Intracellular calcium measurements.** Jurkat cells and LAT-mutant variants were washed with PBS twice and loaded with 1  $\mu$ M Indo-1 AM calcium-indicator dye (Thermo Fisher I1223) at 37°C for 30 min in RPMI medium. The cells were then washed with PBS twice, and transferred into 96-well plates. Changes in the fluorescence ratio (violet/blue) after the addition of anti-CD3 (clone OKT3; Harlan or Tonbo Biosciences cat. no. 70-0037) or ionomycin were recorded with a Flex Station II instrument (Molecular Probes) in SoftMax Pro software. The data were imported into GraphPad Prism software for analysis and production of graphs. Calcium responses in primary thymocytes from bone marrow chimera studies were analyzed through flow cytometry. Cells were loaded with 1.5  $\mu$ M Indo-1 AM at 37°C in RPMI medium supplemented with 5% FBS for 30 min. After being loaded with Indo-1, the cells were stained with antibodies to CD4, CD8, and CD45.2. The cells were analyzed by flow cytometry and stimulated with 1  $\mu$ g/ml anti-CD3 (clone 145-2C11; Harlan), then cross-linked with 50 ng/ml goat anti-Armenian hamster IgG (Jackson ImmunoResearch cat. no. 127-005-099). Changes in intracellular calcium concentrations were monitored as the ratio of Indo-1 (blue/violet) and are displayed as a function of time.

**Immunoblot analysis.** Jurkat and derivative cells were washed with PBS, resuspended at  $5 \times 10^6$  cells/ml, and allowed to rest for 30 min at 37°C. The cells were left unstimulated or were stimulated with anti-CD3 (clone OKT3; Harlan or Tonbo Biosciences cat. no. 70-0037) over time, as described in each experiment.

Then the cells were lysed by direct addition of 10% NP-40 lysis buffer to a final concentration of 1% NP-40 (containing the inhibitors 2 mM NaVO<sub>3</sub>, 10 mM NaF, 5 mM EDTA, 2 mM PMSE, 10  $\mu$ g/ml aprotinin, 1  $\mu$ g/ml pepstatin, and 1  $\mu$ g/ml leupeptin). The lysates were placed on ice and centrifuged at 13,000 g to pellet cell debris. The supernatants were run on NuPAGE 4–12%, 8% or 10% Bis-Tris protein gels (Thermo Fisher) and transferred to PVDF membranes with a Trans-Blot Turbo Transfer System (Bio-Rad). Membranes were blocked with TBS-T buffer containing 3% BSA, then probed with primary antibodies as described, overnight at 4°C or 2 h at room temperature (25°C). The following day, the blots were rinsed and incubated with HRP-conjugated secondary antibodies. The blots were detected with a chemiluminescent substrate and a Bio-Rad Chemi-Doc imaging system. For all antibodies used, the sources and catalog numbers are listed in the Reporting Summary.

**Production of lentivirus expressing WT or AIARSA LAT.** Mouse WT LAT was cloned into the pHR backbone under the control of the *EF1A* promoter. The mouse AIARSA LAT mutant was generated with a QuikChange Lightning site-directed mutagenesis kit (Agilent 210518). A C-terminal P2A self-cleaving peptide followed by mCherry was incorporated to assess transduction efficiency and expression levels. The packaging vector pCMV dR8.91, envelope vector pMD 2.G, and pHR Lck constructs were transiently cotransfected into LX-293T cells with TransIT-LT1 reagent (Mirus Bio Mio2300). Supernatants containing virus particles were collected 48 h after transfection, filtered, and concentrated through PEG 8000 precipitation. The virus particles were resuspended in PBS and stored at -80°C.

**Bone marrow chimeras.** CD45.2<sup>+</sup> B6 hematopoietic stem cells were enriched with an EasySep Mouse Hematopoietic Progenitor Cell Enrichment Kit (StemCell Technology no. 19856), stained for c-Kit and Sca-1, and sorted to enrich an c-Kit<sup>+</sup>Sca-1<sup>+</sup> population on a FACSAriaII flow cytometer. Hematopoietic stem cells were resuspended at a density of  $1 \times 10^6$  cells per 200  $\mu$ l DMEM-F12 containing 10% FCS,  $1 \times$  nonessential amino acids, 2 mM GlutaMax, 1 mM sodium pyruvate, 0.05% gentamicin, 50  $\mu$ M 2-mercaptoethanol, 50 ng/ml stem-cell factor, and 50 ng/ml thrombopoietin per well of a 96-well round-bottom plate. After 18–24 h of culture, 5  $\mu$ l lentivirus stock was added to each well. Cells were adoptively transferred 24 h later into lethally irradiated CD45.1<sup>+</sup> BoyJ mice by tail injection on day 0 (at least  $1 \times 10^4$  hematopoietic stem cells per mouse). After 6–8 weeks of reconstitution, cells were recovered from the thymus and spleen of each recipient mouse, and analyzed on a BD Fortessa flow cytometer with FlowJo software.

**Immunoprecipitation and mass spectrometry analysis.**  $3 \times 10^6$  J.Lat cells reconstituted with WT or AIARSA LAT with the Myc tag fused to the C terminus were harvested and washed with PBS twice. The cells were resuspended in serum-free RPMI at a concentration of  $5 \times 10^6$  cells/ml, then split into three samples. Then the cells were allowed to rest at 37°C for 15 min and were left unstimulated or were stimulated with anti-CD3 for 2 min or 10 min. The stimulation was stopped with ice-cold PBS on ice. The cells were washed with ice-cold PBS, then resuspended in 1 ml 1% NP-40 lysis buffer containing the inhibitors 2 mM NaVO<sub>3</sub>, 10 mM NaF, 5 mM EDTA, 2 mM PMSE, 10  $\mu$ g/ml aprotinin, 1  $\mu$ g/ml pepstatin, and 1  $\mu$ g/ml leupeptin. The cells were centrifuged at 13,000 g, and the supernatants were transferred to clean tubes. Anti-myc magnetic beads (Thermo Fisher Scientific cat. no. 88842) were washed with 1% NP-40 lysis buffer and added to each sample. The samples were rotated at 4°C for 2 h. The beads were washed five times with Tris-NaCl buffer (20 mM Tris, pH 7.4, and 120 mM NaCl) and resuspended in 100  $\mu$ l urea elution buffer (8 M urea, 20 mM Tris, pH 7.5, and 100 mM NaCl) and rotated for 30 min at 25°C with frequent agitation before gentle centrifugation. The beads were collected, and supernatant samples were transferred to clean tubes and frozen at -20°C for mass spectrometry analysis.

Briefly, mass spectrometry analysis was performed with a fully automated proteomic technology platform<sup>45–47</sup>. The tryptic peptides were separated with an Agilent 1200 Series Quaternary HPLC system (Agilent Technologies) and analyzed with a Q Exactive Plus mass spectrometer (Thermo Fisher). For peptide-spectrum matching, MS/MS spectra were searched against a human-specific database (UniProt; downloaded 4 August 2016) with MASCOT v. 2.4.1 (Matrix Science). A concatenated database containing 185,156 'target' and 'decoy reversed' sequences was used to estimate the false discovery rate<sup>48</sup>. Peptide assignments from the database search were filtered down to 1% false discovery rate through MOWSE score filtering, as previously described<sup>45,48</sup>.

Relative quantification of peptide abundance was performed via calculation of selected ion-chromatogram peak areas. Retention-time alignment of individual replicate analyses was performed as previously described<sup>49</sup>. A minimum selected-ion-chromatogram peak area equivalent to the typical spectral noise level of 1,000 was required for all data reported for label-free quantification. Individual selected-ion-chromatogram peak areas were normalized to the peak area of the exogenously spiked peptide DRVYIHPF added before reversed-phase elution into the mass spectrometer. The proteomic datasets have been deposited in the ProteomeXchange Consortium via the PRIDE partner repository under dataset identifier PXD008258. These data are available for review (username, reviewer21222@ebi.ac.uk; password, z11qcj3B).

Samples immunoprecipitated with anti-Myc-tagged LAT were also analyzed through immunoblot analysis and probed for total LAT, Lck, or Grb2 to confirm the mass spectrometry results.

**Immunoprecipitation of proteins associated with TCR complexes.** Anti- $\zeta$ -chain antibody (clone 6B10) was conjugated to Protein G agarose, which was then rinsed twice with 0.2 M sodium borate, pH 9.0. The resin was then resuspended in borate buffer, and solid dimethylpiperimidate was added to a concentration of 20 mM. The resin was incubated for 30 min at room temperature (25 °C) with mixing and then rinsed with 0.2 M ethanolamine, pH 8.0. The resin was then incubated with ethanolamine for 30 min, washed twice with TBS, and stored at 4 °C as a 50% slurry. Before immunoprecipitation, the resin was rinsed with wash buffer (0.1% NP-40 in TBS). Lck-deficient J.Lck cells were transfected to express mouse OT-I TCR and human CD8 with or without FLAG-tagged human Lck.  $1 \times 10^6$  cells were washed with PBS twice, resuspended in serum-free RPMI medium, and allowed to rest at 37 °C for 15 min. The cells were stained with H-2K<sup>b</sup> OVA tetramers (SINFEKL) on ice for 1 h, washed twice with PBS, resuspended again in serum-free RPMI medium, and split into three samples. TCR stimulation was initiated by incubation of samples at 37 °C for 5 min or 15 min; unstimulated samples remained on ice. The cells were directly lysed with 10% NP-40 lysis buffer to a final concentration of 1% NP-40 (containing the inhibitors 2 mM NaVO<sub>3</sub>, 10 mM NaF, 5 mM EDTA, 2 mM PMSE, 10  $\mu$ g/ml aprotinin, 1  $\mu$ g/ml pepstatin, and 1  $\mu$ g/ml leupeptin). Lysates were placed on ice and centrifuged at 13,000g to pellet cell debris. Supernatants were transferred to clean tubes, and anti- $\zeta$ -chain (clone 6B10) resin (50% slurry) was added. Samples were incubated for 2 h at 4 °C before the resin was pelleted and rinsed three times with ice-cold wash buffer in a refrigerated microfuge. Captured proteins were eluted by the addition of SDS sample buffer to the resin and incubation for 5 min at 95 °C.

**HEK293 cell-based reconstitution system.** HEK293 cells were transfected at ~60% confluency with the following constructs: pEF LAT WT or AIARSA (2  $\mu$ g), pEF Zap70<sup>S602</sup> (0.2  $\mu$ g), pEF Lck<sup>S273R</sup> (0.2  $\mu$ g), and empty pcDNA-EGFP vector, for a total of 2.4  $\mu$ g DNA per well (six-well plate). Plasmids were combined in Opti-MEM before addition of Lipofectamine 2000 (Thermo Fisher) (10  $\mu$ l per 4  $\mu$ g DNA), per the manufacturer's instructions. Plasmids were then added to cells for 4 h before the addition of full medium and culturing overnight. After 24 h, the cells were harvested and rinsed, and lysed on ice.

**Preparation of J.OT-I.hCD8.Lck KO cells.** Lck-deficient Jurkat cells<sup>12</sup> were sequentially transfected with hCD8 $\beta$ -T2A-hCD8 $\alpha$  in a lentiviral pHR vector<sup>12</sup> (a gift from W. Paster, Centre for Pathophysiology, Infectiology and Immunology, Medical University of Vienna), OT-I TCR $\beta$  and OT-I TCR $\alpha$  (amplified from OT-I TCR transgenic-mouse DNA) in the retroviral vectors MSCV-IRES-Thy1.1 and MSCV-IRES-GFP, respectively. Human Lck-encoding sequence (a gift from T. Brdicka, IMG, Prague) was fused with a C-terminal FLAG sequence via PCR and cloned into MSCV-IRES-LNGFR.

Lentiviral particles were produced by transfection of HEK293 cells with CD8 $\beta$ -T2A-CD8 $\alpha$ -pHR along with pLP1, pLP2, and pLP-VSVG packaging vectors with Lipofectamine 2000 (Thermo Fisher). Retroviral particles were produced by

transfection of the Phoenix-AMPHO cell line with polyethylenimine. Supernatants were collected and filtered 48 h after transfection, and the Jurkat cells were transfected by centrifugation (45 min, 1,200g) in the presence of 5–8  $\mu$ g/ml polybrene.

Transduced Jurkat cells were labeled with phycoerythrin-conjugated anti-V $\alpha$ 2 (clone B20.1; BD Pharmingen cat. no. 553289), APC-conjugated anti-V $\beta$ 5.1/5.2 (clone MR9-4, both BD Pharmingen), phycoerythrin-Cy7-conjugated anti-Thy1.1 (clone HIS51, eBioscience cat. no. 14-0900-81), and/or APC-conjugated anti-LNGFR (clone ME20.4-1.H4, Miltenyi Biotec cat. no. 130-091-884) antibodies and sorted with a BD Influx sorter (BD Biosciences).

**Statistics and reproducibility.** Statistical analysis was applied to technical replicates or biologically independent mice for each experiment. All experiments described in this study were performed at least twice, and the exact numbers of independent experiments with similar results are indicated in the figure legends. All statistical analyses of experiments were performed with nonparametric, two-tailed Mann–Whitney tests. GraphPad Prism 6 Software (GraphPad Software) was used for data analysis and representation. All bar graphs show means with overlaid scatter dots, or error bars (indicating s.d.), to show the distribution of the data, as indicated in each figure legend. *P* values for comparisons are provided as exact values or as *P* < 0.0001. 95% confidence levels were used to determine statistically significant *P* values.

**Reporting Summary.** Further information on experimental design is available in the Nature Research Reporting Summary linked to this article.

**Data availability.** Mass spectrometry data have been deposited in the ProteomeXchange Consortium repository via PRIDE under dataset identifier PXD008258 (username, reviewer21222@ebi.ac.uk; password, z11qcj3B). The primary data for analysis of all figures and supplementary figures are available upon request. All data necessary to understand and access the conclusions of this study are available in the main text, the supplementary materials, and the indicated repositories.

## References

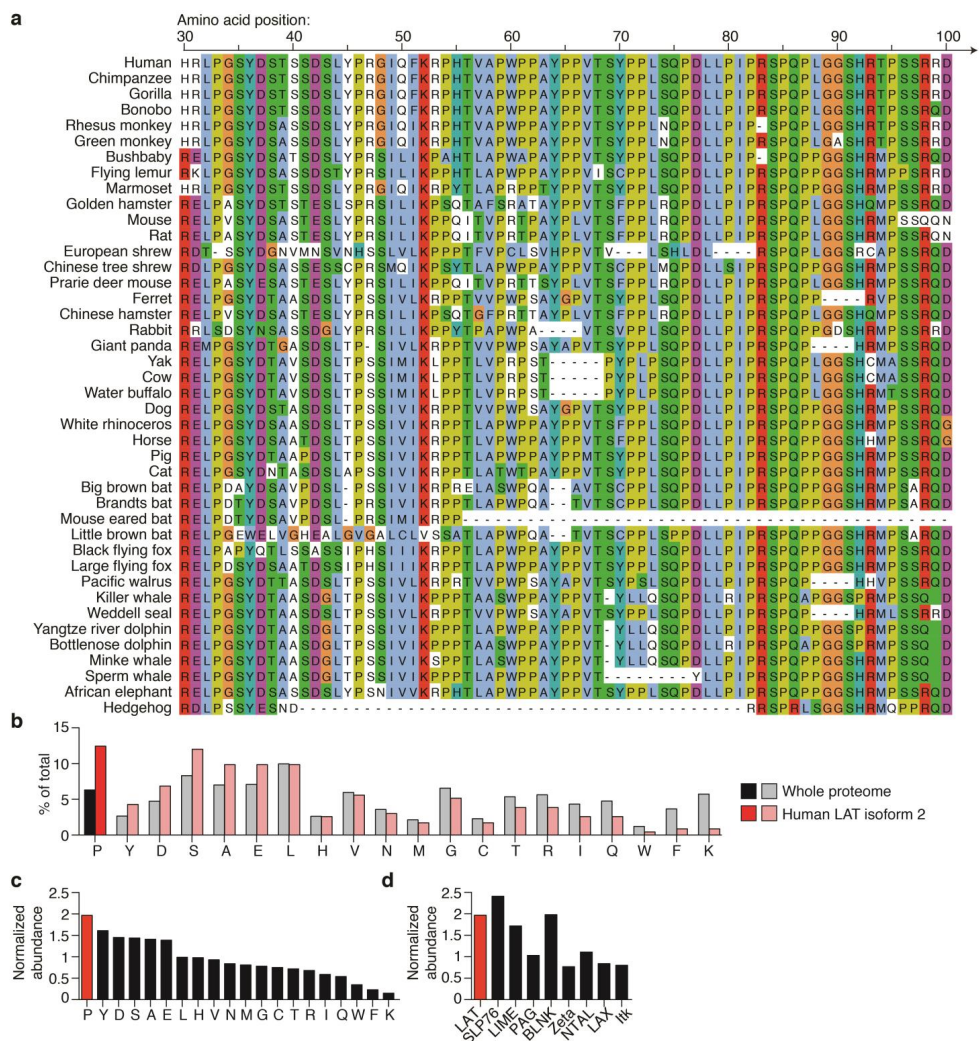
- Crooks, G. E., Hon, G., Chandonia, J. M. & Brenner, S. E. WebLogo: a sequence logo generator. *Genome Res.* **14**, 1188–1190 (2004).
- Yu, K. & Salomon, A. R. PeptideDepot: flexible relational database for visual analysis of quantitative proteomic data and integration of existing protein information. *Proteomics* **9**, 5350–5358 (2009).
- Yu, K. & Salomon, A. R. HTAPP: high-throughput autonomous proteomic pipeline. *Proteomics* **10**, 2113–2122 (2010).
- Ahsan, N., Belmont, J., Chen, Z., Clifton, J. G. & Salomon, A. R. Highly reproducible improved label-free quantitative analysis of cellular phosphoproteome by optimization of LC-MS/MS gradient and analytical column construction. *J. Proteomics* **165**, 69–74 (2017).
- Elias, J. E. & Gygi, S. P. Target-decoy search strategy for increased confidence in large-scale protein identifications by mass spectrometry. *Nat. Methods* **4**, 207–214 (2007).
- Demirkan, G., Yu, K., Boylan, J. M., Salomon, A. R. & Grupp, P. A. Phosphoproteomic profiling of in vivo signaling in liver by the mammalian target of rapamycin complex 1 (mTORC1). *PLoS One* **6**, e21729 (2011).

In the format provided by the authors and unedited.

## Lck promotes Zap70-dependent LAT phosphorylation by bridging Zap70 to LAT

Wan-Lin Lo<sup>1</sup>, Neel H. Shah<sup>2</sup>, Nagib Ahsan<sup>3,4</sup>, Veronika Horkova<sup>5</sup>, Ondrej Stepanek<sup>5</sup>, Arthur R. Salomon<sup>6,7</sup>, John Kuriyan<sup>2,8</sup> and Arthur Weiss<sup>1,9\*</sup>

<sup>1</sup>Division of Rheumatology, Rosalind Russell and Ephraim P. Engleman Arthritis Research Center, Department of Medicine, University of California, San Francisco, San Francisco, CA, USA. <sup>2</sup>Departments of Molecular and Cell Biology, University of California, Berkeley, Berkeley, CA, USA. <sup>3</sup>Division of Biology and Medicine, Alpert Medical School, Brown University, Providence, RI, USA. <sup>4</sup>Center for Cancer Research Development, Proteomics Core Facility, Rhode Island Hospital, Providence, RI, USA. <sup>5</sup>Institute of Molecular Genetics of the Czech Academy of Sciences, Prague, Czech Republic. <sup>6</sup>Department of Chemistry, Brown University, Providence, RI, USA. <sup>7</sup>Department of Molecular Biology, Cell Biology, and Biochemistry, Brown University, Providence, RI, USA. <sup>8</sup>The Howard Hughes Medical Institute, University of California, Berkeley, Berkeley, CA, USA. <sup>9</sup>The Howard Hughes Medical Institute, University of California, San Francisco, San Francisco, CA, USA. \*e-mail: [art.weiss@ucsf.edu](mailto:art.weiss@ucsf.edu)

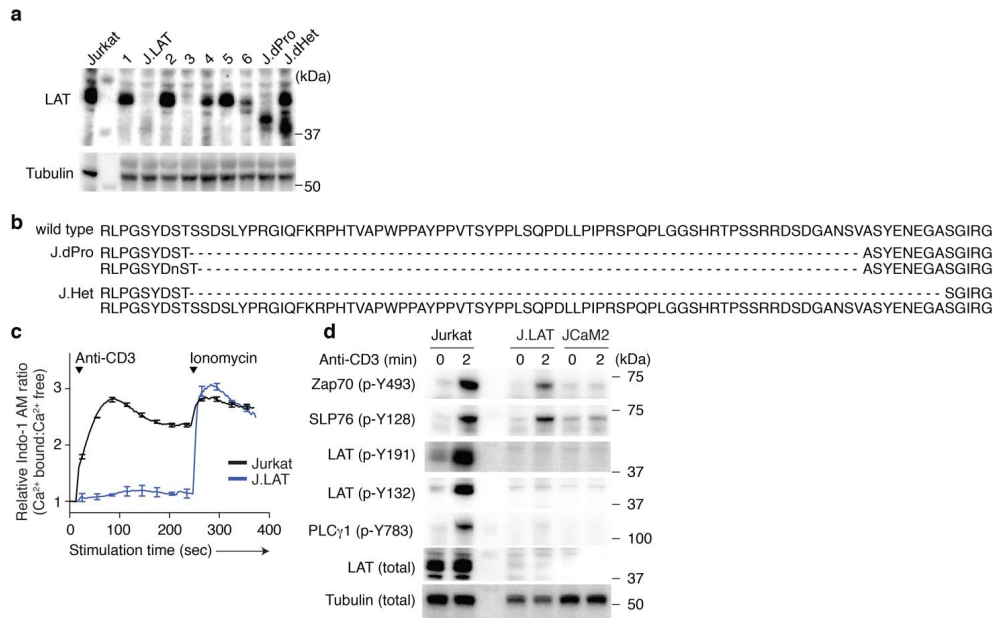


**Supplementary Figure 1**

The proline-rich motif in the membrane-proximal segment of LAT is highly evolutionarily conserved.

**a**, The amino acid sequences of 42 mammalian LATs. **b**, The frequency of individual amino acids in human LAT or the whole human proteome. **c**, Relative frequency of individual amino acids of human LAT normalized to the whole human proteome. **d**, Relative frequency of proline residues of key adaptor or kinase proteins (normalized to the whole human proteome) in the antigen receptor

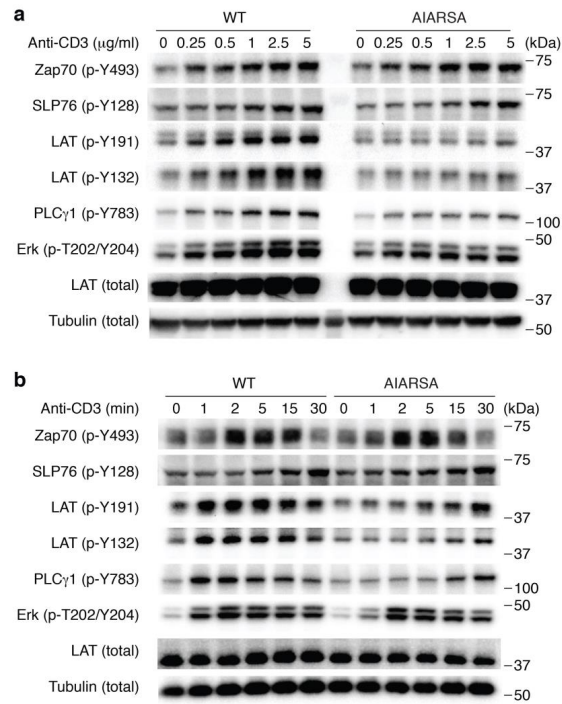
signaling pathway.



**Supplementary Figure 2**

The proline-rich motif in the membrane-proximal segment of LAT promotes TCR signaling.

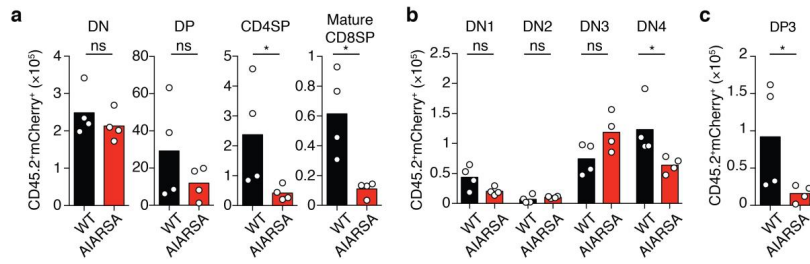
**(a)** Immunoblot analysis of screening LAT mutant Jurkat variants that lack the proline-rich region, probed with anti-C terminal LAT antibody or anti-tubulin antibody (loading control). Numbers to the right of cropped blots indicate molecular masses (kDa). Data are representative of at least two independent experiments. **(b)** Characterization of CRISPR/Cas9-induced amino acid changes of mutant LAT in J.dPro or J.Het cells. Each line represents the amino acid sequences encoded by one allele of DNA. "-" indicates the amino acid deletion. "n" indicates the insertion of asparagine resulted from the CRISPR/Cas9-induced nucleotide insertions. Wild type human LAT sequences are shown at the top. **(c)** CRISPR/Cas9 generated LAT-deficient J.LAT cells, or Jurkat cells were loaded with Indo-1 AM, stimulated with 0.5  $\mu$ g/ml anti-CD3 and the changes in relative calcium-sensitive fluorescence ratios over time are shown. The center of measure indicates mean  $\pm$  s.d.  $n = 3$  technical replicates. Data are representative of two independent experiments. **(d)** Immunoblot analyses of Jurkat, J.LAT cells, or LAT-deficient JCaM2 were left unstimulated or stimulated with 0.5  $\mu$ g/ml anti-CD3 for 2 min. Numbers to the right of cropped blots indicate molecular masses (kDa). Data are representative of at least three independent experiments with similar results.



**Supplementary Figure 3**

The PIPRSP motif in LAT promotes the phosphorylation of LAT and PLCγ1.

Immunoblot analyses of J.LAT cells reconstituted with WT or AIARSA mutant LAT were either unstimulated or stimulated with anti-CD3 (concentration as indicated above blots) for 2 min (**a**), or with 0.5 μg/ml anti-CD3 over time (stimulation time as indicated, **b**). Numbers to the right of cropped blots indicate molecular masses (kDa). Data are representative of four experiments.

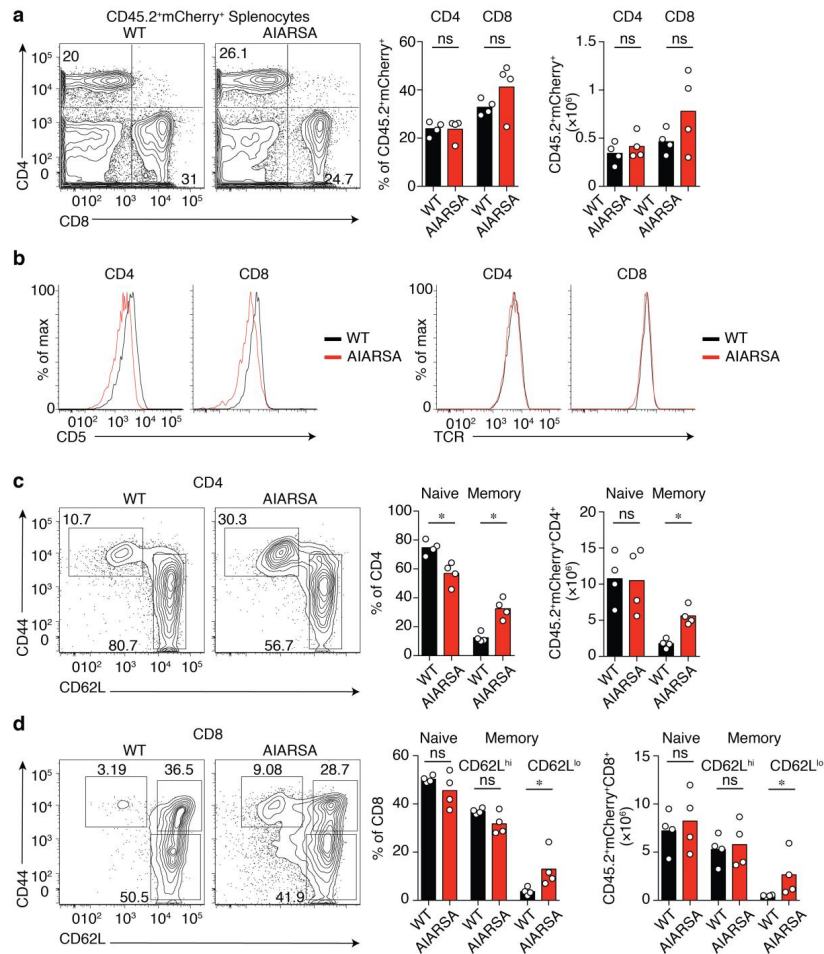


#### Supplementary Figure 4

Mutant AIARSA LAT impedes thymic development.

Absolute number analysis of bone marrow chimeric studies shown in Fig. 3. **(a)** Bar graph showing absolute number of CD45.2<sup>+</sup> mCherry<sup>+</sup> DN, DP, CD4SP, and CD8SP thymocytes as in Fig. 3d. **(b)** Absolute number analysis of CD45.2<sup>+</sup> mCherry<sup>+</sup> DN1, DN2, DN3 and DN4 cells as in Fig. 3f. **(c)** Absolute number analysis of post positive selection CD45.2<sup>+</sup> mCherry<sup>+</sup> DP3 cells as in Fig. 3h. **(a, b, c)** Each symbol represents an individual mouse. All bar graphs indicate mean±s.d. *n* = 4 independent animals. All experiments were repeated twice with four independent animals. \**P* = 0.0286; ns, not significant, two-tailed Mann-Whitney test.



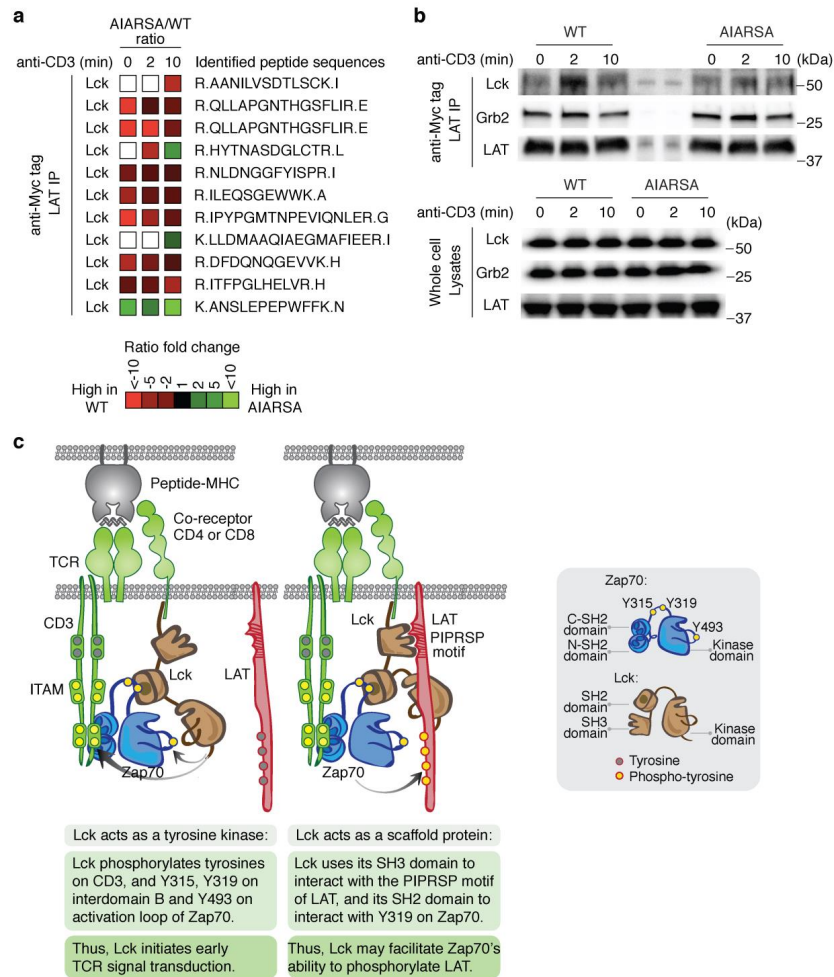


### Supplementary Figure 5

Peripheral T cells ectopically expressing the mutant AIARSA LAT exhibit an increased memory-cell-like phenotype.

Flow cytometry of splenocytes from lethally irradiated bone marrow BoyJ chimeras reconstituted with CD45.2<sup>+</sup> B6 hematopoietic stem cells transduced with lentivirus expressing WT LAT-P2A-mCherry (WT;  $n = 4$  recipients) or mutant AIARSA LAT-P2A-mCherry (AIARSA;  $n = 4$  recipients), as described in Fig. 3. **(a)** Flow cytometric analysis of CD45.2<sup>+</sup> mCherry<sup>+</sup> splenocytes. Numbers in outlined areas indicate percent cells in each quadrant. Bar graph depicts the frequency or the absolute number of CD4<sup>+</sup> and CD8<sup>+</sup> splenocytes among CD45.2<sup>+</sup> mCherry<sup>+</sup> cells (mean $\pm$ s.d.).  $n = 4$  independent animals. ns, not significant; two-tailed Mann-Whitney test. **(b)** Surface expression of TCR or CD5 in CD45.2<sup>+</sup> mCherry<sup>+</sup> CD4<sup>+</sup> or CD8<sup>+</sup> T cells. **(c and d)** Flow cytometric analysis of CD62L versus CD44 expression of CD45.2<sup>+</sup> mCherry<sup>+</sup> CD4<sup>+</sup> **(c)** or CD8<sup>+</sup> **(d)** T cells. Bar graphs present the frequencies or the absolute number of naive cell

populations (CD62L<sup>hi</sup> CD44<sup>lo</sup>), or memory cell populations (CD44<sup>hi</sup>CD62L<sup>lo</sup> or CD44<sup>hi</sup>CD62L<sup>hi</sup>). Bar indicates mean±s.d.  $n = 4$  independent animals. \* $P = 0.0286$ ; ns, not significant, two-tailed Mann-Whitney test. **(a, b, c, d)** Data are representative of two independent experiments.

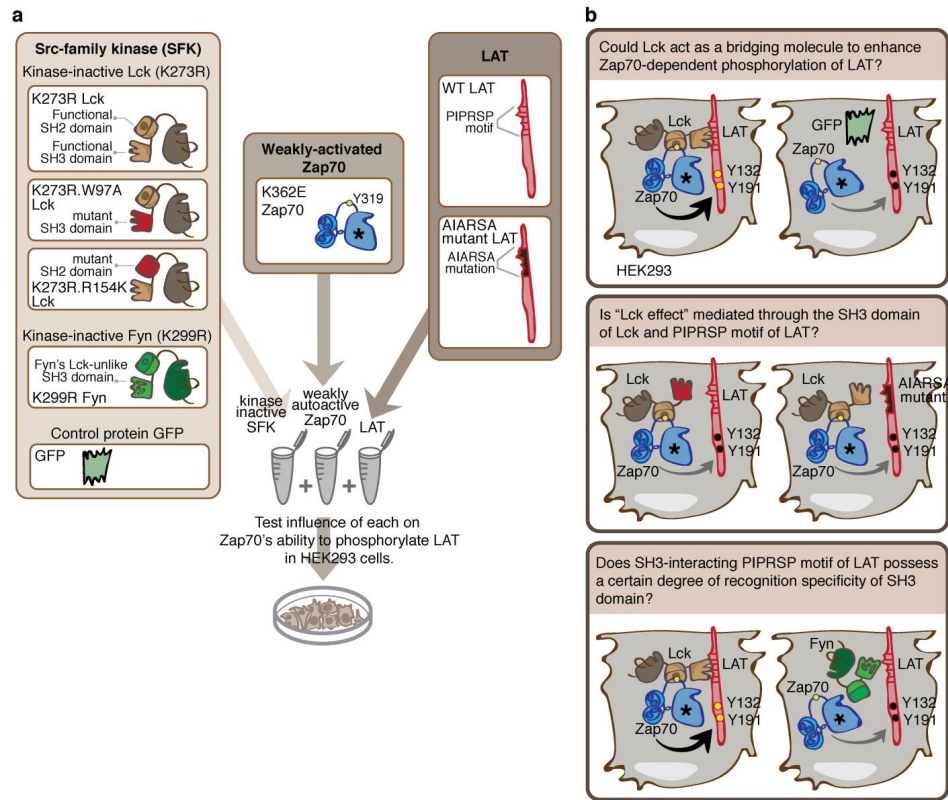


**Supplementary Figure 6**

TCR stimulation induces the interaction of Lck with the LAT PIPRSP motif.

LAT deficient J.LAT cells were reconstituted with WT or AIARSA mutant LAT, fused with a Myc-tag at the C-terminus. Cells were stimulated with 0.5  $\mu$ g/ml anti-CD3 for 0, 2, or 10 min. Samples were immunoprecipitated (IP) with anti-Myc antibody and subjected to mass spectrometry analysis. **(a)** Ratio fold-change in Lck peptides identified by mass spectrometry analysis was illustrated as heat map among each sample. White block indicates peptide was not identified as the peak area was not observed. **(b)** Immunoblot analysis of samples IP'd with anti-Myc or whole cell lysates for Lck (LAT PIPRSP motif dependent), Grb2 (LAT PIPRSP motif independent) or LAT. Data are representative of two independent experiments with similar results. **(c)**, Illustration of the proposed model whereby Lck serves

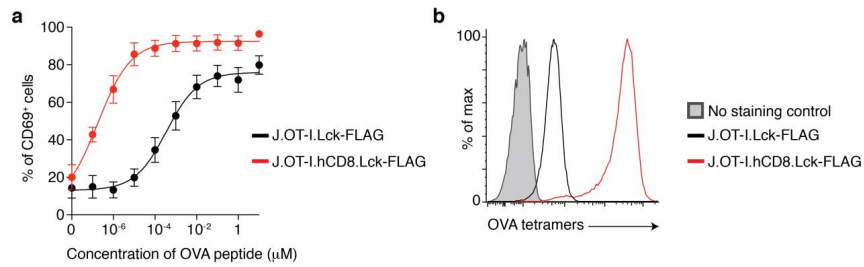
as a kinase and an adaptor protein. New data suggest Lck interacts via its SH3 domain with the LAT PIPRSP motif and also interacts via its SH2 domain with Zap70 phospho-Y319, as well as associating via its unique domain with coreceptor CD4 or CD8 cytoplasmic segment. Arrows indicate Lck's ability to phosphorylate CD3 or Zap70 (left) or Zap70's ability to phosphorylate LAT (right).



**Supplementary Figure 7**

Illustration of a HEK293-cell-based cellular system to examine the adaptor function of Lck and its role in enhancing the phosphorylation of LAT by Zap70.

**a**, Scheme of mutant Lck, Zap70 and LAT variants that were used in experiments in Fig. 5. **b**, Illustration of experimental design using HEK293 cell based system to study Lck's roles as an adaptor protein in Zap70-mediated phosphorylation of LAT.



#### Supplementary Figure 8

The coexpression of human CD8 may assist mouse OT-I TCR in binding the mouse MHC-I H-2K<sup>b</sup>.

**a**, CD69 upregulation assay of human CD8<sup>+</sup> OT-I TCR<sup>+</sup> Jurkat cells cultured with OVA peptide-pulsed antigen presenting T2-K<sup>b</sup> cells over a wide range of OVA peptide concentration. J.OT-I.hCD8.Lck-FLAG cells were retrovirally transduced to express human CD8, whereas J.OT-I.Lck-FLAG cells did not express human CD8. Each symbol represents the mean  $\pm$  s.e.m. of percent of CD69<sup>+</sup> cells.  $n = 4$  independent experiments at OVA concentration of  $10^{-6}$ ,  $10^{-7}$ ,  $10^{-8}$   $\mu\text{M}$ ;  $n = 6$  independent experiments at OVA concentration between 1 and  $10^{-6}$   $\mu\text{M}$ . Data are representative of six independent experiments. **b**, The flow cytometry analysis of MHC class I H-2K<sup>b</sup> OVA tetramers staining of J.OT-I.hCD8.Lck-FLAG cells or J.OT-I.Lck-FLAG cells. The unstained sample of J.OT-I.hCD8.Lck-FLAG cells was used as the no stained control. Experiments were repeated independently twice with similar results.

## **Attachment 6**

# CD45 Functions as a Signaling Gatekeeper in T cells

## IMMUNOLOGY

## CD45 functions as a signaling gatekeeper in T cells

Adam H. Courtney<sup>1,2\*</sup>, Alexey A. Shvets<sup>3</sup>, Wen Lu<sup>1</sup>, Gloria Griffante<sup>4†</sup>, Marianne Mollenauer<sup>5</sup>, Veronika Horkova<sup>6</sup>, Wan-Lin Lo<sup>1</sup>, Steven Yu<sup>5</sup>, Ondrej Stepanek<sup>6</sup>, Arup K. Chakraborty<sup>3,7,8,9,10</sup>, Arthur Weiss<sup>1,5\*</sup>

T cells require the protein tyrosine phosphatase CD45 to detect and respond to antigen because it activates the Src family kinase Lck, which phosphorylates the T cell antigen receptor (TCR) complex. CD45 activates Lck by opposing the negative regulatory kinase Csk. Paradoxically, CD45 has also been implicated in suppressing TCR signaling by dephosphorylating the same signaling motifs within the TCR complex upon which Lck acts. We sought to reconcile these observations using chemical and genetic perturbations of the Csk/CD45 regulatory axis incorporated with computational analyses. Specifically, we titrated the activities of Csk and CD45 and assessed their influence on Lck activation, TCR-associated  $\zeta$ -chain phosphorylation, and more downstream signaling events. Acute inhibition of Csk revealed that CD45 suppressed  $\zeta$ -chain phosphorylation and was necessary for a regulatable pool of active Lck, thereby interconnecting the activating and suppressive roles of CD45 that tune antigen discrimination. CD45 suppressed signaling events that were antigen independent or induced by low-affinity antigen but not those initiated by high-affinity antigen. Together, our findings reveal that CD45 acts as a signaling "gatekeeper," enabling graded signaling outputs while filtering weak or spurious signaling events.

## INTRODUCTION

Antigens derived from foreign pathogens or malignant cells are detected by a cognate T cell using its T cell antigen receptor (TCR). Because antigen detection is essential for a T cell response, the TCR is critical to human adaptive immunity and current efforts to harness T cells therapeutically. Antigen detection occurs when the TCR binds to agonist peptide–major histocompatibility complex (MHC) (pMHC) complexes on the surface of an antigen-presenting cell (APC). Because it lacks intrinsic kinase activity, the TCR requires the Src family kinase (SFK) Lck to detect and respond to antigen (1, 2). Lck phosphorylates immunoreceptor tyrosine-based activation motifs (ITAMs) within the TCR-associated CD3 and  $\zeta$ -chains (denoted as the TCR complex). Phosphorylated ITAMs recruit the Zap70 kinase where it is then also phosphorylated by Lck to activate it and propagate signaling events that are necessary for T cell activation to occur (3–5). Because Lck is required to initiate signals through the TCR, its regulation is critical to T cell function. In T cells, Lck activity is controlled by the phosphatase CD45 whose action on Lck is opposed by the inhibitory kinase Csk.

Lck activity is regulated by modulating the conformation of its kinase domain through the phosphorylation of critical regulatory sites (6, 7). CD45 activates Lck by dephosphorylating a tyrosine in its inhibitory C-terminal tail (8–10). Dephosphorylation of the inhibitory C-terminal tail allows Lck to adopt an active open conformation, which is stabilized through trans-autophosphorylation of a tyrosine in its activation loop (11). The inhibitory kinase Csk opposes CD45 and phosphorylates the C-terminal tail of Lck to stabilize the closed autoinhibited conformation (12, 13). Loss of CD45 causes hyperphosphorylation of the Lck C-terminal tail and markedly reduces the amount of active Lck. Because active Lck amounts are reduced, T cell development is impaired when TCR signaling is required, such as during positive selection (14–16). In contrast, loss of Csk activity causes increased activation of Lck and results in the aberrant survival of thymocytes lacking a functional TCR (12, 17, 18). Therefore, Csk and CD45 comprise a regulatory axis that controls active Lck amounts, which is important for T cell development. In mature peripheral T cells, before TCR engagement, there is a basal pool of active Lck (19, 20). Consistent with active Lck amounts setting a threshold for T cell activation, T cell responses to low-affinity antigen are potentiated by increasing active Lck abundance through inhibition of Csk (21). Memory T cells have increased amounts of active Lck, which corresponds with their augmented response to antigen (22). Therefore, Csk is a critical inhibitor of Lck, which reduces active Lck amounts. The role of CD45, however, is less clear.

CD45 is a receptor-type protein tyrosine phosphatase (RT-PTP) that is among the most abundant proteins within the T cell plasma membrane, yet its role in regulating T cell function remains enigmatic (23). CD45 is required for TCR signaling because it activates Lck, which is required to phosphorylate the TCR complex. However, CD45 has also been observed to associate with the phosphorylated  $\zeta$ -chain, a component of the TCR complex, and to dephosphorylate it in vitro (24, 25). Consistent with a negative regulatory role, CD45 is excluded from the site of contact when a T cell encounters a cell bearing antigen (26, 27). The segregation of CD45 within the T cell plasma membrane is thought to be important for T cell activation because when this process is disrupted, T cell activation is attenuated

<sup>1</sup>Rosalind Russell and Ephraim P. Engleman Arthritis Research Center, Division of Rheumatology, Department of Medicine, University of California, San Francisco, San Francisco, CA 94143, USA. <sup>2</sup>Department of Pharmacology, University of Michigan, Ann Arbor, MI 48109, USA. <sup>3</sup>Institute for Medical Engineering and Science, Massachusetts Institute of Technology, Cambridge, MA 02139, USA. <sup>4</sup>Division of Molecular Immunology, Department of Internal Medicine, University Hospital Erlangen and Friedrich-Alexander University of Erlangen-Nürnberg, 91054 Erlangen, Germany. <sup>5</sup>Howard Hughes Medical Institute (HHMI), San Francisco, CA 94143, USA. <sup>6</sup>Laboratory of Adaptive Immunity, Institute of Molecular Genetics of the Czech Academy of Sciences, 142 20 Prague 4, Czech Republic. <sup>7</sup>Department of Chemical Engineering, Massachusetts Institute of Technology, Cambridge, MA 02139, USA. <sup>8</sup>Department of Physics, Massachusetts Institute of Technology, Cambridge, MA 02139, USA. <sup>9</sup>Ragon Institute of Massachusetts General Hospital, Massachusetts Institute of Technology and Harvard University, Cambridge, MA 02139, USA. <sup>10</sup>Department of Chemistry, Massachusetts Institute of Technology, Cambridge, MA 02139, USA.

\*Corresponding author. Email: aweiss@medicine.ucsf.edu (A.W.); adamhc@umich.edu (A.H.C.)

†Present address: Department of Public Health and Pediatric Sciences, University of Turin, 10126 Turin, Italy.



(28, 29). Altered levels of CD45 expression can also affect T cell development within the thymus. In contrast to mice deficient for CD45, those that express low levels of CD45 have more thymocytes undergoing positive selection, which indicates increased sensitivity toward self-antigens (30). In aggregate, CD45 is required for T cell function; however, differing experimental observations suggest that it can positively or negatively affect TCR signaling.

A potential explanation for the divergent roles attributed to CD45 is that it acts on multiple substrates. Because the importance of a given substrate will likely depend on the experimental context, assigning a specific role to CD45 has been challenging. We therefore sought to reconcile the various roles attributed to CD45 by performing a series of chemical and genetic perturbations to the Csk/CD45 regulatory axis. We reasoned that such an approach would reveal whether CD45 acts differentially on multiple substrates in T cells, including Lck and the TCR complex. Transgenic mice and cell lines modified using CRISPR-Cas9 were used to assess the consequences of CD45 deficiency and Csk inhibition on TCR signaling pathways. We report two critical and interdependent roles of CD45. CD45 is required for graded changes in active Lck amounts and suppression of  $\zeta$ -chain phosphorylation in intact cells. Moreover, our findings reveal that negative regulation of the TCR by CD45 prevents antigen-independent or weak signals but permits sustained signaling by high-affinity antigens. Together, these features are critical to graded signaling responses required for antigen discrimination.

## RESULTS

### Antigen discrimination is sensitive to active Lck abundance

We previously reported that the T cell response to low-affinity antigens is potentiated by increasing the amount of active Lck (21). Specifically, by inhibiting Csk, a negative regulator of Lck, active Lck amounts increase and TCR signaling in response to weak stimuli is augmented. The amount of active Lck and its recruitment to TCR:pMHC is thought to set a threshold, which controls the extent of signaling (31). Because antigen discrimination is a critical hallmark of the T cell response, we sought to better understand how manipulation of active Lck amounts influences T cell activation. To increase active Lck, we used a previously described analog-sensitive allele of Csk (Csk<sup>AS</sup>) that can be inhibited using the small molecule 3-IB-PP1 (hereafter denoted as Csk inhibitor) (Fig. 1A) (32, 33). We also assessed the effect of decreasing active Lck amounts using a SFK inhibitor (PP2). The response of T cells to antigens of differing affinities was assessed using the OT1 TCR transgene. The OT1 TCR binds to a peptide derived from ovalbumin (OVA), and variants of this peptide sequentially reduce the binding affinity. During thymic selection, high-affinity peptides act as agonists, which cause negative selection, whereas lower-affinity variants act as partial or nonagonists (34, 35). Therefore, by assessing a panel of peptide antigens of differing affinities, the OT1 TCR provides a readout of TCR sensitivity.

To monitor how active Lck amounts affect antigen discrimination, we used two readouts of T cell activation: Nur77-GFP (green fluorescent protein) and CD69 up-regulation. The Nur77-GFP transcriptional reporter provides a readout of TCR integrated signaling involving several downstream pathways and is less sensitive to other mitogenic signals (36, 37). Csk analog-sensitive mice were crossed to incorporate both the OT1 TCR transgene and the Nur77-GFP reporter. CD8<sup>+</sup> T cells from these mice up-regulate Nur77-GFP

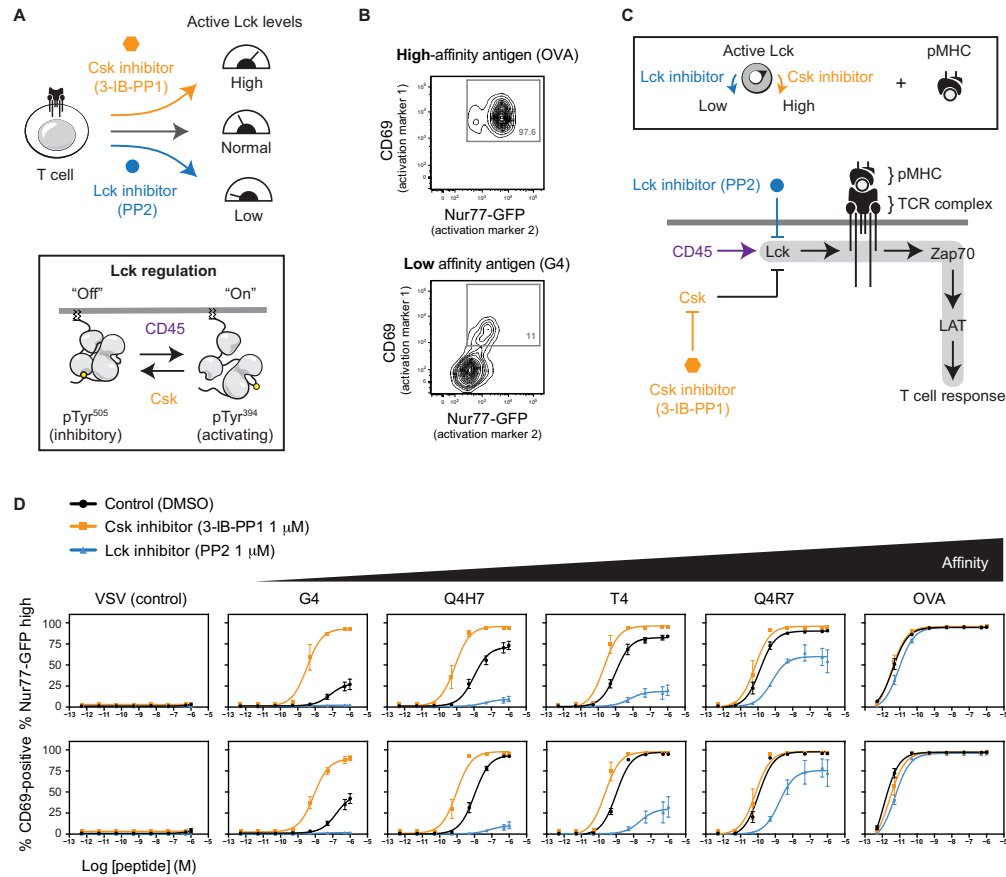
and CD69 when cocultured with splenocytes that display the high-affinity OVA peptide but only weakly respond to the low-affinity G4 peptide (Fig. 1B). To assess the influence of active Lck amounts on T cell activation, purified CD8 T cells were treated with an intermediate dose of either the Csk inhibitor (3-IB-PP1) or the Lck inhibitor (PP2) (Fig. 1C).

Consistent with our previous findings, inhibition of Csk potentiated responses to low-affinity antigens resulting in both Nur77-GFP and CD69 up-regulation, whereas up-regulation of both Nur77-GFP and CD69 was insensitive to Csk inhibition when cells were exposed to antigens of high affinity. Conversely, low-affinity antigens were markedly sensitive to partial Lck inhibition by PP2 causing reduced Nur77-GFP and CD69 up-regulation. The high-affinity OVA antigen responded similarly regardless of whether PP2 was present (Fig. 1D). These findings demonstrate, using two readouts of T cell activation, that the capacity of the TCR to distinguish between antigens that bind with differing affinities is markedly sensitive to changes in active Lck amounts. Because Csk and CD45 cooperate to affect active Lck amounts, we used Csk inhibition to study the role of CD45.

### Csk inhibition can activate Lck when CD45 is absent

Important regulatory features of CD45 could be unmasked if Lck were activated in its absence. For example, CD45-mediated dephosphorylation of phosphorylated ITAMs within the TCR complex has been reported *in vitro* using purified proteins (24). However, this has been challenging to observe *in vivo* in T cells because the loss of CD45 impairs Lck activation. We therefore sought to uncouple Lck activation from CD45 expression using Csk inhibition. CD45 is normally required to activate Lck in T cells, but inhibition of Csk can relieve negative regulation of Lck and allow for its activation when CD45 is reduced or absent. Because loss of CD45 prevents proper T cell development in mice, we used a more genetically tractable system. Using Jurkat T cells, we were able to delete both Csk and CD45 using CRISPR-Cas9 and install a Csk analog-sensitive allele (Csk<sup>AS</sup>), which can be inhibited (fig. S1, A to E) (32, 38, 39). These cells were then treated with an anti-TCR antibody to initiate signaling or with the Csk<sup>AS</sup> inhibitor. To assess signaling, we monitored global increases in protein tyrosine phosphorylation (Fig. 2A). Jurkat T cells respond to the anti-TCR antibody, as revealed by a marked increase in overall protein phosphorylation, but do not respond to Csk inhibition because they lack the Csk<sup>AS</sup> allele. Jurkat T cells that were made deficient in Csk that were reconstituted with Csk<sup>AS</sup> (J.Csk<sup>AS</sup>) respond to both anti-TCR stimulation and the Csk inhibitor. Cells expressing the Csk<sup>AS</sup> allele and are deficient for CD45 (J.Csk<sup>AS</sup>/CD45) display attenuated signaling in response to anti-TCR stimulation consistent with impaired Lck activation. Despite a lack of CD45, the Csk inhibitor caused robust protein tyrosine phosphorylation.

We next monitored phosphorylation of specific signaling effectors as a readout of their activation status (Fig. 2B). When CD45 is present, TCR stimulation causes robust phosphorylation of the  $\zeta$ -chain, Zap70, linker of activated T cells (LAT), and extracellular signal-regulated kinase (ERK). We also assessed Lck activation by monitoring Lck regulatory site phosphorylation, and these were not substantially affected by TCR stimulation. Because CD45 activates Lck, its loss causes hyperphosphorylation of the inhibitory C-terminal tail (Tyr<sup>505</sup>) of Lck, which reduces active Lck amounts and can be read out by decreased Lck autophosphorylation (Tyr<sup>394</sup>). Upon TCR stimulation, cells deficient for CD45 display impaired phosphorylation



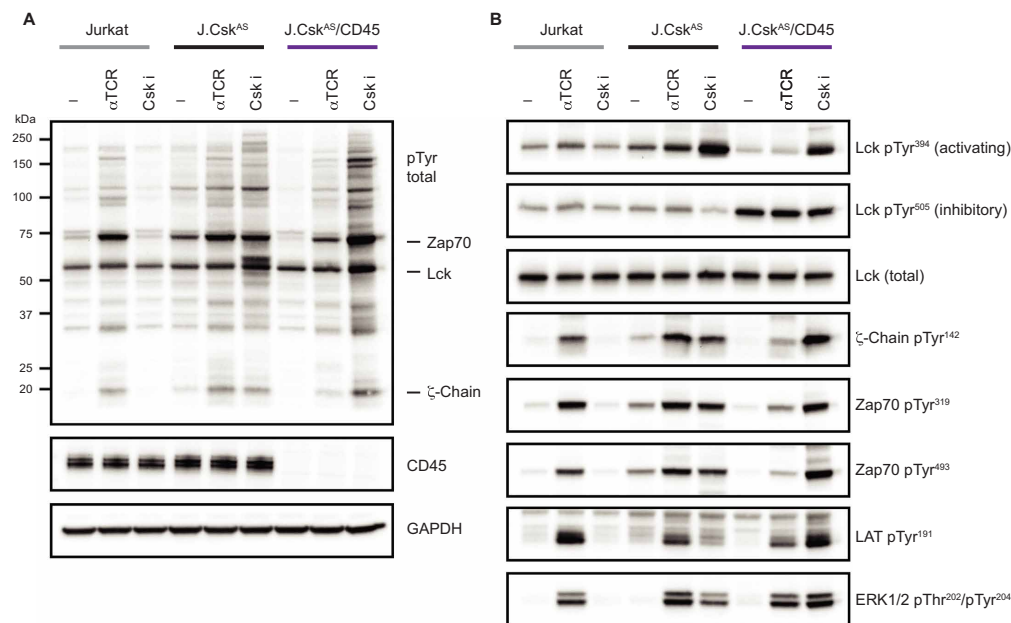
**Fig. 1. The amount of active Lck alters antigen discrimination by T cells.** (A) Depiction of small-molecule inhibition to manipulate the amount of basally active Lck in OT1 CD8<sup>+</sup> T cells. (B) When cocultured with splenocytes and the high-affinity OVA peptide antigen, OT1 T cells up-regulate two readouts of T cell activation: Nur77-GFP reporter and CD69. A low-affinity peptide variant only weakly activates Nur77-GFP and CD69. (C and D) OT1 T cells were cocultured with a series of OVA peptide variants that bind with altered affinity. Active Lck amounts were manipulated by adding intermediate doses (1  $\mu$ M) of PP2 or Csk inhibitor. Error bars represent means  $\pm$  SEM of at least three independent experiments. VSV, vesicular stomatitis virus peptide.

of the  $\zeta$ -chain, Zap70, and LAT. Therefore, TCR stimulation causes signaling when CD45 is present, and signaling is attenuated when CD45 is absent because of reduced active Lck amounts.

We contrasted signaling that occurs upon TCR stimulation with that initiated by acute Csk inhibition. When CD45 is present, Csk inhibition causes increased Lck activation and a corresponding decrease in phosphorylation of the inhibitory C-terminal tail. Because the amount of active Lck is increased, its substrates the  $\zeta$ -chain and Zap70 are phosphorylated. In contrast, in resting CD45-deficient cells, the inhibitory C-terminal tail of Lck is hyperphosphorylated and its activation loop is predominately unphosphorylated, indi-

cating that it is mostly autoinhibited. Unexpectedly, Csk inhibition causes a marked increase in Lck autophosphorylation and therefore active Lck amounts, despite no appreciable dephosphorylation of the inhibitory C-terminal tail. When Lck is doubly phosphorylated on both its inhibitory C-terminal tail (Tyr<sup>505</sup>) and its activation loop (Tyr<sup>394</sup>), it is active (19, 24). In this way, inhibition of Csk could allow some activation of Lck despite the loss of CD45 if a very small pool of Lck was transiently in the open conformation due to the inefficient actions of other transmembrane or cytoplasmic PTPs. Consistent with this reasoning, we observed robust phosphorylation of the  $\zeta$ -chain and Zap70. Phosphorylation of the

Downloaded from <http://sike.sciencemag.org/> on October 31, 2019



**Fig. 2. Csk inhibition activates Lck in the absence of CD45.** (A) Cells were stimulated for 2 min by either anti-TCR cross-linking or Csk inhibition (5  $\mu$ M 3-IB-PP1), and lysates were analyzed by immunoblot. Total protein tyrosine phosphorylation was assessed, and the mobilities of specific proteins are denoted. (B) Phosphorylation of specific regulatory sites was assessed using site-specific antibodies. Data are representative of three independent experiments. GAPDH, glyceraldehyde-3-phosphate dehydrogenase.

$\zeta$ -chain appeared increased when Lck was activated in the absence of CD45.

#### CD45 suppresses $\zeta$ -chain phosphorylation

To better understand the role of CD45 in Lck activation, we evaluated the effects of the extent of Csk inhibition. We found that higher doses of Csk inhibitor were required to activate Lck in CD45-deficient cells, consistent with CD45 facilitating Lck activation (Fig. 3A and fig. S2A). In the absence of CD45, no appreciable change to phosphorylation of the inhibitory C-terminal tail (Tyr<sup>505</sup>) could be detected (Fig. 3A). However, in the absence of CD45, a small reduction in Tyr<sup>505</sup> by other PTPs could facilitate Lck activation through trans-autophosphorylation of the activation loop (19, 24). Consistent with this reasoning, the extent of  $\zeta$ -chain phosphorylation was markedly increased (fourfold) when Lck was activated in the absence of CD45 (Fig. 3, A and B). We also noted that in the absence of CD45, a more abrupt change in Lck activation occurred with higher concentrations of Csk inhibitor (fig. S2A). The extent of Lck activity was confirmed using Lck isolated from cellular extracts (fig. S2B). Because changes in Lck activity affect  $\zeta$ -chain phosphorylation, and both appear to be regulated by CD45, a computational model was constructed to explore these complex behaviors.

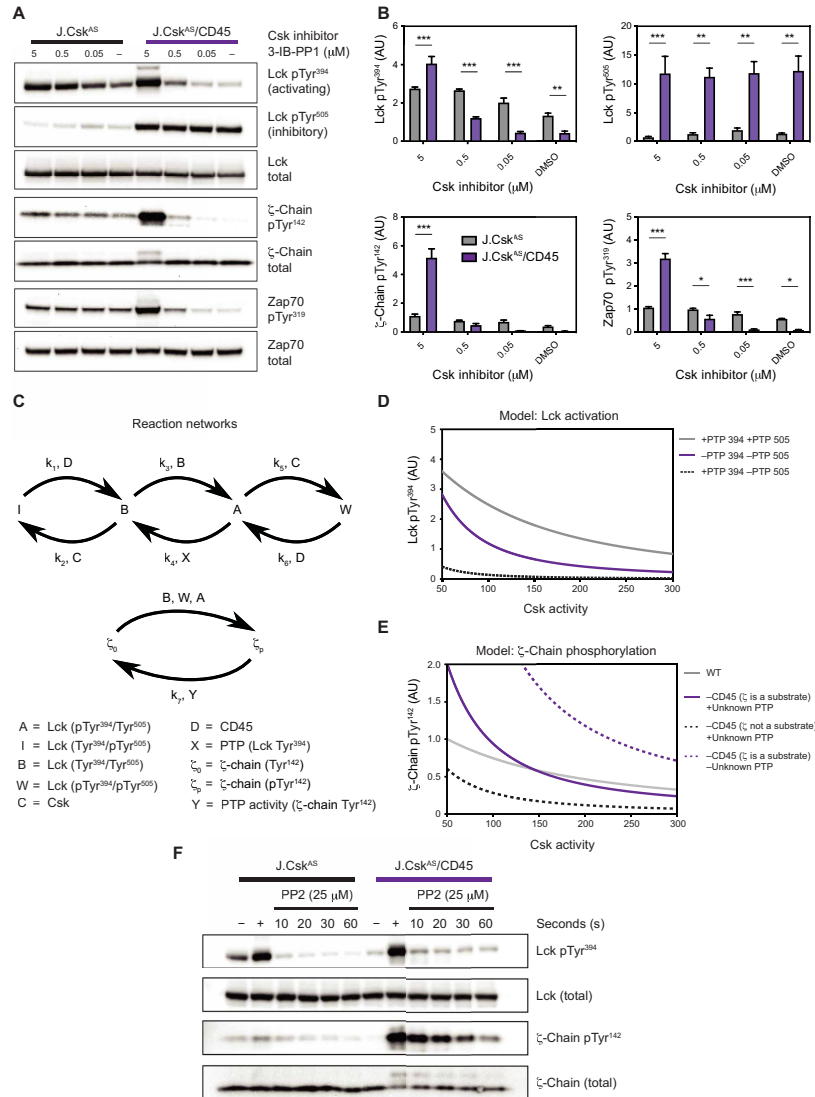
Our model considers phosphorylation of regulatory sites within Lck because these sites control its activity. To deactivate Lck, the

C-terminal tail of Lck (Tyr<sup>505</sup>) is phosphorylated by Csk, and CD45 reverses this modification. Dephosphorylation of Lck Tyr<sup>505</sup> by CD45 results in a basally active unphosphorylated state. When trans-autophosphorylation of Tyr<sup>394</sup> within the activation loop occurs in the basal state (pTyr<sup>394</sup>), it becomes fully active. Our model considers the doubly phosphorylated form of Lck (pTyr<sup>394</sup>/pTyr<sup>505</sup>) because it is reported to have similar activity to basally active Lck (19, 24). Thus, in the computational model, there are four possible states for Lck: activated, A (pTyr<sup>394</sup>, Tyr<sup>505</sup>); basal state, B (Tyr<sup>394</sup>/Tyr<sup>505</sup>); doubly phosphorylated, W (pTyr<sup>394</sup>/pTyr<sup>505</sup>); and inactive, I (Tyr<sup>394</sup>, pTyr<sup>505</sup>).

A reaction network was constructed to compute changes in Lck and  $\zeta$ -chain phosphorylation as Csk activity is reduced (Fig. 3C). The kinetic processes within the reaction network were described mathematically using mass action kinetics, and the resulting differential equations were solved (text S1). We considered different identities for the phosphatase (denoted X) that predominately acts on the activation loop of Lck. Using our model, we evaluated whether our experimental findings were best recapitulated with X being CD45 or another phosphatase. We found that our model best recapitulated the experimental changes in Lck autophosphorylation if the identity of X is CD45, consistent with previous findings (Fig. 3D) (24, 40).

We next computationally evaluated the consequences of Lck activation on  $\zeta$ -chain phosphorylation. Two states for  $\zeta$ -chain

**Fig. 3. CD45 suppresses  $\zeta$ -chain phosphorylation.** (A and B) Cells were treated with decreasing amounts of Csk inhibitor, and protein phosphorylation was assessed after 2 min by immunoblot, represented in (A) and quantified in (B). Protein phosphorylation was normalized to total protein. Data were pooled from three independent experiments ( $n = 3$ ). Error bars represent the means  $\pm$  SEM and \* $P < 0.05$ , \*\* $P < 0.01$ , \*\*\* $P < 0.001$  [two-way analysis of variance (ANOVA) Bonferroni multiple comparisons test]. AU, arbitrary units. (C) Reaction network that describes Lck in its active ("A"), basal ("B"), inactive ("I"), and doubly phosphorylated state ("W"); "D" is CD45, and "C" is Csk; "X" and "Y" are phosphatases whose identities were explored. (D) Computational model to assess PTP activities affecting Lck sites. (E) Computational model to evaluate effects of CD45 on  $\zeta$ -chain phosphorylation. (F) Cells were treated with either DMSO control (–) or Csk inhibitor (5  $\mu$ M) for 0.5 min. To assess the extent of phosphorylation cells were treated with Csk inhibitor alone (+). After Lck activation with Csk inhibitor, PP2 (25  $\mu$ M) was added to block Lck activity, and dephosphorylation was assessed over time by immunoblot. Data are representative of two independent experiments.



Tyr<sup>142</sup> were designated:  $\zeta_0$  (unphosphorylated) and  $\zeta_p$  (phosphorylated). Within our model, the  $\zeta$ -chain is dephosphorylated by phosphatase(s) that we label Y. Our calculations explored three scenarios to evaluate whether our experimental data are consistent with Y being: (i) CD45, (ii) another unknown phosphatase, or (iii)

CD45 and another phosphatase, which both act on  $\zeta$  (Fig. 3E). Our model predicts that if CD45 is the only phosphatase that acts on the  $\zeta$ -chain, then active  $\zeta$ -chain should be higher in CD45-deficient cells at all levels of Csk activity because of the loss-negative regulation. Alternatively, if  $\zeta$  is not a substrate for CD45, and Y is

an unknown phosphatase, then  $\zeta$ -chain phosphorylation is predicted to be lower in CD45-deficient cells at all levels of Csk activity because CD45-mediated activation of Lck is lost whereas the capacity to dephosphorylate  $\zeta$  is unaffected. Only in the case where CD45 and another phosphatase both act on  $\zeta$  do the computational results mirror our experimental findings. Within this scenario, in CD45-deficient cells, a transition occurs where  $\zeta$  phosphorylation is lower at high levels of Csk activity, and as Csk activity is reduced,  $\zeta$  phosphorylation becomes higher. Such a transition occurs because at high levels of Csk activity, only a small amount of Lck is active, and therefore,  $\zeta$ -chain phosphorylation is low and another phosphatase is present to act on  $\zeta$ . When Csk activity is reduced, the amount of active Lck is increased and  $\zeta$ -chain phosphorylation is also increased because CD45 is absent. Therefore, our experimental findings and computational analysis reveal that both CD45 and an unknown phosphatase regulate  $\zeta$ -chain phosphorylation.

To further evaluate suppression of  $\zeta$ -chain phosphorylation by CD45 experimentally, we inhibited Csk to phosphorylate the  $\zeta$ -chain and then inhibited Lck. We monitored Lck and  $\zeta$ -chain dephosphorylation and found that activation loop (Tyr<sup>394</sup>) phosphorylation was rapidly diminished after Lck inhibition. Despite the loss of Lck autophosphorylation,  $\zeta$ -chain phosphorylation was dephosphorylated very slowly in the absence of CD45, implicating the importance of CD45 in  $\zeta$ -chain dephosphorylation but also implicating another PTP (Fig. 3F).

#### Titration of CD45 expression unmasks opposing regulatory roles

Having found that CD45 can affect dephosphorylation of both Lck and  $\zeta$ , we explored a more downstream readout of TCR signaling, Erk phosphorylation (Fig. 4A). We reasoned that Erk would provide an integrated readout of the influence of CD45 on TCR signaling. We therefore assessed the proportion of phospho-ERK-positive cells in response to Csk inhibition. We found that in the presence or absence of CD45, at high levels of Csk inhibition, cells were phospho-ERK positive. However, as Csk inhibition was reduced, the proportion of cells that became phospho-ERK positive drastically declined in the absence of CD45. It is apparent that more graded activation of signaling occurs in the presence of CD45. In contrast, in the absence of CD45, switch-like or cooperative signaling occurs (Hill coefficient  $n_H = 4.9$ ) (Fig. 4B).

Because reducing CD45 levels influenced both Lck activation and signaling, we sought to unmask regulatory trends by surveying a broad range of CD45 levels. We therefore titrated CD45 expression and assessed sensitivity to Csk inhibition. We used single-cell analysis to monitor the amount of CD45 on a cell and its response to Csk inhibition. Specifically, CD45-deficient cells (J.Csk<sup>AS</sup>/CD45) were reconstituted with CD45 to generate a diverse expression profile. The proportion of phospho-ERK-positive cells provided a readout of TCR signaling, which was plotted as a moving average versus CD45 levels (Fig. 4C). When CD45 was greatly diminished or absent, we again observed all-or-none activation, where high levels of Csk inhibition caused signaling and low levels did not (Fig. 4D and fig. S3, A and B). However, as CD45 levels increased to an intermediate amount, hypersensitivity to Csk inhibition occurred. Within this range of CD45, even small amounts of Csk inhibition cause signaling. Last, when CD45 is very abundant, signaling was suppressed even at the highest level of Csk inhibition.

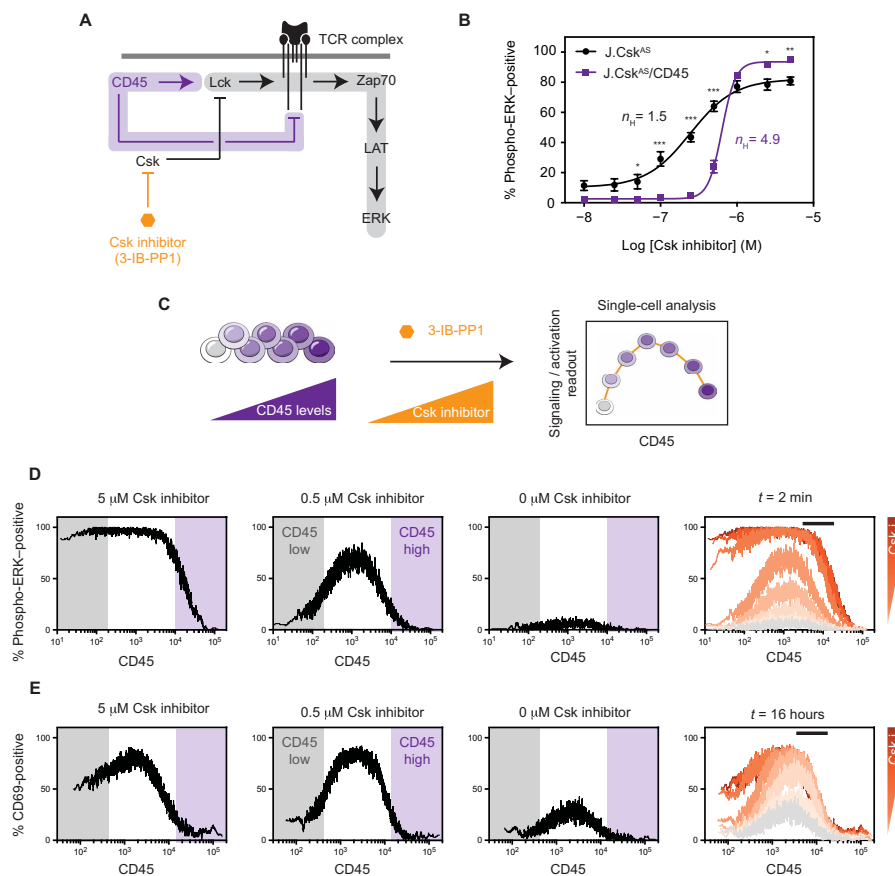
Erk phosphorylation occurs rapidly, so we also evaluated a readout of sustained signaling, CD69 up-regulation. We performed similar single-cell analysis using CD45-deficient cells reconstituted with variable levels of CD45. Cells were then cultured in the presence of Csk inhibitor for 16 hours, and up-regulation of CD69 was assessed. The obtained activation profile was qualitatively similar to that observed using phospho-ERK as a readout (Fig. 4E and fig. S3C). Specifically, upon Csk inhibition, cells displayed a more switch-like response in the absence of CD45, intermediate CD45 levels caused hypersensitivity, and high amounts of CD45 suppressed signaling. Overall, our findings indicate that changes in CD45 activity can cause divergent responses to Csk inhibition that range from hypersensitivity to suppression of activation.

Mice that express a CD45 variant (*LL*) that results in reduced levels of CD45 [ $\sim 10$  to 14% of wild-type (WT)] were anticipated to be hyperresponsive to Csk inhibition, much as immature thymocytes from the *LL* mice have been shown to be hyperresponsive to TCR stimulation. We therefore crossed CD45-low (*LL*) mice to incorporate the Csk<sup>AS</sup> allele (30). Consistent with increased reactivity, we found that CD8<sup>+</sup> T cells isolated from mice with low CD45 had reduced TCR levels and an increased proportion of memory T cells, which are hallmarks of chronic stimulation (fig. S4, A to C). CD8<sup>+</sup> T cells were isolated and treated with Csk inhibitor at different concentrations. Csk inhibition caused an increase in  $\zeta$ -chain phosphorylation in mice with WT or reduced CD45 levels (fig. S4D). However, the extent of  $\zeta$ -chain phosphorylation in CD45-low mice did not reach that of WT, perhaps because of chronic TCR stimulation and down-regulation of the TCR in vivo. Despite a lower extent of  $\zeta$ -chain phosphorylation, CD45-low mice display increased Zap70 activation and LAT phosphorylation, as well as increased global protein tyrosine phosphorylation. Not seen in CD45 null Jurkat cells, the phosphorylation of Lck Tyr<sup>505</sup> decreased at high levels of Csk inhibition, perhaps reflective of the action of the low level of CD45 in these cells (Fig. 3A and fig. S4D).

#### CD45 enables graded signaling outputs

Because changes in CD45 expression affect sensitivity to Csk inhibition (Fig. 4D and fig. S2A), CD45 appears necessary to maintain a basally active pool of Lck while suppressing antigen-independent signals. To further evaluate this model, the TCR was stimulated while Csk was inhibited. We reasoned that loss of CD45 would narrow the range of TCR stimuli to which cells could respond. We treated cells with differing concentrations of stimulatory anti-CD3 antibody and Csk inhibitor and assessed ERK phosphorylation (Fig. 5A). In the presence of CD45, Csk inhibition causes an incremental increase in the proportion of phospho-ERK-positive cells. Despite this basal increase, except at the highest levels of Csk inhibition, TCR stimulation further increases the proportion of phospho-ERK-positive cells. In contrast, CD45-deficient cells were markedly less responsive to TCR stimulation. At higher levels of Csk inhibition, cells were predominately activated and therefore could not respond to further stimuli, and when Csk inhibition is decreased, CD45-deficient cells respond only weakly to TCR stimulation.

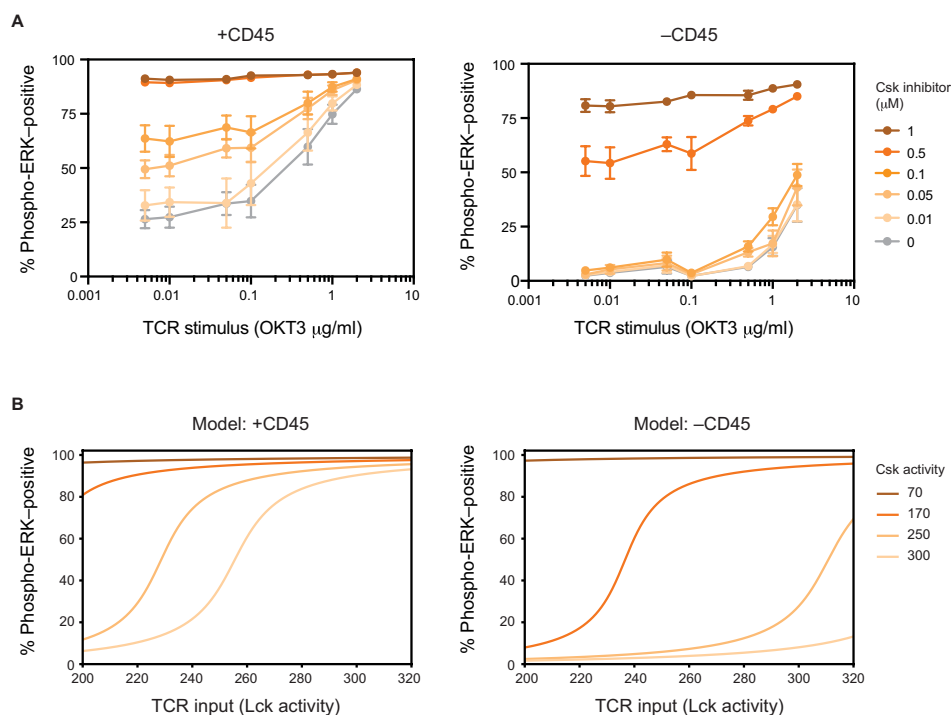
To better understand ERK activation in the absence of CD45, we constructed a computational model. We previously reported that Ras/SOS/ERK pathway behavior in T cells can be recapitulated computationally (41). Positive feedback mediated by SOS-catalyzed Ras activation creates a digital response (i.e., within a given cell,



**Fig. 4. Titration of CD45 expression unmasks opposing regulatory roles.** (A) Revised model where CD45 acts to both activate Lck kinase but also dephosphorylate its substrate, the TCR complex. (B) The proportion of phospho-ERK positive cells was quantified as an integrated readout of TCR signaling by flow cytometry using a range of Csk inhibition. Error bars represent the means  $\pm$  SEM ( $N = 3$ ) and \* $P < 0.05$ , \*\* $P < 0.01$ , \*\*\* $P < 0.001$  (two-way ANOVA Bonferroni multiple comparisons test). (C) CD45-deficient cells (J.Csk<sup>Δ5</sup>/CD45) were transfected with CD45 to generate a broad range of CD45 expression levels. Cells were then treated with Csk inhibitor and assessed by flow cytometry. (D) Analysis of cells with high and low CD45 levels treated with 5 μM Csk inhibitor (3-IB-PP1) for 2 min using phospho-ERK as a readout. The percentage of phospho-ERK-positive cells was plotted as a moving average versus CD45 levels over a range of inhibitor concentrations. (E) To assess sustained signaling, cells were treated with Csk inhibitor for 16 hours. The percentage of activated (CD69-positive) cells was plotted as a moving average versus CD45 levels. For (D) and (E), the far-right panel depicts an overlay of results obtained with different Csk inhibitor concentrations. The black bar denotes approximate WT level of CD45. Histograms can be found in the Supplementary Materials. All data are representative of three independent experiments.

ERK is either activated or not). Using this model, we sought to explore how changes in Lck activity and  $\zeta$ -chain phosphorylation that occur in the presence or absence of CD45 affect ERK activation (Fig. 5B). We therefore incorporated the Csk/CD45 regulatory axis into a simplified model of ERK activation. Within our model, we considered the amount of active Lck as a proxy for TCR input or stimulation level. We found that our experimental observations

could be broadly recapitulated by considering a linear relationship between the amount of phosphorylated  $\zeta$ -chain and active SOS. The increased sensitivity of CD45-sufficient cells can be attributed to the role of CD45 in activating Lck. When cells are CD45 deficient, low basally active Lck amounts propagate through the system. These findings highlight the importance of the positive regulatory role of CD45 upon Lck activation at high levels of Csk activity and



**Fig. 5. CD45 is necessary for regulatable activation of Lck and TCR responsiveness.** (A) The amount of active Lck was perturbed through Csk inhibition of cells that were CD45 positive (left) and CD45 negative (right) in combination with TCR stimulation using anti-CD3 cross-linking. Signaling was assessed by monitoring the proportion of phospho-ERK-positive cells. Error bars represent the means  $\pm$  SEM of four independent experiments ( $N = 4$ ). (B) A computational model was generated to evaluate the effects of CD45 on the SOS/RAS/ERK pathway.

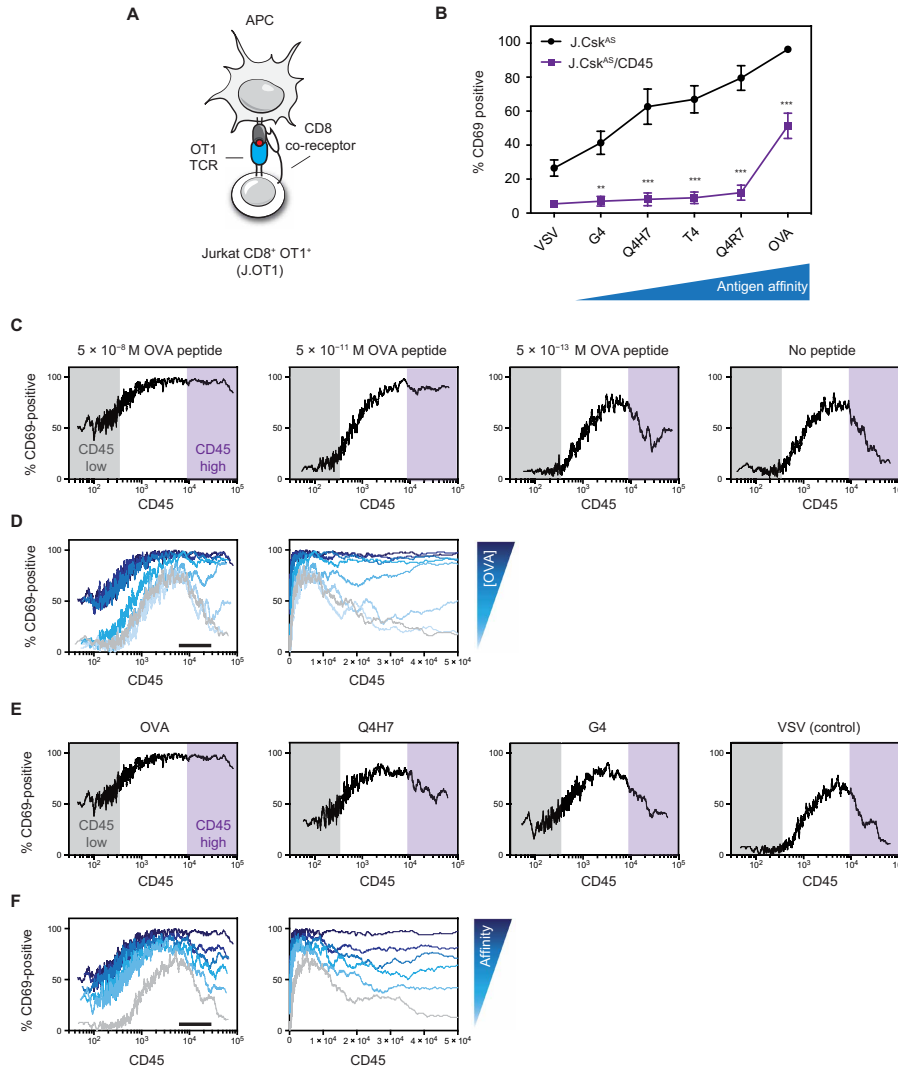
of its negative regulatory roles, such as  $\zeta$ -chain dephosphorylation, at low levels Csk activity. These roles underlie the experimental changes in Erk activation, which occur as CD45 levels are altered (Fig. 4D). Using the model described above, our calculations recapitulate the nonmonotonic dependence of ERK activation on the level of CD45 (text S1).

#### CD45 is required for antigen affinity discrimination

High levels of CD45 suppress antigen-independent signals (Fig. 4). We therefore sought to evaluate whether antigen-dependent signals were affected similarly. Antigen-dependent signaling was tuned using peptide antigens that bind the TCR with differing affinities (Fig. 1). We used Jurkat T cells that were engineered to express the OT1 TCR transgene and CD8 co-receptor. Jurkat OT1<sup>+</sup> CD8<sup>+</sup> (J.OT1) cells were used to generate a CD45-deficient variant (J.OT1/CD45) (Fig. 6A and fig. S5, A to C) (42). Similar to primary T cells, J.OT1 cells display a graded response to APCs, displaying altered peptide ligands (Fig. 6B). The high-affinity OVA epitope elicited robust activation as read out by CD69 up-regulation. In contrast, the low-affinity antigen resulted in only weak activation.

When compared to CD45-deficient cells, however, only the highest affinity OVA antigen was able to elicit partial activation. Even when no peptide is present, an increased proportion of activated cells is observed when CD45 is reduced, which is consistent with CD45 suppressing weak signals that occur in the absence of cognate antigen in cells where Lck is active. Consistent with the ability of high-affinity antigens to elicit activation, we observed surfaces coated with immobilized high-affinity OVA pMHC or anti-TCR-facilitated robust cell spreading when a synapse is formed with the surface (fig. S6, A and B). In contrast, surfaces displaying lower-affinity peptide displayed reduced spreading. The capacity of CD45-deficient cells to form a synapse was reduced, particularly in response to lower-affinity antigen (fig. S6, A and B).

We next reconstituted CD45-deficient cells to generate a range of CD45 levels. Activation of single cells was monitored as a function of CD45 level in response to differing doses of the OVA peptide (Fig. 6, C and D, and fig. S7A). At low levels of CD45, cells were less responsive to antigen, particularly as the antigen concentration was reduced. At intermediate levels of CD45 expression, cells were increasingly sensitive with substantial activation even when antigen



**Fig. 6. CD45 is required for affinity discrimination of antigen.** (A) Jurkat T cells were engineered to express the OT1 TCR transgene and the CD8 co-receptor (J.OT1). CD45 was deleted from J.OT1 cells using CRISPR-Cas9 (J.OT1/CD45). (B) Cells were cocultured with T2-Kb APCs pulsed with the indicated peptide antigens (0.05 nM), and up-regulation of CD69 was assessed as a readout of T cell activation. Error bars represent the means  $\pm$  SEM ( $N = 3$ ) and  $^{**}P < 0.01$ ,  $^{***}P < 0.001$  (two-way ANOVA Bonferroni multiple comparisons test). (C to F) CD45-deficient cells (J.OT1/CD45) were transiently transfected with CD45 to generate a broad range of CD45 levels. Cells were then cocultured with T2-Kb cells and peptide antigen for 16 hours. The percentage of CD69-positive cells was plotted as a moving average versus CD45 expression levels. Differing concentrations of OVA peptide (C) and overlay of OVA concentrations on a log scale (left) or linear (right) axis (D). Black bar denotes approximate WT level of CD45. (E) Altered peptide ligands at a fixed concentration (50 nM) and (F) overlay of altered peptide ligands on a log scale (left) or linear (right) axis. Black bar denotes approximate WT level of CD45. Histograms can be found in the Supplementary Materials. All data are representative of three independent experiments.



was greatly reduced or absent. In contrast to Csk inhibition, we observed that the high-affinity OVA peptide could cause robust activation even at high levels of CD45. To expand this finding, we assessed variants of the OVA peptide that bind with reduced affinity (Fig. 6, E and F, and fig. S7, B and C). At high levels of CD45, the proportion of cells that became activated declined as antigen affinity was decreased.

## DISCUSSION

T cells can distinguish between antigens of differing affinities (35, 43, 44). Recent efforts have revealed that not only the affinity of the TCR:pMHC interaction is critical but also its strength under exerted force (45–49). How TCR signaling events enforce antigen discrimination remains unclear. The kinetic proofreading model proposes that once initiated, signaling must accumulate to a point of commitment before dissociation of the TCR from pMHC (50, 51). An expanded kinetic proofreading model has found recruitment of active Lck and co-receptor to the TCR:pMHC to be critical for this process (31, 49). Studies have implicated active Lck abundance in setting a threshold for T cell activation (21, 22, 52). We demonstrate using two readouts of T cell activation that increasing active Lck amounts potentiate responses to low-affinity antigens, and conversely, the response to these weak antigens is attenuated when active Lck is reduced. In contrast to low-affinity antigens, high-affinity antigens are less sensitive to changes in the abundance of active Lck. Although we focus predominately on Lck, T cells also have another less abundant SFK, Fyn (23, 53). Fyn is dispensable for T cell development but is reported to contribute to antigen recognition in the periphery (52, 54). Overall, our findings are consistent with Csk repressing active SFK amounts to set a threshold for T cell activation.

Because Csk-mediated inhibition of Lck is opposed by CD45, we investigated the contributions of both regulators simultaneously using intact cells. We found that inhibition of Csk could activate Lck in the absence of CD45 despite no appreciable dephosphorylation of the inhibitory C-terminal tail (Tyr<sup>505</sup>). Because a greater extent of Csk inhibition is required when CD45 is absent, we speculate that another phosphatase may weakly act on this site, and when Csk activity is abolished, Lck trans-autophosphorylation can occur independently of CD45. Phosphorylation of Lck (Tyr<sup>394</sup>) has been demonstrated to activate the kinase even when its inhibitory C-terminal tail remains phosphorylated (19, 24). Activation of Lck in this way allowed us to assess the role of CD45. Our findings indicate that CD45 acts on multiple substrates, facilitating Lck activation while also suppressing phosphorylation of its substrate, the  $\zeta$ -chain. Computational modeling of our Csk inhibition results confirm that suppression of  $\zeta$ -chain phosphorylation is recapitulated only if  $\zeta$  is a CD45 substrate. Our computational analysis also implicates an additional phosphatase, which can dephosphorylate the  $\zeta$ -chain because deletion of CD45 would otherwise be predicted to cause constitutive  $\zeta$ -chain phosphorylation. The contribution of an additional phosphatase to suppression of TCR signaling is consistent with roles attributed to phosphatases, including SHP1, PTPN22, and others, thought to be important for regulating T cell reactivity in the periphery (5, 55, 56). Here and in previous reports, when CD45 was reduced but not absent, cells became hyperresponsive to stimuli (30). Consistent with increased reactivity, T cells that we isolated from mice with low levels of CD45 displayed hallmarks

of chronic stimulation: reduced TCR and a higher proportion of memory T cells. Together, these observations suggest that numerous adaptations can occur in the periphery to suppress TCR signaling when CD45 is reduced, which could affect  $\zeta$ -chain phosphorylation.

Because CD45 acts on  $\zeta$ , Lck, and potentially additional substrates, we altered Csk and CD45 activity and assessed an integrated readout of TCR signaling (Erk phosphorylation). Critical features of CD45-mediated regulation emerged as follows: (i) a switch-like response in its absence, (ii) hypersensitivity to changes in Csk activity at reduced CD45 levels, and (iii) suppression at high levels of CD45. These findings reveal a marked interdependence between CD45-mediated activation of Lck and suppression of TCR signaling. Our findings highlight how quantitative manipulation of Csk and CD45 activities can achieve distinct signaling behaviors. We also found that CD45 was required for TCR agonist-induced signaling. Our findings were modeled computationally and reveal that CD45 is required to suppress  $\zeta$ -chain phosphorylation when Csk activity is low. Specifically, when CD45 is absent, and Csk activity is reduced to activate Lck, the loss of  $\zeta$ -chain suppression causes cells to signal in the absence of TCR stimuli, rendering them unresponsive to further TCR stimuli. Therefore, CD45 is required for inducible signaling because it provides for a regulatable pool of basally active Lck while suppressing phosphorylation of its substrate, the  $\zeta$ -chain, until TCR stimuli are encountered. In vitro analyses of CD45 have generally emphasized its negative regulatory role ( $\zeta$ -chain dephosphorylation). However, our findings reveal the importance of CD45 in maintaining a regulatable pool of active Lck. Loss of Lck regulation, for example, in CD45-deficient or CD45-low mice and cells, affects the capacity of T cells to properly discern antigen strength. In this way, the capacity of a T cell to initiate signals that correspond to the appropriate cellular response is disrupted. Moreover, feedback mechanisms that tune TCR signaling have been implicated in regulating active Lck amounts. For example, Csk resides within the cytoplasm unless it is recruited to the plasma membrane where it can inhibit Lck. Recruitment of Csk is mediated by phosphorylated adaptor proteins, such as PAG (57, 58). In addition, a Zap70-dependent negative regulatory loop is thought to phosphorylate a conserved site (Tyr<sup>192</sup>) within the SH2 domain of Lck (59, 60). Modification of Tyr<sup>192</sup> disrupts the ability of CD45 to interact with Lck and dephosphorylate its inhibitory C-terminal tail (59). Such negative feedback mechanisms highlight the capacity of a T cell to tune its basal pool of active Lck. It is anticipated that tuning Lck activity is important for T cells to generate graded signaling outputs that ultimately influence cellular programs (5, 61–63).

CD45 has been previously reported to suppress T cell activation because it is excluded from the TCR as a synapse is formed between a T cell and an APC-bearing cognate antigen. Within the synapse, many proteins are redistributed within the plasma membrane of the T cell. Over time, the TCR becomes concentrated at the center of the synapse, whereas CD45 is excluded (27). Because CD45 is excluded, it has been proposed that the segregation of CD45 itself may be sufficient to initiate TCR signaling (26). However, studies using tethered antibodies that bind to the TCR with high affinity indicate that exclusion of CD45 is not a strict requirement (64). Additional studies have reported that the T cell:APC synapse also functions as a site of sustained signaling and receptor down-regulation upon strong stimulation (65, 66). We did not investigate whether the exclusion of CD45 initiates TCR signaling; however, we found that high-affinity antigens can overcome suppression that occurs at high

levels of CD45 expression. In contrast, low-affinity antigens and antigen-independent signaling (Csk inhibition) are suppressed by CD45. Our findings appear consistent with the T cell:APC synapse, facilitating sustained signaling. Specifically, we anticipate that sustained signaling over time through a synapse could overcome CD45-mediated suppression through exclusion of CD45 and/or the local concentration of signaling components. This would not occur during antigen-independent signaling (Csk inhibition).

Overall our findings reveal that CD45 acts as a signaling gatekeeper in T cells because it enables a regulatable pool of basally active Lck while suppressing weak or spurious TCR signaling. We anticipate that CD45 could fulfill a similar role in other immune cells having ITAM receptors, and by extension, other receptor-mediated signaling pathways having RT-PTPs.

## MATERIALS AND METHODS

### Mice

All mice were bred and maintained on the C57BL/6 genetic background. For experiments, mice were used at between 6 and 12 weeks of age. All animals were housed in a specific pathogen-free facility at University of California, San Francisco (UCSF) and were treated according to protocols that were approved by UCSF animal care ethics and veterinary committees and are in accordance with National Institutes of Health (NIH) guidelines. The OT1 TCR transgene was crossed to Csk<sup>AS</sup> transgenic and Nur77-GFP reporter mice (33, 67). The lightning allele (LL or CD45-low) was similarly crossed to mice harboring the Csk<sup>AS</sup> transgene (30). To assess cell populations, spleen and lymph nodes were isolated from mice, and organs were dissociated in complete medium [RPMI supplemented with 10% fetal bovine serum (FBS), 2 mM glutamine, nonessential amino acids (Gibco), penicillin and streptomycin (Gibco), 1 mM sodium pyruvate, 50  $\mu$ M 2-mercaptoethanol, and 10 mM HEPES]. Red blood cells were removed using ammonium-chloride-potassium (ACK) lysis. Cells were washed and resuspended in fluorescence-activated cell sorting (FACS) buffer [phosphate-buffered saline (PBS) supplemented with 2% FBS and 2 mM EDTA] and stained using fluorescently labeled antibodies. Cells were analyzed using a BD Fortessa, and quantification was carried out using FlowJo software.

### Antibodies

A table of antibodies used in this study can be found in table S1.

### Cell lines

Jurkat T cell lines were maintained by the Weiss laboratory and are routinely analyzed for the expression of CD3 or TCR $\beta$  and other surface markers by flow cytometry. Cells were maintained in a tissue culture incubator at 37°C with 5% CO<sub>2</sub> in culture medium (RPMI supplemented with 10% FBS and 2 mM glutamine). Jurkat variants deficient for specific proteins of interest were generated using CRISPR-Cas9-targeted gene deletion. J.Csk<sup>AS</sup> (B2C9-26) and J.Csk<sup>AS</sup>/CD45 (C14) were maintained in medium supplemented with blasticidin (10  $\mu$ g/ml).

### CRISPR-Cas9

CD45-deficient cell lines were generated using the pX330 vector (38) and guide RNAs targeting CD45 (59). The pX330 vector was introduced using electroporation and cultured for ~4 days. Cells were stained for surface CD45, and cells with low CD45 expression

were sorted into 96-well plates using a BD FACSAria. Cells were expanded and analyzed for CD45 expression using flow cytometry and immunoblot to confirm CD45-deficient clones. Mutations to *PTPRC*, which encodes CD45, were confirmed by sequencing. The target site was amplified by polymerase chain reaction using genomic DNA isolated from cell lines and cloned into a Topo vector. Cell lines that were reconstituted with Csk<sup>AS</sup> were confirmed by immunoblot using anti-Csk and anti-Myc tag antibodies.

### Electroporation

DNA constructs were introduced into Jurkat T cell lines using a Bio-Rad Gene Pulser Xcell. Cells were washed and resuspended with RPMI medium. Four hundred microliters of cells ( $15 \times 10^6$  total cells) were added to a 0.4-cm cuvette. Typically, 10  $\mu$ g of DNA was added and cells were electroporated (260 V, 1250  $\mu$ F). Immediately after electroporation, cells were recovered into prewarmed culture medium and incubated at 37°C for 48 hours. For transient expression of CD45, cells were electroporated with a pEF CD45RO construct. For stable reconstitution, cells were electroporated with pEF Csk<sup>AS</sup> and recovered for 48 hours. Stable clones were isolated using limiting dilution. Cells were diluted and cultured in selective medium containing blasticidin (10  $\mu$ g/ml) in 96-well plates. After ~3 weeks, clones were assessed for Csk expression using immunoblot and expanded further.

### Immunoblotting

Jurkat T cells were rinsed with RPMI and resuspended at  $5 \times 10^6$  cells/ml and rested for 15 min at 37°C. Cells were treated with anti-TCR antibody (C305, 0.85  $\mu$ g/ml) or Csk<sup>AS</sup> inhibitor 3-IB-PP1 (provided by the Shokat laboratory), PP2 (Toocris), or dimethyl sulfoxide (DMSO). Cells were then lysed through addition of lysis buffer containing a final concentration of the following: 1% NP-40, NaVO<sub>4</sub> (2 mM), NaF (10 mM), EDTA (5 mM), phenylmethylsulfonyl fluoride (2 mM), aprotinin (10  $\mu$ g/ml), pepstatin (1  $\mu$ g/ml), leupeptin (1  $\mu$ g/ml), and PP2 (25  $\mu$ M). Lysates were placed on ice, and debris were pelleted at 13,000g. Primary T cells were resuspended at 20 to  $40 \times 10^6$  cells/ml and lysed using 6 $\times$  SDS-polyacrylamide gel electrophoresis sample buffer. DNA was pelleted in an ultracentrifuge at 70,000 rpm. Supernatants were run on 4 to 12% NuPage or 10% bis-tris gels and transferred to polyvinylidene difluoride membranes. Membranes were incubated with blocking buffer [2% bovine serum albumin tris-buffered saline with 0.1% Tween-20 (TBS-T)] and then probed with primary antibodies overnight at 4°C. The following day, blots were rinsed and incubated with horseradish peroxidase-conjugated secondary antibodies (diluted 1:5000). All antibodies used for immunoblotting were diluted 1:2000 in blocking buffer unless otherwise stated. Blots were detected using chemiluminescent substrate and a ChemiDoc (Bio-Rad) or iBright (Invitrogen) imaging system. Phosphorylation was assessed at 2 min after acute treatment with inhibitor or anti-TCR stimulation unless otherwise stated. Quantification was performed using Image Lab or iBright analysis software.

### OT1 coculture

Cells were isolated from the spleen and lymph node. CD8<sup>+</sup> OT1 T cells were purified by negative selection using biotinylated antibodies and magnetic beads as previously described (68). Splenocytes were used as APCs and were isolated from T cell-deficient mice (Ca<sup>-/-</sup> or Zap70<sup>-/-</sup>). Before culture, red blood cells removed using ACK lysis. Splenocytes were incubated with peptide antigens for

1 hour at 37°C. Small-molecule inhibitors (3-IB-PP1 or PP2) or DMSO control were then added followed immediately by OT1 T cells at a ratio of 5:1 (APC:T cell). Cells were cultured overnight at 37°C for a total of 16 hours and placed on ice before staining for CD69 and other surface markers (CD19/B220, CD8 $\alpha$ , TCR $\beta$ , or V $\alpha$ 2) using an antibody dilution of 1:200 in FACS buffer and Fc blocking antibody (2.4G2) at 1:1000. Up-regulation of CD69 or Nur77-GFP was assessed by flow cytometry using a BD Fortessa and quantified using FlowJo software. The OVA peptide (SIINFEKL), its variants (Q4R7, T4, Q4H7, and G4), and the VSV peptide were synthesized by GenScript.

#### J.OT1 coculture

J.OT1 activation assays were performed similarly to primary CD8<sup>+</sup> OT1 T cell cocultures. J.OT1 cells ( $5 \times 10^4$ ) were combined with T2-Kb cells (APCs) that had been incubated with peptide antigen for 1 hour at a ratio of 3:1 (APC:J.OT1). Cells were cultured for 16 hours and then placed on ice and stained for CD69 (1:200 in FACS buffer). CD69 up-regulation was assessed by flow cytometry using a BD Fortessa and quantified using FlowJo software.

#### Phospho-ERK staining

Cells were stimulated in RPMI and fixed by adding 4% formaldehyde PBS (1:1) and incubating for 12 min at room temperature. Cells were pelleted and rinsed with FACS buffer (PBS supplemented with 2% FBS and 2 mM EDTA). Cells were then placed on ice and ice-cold 90% methanol added to permeabilize the cells for 45 min. Cells were then rinsed three times with FACS buffer and resuspended in staining solution (anti-phospho-ERK 1:100 in FACS buffer). Cells were stained for either 1 hour at room temperature or overnight at 4°C. Cells were rinsed three times and stained with anti-rabbit PE (R-phycoerythrin) antibody and anti-CD45 AF647 antibody (1:100 in FACS buffer) for 45 min at room temperature. Cells were rinsed two times and analyzed by flow cytometry using a BD Fortessa and quantification performed using FlowJo software. For Csk inhibitor dose-response curves, data were fit using agonist versus response with variable slope in GraphPad Prism.

#### Single-cell analysis

FACS data were exported from FlowJo in CSV format and analyzed with R Studio using the Zoo package. The proportion of phospho-ERK- or CD69-positive cells was calculated as a moving average. Graphs were generated using GraphPad Prism software.

#### In vitro kinase assay

Cells were washed and resuspended in RPMI. Cells were incubated at 37°C for 10 to 15 min before treatment with inhibitors (25 or 5  $\mu$ M 3-IP-PP1) for 1 min. Cells were lysed by adding concentrated lysis buffer to a final concentration of the following: 1% NP-40, NaVO<sub>4</sub> (2 mM), NaF (10 mM), EDTA (5 mM), and HALT protease inhibitor cocktail (Invitrogen). Samples were vortexed briefly and placed on ice for 10 min and then centrifuged to pellet debris. Anti-Lck beads [25  $\mu$ l per immunoprecipitation (IP)] were added and mixed for 1.5 hours at 4°C. Beads were rinsed with ice-cold lysis buffer twice followed by kinase buffer [50 mM Hepes (pH 7.0), 2 mM dithiothreitol, 5 mM MgCl<sub>2</sub>, 0.2 mM NaVO<sub>4</sub>, and 0.5 mM  $\beta$ -glycerophosphate]. Beads were resuspended in 60  $\mu$ l of kinase buffer containing substrate [1  $\mu$ g of glutathione S-transferase (GST) CD3 $\zeta$ , Sino Biological] and adenosine 5'-triphosphate added to 0.2 mM. Samples were in-

cubated with agitation at 25°C for 5 min and placed on ice. Supernatant containing substrate was collected. Phosphorylation status of substrate (GST CD3 $\zeta$ ) and immunoprecipitated Lck were assessed by immunoblot.

#### Anti-Lck resin

Protein G Dynabeads (1 ml, Invitrogen) were washed and incubated with 200  $\mu$ g of anti-Lck (1F6) in binding buffer (sodium borate, pH 9) for 1 hour at room temperature. Beads were rinsed and resuspended in 10 ml of binding buffer. Dimethyl pimelimidate (DMP) (50 mg) was added and mixed for 30 min. Beads were rinsed and resuspended in 0.1 M ethanolamine (pH 8) and incubated for 30 min. Unconjugated antibody was released by washing with 0.1 M glycine (pH 3). Beads were washed twice with tris-buffered saline (TBS, pH 7.4). Beads were resuspended in 1 ml of TBS and stored at 4°C.

#### Microscopy

Glass surfaces were coated with either stimulatory antibody (C305) or streptavidin (SA). Surfaces were then washed, and biotinylated monomeric pMHC complexes were incubated with streptavidin surfaces to immobilize them. Surfaces were then washed and used for antigen presentation. To assess synapse formation, J.OT1 cells were dropped onto cover glass coated with various stimulatory reagents for 30 min at 37°C. Cells were subsequently fixed with 4% paraformaldehyde. After fixation, the cell membrane was stained using either AF-594 anti-human-CD45 (Biolegend) or AF-594 wheat germ agglutinin (Thermo Fisher Scientific). Fixed immunological synapses formed on glass surfaces were imaged with the Nikon Ti Microscope using total internal reflection fluorescence microscopy at the UCSF Nikon Imaging Center. The areas of synapses were processed and quantified using ImageJ software. The pMHC complexes were provided by the Palmer laboratory and the NIH tetramer core.

#### SUPPLEMENTARY MATERIALS

stke.sciencemag.org/cgi/content/full/12/604/eaaw8151/DC1

Text S1. Details of the computational model.

Fig. S1. Csk analog-sensitive Jurkat T cell characterization.

Fig. S2. Effects of Csk inhibition on CD45-deficient Jurkat T cells.

Fig. S3. FACS analysis of Csk inhibition.

Fig. S4. CD45-low (LL) mice have increased memory CD8<sup>+</sup> T cells and lower TCR levels.

Fig. S5. OT1 Jurkat T cells.

Fig. S6. Contact area is influenced by antigen affinity and CD45.

Fig. S7. FACS analysis of J.OT1/CD45 cells.

Table S1. Antibodies.

[View/request a protocol for this paper from Bio-protocol.](#)

#### REFERENCES AND NOTES

1. T. J. Molina, K. Kishihara, D. P. Siderovski, W. van Ewijk, A. Narendran, E. Timms, A. Wakeham, C. J. Paige, K. U. Hartmann, A. Veillette, D. Davidson, T. W. Mak, Profound block in thymocyte development in mice lacking p56<sup>lck</sup>. *Nature* **357**, 161–164 (1992).
2. D. B. Straus, A. Weiss, Genetic evidence for the involvement of the Lck tyrosine kinase in signal transduction through the T cell antigen receptor. *Cell* **70**, 585–593 (1992).
3. A. H. Courtney, W.-L. Lo, A. Weiss, TCR signaling: Mechanisms of initiation and propagation. *Trends Biochem. Sci.* **43**, 108–123 (2018).
4. J. E. Smith-Garvin, G. A. Koretzky, M. S. Jordan, T cell activation. *Annu. Rev. Immunol.* **27**, 591–619 (2009).
5. G. Gaud, R. Lesourne, P. E. Love, Regulatory mechanisms in T cell receptor signalling. *Nat. Rev. Immunol.* **18**, 485–497 (2018).
6. F. Sicheri, I. Moarefi, J. Kuriyan, Crystal structure of the Src family tyrosine kinase Hck. *Nature* **385**, 602–609 (1997).
7. W. Xu, S. C. Harrison, M. J. Eck, Three-dimensional structure of the tyrosine kinase c-Src. *Nature* **385**, 595–602 (1997).

8. T. Mustelin, K. M. Coggeshall, A. Altman, Rapid activation of the T-cell tyrosine protein kinase pp56lck by the CD45 phosphotyrosine phosphatase. *Proc. Natl. Acad. Sci. U.S.A.* **86**, 6302–6306 (1989).
9. H. L. Ostergaard, D. A. Shackelford, T. R. Hurler, P. Johnson, R. Hyman, B. M. Sefton, I. S. Trowbridge, Expression of CD45 alters phosphorylation of the lck-encoded tyrosine protein kinase in murine lymphoma T-cell lines. *Proc. Natl. Acad. Sci. U.S.A.* **86**, 8959–8963 (1989).
10. M. Sieh, J. B. Bolen, A. Weiss, CD45 specifically modulates binding of Lck to a phosphopeptide encompassing the negative regulatory tyrosine of Lck. *EMBO J.* **12**, 315–321 (1993).
11. H. Yamaguchi, W. A. Hendrickson, Structural basis for activation of human lymphocyte kinase Lck upon tyrosine phosphorylation. *Nature* **384**, 484–489 (1996).
12. M. Bergman, T. Mustelin, C. Oetken, J. Partanen, N. A. Flint, K. E. Amrein, M. Autero, P. Burn, K. Alitalo, The human p50csk tyrosine kinase phosphorylates p56lck at Tyr-505 and down regulates its catalytic activity. *EMBO J.* **11**, 2919–2924 (1992).
13. N. M. Levinson, M. A. Seeliger, P. A. Cole, J. Kuriyan, Structural basis for the recognition of c-Src by its inactivator Csk. *Cell* **134**, 124–134 (2008).
14. K. Kishihara, J. Penninger, V. A. Wallace, T. M. Kundig, K. Kawai, A. Wakeham, E. Timms, K. Pfeffer, P. S. Ohashi, M. L. Thomas, C. Furlonger, C. J. Paige, T. W. Mak, Normal B lymphocyte development but impaired T cell maturation in CD45-exon6 protein tyrosine phosphatase-deficient mice. *Cell* **74**, 143–156 (1993).
15. J. T. Pingel, M. L. Thomas, Evidence that the leukocyte-common antigen is required for antigen-induced T lymphocyte proliferation. *Cell* **58**, 1055–1065 (1989).
16. G. A. Koretzky, J. Picus, M. L. Thomas, A. Weiss, Tyrosine phosphatase CD45 is essential for coupling T-cell antigen receptor to the phosphatidylinositol pathway. *Nature* **346**, 66–68 (1990).
17. S. Nada, T. Yagi, H. Takeda, T. Tokunaga, H. Nakagawa, Y. Ikawa, M. Okada, S. Aizawa, Constitutive activation of Src family kinases in mouse embryos that lack Csk. *Cell* **73**, 1125–1135 (1993).
18. C. Schmidt, K. Sajjo, T. Niidome, R. Kühn, S. Aizawa, A. Tarakhovskiy, Csk controls antigen receptor-mediated development and selection of T-lineage cells. *Nature* **394**, 901–904 (1998).
19. K. Nika, C. Soldani, M. Salek, W. Paster, A. Gray, R. Etzensperger, L. Fugger, P. Polzella, V. Cerundolo, O. Dushkek, T. Höfer, A. Viola, O. Acuto, Constitutively active Lck kinase in T cells drives antigen receptor signal transduction. *Immunity* **32**, 766–777 (2010).
20. A. Stirnweiss, R. Hartig, S. Gieseeler, J. A. Lindquist, P. Reichardt, L. Philipsen, L. Simeoni, M. Poltorak, C. Merten, W. Zschatterer, Y. Prokakov, W. Paster, H. Stockinger, T. Harder, M. Gunzer, B. Schraven, T cell activation results in conformational changes in the Src family kinase Lck to induce its activation. *Sci. Signal.* **6**, ra13 (2013).
21. B. N. Manz, Y. X. Tan, A. H. Courtney, F. Rutaganira, E. Palmer, K. M. Shokat, A. Weiss, Small molecule inhibition of Csk alters affinity recognition by T cells. *eLife* **4**, e08088 (2015).
22. D. Moogk, S. Zhong, Z. Yu, I. Liadi, W. Rittase, V. Fang, J. Dougherty, A. Perez-Garcia, I. Osman, C. Zhu, N. Varadarajan, N. P. Restifo, A. B. Frey, M. Krogsgaard, Constitutive Lck activity drives sensitivity differences between CD8<sup>+</sup> memory T cell subsets. *J. Immunol.* **197**, 644–654 (2016).
23. J. L. Hukelmann, K. E. Anderson, L. V. Sinclair, K. M. Grzes, A. B. Murillo, P. T. Hawkins, L. R. Stephens, A. I. Lamond, D. A. Cantrell, The cytotoxic T cell proteome and its shaping by the kinase mTOR. *Nat. Immunol.* **17**, 104–112 (2016).
24. E. Hui, R. D. Vale, In vitro membrane reconstitution of the T-cell receptor proximal signaling network. *Nat. Struct. Mol. Biol.* **21**, 133–142 (2014).
25. T. Furukawa, M. Itoh, N. X. Krueger, M. Streuli, H. Saito, Specific interaction of the CD45 protein-tyrosine phosphatase with tyrosine-phosphorylated CD3 zeta chain. *Proc. Natl. Acad. Sci. U.S.A.* **91**, 10928–10932 (1994).
26. P. Anton van der Merwe, S. J. Davis, A. S. Shaw, M. L. Dustin, Cytoskeletal polarization and redistribution of cell-surface molecules during T cell antigen recognition. *Semin. Immunol.* **12**, 5–21 (2000).
27. S. K. Bromley, W. R. Burack, K. G. Johnson, K. Somersalo, T. N. Sims, C. Sumen, M. M. Davis, A. S. Shaw, P. M. Allen, M. L. Dustin, The immunological synapse. *Annu. Rev. Immunol.* **19**, 375–396 (2001).
28. V. T. Chang, R. A. Fernandes, K. A. Ganzinger, S. F. Lee, C. Siebold, J. McColl, P. Jönsson, M. Palayre, K. Harlos, C. H. Coles, E. Y. Jones, Y. Lui, E. Huang, R. J. C. Gilbert, D. Klenerman, A. R. Aricescu, S. J. Davis, Initiation of T cell signaling by CD45 segregation at 'close contacts'. *Nat. Immunol.* **17**, 574–582 (2016).
29. K. Choudhuri, D. Wiseman, M. H. Brown, K. Gould, P. A. van der Merwe, T-cell receptor triggering is critically dependent on the dimensions of its peptide-MHC ligand. *Nature* **436**, 578–582 (2005).
30. J. Zikherman, C. Jenne, S. Watson, K. Doan, W. Raschke, C. C. Goodnow, A. Weiss, CD45-Csk phosphatase-kinase titration uncouples basal and inducible T cell receptor signaling during thymic development. *Immunity* **32**, 342–354 (2010).
31. O. Stepanek, A. S. Prabhakar, C. Osswald, C. G. King, A. Bulek, D. Naeher, M. Beaufils-Hugot, M. L. Abanto, V. Galati, B. Hausmann, R. Lang, D. K. Cole, E. S. Huseby, A. K. Sewell, A. K. Chakraborty, E. Palmer, Coreceptor scanning by the T cell receptor provides a mechanism for T cell tolerance. *Cell* **159**, 333–345 (2014).
32. J. R. Schoenborn, Y. X. Tan, C. Zhang, K. M. Shokat, A. Weiss, Feedback circuits monitor and adjust basal Lck-dependent events in T cell receptor signaling. *Sci. Signal.* **4**, ra59 (2011).
33. Y. X. Tan, B. N. Manz, T. S. Freedman, C. Zhang, K. M. Shokat, A. Weiss, Inhibition of the kinase Csk in thymocytes reveals a requirement for actin remodeling in the initiation of full TCR signaling. *Nat. Immunol.* **15**, 186–194 (2014).
34. K. A. Hogquist, S. C. Jameson, W. R. Heath, J. L. Howard, M. J. Bevan, F. R. Carbone, T cell receptor antagonist peptides induce positive selection. *Cell* **76**, 17–27 (1994).
35. M. A. Daniels, E. Teixeira, J. Gill, B. Hausmann, D. Roubaty, K. Holmberg, G. Werlen, G. A. Holländer, N. R. J. Gascoigne, E. Palmer, Thymic selection threshold defined by compartmentalization of Ras/MAPK signalling. *Nature* **444**, 724–729 (2006).
36. A. E. Moran, K. L. Holzappel, Y. Xing, N. R. Cunningham, J. S. Maltzman, J. Punt, K. A. Hogquist, T cell receptor signal strength in T<sub>H</sub>1 and iNKT cell development demonstrated by a novel fluorescent reporter mouse. *J. Exp. Med.* **208**, 1279–1289 (2011).
37. M. Noviski, J. L. Mueller, A. Satterthwaite, L. A. Garrett-Sinha, F. Brombacher, J. Zikherman, IgM and IgD B cell receptors differentially respond to endogenous antigens and control B cell fate. *eLife* **7**, e35074 (2018).
38. L. Cong, F. A. Ran, D. Cox, S. Lin, R. Barretto, N. Habib, P. D. Hsu, X. Wu, W. Jiang, L. A. Marraffini, F. Zhang, Multiplex genome engineering using CRISPR/Cas systems. *Science* **339**, 819–823 (2013).
39. M. Jinek, K. Chylinski, I. Fonfara, M. Hauer, J. A. Doudna, E. Charpentier, A programmable dual-RNA-guided DNA endonuclease in adaptive bacterial immunity. *Science* **337**, 816–821 (2012).
40. L. McNeill, R. J. Salmond, J. C. Cooper, C. K. Carret, R. L. Cassidy-Cain, M. Roche-Molina, P. Tandon, N. Holmes, D. R. Alexander, The differential regulation of Lck kinase phosphorylation sites by CD45 is critical for T cell receptor signaling responses. *Immunity* **27**, 425–437 (2007).
41. M. Das, M. Ho, J. Zikherman, C. Govern, M. Yang, A. Weiss, A. K. Chakraborty, J. P. Roose, Digital signaling and hysteresis characterize ras activation in lymphoid cells. *Cell* **136**, 337–351 (2009).
42. W.-L. Lo, N. H. Shah, N. Ahsan, V. Horkova, O. Stepanek, A. R. Salomon, J. Kuriyan, A. Weiss, Lck promotes Zap70-dependent LAT phosphorylation by bridging Zap70 to LAT. *Nat. Immunol.* **19**, 733–741 (2018).
43. D. Zehn, S. Y. Lee, M. J. Bevan, Complete but curtailed T-cell response to very low-affinity antigen. *Nature* **458**, 211–214 (2009).
44. J. Huang, V. I. Zarnitsyna, B. Liu, L. J. Edwards, N. Jiang, B. D. Evavold, C. Zhu, The kinetics of two-dimensional TCR and pMHC interactions determine T-cell responsiveness. *Nature* **464**, 932–936 (2010).
45. L. V. Sibener, R. A. Fernandes, E. M. Kolawole, C. B. Carbone, F. Liu, D. McAffee, M. E. Birnbaum, X. Yang, L. F. Su, W. Yu, S. Dong, M. H. Gee, K. M. Jude, M. M. Davis, J. T. Groves, W. A. Goddard III, J. R. Heath, B. D. Evavold, R. D. Vale, K. C. Garcia, Isolation of a structural mechanism for uncoupling T cell receptor signaling from peptide-MHC binding. *Cell* **174**, 672–687.e27 (2018).
46. S. T. Kim, K. Takeuchi, Z.-Y. Sun, M. Touma, C. E. Castro, A. Fahmy, M. J. Lang, G. Wagner, E. L. Reinherz, The  $\alpha\beta$  T cell receptor is an anisotropic mechanosensor. *J. Biol. Chem.* **284**, 31028–31037 (2009).
47. Y. Feng, E. L. Reinherz, M. J. Lang,  $\alpha\beta$  T cell receptor Mechanosensing forces out serial engagement. *Trends Immunol.* **39**, 596–609 (2018).
48. B. Liu, W. Chen, B. D. Evavold, C. Zhu, Accumulation of dynamic catch bonds between TCR and agonist peptide-MHC triggers T cell signaling. *Cell* **157**, 357–368 (2014).
49. J. Hong, C. Ge, P. Jothikumar, Z. Yuan, B. Liu, K. Bai, K. Li, W. Rittase, M. Shinzawa, Y. Zhang, A. Palini, P. Love, X. Yu, K. Salaita, B. D. Evavold, A. Singer, C. Zhu, A TCR mechanotransduction signaling loop induces negative selection in the thymus. *Nat. Immunol.* **19**, 1379–1390 (2018).
50. T. W. McKeithan, Kinetic proofreading in T-cell receptor signal transduction. *Proc. Natl. Acad. Sci. U.S.A.* **92**, 5042–5046 (1995).
51. M. Lever, P. K. Maini, P. A. van der Merwe, O. Dushkek, Phenotypic models of T cell activation. *Nat. Rev. Immunol.* **14**, 619–629 (2014).
52. M. Lovatt, A. Filby, V. Parravicini, G. Werlen, E. Palmer, R. Zamoyska, Lck regulates the threshold of activation in primary T cells, while both Lck and Fyn contribute to the magnitude of the extracellular signal-related kinase response. *Mol. Cell. Biol.* **26**, 8655–8665 (2006).
53. S. C. Ley, M. Marsh, C. R. Bebbington, K. Proudfoot, P. Jordan, Distinct intracellular localization of Lck and Fyn protein tyrosine kinases in human T lymphocytes. *J. Cell Biol.* **125**, 639–649 (1994).
54. R. Zamoyska, A. Basson, A. Filby, G. Legname, M. Lovatt, B. Seddon, The influence of the src-family kinases, Lck and Fyn, on T cell differentiation, survival and activation. *Immunol. Rev.* **191**, 107–118 (2003).

55. Y. Bounab, A. Getahun, J. C. Cambier, M. Daéron, Phosphatase regulation of immunoreceptor signaling in T cells, B cells and mast cells. *Curr. Opin. Immunol.* **25**, 313–320 (2013).
56. R. J. Salmond, R. J. Brownlie, V. L. Morrison, R. Zamoyska, The tyrosine phosphatase PTPN22 discriminates weak self peptides from strong agonist TCR signals. *Nat. Immunol.* **15**, 875–883 (2014).
57. L. Simeoni, S. Kliche, J. Lindquist, B. Schraven, Adaptors and linkers in T and B cells. *Curr. Opin. Immunol.* **16**, 304–313 (2004).
58. L. M. Chow, M. Fournel, D. Davidson, A. Veillette, Negative regulation of T-cell receptor signalling by tyrosine protein kinase p50<sup>lck</sup>. *Nature* **365**, 156–160 (1993).
59. A. H. Courtney, J. F. Amacher, T. A. Kadlecik, M. N. Mollnauer, B. B. Au-Yeung, J. Kuriyan, A. Weiss, A phosphosite within the SH2 domain of Lck regulates its activation by CD45. *Mol. Cell.* **67**, 498–511.e6 (2017).
60. H. Sjölin-Goodfellow, M. P. Frushicheva, Q. Ji, D. A. Cheng, T. A. Kadlecik, A. J. Cantor, J. Kuriyan, A. K. Chakraborty, A. R. Salomon, A. Weiss, The catalytic activity of the kinase ZAP-70 mediates basal signaling and negative feedback of the T cell receptor pathway. *Sci. Signal.* **8**, ra49 (2015).
61. J. M. Conley, M. P. Gallagher, L. J. Berg, T cells and gene regulation: The switching on and turning up of genes after T cell receptor stimulation in CD8 T cells. *Front. Immunol.* **7**, 76 (2016).
62. R. Nayar, E. Schutten, B. Bautista, K. Daniels, A. L. Prince, M. Enos, M. A. Brehm, S. L. Swain, R. M. Welsh, L. J. Berg, Graded levels of IRF4 regulate CD8<sup>+</sup> T cell differentiation and expansion, but not attrition, in response to acute virus infection. *J. Immunol.* **192**, 5881–5893 (2014).
63. K. Man, M. Miasari, W. Shi, A. Xin, D. C. Henstridge, S. Preston, M. Pellegrini, G. T. Belz, G. K. Smyth, M. A. Febbraio, S. L. Nutt, A. Kallies, The transcription factor IRF4 is essential for TCR affinity-mediated metabolic programming and clonal expansion of T cells. *Nat. Immunol.* **14**, 1155–1165 (2013).
64. M. A. Al-Aghbar, Y.-S. Chu, B.-M. Chen, S. R. Roffler, High-affinity ligands can trigger T cell receptor signaling without CD45 segregation. *Front. Immunol.* **9**, 713 (2018).
65. S. Cemerski, J. Das, E. Giurisato, M. A. Markewicz, P. M. Allen, A. K. Chakraborty, A. S. Shaw, The balance between T cell receptor signaling and degradation at the center of the immunological synapse is determined by antigen quality. *Immunity* **29**, 414–422 (2008).
66. T. Yokosuka, K. Sakata-Sogawa, W. Kobayashi, M. Hiroshima, A. Hashimoto-Tane, M. Tokunaga, M. L. Dustin, T. Saito, Newly generated T cell receptor microclusters initiate and sustain T cell activation by recruitment of Zap70 and SLP-76. *Nat. Immunol.* **6**, 1253–1262 (2005).
67. J. Zikherman, R. Parameswaran, A. Weiss, Endogenous antigen tunes the responsiveness of naive B cells but not T cells. *Nature* **489**, 160–164 (2012).
68. B. B. Au-Yeung, G. A. Smith, J. L. Mueller, C. S. Heyn, R. G. Jaszczak, A. Weiss, J. Zikherman, IL-2 modulates the TCR signaling threshold for CD8 but not CD4 T cell proliferation on a single-cell level. *J. Immunol.* **198**, 2445–2456 (2017).

**Acknowledgments:** We thank the Shokat laboratory at UCSF for providing the 3-IB-PP1 compound, the Palmer laboratory at the University of Basel, and the NIH tetramer core for providing pMHC. We thank B. Au-Yeung and E. Jutkiewicz for providing feedback on the manuscript. Microscopy was conducted at the UCSF Nikon Imaging Center, and cell sorting was carried out using the flow cytometry core at UCSF. We thank A. Roque for assisting with animal husbandry. **Funding:** A.H.C. was supported by a Robertson Foundation/Cancer Research Institute fellowship. G.G. was supported by the doctoral training program GRK1660 from the German Research Foundation (DFG). This work was supported, in part, by the Howard Hughes Medical Institute, the NIH, NIAID PO1 AI091580 (A.W. and A.K.C.), and the Czech Science Foundation, 16-09208Y (O.S.). **Author contributions:** A.H.C., A.A.S., W.L., A.K.C., and A.W. contributed to experimental design. A.H.C., W.L., and G.G. carried out experiments. A.A.S. and A.K.C. developed computational models. V.H. and O.S. developed the J.OT1 cell line. W.-L.L. contributed reagents. M.M. and S.Y. provided technical assistance. The manuscript was written and edited by A.H.C., A.A.S., A.K.C., and A.W. All authors reviewed the manuscript.

**Competing interests:** The authors declare that they have no competing interests. **Data and materials availability:** All data needed to evaluate the conclusions in the paper are present in the paper or the Supplementary Materials.

Submitted 29 January 2019

Accepted 6 September 2019

Published 22 October 2019

10.1126/scisignal.aaw8151

**Citation:** A. H. Courtney, A. A. Shvets, W. Lu, G. Griffante, M. Mollnauer, V. Horkova, W.-L. Lo, S. Yu, O. Stepanek, A. K. Chakraborty, A. Weiss, CD45 functions as a signaling gatekeeper in T cells. *Sci. Signal.* **12**, eaaw8151 (2019).

## Supplementary Materials for

### CD45 functions as a signaling gatekeeper in T cells

Adam H. Courtney\*, Alexey A. Shvets, Wen Lu, Gloria Griffante, Marianne Mollenauer, Veronika Horkova, Wan-Lin Lo, Steven Yu, Ondrej Stepanek, Arup K. Chakraborty, Arthur Weiss\*

\*Corresponding author. Email: aweiss@medicine.ucsf.edu (A.W.); adamhc@umich.edu (A.H.C.)

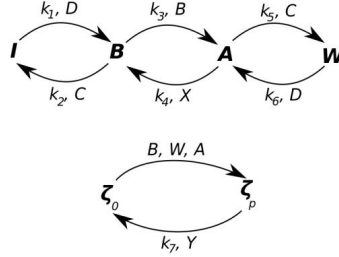
Published 22 October 2019, *Sci. Signal.* **12**, eaaw8151 (2019)  
DOI: 10.1126/scisignal.aaw8151

#### This PDF file includes:

Text S1. Details of the computational model.  
Fig. S1. Csk analog-sensitive Jurkat T cell characterization.  
Fig. S2. Effects of Csk inhibition on CD45-deficient Jurkat T cells.  
Fig. S3. FACS analysis of Csk inhibition.  
Fig. S4. CD45-low (LL) mice have increased memory CD8<sup>+</sup> T cells and lower TCR levels.  
Fig. S5. OT1 Jurkat T cells.  
Fig. S6. Contact area is influenced by antigen affinity and CD45.  
Fig. S7. FACS analysis of J.OT1/CD45 cells.  
Table S1. Antibodies.

## Text S1. Details of the computational model.

### *Lck activation*



*Schematic diagram of the reaction network used in the model (same as Fig 3C in main text).*

The above is a minimal network model consisting of phosphoforms of *Lck* and their regulation by *Csk*, *CD45* and two other phosphatases *X* and *Y*. We explored various possibilities for the identities of *X* and *Y*, including whether they were actually *CD45*. In this figure, A, B, I and W corresponds to *Lck* in its active (pY394/Y505), basal (Y394/Y505), inactive (Y394/pY505) and doubly phosphorylated state (pY394/pY505); D is *CD45* and C is *Csk*. The rate constants for each reaction is shown above the arrows.

The following system of differential equations describe the biochemical network in the figure.

$$\begin{aligned}\frac{\partial I}{\partial t} &= -k_1 I D + k_2 B C \\ \frac{\partial A}{\partial t} &= k_3 B^2 - k_4 A X - k_5 A C + k_6 D W \\ \frac{\partial W}{\partial t} &= k_5 A C - k_6 D W \\ \frac{\partial \xi_p}{\partial t} &= (k_a A + k_b B + k_w W) \xi_0 - k_7 \xi_p Y \\ \frac{\partial B}{\partial t} &= k_1 I D - k_2 C\end{aligned}$$

where  $C \equiv Csk$  and  $D \equiv CD45$ . Denoting the total *Lck* concentration as  $L = I + A + B + W$ , the total ITAM (Y142) concentration as  $\xi = \xi_0 + \xi_p$ ,  $k_D = k_1/k_2$ ,  $k_X = k_4/k_3$ ,  $k_C = k_5/k_6$  and  $k_A = k_7/k_7$  ( $k_B = k_b/k_7$ ,  $k_W = k_w/k_7$ ), we can obtain the steady state concentrations of various species by solving the following algebraic equations:

$$\begin{aligned}k_D I D - (L - A - I - W) &= 0 \\ k_C A C - D W &= 0 \\ k_X A X - (L - A - I - W)^2 &= 0 \\ \xi_p Y - (k_A A + k_B B + k_W W) \xi_0 &= 0\end{aligned}$$

The solution of the system of steady state equations is:

$$A = \frac{1}{2(1+k_C C/D)^2} (P - (1 + C/k_D D)^2 \sqrt{k_X X} \sqrt{P + 2L(1 + k_C C/D)^2})$$

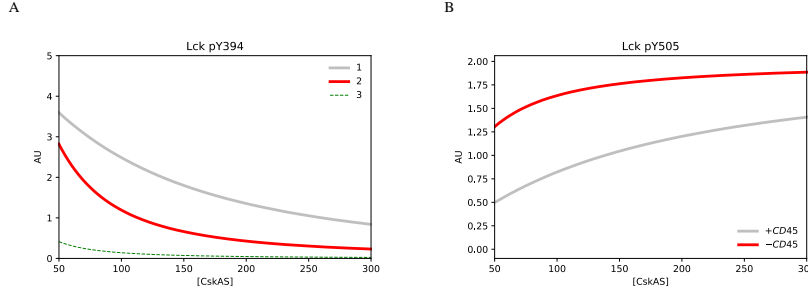
for the active *Lck*, where we denote

$$P \equiv 2L(1 + k_c C/D) + (1 + C/k_D D)^2 X$$

and

$$I = \frac{(L - (1 + k_c C/D)A)C}{C + k_D D}$$

for inactive Lck.



Changes in Lck phosphorylation and activation. The dependence of active Lck (pTyr<sup>394</sup>) on Csk concentration in the presence or absence of CD45 (A; same as shown in main text, Fig 3D), and the corresponding decrease in Lck C-terminal tail phosphorylation (B; pTyr<sup>505</sup>).

In the above model, we consider the following cases: 1) WT case or CD45-sufficient/X-sufficient (gray line); 2) CD45-deficient/X-deficient (red line); 3) CD45-deficient/X sufficient case (dashed green line). Total amount of Lck is  $L=100$  molecules. We also divided active Lck concentration by 7 to make the same scale as experimental data. Our model recapitulates the experimental changes in Lck activity that occur in the presence or absence of CD45. We used unknown phosphatases (X & Y) in our model to explore the contributions of poorly defined phosphatase activities that could be attributed to CD45 or another phosphatase.

We consider the rates at which CD45 dephosphorylates Tyr<sup>505</sup> and Tyr<sup>394</sup> residues to be equal and  $k_C < 0.05$  (i.e.  $k_5 < 0.05k_6$ , the unknown parameters pertinent to Lck activation are incorporated in the range of concentrations of Csk and CD45 in the cells). Moreover, we consider the activity of Lck acting on its substrate, the  $\zeta$ -chain, to be in the range of  $0 < k_B/k_A = k_W/k_A < 0.5$  based on results obtained by Hui and Vale, 2014.

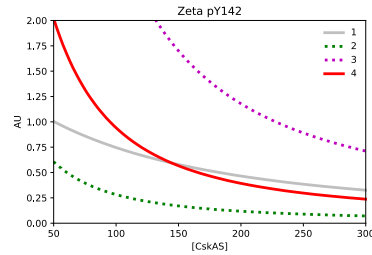
We qualitatively recapitulate our experimental findings by using a maximum Csk level of 300 molecules and a minimum amount (at the highest inhibitor concentration) to be 50 molecules (Fig 2A). Similarly, CD45 levels were set to 100 molecules for CD45 sufficient cells and 10 molecules in CD45-deficient cells. Importantly, the CD45 level in CD45-deficient cells may be considered a proxy for trace amounts of CD45 (or another similar phosphatase) or other phosphatases that weakly act on Lck. We first carried out calculations without inclusion of the doubly phosphorylated form of Lck (W), and found a range of parameters that recapitulated the basic experimental data. We then included W, and found that a low rate of formation of this species did not change the qualitative behavior. This is supported also by the qualitative arguments reported in the main text regarding the results for  $\zeta$  chain phosphorylation (next figure, below) and whether or not CD45 is the only phosphatase that acts on  $\zeta$ . Therefore, we have not carried out an extensive parameter search that includes varying the parameters pertinent to W along with all others.

Within our model, we found CD45-deficient cells to have lower amounts of active Lck at all levels of Csk inhibition because under these conditions the positive role of CD45 (Lck activation) becomes dominant. The model also reproduces the expected observed behavior regarding the phosphorylation state of Tyr<sup>505</sup> (panel B in the above figure). Because the Csk and CD45 levels noted above recapitulate our experimental findings, they were used to explore models for regulation of  $\zeta$  chain phosphorylation. We also emphasize that the goal of our



modeling studies is not the quantitative recapitulation of data, but to obtain mechanistic insight from qualitative trends.

#### $\zeta$ -chain phosphorylation



The influence of Csk activity on  $\zeta$ -chain phosphorylation in the presence or absence of CD45.

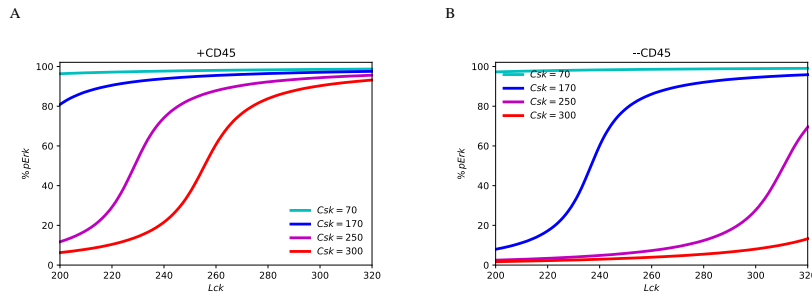
Our model considers the following cases (depicted in the figure above): 1) WT case (gray line); 2) *CD45*-deficient and only *Y* acts on  $\zeta$  chain (dashed green line); 3) *CD45* deficient and only *CD45* acts on  $\zeta$  chain (dashed magenta line); 4)  $\zeta$  chain is deactivated by *CD45* as well as by other undefined phosphatase *Y* (red line). Total amount of Lck is  $L=100$  molecules and *ITAMs*  $\zeta=100$  molecules.  $\zeta$  chain concentration and the axis was rescaled for comparison with experimental data. Our model assesses  $\zeta$  chain phosphorylation (Tyr<sup>142</sup>) by Lck where we consider three different models for the phosphatase that acts on Y142 of  $\zeta$ . We consider the scenarios where: CD45 is the only phosphatase that acts on  $\zeta$ , or another phosphatase, *Y*, is the only one that acts on  $\zeta$ , or CD45 and *Y* both act on  $\zeta$ . As before, for CD45-sufficient and deficient cells, there are 100 and 10 molecules of CD45, respectively. In the case wherein both *CD45* and *Y* can deactivate the  $\zeta$  chain, for the results shown in the above figure, we take the ratio of the activity of CD45 ( $k_{\text{D}}$ ) acting on  $\zeta$  and the activity of *Y* acting on  $\zeta$  in CD45-sufficient cells to be 2.33.

Using our model, we found that if the only phosphatase that acts on the  $\zeta$  chain is CD45, then active  $\zeta$  chain levels are predicted to be higher at all Csk levels for *CD45*-deficient cells, compared to CD45-sufficient cells. In this case, the two negative regulatory roles for CD45 (acting on Lck and  $\zeta$ ) dominate. If  $\zeta$  is not a substrate for CD45 (only *Y* acts on  $\zeta$ ), then active  $\zeta$  chain levels are predicted to be lower at all Csk levels for CD45-deficient cells, compared to CD45-sufficient cells. This is because CD45's positive regulatory role, which initiates Lck activity is dominant. Only in the case where CD45 and another phosphatase both act on  $\zeta$ , do the computational results mirror the experimental finding that active  $\zeta$  levels are lower at high Csk levels and higher at low Csk levels for CD45-deficient cells, compared to CD45-sufficient cells. The reason for this can be understood as follows: at high Csk levels, there is only a small amount of active Lck, and so there is only a small amount of active  $\zeta$ . Therefore, the phosphatase, *Y*, is sufficient for suppressing  $\zeta$  phosphorylation. Therefore, as in the model where  $\zeta$  is not a substrate for CD45, the positive regulatory role of CD45 is dominant. At low Csk levels, as Lck activity increases,  $\zeta$  chain phosphorylation is also increased. Therefore, both *Y* and CD45 are important for negative regulation of  $\zeta$  phosphorylation (meaning, *Y* is not sufficient).

#### ERK activation

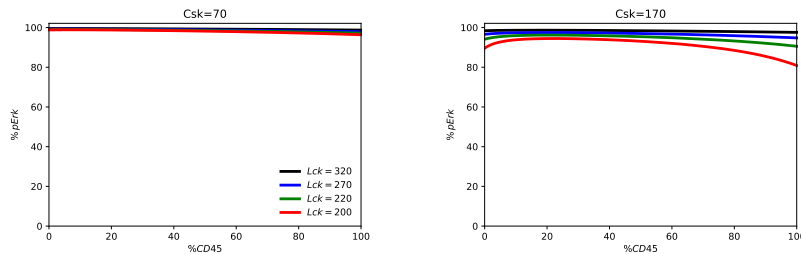
Our experimental findings show that cells are less responsive to stimuli in the absence of CD45 (consistent with the loss of CD45 causing a defect in TCR signaling). The decreased sensitivity to stimuli in the absence of CD45, reflects the importance of the positive regulatory role of CD45 at high levels of Csk activity. To explore these behaviors further, we coupled our model of Lck and  $\zeta$  chain activation (described above) with a simplified model for ERK activation.

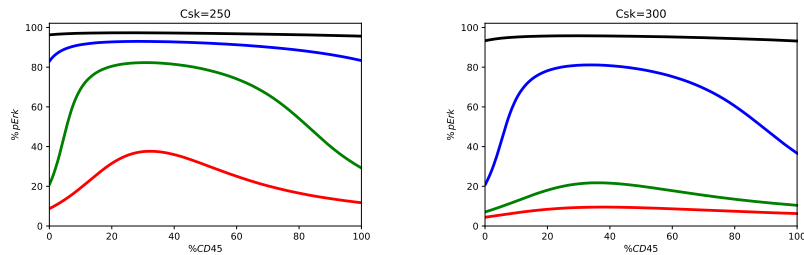
In T cells, Lck phosphorylates the TCR complex, which includes the  $\zeta$  chain, resulting in the recruitment of Zap70. Zap70 is also phosphorylated by Lck which activates it to phosphorylate the critical adapter protein LAT on several tyrosine sites. Once phosphorylated, LAT assembles a signaling complex which includes: PLC $\gamma$ 1, Gads, SLP76, ITK, Vav, and a complex consisting of Grb2 and SOS. Both RasGRP and SOS activate Ras. Previously, we have shown that, because of a positive feedback loop in SOS-catalyzed Ras activation, Ras activation is digital; i.e., the cellular response is bimodal in Ras activity with some cells showing high Ras activity and others not. For population-level measurements that do not resolve single cells, this results in a sharp increase in active Ras levels above a threshold value of SOS recruited to the membrane. Because the experimental results reported in this paper measure only population level responses, we use such a sharp function to define the dependence of Ras activity on SOS (41).



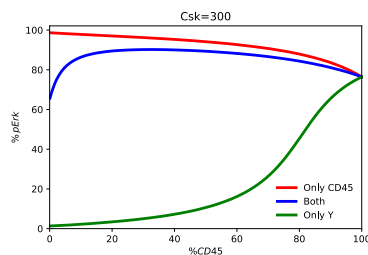
The proportion of phospho-ERK positive cells as a function of total Lck for different values of Csk in CD45-sufficient (A) and CD45-deficient (B) cells. Graphs depict four different levels of Csk which corresponds to different levels of inhibitor in our experimental results.

Active Ras engages the MAPK pathway to activate ERK. As in our past work, which was validated experimentally, we take Ras activity to be a proxy for active ERK. In this study, because our purpose was to see whether the upstream model for regulation of Lck and  $\zeta$  is consistent with the results for ERK activation, we considered a linear relationship between active  $\zeta$  chains and active SOS levels. We found that this simple ansatz recapitulates the experimental observations for ERK activation. We also used the total amount of Lck activity to be a proxy for stimulation level. Experimentally CD45 is necessary for cells to respond to TCR stimuli. Our calculations show that the reason that CD45-sufficient cells are more sensitive at low levels of stimuli and high Csk levels is the positive regulatory role of CD45 in Lck activation. Lack of CD45 results in low levels of basally active Lck, and this effect propagates through the system.



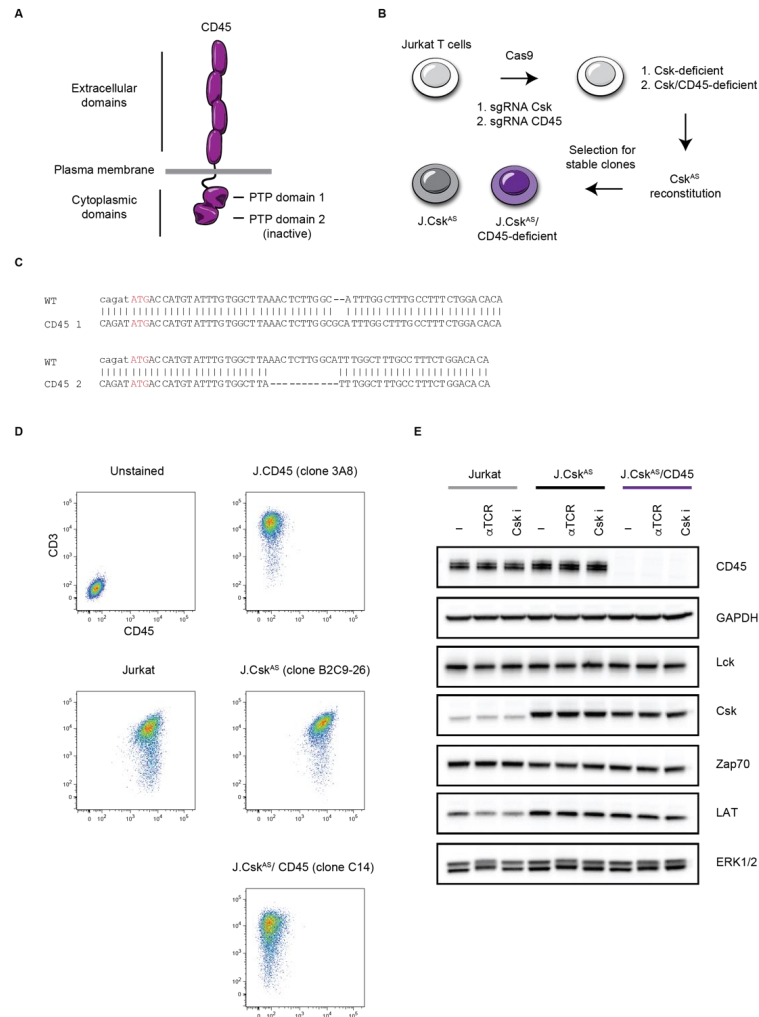


*Predictions for the influence of CD45 concentration on the proportion of phospho-ERK positive cells for concentrations of stimulus and Csk inhibitor.*

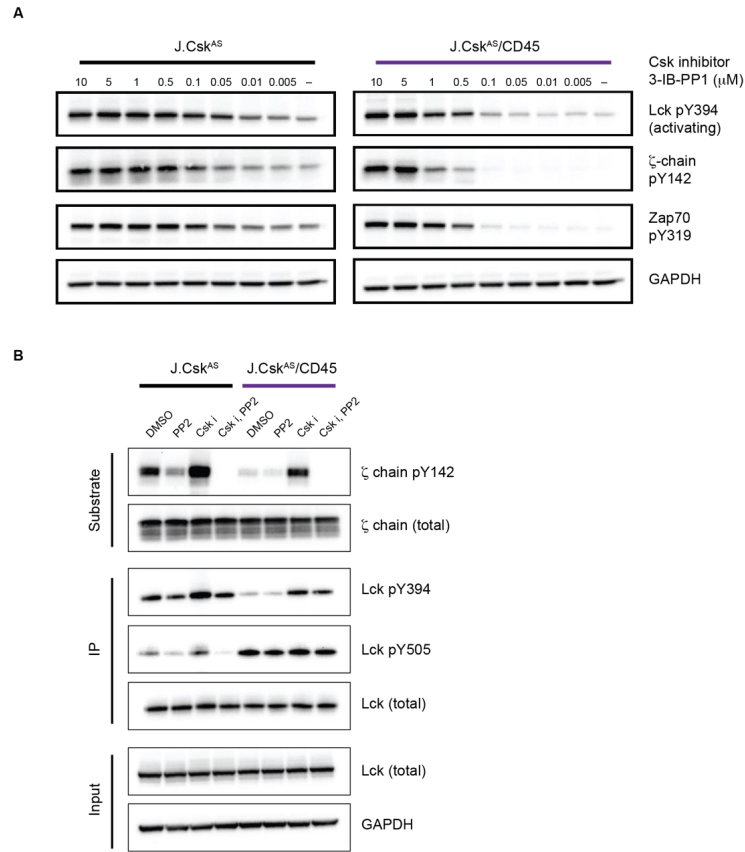


*Predictions for the influence of CD45 concentration on the proportion of phospho-ERK positive cells where we explore only CD45 acting on the  $\zeta$ -chain (red line); only undefined phosphatase acting on  $\zeta$ -chain (green line); both, CD45 and undefined phosphatase acting on  $\zeta$ -chain. The total amount of Lck = 270 molecules.*

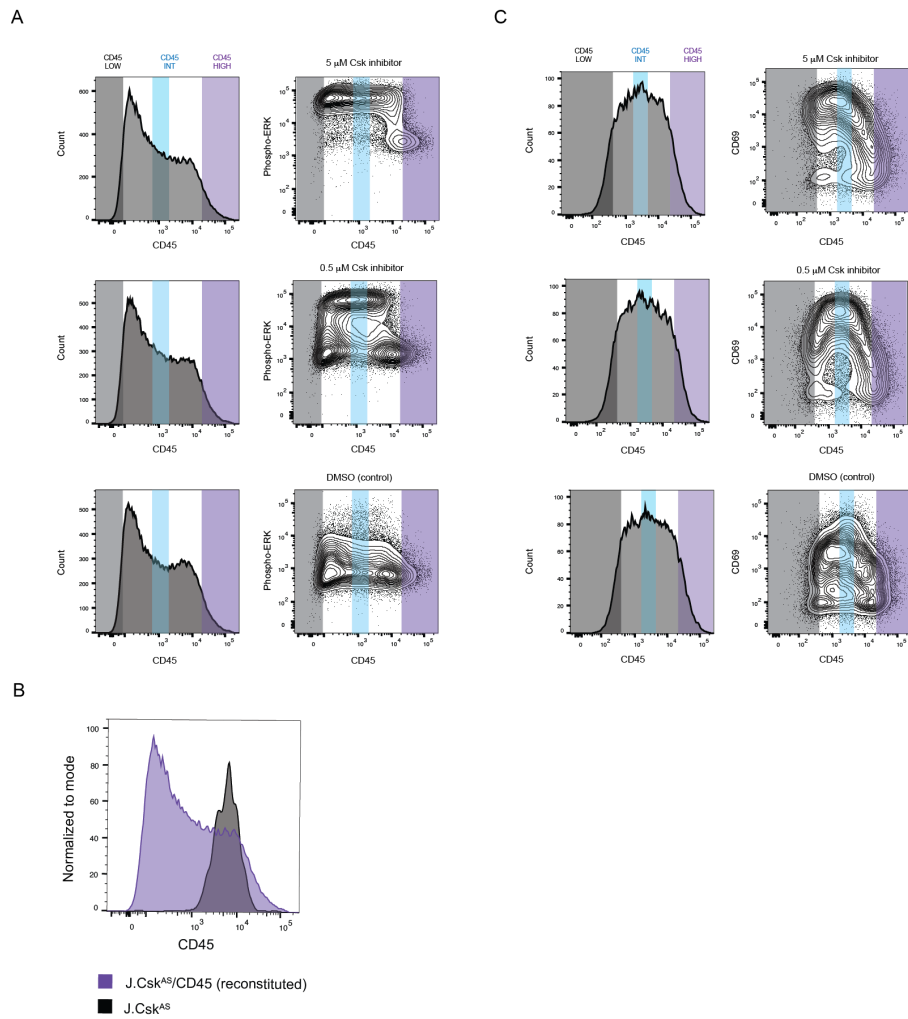
Notably, our model predicts that the non-monotonic dependence of ERK activation on CD45 would not occur if CD45 was the only phosphatase acting on  $\zeta$  or, if it did, not act on it at all (depicted above). This occurs because if CD45 is the only phosphatase that acts on the  $\zeta$ -chain, then active  $\zeta$  chain levels are higher at all Csk levels for CD45-deficient cells, compared to CD45-sufficient cells. Similar to the situation in the second figure above, the negative regulatory roles of CD45 (acting on Lck and  $\zeta$ ) dominate over its one positive regulatory role (activating Lck). This trend holds at all CD45 levels, not just for CD45-sufficient and deficient cells. If  $\zeta$  is not a substrate for CD45 (only Y acts on  $\zeta$ ), then active  $\zeta$  chain levels are lower at all Csk levels for CD45-deficient cells, compared to CD45-sufficient cells. This occurs because the positive regulatory role of CD45 (Lck activation) is dominant. Only in the case where CD45 and another phosphatase act on  $\zeta$ , is there a shift between the relative dominance of the positive and negative regulatory roles of CD45 at low and high CD45 levels.



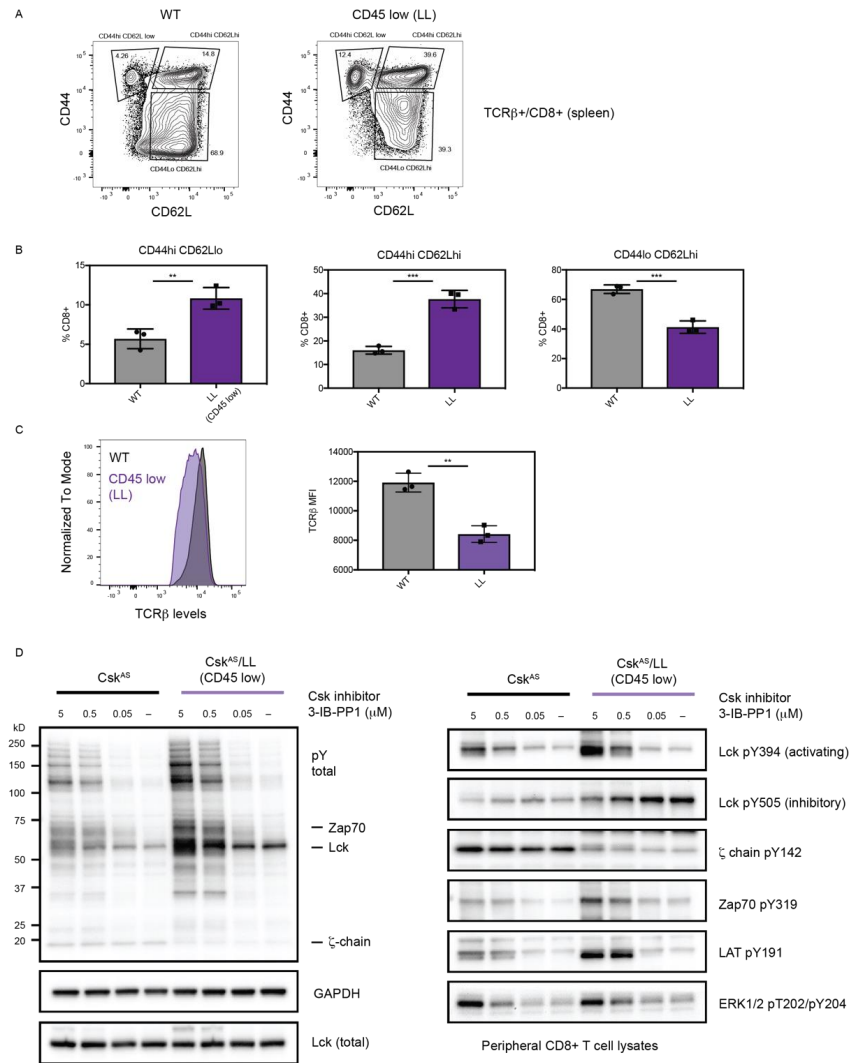
**Fig. S1. Csk analog-sensitive Jurkat T cell characterization.** (A) Diagram depicting the protein tyrosine phosphatase CD45. (B) Csk-deficient Jurkat T cells were generated using CRISPR/Cas9. Csk/CD45 doubly deficient cells were similarly generated. Cells were reconstituted with a previously described Csk analog-sensitive allele (Csk<sup>AS</sup>). (C) Sequence of CD45-deficient (J.Csk<sup>AS</sup>/CD45) genomic DNA targeted using CRISPR/Cas9. Start codon is showing in red. (D) Cells were characterized by flow cytometry to assess surface expression of CD45 and CD3. (E) Expression of important TCR signaling proteins were assessed by immunoblot. Data are representative of three independent experiments.



**Fig. S2. Effects of Csk inhibition on CD45-deficient Jurkat T cells. (A)** Phosphorylation of specific regulatory sites was assessed over an extended range of Csk inhibitor concentrations. Data are representative of three independent experiments. **(B)** Cells were treated with control (DMSO), PP2 (25 μM), or Csk inhibitor (5 μM – denoted Csk i) for 1 minute. Lck was immunoprecipitated and an in vitro kinase assay performed using recombinant GST CD3 ζ as a substrate. To assess the extent of on-bead autophosphorylation that occurs following immunoprecipitation a control was performed (Csk i, PP2). For ‘Csk i, PP2 control’, cells were first treated with Csk inhibitor and IP was performed. Subsequently, PP2 (50 μM) was added to the kinase reaction to inhibit Lck autophosphorylation (and also substrate phosphorylation) in the 4th and 8th lanes from the left. Phosphorylation was assessed by immunoblot. Data are representative of two independent experiments.

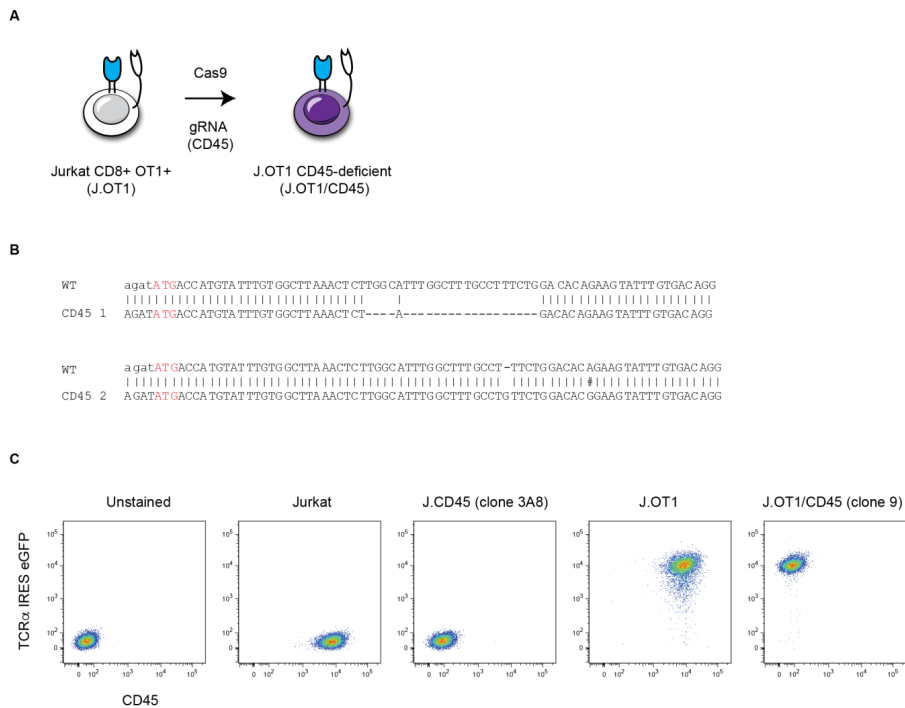


**Fig. S3. FACS analysis of Csk inhibition.** (A) Representative FACS plots depicting CD45 reconstitution and ERK phosphorylation in response to Csk inhibition for 2 min. (B) Histogram showing CD45 staining of J.Csk<sup>AS</sup> cells and reconstituted J.Csk<sup>AS</sup>/CD45 cells. (C) Representative FACS plots depicting CD45 reconstitution and CD69 upregulation in response to Csk inhibition for 16 hours. Data are representative of three independent experiments.



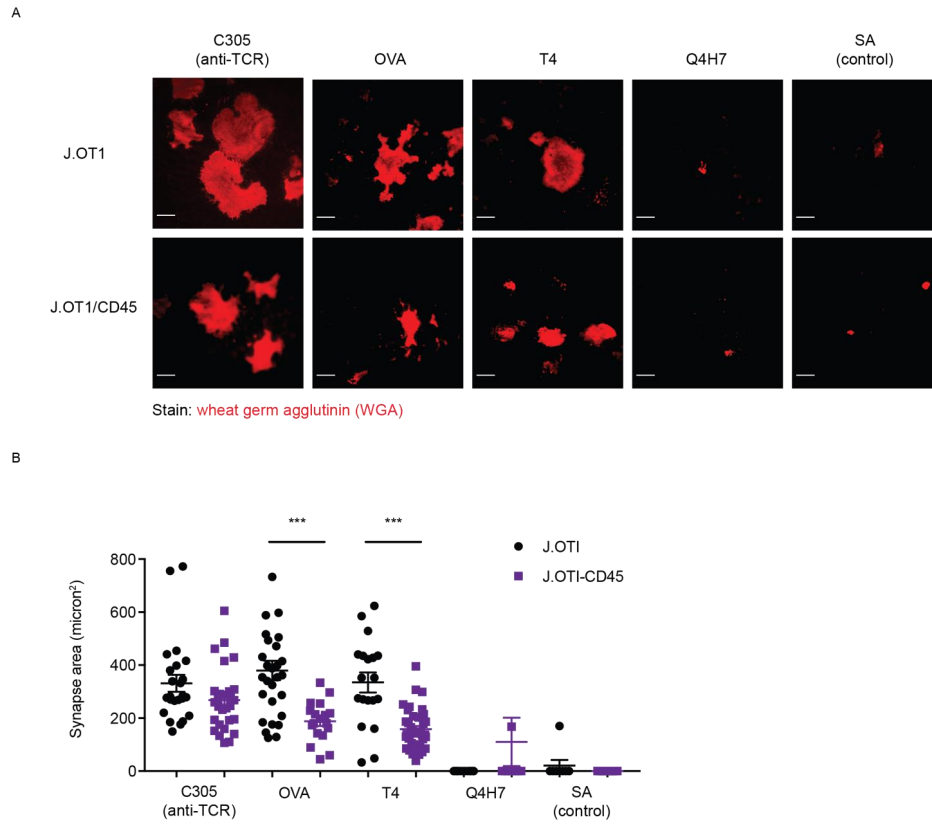
**Fig. S4. CD45-low (LL) mice have increased memory CD8<sup>+</sup> T cells and lower TCR levels. (A)** FACs analysis of CD8<sup>+</sup> T cells isolated from the spleen. **(B)** Quantification of CD8<sup>+</sup> T cell populations (CD44<sup>hi</sup>/CD62L<sup>lo</sup>, CD44<sup>hi</sup>/CD62L<sup>hi</sup>, CD44<sup>lo</sup>/CD62L<sup>hi</sup>). **(C)** Histogram of TCR $\beta$  staining of total

splenic CD8<sup>+</sup> T cells (left), and quantification of TCR $\beta$  staining (right). Error bars represent the means  $\pm$  SD for N=3 mice, \*\* denotes  $p < 0.01$ , \*\*\* denotes  $p < 0.001$ . The unpaired Student's  $t$  test was used to calculate  $p$  values. **(D)** Peripheral CD8<sup>+</sup> T cells were isolated from the indicated mice and treated with differing doses of Csk inhibitor for 2 minutes. Total protein tyrosine phosphorylation was assessed by immunoblot, the molecular weights (MW) of specific proteins are denoted. Phosphorylation of specific regulatory sites was assessed with phosphor-site specific antibodies as a readout of their activation status. Immunoblot data are representative of three independent experiments.



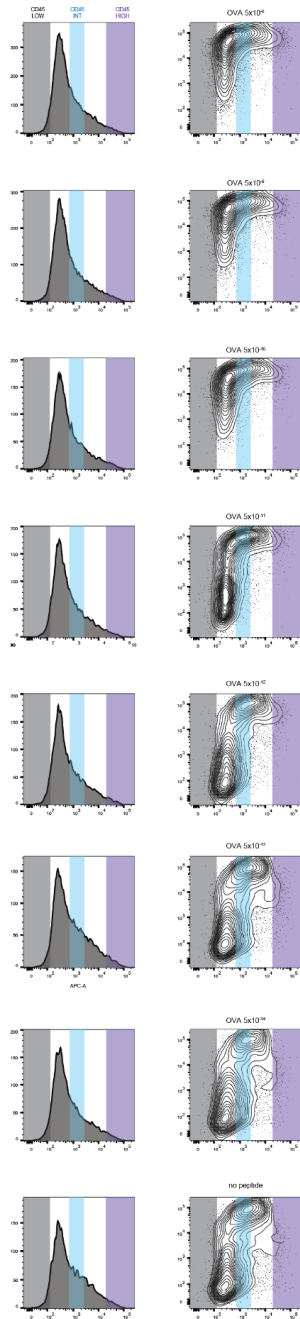
**Fig. S5. OT1 Jurkat T cells.** **(A)** Jurkat T cells which stably express the OT-1 TCR and CD8 coreceptor have been previously described. CD45-deficient Jurkat OT-1<sup>+</sup> CD8<sup>+</sup> cells were generated using CRISPR/CAS9. **(B)** Sequence of CD45-deficient (J.OT1/CD45) genomic DNA. Start codon is showing in red. **(C)** Expression of the OT-1 TCR was assessed by GFP expression and CD45 levels assessed by surface staining. Data are representative of three independent experiments.



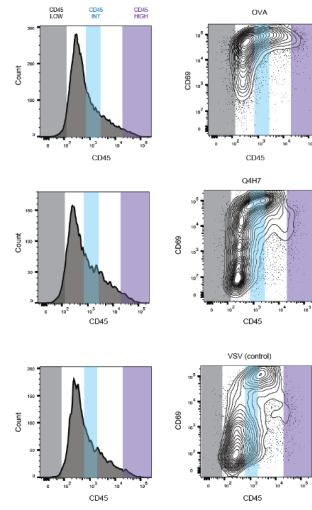


**Fig. S6. Contact area is influenced by antigen affinity and CD45.** (A) J.OT1 and J.OT1/CD45 (CD45 deficient) cells were stimulated for 30 mins at 37 °C using surfaces coated with stimulatory anti-TCR antibody (C305), or surfaces coated with streptavidin followed by biotinylated monomeric pMHC (OVA, T4, Q4H7), or streptavidin alone (SA). Cell membranes were stained with wheat germ agglutinin (WGA). Contact areas of cells with the stimulatory surface were imaged by the TIRF microscopy. Scale bar represents 10  $\mu$ M. (B) Contact areas for each condition were quantified. Each data point represents a unique cell. Error bars represent the means  $\pm$  SEM for  $N \geq 8$  cells, NS denotes  $P \geq 0.05$  and \*\*\*  $p < 0.0001$ . The Mann-Whitney test was used to calculate  $P$  values.

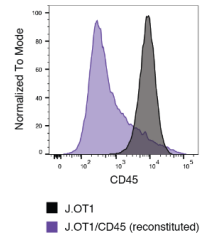
A



B



C



**Fig. S7. FACS analysis of J.O1/CD45 cells.** (A) Representative FACS plots depicting CD45 reconstitution and CD69 upregulation. J.O1 cells were cultured with T2-Kb cells and serial dilutions of OVA peptide for 16 hours. (B) Representative FACS plots depicting CD45 reconstitution and CD69 upregulation in response to coculture with OVA, Q4H7 and VSV peptides (5 nM) and T2Kb cells for 16 hours. (C) Histogram showing CD45 staining of J.O1 cells and reconstituted J.O1/CD45 cells. Data are representative of three independent experiments.



## **Attachment 7**

Slow Phosphorylation of a Tyrosine Residue  
in LAT Optimizes T cell Ligand  
Discrimination

# Slow phosphorylation of a tyrosine residue in LAT optimizes T cell ligand discrimination

Wan-Lin Lo<sup>1</sup>, Neel H. Shah<sup>2,10</sup>, Sara A. Rubin<sup>3,4</sup>, Weiguo Zhang<sup>5</sup>, Veronika Horkova<sup>6</sup>, Ian R. Fallahee<sup>2</sup>, Ondrej Stepanek<sup>6</sup>, Leonard I. Zon<sup>3,4,7</sup>, John Kuriyan<sup>2,8</sup> and Arthur Weiss<sup>1,9\*</sup>

**Self-non-self discrimination is central to T cell-mediated immunity. The kinetic proofreading model can explain T cell antigen receptor (TCR) ligand discrimination; however, the rate-limiting steps have not been identified. Here, we show that tyrosine phosphorylation of the T cell adapter protein LAT at position Y132 is a critical kinetic bottleneck for ligand discrimination. LAT phosphorylation at Y132, mediated by the kinase ZAP-70, leads to the recruitment and activation of phospholipase C- $\gamma$ 1 (PLC- $\gamma$ 1), an important effector molecule for T cell activation. The slow phosphorylation of Y132, relative to other phosphosites on LAT, is governed by a preceding glycine residue (G131) but can be accelerated by substituting this glycine with aspartate or glutamate. Acceleration of Y132 phosphorylation increases the speed and magnitude of PLC- $\gamma$ 1 activation and enhances T cell sensitivity to weaker stimuli, including weak agonists and self-peptides. These observations suggest that the slow phosphorylation of Y132 acts as a proofreading step to facilitate T cell ligand discrimination.**

T cell responses, mediated by T cell antigen receptors (TCRs), are remarkable for their high sensitivity, exquisite specificity, and rapidity<sup>1</sup>. T cells can be activated in response to very few foreign peptide major histocompatibility complex (pMHC) ligands (one to ten)<sup>2–4</sup>, with a small error rate ( $10^{-4}$  to  $10^{-6}$ )<sup>5,6</sup> and rapid response time (seconds to a few minutes)<sup>7</sup>. This rapid and highly accurate responsiveness allows T cells to detect peptides derived from foreign pathogens or abnormal cells early and efficiently without reacting to self-tissues. Several factors have been proposed to affect T cell discrimination and correlate with responsiveness, including subtle differences in TCR–pMHC off-rates, on-rates, affinities, and catch-bond formation. However, differences in these factors for agonist and non-agonist ligands are not always sufficient to explain the actual T cell error rate<sup>8,9</sup>.

The remarkable selectivity of T cells may be explained by a kinetic proofreading model<sup>3,6</sup>. Following ligand binding, TCR proximal signaling molecules undergo a series of biochemical reactions, such as phosphorylation, and these multiple steps create a time delay between the input signal (pMHC recognition) and the output response (T cell activation)<sup>6</sup>. If these signaling steps are rapidly reversible following removal of the stimulus (for example, through dephosphorylation by phosphatases), the TCR–pMHC interaction would have to persist for a sufficient duration to initiate successful activation. By this mechanism, small differences in TCR–pMHC affinities or off-rates could lead to vastly different cellular outcomes, with each signaling step functioning as a ‘proofreader’ to allow only a bona fide activation signal to propagate downstream. Thus far, most efforts to assess the importance of kinetic proofreading in TCR signaling have been restricted to biochemical or mathematical models, and have failed to account for the role of

endogenous self-peptides and changes in ligand discrimination during development<sup>1,10,11</sup>.

LAT (the linker for activation of T cells) is an important scaffold that coordinates TCR proximal signals in a phosphorylation-dependent manner following receptor stimulation<sup>12,13</sup>. Although there are several phosphorylation sites in LAT that have a role in signal transduction, Y132 is the only residue in LAT that recruits phospholipase C- $\gamma$ 1 (PLC- $\gamma$ 1) following its phosphorylation by ZAP-70. Binding of PLC- $\gamma$ 1 to phosphorylated Y132 (p-Y132) in LAT leads to the Tec family kinase ITK-mediated PLC- $\gamma$ 1 phosphorylation and activation<sup>14</sup>. This activation of PLC- $\gamma$ 1 ultimately leads to calcium mobilization, ERK and protein kinase C (PKC) activation, and eventually cellular effector and transcriptional responses<sup>12</sup>. Interestingly, despite the importance of LAT p-Y132, the presence of a glycine at position 131 in LAT makes Y132 a particularly poor substrate for ZAP-70 because the kinase domain of ZAP-70 strongly favors an acidic residue (aspartate or glutamate) at the –1 position relative to substrate tyrosine residues<sup>15</sup>.

Here, we show that substitution of the glycine residue at the –1 position with aspartate or glutamate markedly increases the phosphorylation rate of LAT Y132 in T cells. This focused amino acid substitution in a signaling scaffold protein is sufficient to enhance T cell responsiveness to weak antigens or self-peptides. We demonstrate that slow phosphorylation of Y132 in LAT serves as an essential rate-limiting step in TCR signaling to enable ligand discrimination. Although a glycine at position 131 in LAT is highly conserved in tetrapods, some fish have other residues preceding the homologous tyrosine residue, including aspartate and glutamate, that are more optimal for phosphorylation by ZAP-70. Our results suggest that the slow phosphorylation of LAT Y132 is an important

<sup>1</sup>Division of Rheumatology, Rosalind Russell and Ephraim P. Engleman Arthritis Research Center, Department of Medicine, University of California, San Francisco, San Francisco, CA, USA. <sup>2</sup>Department of Molecular and Cell Biology, University of California, Berkeley, Berkeley, CA, USA. <sup>3</sup>Harvard Stem Cell Institute, Harvard University, Cambridge, MA, USA. <sup>4</sup>Stem Cell Program and Division of Hematology/Oncology, Boston Children’s Hospital and Dana-Farber Cancer Institute; Program in Immunology, Harvard Medical School, Boston, MA, USA. <sup>5</sup>Department of Immunology, Duke University Medical Center, Durham, NC, USA. <sup>6</sup>Institute of Molecular Genetics of the Czech Academy of Sciences, Prague, Czech Republic. <sup>7</sup>Howard Hughes Medical Institute, Boston Children’s Hospital and Harvard University, Boston, MA, USA. <sup>8</sup>Howard Hughes Medical Institute, University of California, Berkeley, Berkeley, CA, USA. <sup>9</sup>Howard Hughes Medical Institute, University of California, San Francisco, San Francisco, CA, USA. <sup>10</sup>Present address: Department of Chemistry, Columbia University, New York, NY, USA. \*e-mail: [art.weiss@ucsf.edu](mailto:art.weiss@ucsf.edu)

regulatory mechanism that contributes to T cell ligand discrimination in most jawed vertebrates and might underlie the remarkable selectivity of T cells.

## Results

**Mammalian LAT Y132 has a glycine at the –1 position, unlike other ZAP-70 substrates.** LAT and SLP-76 are two adaptors in T cells that rely on their phosphorylation by ZAP-70 to link initial TCR signals to many downstream cellular events required for full T cell activation (Fig. 1a)<sup>15</sup>. ZAP-70 has a strong preference for its substrate tyrosine residues to be surrounded by acidic residues (that is, aspartate and glutamate)<sup>15,16</sup>. These acidic residues facilitate substrate interaction with the ZAP-70 kinase domain, which is rich in basic residues in the substrate-binding region<sup>15</sup>.

The marked preference for aspartate and glutamate at the –1 position in ZAP-70 substrates is reflected in almost all reported substrates of human ZAP-70, except for the Y132 residue in LAT (Fig. 1b). Human LAT Y132 has an unusually placed, small neutral glycine residue (G131) at the –1 position (Fig. 1b), making Y132 a potentially poor substrate for ZAP-70. In support of this view, Y132 phosphorylation is delayed compared to that of the distal tyrosines on LAT and is coincident with PLC- $\gamma$ 1 phosphorylation<sup>17</sup>. This uniquely positioned glycine preceding LAT Y132 was observed at the homologous position in virtually all 68 mammalian species examined (Fig. 1c). Consistent with the distinct sequence features of the Y132 phosphosite, *in vitro* phosphorylation assays with the ZAP-70 kinase domain and the cytoplasmic region of LAT showed that LAT Y132 was phosphorylated by ZAP-70 with substantially slowed kinetics relative to the rate of total tyrosine phosphorylation in LAT (Fig. 1d). Of note, mutation of Y127 to phenylalanine did not affect phosphorylation of Y132 in the *in vitro* kinase assay, suggesting that this nearby site of phosphorylation does not have a priming effect.

To extend this analysis to cells, we used Csk-deficient Jurkat cells reconstituted with a PPI analog-sensitive Csk mutant (J.CskAS), to rapidly activate Lck by inhibiting Csk-dependent phosphorylation of an inhibitory tyrosine in Lck (data not shown)<sup>18</sup>. Activated Lck could then phosphorylate TCR ITAMs and ZAP-70, allowing ZAP-70 to initiate its kinase activities in its native cellular environment without triggering the TCR. Such treatment showed slower tyrosine phosphorylation of Y132 than of Y171, and the phosphorylation of PLC- $\gamma$ 1 exhibited similar time-dependent phosphorylation to Y132 (Supplementary Fig. 1a,b).

Scanning mutagenesis screens with LAT-derived peptides suggested that the substitution of G131 with almost any other amino acid should enhance Y132 phosphorylation, with aspartate and glutamate substitutions showing the greatest enhancement (Supplementary Fig. 1c)<sup>15</sup>. In a colorimetric *in vitro* kinase assay, in which ATP consumption is coupled to NADH oxidation, the ZAP-70 kinase domain showed negligible activity towards a wild-type peptide encompassing Y132 (Fig. 1e,f). Replacement of the glycine at the –1 position with aspartate or glutamate greatly increased the phosphorylation efficiency of Y132 (Fig. 1e,f). Despite its slow phosphorylation by ZAP-70, LAT Y132 is a bona fide well-established ZAP-70 substrate, as shown in the kinase assay (Fig. 1d) and in the experiments in which ZAP-70 deficiency but not ITK deficiency eliminated Y132 phosphorylation (Supplementary Fig. 1d), and as reported in the literature<sup>19</sup>.

Since p-Y132 in LAT is directly upstream of PLC- $\gamma$ 1, we examined the possibility that the glycine at position 131 might have been selected to promote a better PLC- $\gamma$ 1 interaction with the p-Y132 site. Phosphorylated Y132 interacts with the N-terminal SH2 domain of PLC- $\gamma$ 1 (refs. 19,20). A peptide with glycine preceding Y132 had similar binding affinity to the PLC- $\gamma$ 1 N-SH2 domain, as did a peptide with aspartate preceding Y132 (Supplementary Fig. 2a,b). A scanning mutagenesis screen for PLC- $\gamma$ 1 N-terminal

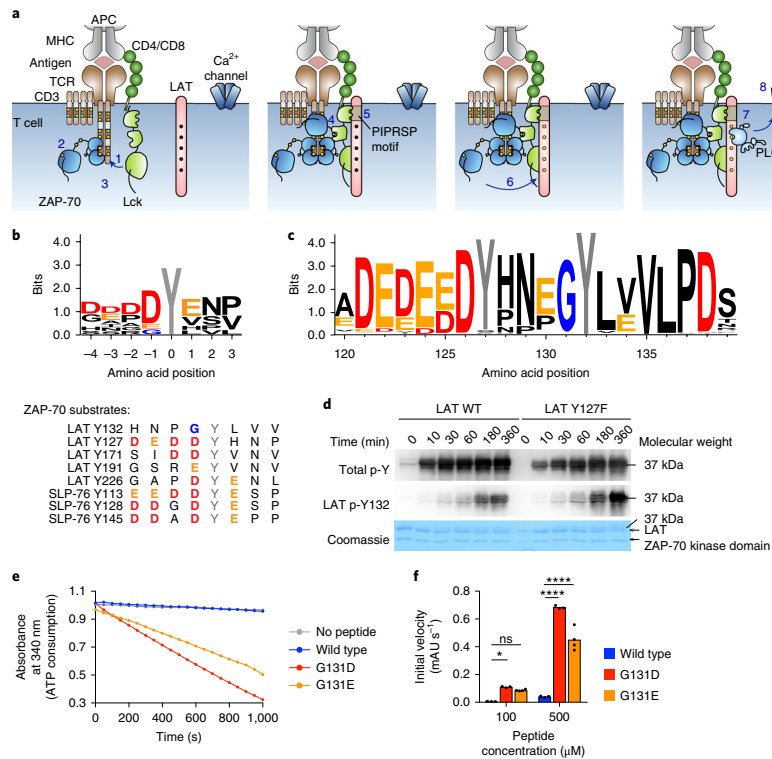
SH2 binding to LAT p-Y132 peptide mutants confirmed that most substitutions at G131 do not affect SH2 binding, whereas polar substitutions at V135 (the +3 position) in the p-Y132-containing peptide impaired SH2 binding, consistent with the known binding motif preference for PLC- $\gamma$ 1 N-terminal SH2 (Supplementary Fig. 2c)<sup>21</sup>. It is also unlikely that the G131D and G131E mutations would change which kinase phosphorylates this site, because the aspartate or glutamate residue at the –1 position is disfavored by Src family kinases and Tec family kinases<sup>15,16</sup>. Therefore, this highly conserved glycine at the –1 position impedes the efficiency of LAT Y132 phosphorylation by ZAP-70.

**Mutation of LAT G131 to an aspartate or glutamate enhances calcium responses.** To determine how the G131 residue preceding Y132 affects PLC- $\gamma$ 1-dependent signal transduction (for example, calcium responses), we substituted G131 with aspartate or glutamate in T cells. LAT and its G131 variants were used to reconstitute CRISPR-Cas9-generated LAT-deficient human Jurkat cells (J.LAT), hereafter termed J.LAT.WT, J.LAT.G131D, and J.LAT.G131E. When these cells were stimulated with anti-CD3 mAb (OKT3), the G131D and G131E LAT variants markedly augmented the magnitude of maximal calcium peaks (Fig. 2a,b). Particularly evident at lower doses of anti-CD3, expression of G131D and G131E mutant LAT molecules endowed cells with faster and larger calcium responses than did wild-type LAT (Fig. 2a,c). Thus, by mutating G131 to an aspartate or glutamate, the reconstituted J.LAT cells had increased sensitivity and decreased response times to weak anti-CD3 stimuli.

We examined whether the elevated calcium mobilization in J.LAT.G131D and J.LAT.G131E cells resulted from alteration of LAT Y132 and PLC- $\gamma$ 1 phosphorylation. J.LAT.G131D and J.LAT.G131E cells responded to lower anti-CD3 concentrations than did wild-type cells (Fig. 2d and Supplementary Fig. 3a). The mutation at G131 did not influence the activation of Lck and ZAP-70 (Supplementary Fig. 3a,b), but LAT Y132 and PLC- $\gamma$ 1 phosphorylation were greatly enhanced in G131D- and G131E-expressing cells (Fig. 2d and Supplementary Fig. 3a,c). Notably, we sometimes observed an enhancement in the phosphorylation of the distal tyrosine residues in cells expressing LAT G131D; however, this effect was not consistently observed (Fig. 2d and Supplementary Fig. 3b). In time-course experiments, G131D and G131E LAT also accelerated the phosphorylation of LAT Y132 and PLC- $\gamma$ 1 (Fig. 2e). These results suggest that LAT G131D and G131E lowered the TCR response threshold and amplified T cell responsiveness by promoting the phosphorylation of LAT Y132 and PLC- $\gamma$ 1.

**Enhanced Y132-PLC- $\gamma$ 1-derived signals allow T cells to respond to low-affinity ligands.** The OT-I TCR recognizes a peptide spanning residues 257–264 from chicken ovalbumin (OVA) presented by the H-2K<sup>b</sup> MHC molecules. Substitutions of one or two amino acids convert the full agonist OVA peptide into partial or weak agonists, all termed altered peptide ligands (APLs), which provide a sensitive and specific system to examine the capability of T cell ligand discrimination.

We reconstituted LAT-deficient OT-I<sup>h</sup>CD8<sup>+</sup> Jurkat cells with wild-type LAT or the G131D or G131E variants (termed J.OT-I.LAT.WT, J.OT-I.LAT.G131D, and J.OT-I.LAT.G131E, respectively). Each cell clone was stimulated with OVA APL-pulsed H-2K<sup>b</sup>-expressing T2 cells (T2-K<sup>b</sup>)<sup>22</sup>. Cells upregulated the activation marker CD69 in response to OVA stimulation but remained unresponsive towards an unrelated peptide, VSV (Fig. 3a). When the cells were stimulated with OVA or partial agonists Q4R7 or T4, G131D-LAT- and G131E-LAT-expressing J.OT-I<sup>+</sup> cells were approximately tenfold more sensitive to the peptide stimulus. Q4H7 is a very weak agonist and activated only approximately 30% of the J.OT-I.LAT.WT cells, but approximately 60% of J.OT-I.LAT.G131D and 50% of J.OT-I.LAT.G131E cells were able to respond to Q4H7, as measured by CD69

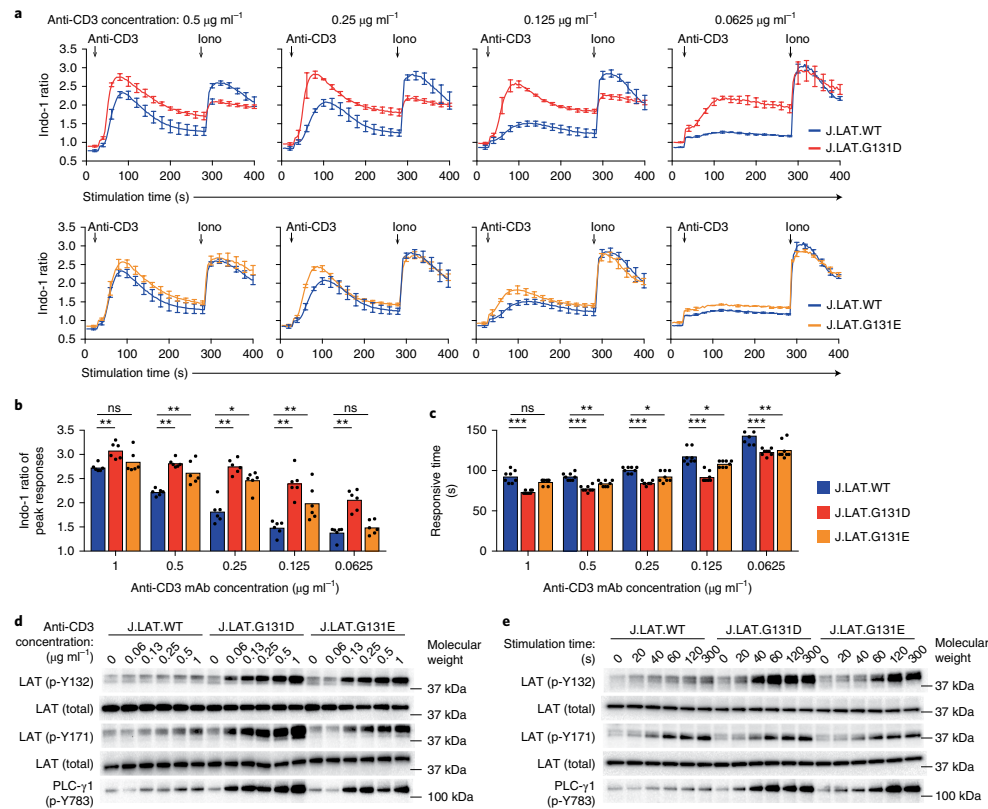


**Fig. 1 | Mammalian LAT has a glycine preceding Y132 that decreases the phosphorylation efficiency of Y132.** **a**, An illustration of TCR proximal signaling after TCR–pMHC engagement. Step 1, TCR–pMHC engagement colocalizes the co-receptor-associated Lck with the pMHC-stimulated TCR, where Lck phosphorylates tyrosines on ITAMs of the CD3 and  $\zeta$ -chains. Step 2, ZAP-70 is recruited and bound to doubly phosphorylated ITAMs. Step 3, Lck phosphorylates ZAP-70, stabilizing its open conformation and activating the ZAP-70 catalytic domain. Step 4, Lck SH2 domain binds to ZAP-70 p-Y319, stabilizing the open conformation of Lck<sup>315,32</sup>. Step 5, Lck SH3 domain binds to the PIPRSP motif of LAT to facilitate the accessibility of LAT to the kinase ZAP-70 (ref. <sup>33</sup>). Step 6, activated ZAP-70 phosphorylates tyrosine residues on LAT or SLP-76 (SLP-76 not shown). Step 7, phosphorylated LAT Y132 recruits PLC- $\gamma$ 1, leading to ITK-mediated PLC- $\gamma$ 1 phosphorylation and activation. Step 8, activated PLC- $\gamma$ 1 induces calcium increase and PKC and Ras–MAPK activation (not shown), eventually leading to T cell activation. APC, antigen-presenting cell. **b**, Sequence logo (top) and individual sequences (bottom) showing the conservation of amino acids spanning the target tyrosine residues of reported ZAP-70 substrates in humans. The tyrosine substrate of ZAP-70 is referred to as position 0, whereas the preceding residue is position –1. **c**, Sequence conservation of LAT in 68 mammalian species, depicted in the regions surrounding tyrosine residues Y127 and Y132 of LAT. The amino acid position is numbered on the basis of human LAT isoform 2. **d**, Immunoblot analysis of in vitro LAT phosphorylation reactions, monitoring site-specific phosphorylation at Y132 as well as total tyrosine phosphorylation. Purified LAT or a Y127F mutant cytoplasmic domain (5  $\mu$ M) were phosphorylated by purified ZAP-70 kinase domain (1  $\mu$ M). The phosphorylation of Y132 on LAT was assessed using an anti-LAT p-Y132 antibody. The total phosphorylation level of LAT was assessed using an anti-p-Y antibody (clone 4G10). A Coomassie Blue-stained membrane below shows loading levels. Data are representative of three independent experiments. **e**, Phosphorylation of peptides spanning LAT Y132 with the wild-type G131 residue, the G131D mutation, or the G131E mutation, using a colorimetric assay in which ATP consumption is enzymatically coupled to stoichiometric oxidation of NADH, with concomitant loss of NADH absorbance at 340 nm. The ZAP-70 kinase domain was used at a concentration of 1  $\mu$ M and peptides were at a concentration of 500  $\mu$ M. A control reaction lacking substrate peptide was also carried out to measure the background level of kinase-mediated ATP hydrolysis. At least three experiments were repeated independently with similar results. **f**, Background-subtracted rates of in vitro LAT Y132 phosphorylation using the assay described in **e**. Bar graphs show the mean rate from at least three independent experiments for each kinase–substrate pair at two substrate concentrations. Each symbol represents an individual result.  $n = 3$  independent results (wild type and G131D),  $n = 4$  independent results (G131E). \* $P = 0.0389$ , \*\*\*\* $P < 0.0001$ ; ns, not significant; one-way analysis of variance (ANOVA) analysis.

upregulation (Fig. 3a,b). Another weak OVA APL peptide, G4, did not stimulate J.OT-I.LAT.WT cells to upregulate CD69, but was able to activate about 40% of G131D-expressing J.OT-I<sup>+</sup> T cells and 20% of G131E-expressing cells (Fig. 3a,b). The responses to Q4H7 and

G4 peptides are noteworthy because both peptides can promote positive selection of OT-I<sup>+</sup> T cells in fetal thymic organ cultures and, as such, are considered to have an affinity in the range of positively selecting self-peptides<sup>23,24</sup>.

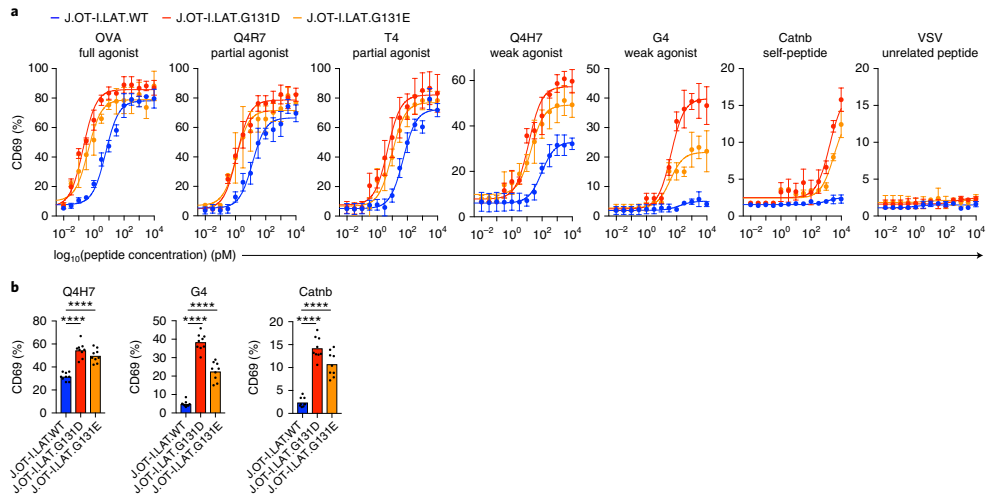




**Fig. 2 | Mutation of LAT G131 to an aspartate or glutamate facilitates calcium responses by augmenting PLC- $\gamma$ 1 signaling. a**, CRISPR-Cas9-generated LAT-deficient J.LAT cells were reconstituted with wild-type LAT or mutant LAT with G131D (top) or G131E (bottom) substitutions, as indicated. Cells were loaded with the calcium-sensitive dye Indo-1 AM and stimulated with a range of anti-CD3 (clone OKT3) concentrations starting at 0.5  $\mu\text{g ml}^{-1}$  (left) followed by a series of twofold dilutions (0.25  $\mu\text{g ml}^{-1}$ , 0.125  $\mu\text{g ml}^{-1}$ , and 0.0625  $\mu\text{g ml}^{-1}$ , from left to right). The changes in relative calcium-sensitive fluorescence ratios over time for 400 s are shown (mean  $\pm$  s.d.,  $n = 3$  technical replicates). Ionomycin treatment was used as a positive control. Data are representative of at least three experiments. **b**, The plot shows the mean of the maximal calcium peak at different concentrations of anti-CD3 stimuli (mean  $\pm$  s.d.,  $n = 8$  samples from three independent experiments). Diminishing amounts of anti-CD3 were added, starting at 1  $\mu\text{g ml}^{-1}$ , followed by a series of twofold dilutions. Data were pooled from three independent experiments. \*\* $P = 0.0022$ , \* $P = 0.0043$ ; ns, not significant ( $P = 0.1327$ ); two-tailed Mann-Whitney U test. **c**, Bar graphs summarize the response times to reach the peak calcium increases (mean  $\pm$  s.d.,  $n = 8$  samples from three independent experiments). Anti-CD3 stimulation starts at 1  $\mu\text{g ml}^{-1}$ , followed by a series of twofold dilutions. Data were pooled from three independent experiments. \*\*\* $P = 0.0002$ ; ns, not significant ( $P = 0.3095$ ); \*\* $P = 0.0031$ , \* $P$  (left) = 0.0123, \* $P$  (right) = 0.0228, \*\* $P$  (right) = 0.0053; two-tailed Mann-Whitney U test. **d**, Immunoblot analyses of J.LAT cells that were reconstituted with wild-type LAT, G131D or G131E mutant LATs, and were left unstimulated or were stimulated with anti-CD3 stimulation (clone OKT3) starting at 0.5  $\mu\text{g ml}^{-1}$  with serial twofold dilutions at 37  $^{\circ}\text{C}$  for 1 min. Data are representative of at least five experiments. Note that the same lysates were run on two separate gels to blot for p-Y171 and p-Y132; hence, blots for LAT loading are provided twice. **e**, Immunoblot analyses of J.LAT cells that were reconstituted with wild-type LAT, or G131D or G131E mutant LATs, and were left unstimulated or were stimulated with anti-CD3 stimulation at 1  $\mu\text{g ml}^{-1}$  (clone OKT3) at 37  $^{\circ}\text{C}$  for different durations (as indicated above the blots). Data are representative of at least five experiments. Note that the same lysates were run on two separate gels to blot for p-Y171 and p-Y132; hence, blots for LAT loading are provided twice.

G131D- or G131E-expressing J.Ot-I $^{+}$  cells were also weakly activated by the naturally occurring positively selecting self-peptide for OT-I TCR, Catnb (derived from  $\beta$ -catenin residues 329–336)<sup>25</sup>, whereas wild-type LAT-expressing cells were not (Fig. 3a,b). We compared the potency of each OVA APL peptide and

the self-peptide Catnb using J.Ot-I $^{+}$  G131D and G131E versus wild-type LAT-expressing cells (Table 1). Peptide potencies were quantified by calculating EC<sub>50</sub> (half maximal responses) in the CD69 upregulation assays and normalizing these values to the percentage of maximal CD69 responses<sup>26</sup>. These results suggest that



**Fig. 3 | Enhanced Y132 phosphorylation allows T cells to react with low-affinity ligands.** **a**, LAT-deficient J.OT-I.hCD8<sup>+</sup> Jurkat variants were reconstituted with wild-type LAT, or G131D or G131E mutant LATs. Cells were stimulated with T2-K<sup>b</sup> antigen-presenting cells pulsed with OVA peptide, OVA APL peptides, self-peptide Catnb, or VSV control peptide over a wide range of peptide concentrations. The next day, the expression of CD69 was assessed by flow cytometry. Percentages of CD69<sup>+</sup> cells were plotted against peptide concentrations (mean  $\pm$  s.d.,  $n = 3$  technical replicates). Data are representative of at least five experiments. **b**, Bar graph depicts the mean percentages of CD69<sup>+</sup> cells after stimulation with Q4H7, G4, or Catnb peptides. Each symbol represents the result of a technical replicate (mean  $\pm$  s.d.,  $n = 9$  samples from three independent experiments).  $P^{****} < 0.0001$ , two-tailed Mann-Whitney U test.

**Table 1 | EC<sub>50</sub> (pM) and ligand potency analysis of CD69 upregulation**

Peptide	Selecting effect on thymocytes	K <sub>0</sub> by SPR	EC <sub>50</sub>			1/potency		
			WT	G131D	G131E	WT	G131D	G131E
OVA	Negative selection	54 $\mu$ M	6.19	0.69	1.24	1	0.1	0.2
Q4R7	Partial	288 $\mu$ M	14.92	4.23	4.27	2.7	0.6	0.7
T4	Partial/boarder	444 $\mu$ M	82.67	4.89	9.34	13.8	0.7	1.5
Q4H7	Positive selection	847 $\mu$ M	87.89	15.56	18.11	34.5	3.5	4.5
G4	Positive selection	>1000 $\mu$ M	231.4	39.04	97.24	588.0	19.2	60.6
Catnb	Positive selection	N.A.	N.A.	1246	2116	N.A.	1090.4	2453.2

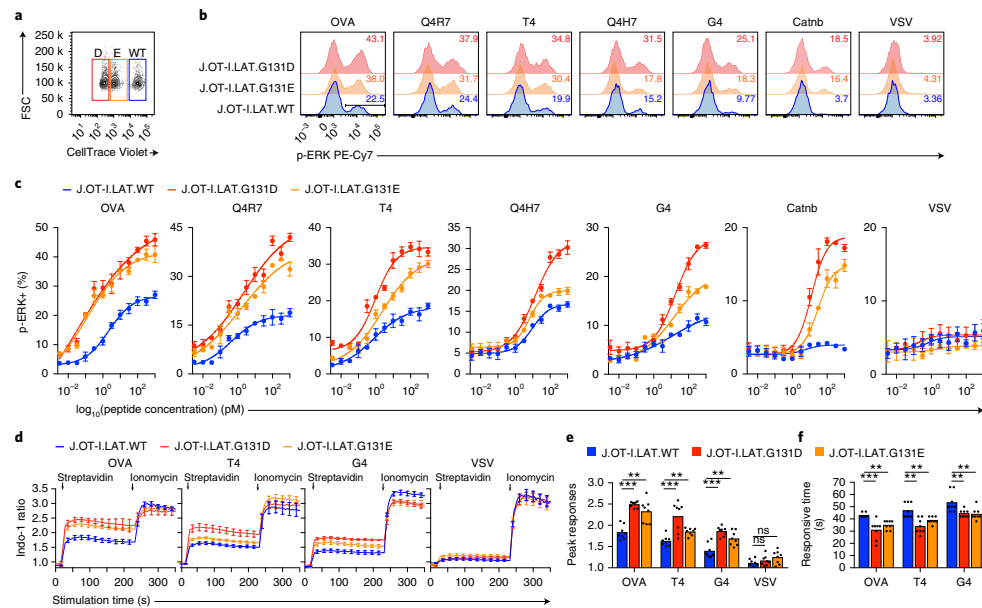
The table shows EC<sub>50</sub> (pM) and ligand potency analysis of CD69 upregulation from assays as in Fig. 3a. K<sub>0</sub> values, determined by surface plasmon resonance (SPR), were obtained from the literature<sup>30</sup>. N.A., not applicable. WT, wild type.

augmented LAT Y132 phosphorylation disrupted the ability of the cells to accurately discriminate ligands with different potencies. G131D-expressing cells exhibited a lower ligand responsiveness threshold than did wild-type LAT-expressing cells.

CD69 upregulation is a prominent feature of T cell activation, but its expression can also be induced by exposure to cytokines<sup>27</sup>. Therefore, we examined TCR-induced proximal signals, including phosphorylation of ERK and calcium flux, in response to OVA APL or self-peptide stimulation of J.OT-I<sup>+</sup> cells expressing LAT variants. LAT.WT-, G131D- or G131E-expressing J.OT-I<sup>+</sup> cells were first 'bar-coded' by labeling them with different dilutions of CellTrace Violet. All three variants were pooled and incubated with various peptide-pulsed T2-K<sup>b</sup> cells at 37 °C for 5 min (Fig. 4a). Stimulation with the OVA peptide induced the phosphorylation of ERK in all three J.OT-I<sup>+</sup> cell variants, but stimulation with the control peptide VSV

did not (Fig. 4b and Supplementary Fig. 4a,b). Across all OVA and the APL peptide stimuli, a substantially larger population of G131D-expressing J.OT-I<sup>+</sup> cells exhibited ERK phosphorylation than did G131E-expressing J.OT-I<sup>+</sup> cells; the wild-type-expressing J.OT-I<sup>+</sup> cells were the least responsive. Dose–response analyses of the phospho-ERK induction further supported the strengthened responses of LAT G131D- or G131E-expressing J.OT-I<sup>+</sup> cells towards full or partial agonist stimuli (Fig. 4c). Moreover, approximately 20% of G131D-expressing J.OT-I cells and 15% of G131E-expressing cells acquired the ability to upregulate ERK phosphorylation following stimulation with the self-peptide Catnb, whereas wild-type-expressing J.OT-I cells were unresponsive (Fig. 4c).

Next, we used OVA- or APL-loaded biotinylated pMHC monomers and streptavidin to analyze antigen-specific calcium responses. Expression of G131D or G131E LAT augmented calcium mobilization

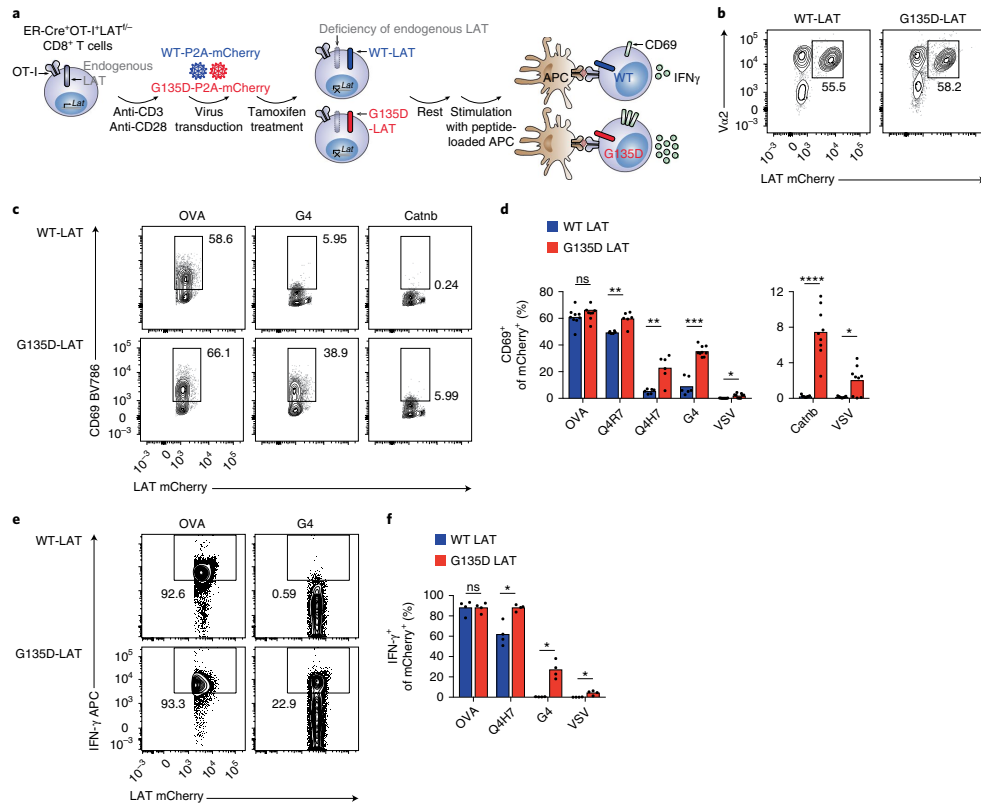


**Fig. 4 | Substitution of G131D or G131E in LAT promotes ERK activation and calcium increase in response to weak ligand or self-peptide stimulation.** **a–c.** Wild-type (WT), and G131D- (D) and G131E-expressing (E) LAT-deficient J.OT-I<sup>+</sup>hCD8<sup>+</sup> Jurkat variants were first individually labeled with CellTrace Violet dye at different concentrations. Cells were washed and pooled together for the experiments. T2-K<sup>+</sup> cells were pulsed with OVA peptides, APL ligands, the self-peptide Catnb, or VSV control peptide. Pooled J.OT-I<sup>+</sup>hCD8<sup>+</sup> Jurkat variants and peptide-pulsed T2-K<sup>+</sup> cells were mixed on ice, and quickly centrifuged. Cells were then stimulated by moving them to 37°C for 5 min, and then fixed with 4% PFA to terminate the stimulation. Cells were then subjected to flow cytometry-based p-ERK analysis. Data are representative of four independent experiments. **a.** Representative flow cytometry plot of J.OT-I<sup>+</sup>hCD8<sup>+</sup> Jurkat variants barcoded with titrated amounts of CellTrace Violet dye. FSC, forward scatter. **b.** Representative histograms for ERK phosphorylation responses in G131D, G131E, and wild-type LAT-expressing J.OT-I<sup>+</sup>hCD8<sup>+</sup> Jurkat variants stimulated with T2-K<sup>+</sup> cells pulsed with 1000 pM of each peptide as indicated. The black bar in the first panel depicts the gate used to define the p-ERK-induced population in **c.** Percentages of positive cells are indicated. Ligands used for stimulation are indicated above the plots. **c.** Analysis of the p-ERK<sup>+</sup> population of G131D, G131E, or wild-type LAT-expressing J.OT-I<sup>+</sup>hCD8<sup>+</sup> Jurkat variants stimulated with the indicated concentrations of peptide-pulsed T2-K<sup>+</sup> cells. Data were pooled from four independent experiments (mean  $\pm$  s.d.,  $n = 4$  in four independent experiments). Ligands used for stimulation are indicated above the plots. **d.** Wild-type, and G131D- and G131E-expressing LAT-deficient J.OT-I<sup>+</sup>hCD8<sup>+</sup> Jurkat variants were loaded with the calcium-sensitive dye Indo-1, and labeled with 1:100 biotinylated OVA/H-2K<sup>b</sup>, T4/H-2K<sup>b</sup>, G4/H-2K<sup>b</sup>, or VSV/H-2K<sup>b</sup> monomers. Cells were then subjected to calcium mobilization assays on Flex Station II. Indo-1 ratios were first recorded for 30 s to determine a relative baseline calcium level, followed by streptavidin addition to trigger the TCR-induced calcium response. Ionomycin was added at 240 s as a positive control. Representative calcium traces are shown. Each stimulus is as indicated. Data are representative of three independent experiments (mean  $\pm$  s.d.,  $n = 3$  technical replicates). **e.** Bar graphs depict the statistical analysis of the fold change of the peak. Each symbol represents a technical replicate (mean  $\pm$  s.d.,  $n = 8$  samples in three independent experiments). \*\*\* $P = 0.0002$  (OVA), \*\*\* $P = 0.0006$  (T4), \*\*\* $P = 0.0003$  (G4), \*\* $P = 0.0047$  (OVA), \*\* $P = 0.0020$  (T4), \*\* $P = 0.0070$  (G4); ns, not significant;  $P = 0.3823$  (VSV, left),  $P = 0.0830$  (VSV, right); two-tailed Mann-Whitney U test. **f.** Bar graphs depict the statistical analysis of the response time to reach the peak (mean  $\pm$  s.d.,  $n = 8$  samples in three independent experiments). Each symbol represents a technical replicate. \*\*\* $P = 0.0002$  (OVA), \*\* $P = 0.0011$  (OVA), \*\* $P = 0.0054$  (T4, top), \*\* $P = 0.0023$  (T4, bottom) \*\* $P = 0.0059$  (G4, top), \*\* $P = 0.0076$  (G4, bottom), two-tailed Mann-Whitney U test.

(Fig. 4d), enabling more rapid responses, and 1.52-fold increases in the magnitude of the peak responses (Fig. 4e,f). Thus, a negatively charged residue preceding Y132 in LAT enhanced the sensitivity of T cells to full or partial agonist stimuli, and bestowed on T cells the ability to respond, albeit weakly, to self-peptide stimulation.

**Murine T cells rely on slow phosphorylation kinetics of Y136 in LAT to allow self-non-self antigen discrimination.** The mutations at LAT residue 131 elicited similar functional consequences in primary mouse T cells. Ectopic over-expression of the G135D mutant LAT (Y136 is the murine ortholog of human Y132) in

the presence of endogenous LAT was sufficient to endow OT-I<sup>+</sup> CD8 and OT-II<sup>+</sup> CD4 T cells with a gain-of-function ability to respond to low-affinity ligands (Supplementary Fig. 5). OT-I<sup>+</sup> CD8 or OT-II<sup>+</sup> CD4 T cells transduced with a retrovirus encoding wild-type LAT-P2A-BFP or G135D LAT-P2A-BFP were stimulated with various peptide-pulsed T cell-deficient splenocytes. In response to stimulation with G4 peptide-pulsed splenocytes, the expression of G135D LAT enabled OT-I<sup>+</sup> CD8 T cells to increase the expression of the key transcriptional factor IRF4 and activation marker CD69 (Supplementary Fig. 5a), augmented the activation of ERK phosphorylation (Supplementary Fig. 5b), and



**Fig. 5 | The G135D mutation in LAT promotes primary mouse T cells to respond to low-affinity antigen or self-peptide stimulation. a**, The diagram shows the experimental flow. Naive ER-Cre<sup>+</sup>OT-I<sup>+</sup>LAT<sup>-/-</sup> CD8<sup>+</sup> T cells were isolated and lentivirally transduced to express wild-type LAT or G135D LAT and tamoxifen-treated for 4 d to delete endogenous LAT. Mouse G135D is homologous to human G131D. The wild-type or G135D LAT was conjugated to mCherry fluorescent protein through a self-cleaving P2A peptide. Cells with successful tamoxifen-induced deletion of endogenous LAT are GFP<sup>+</sup> (efficiency > 90%). Cells were rested for 1 d and stimulated with peptide-pulsed TCR  $\alpha$ -deficient splenocytes overnight. TCR  $\alpha$ -deficient splenocytes were pulsed with 1  $\mu$ M of OVA, T4, or G4 peptide, 10  $\mu$ M of Catnb peptide, or 10  $\mu$ M of VSV peptide. Cells were then analyzed for their ability to upregulate CD69 and produce IFN- $\gamma$ . Numbers in all flow cytometry plots indicate the percentages of positive cells. **b**, Representative contour plots depict the expression of Va2 (OT-I TCR  $\alpha$  chain) and mCherry after cells were transduced with lentivirus expressing wild-type LAT-P2A-mCherry or G135D LAT-P2A-mCherry. Data are representative of three experiments. **c**, Flow cytometric analysis of CD69 expression in mCherry<sup>+</sup> subpopulations of GFP<sup>+</sup>Va2<sup>+</sup>CD8<sup>+</sup> T cells, pulsed with OVA peptide, G4 peptide, or Catnb self-peptide. **d**, Bar graphs represent the mean of CD69<sup>+</sup> cells in the peptide stimulation assay. Each symbol represents one technical replicate (mean  $\pm$  s.d.,  $n = 9$  samples in three independent experiments). \*\* $P = 0.0043$  (Q4R7), \*\* $P = 0.0022$  (Q4H7), \*\*\* $P = 0.0004$ , \*\*\*\* $P < 0.0001$  (Catnb), \* $P = 0.0294$  (VSV). ns, not significant ( $P = 0.1359$ ); two-tailed Mann-Whitney U test. **e**, Flow cytometric analysis of IFN- $\gamma$ -producing ability in mCherry<sup>+</sup> subpopulations of GFP<sup>+</sup>Va2<sup>+</sup>CD8<sup>+</sup> T cells, pulsed with various peptides. **f**, Bar graph demonstrates the mean of IFN- $\gamma$ -producing cells in the peptide-stimulation assay. Each symbol represents one technical replicate (mean  $\pm$  s.d.,  $n = 4$  samples in two independent experiments.) \* $P = 0.0286$ ; ns, not significant ( $P = 0.8857$ ); two-tailed Mann-Whitney U test.

promoted the mobilization of calcium (Supplementary Fig. 5c). Similar gain of function was observed in G135D LAT-expressing OT-II<sup>+</sup> CD4 T cells when stimulated with the E336Q peptide, a partial agonist of OVA peptide (residues 329–336) specific for OT-II<sup>+</sup> TCR (Supplementary Fig. 5a,b).

Our data suggest that the human G131–Y132 and the homologous mouse G135–Y136 LAT sequences may place an important regulatory constraint on TCR signaling that enables ligand discrimination. To further test this hypothesis in the absence of

endogenous LAT, we used a mouse expressing a floxed *Lat* allele in which germline *Lat* could be deleted by tamoxifen treatment<sup>28</sup>. Endogenous, wild-type LAT is expressed during thymic selection in the CD8 lineage of ER-Cre<sup>+</sup>OT-I<sup>+</sup>LAT<sup>-/-</sup> mouse. We used wild-type or G131D-expressing lentivirus to transduce the peripheral ER-Cre<sup>+</sup>OT-I<sup>+</sup>LAT<sup>-/-</sup> CD8 T cells from these mice. Tamoxifen treatment was then used in vitro to delete endogenous *Lat* in mature OT-I<sup>+</sup> T cells, enabling experimental assessment of the function of the lentivirally expressed LAT mutant (Fig. 5a).

ERC<sup>Cre</sup>OT-I<sup>+</sup>Lat<sup>fl/fl</sup> CD8 T cells transduced with wild-type or G135D-P2A-mCherry lentivirus showed similar transduction frequencies and expression (Fig. 5b). The P2A sequence allows the mCherry fluorescence to function as a marker for successful transduction<sup>19</sup> and its fluorescence intensity can serve as a surrogate marker for protein expression without interfering with LAT function. The mCherry<sup>+</sup> ERC<sup>Cre</sup>OT-I<sup>+</sup>Lat<sup>fl/fl</sup> CD8 T cells regained the ability to respond to stimulation with OVA and the partial agonist Q4R7, as shown by the upregulation of CD69, but the non-transduced mCherry-negative cells did not (Supplementary Fig. 6). Expression of the G135D LAT mutant lowered the reactivity threshold to allow for an increased percentage of cells to be activated compared with that of wild-type LAT. The difference was particularly noteworthy when cells were stimulated with low-affinity peptides, such as the G4 peptide or the natural self-peptide Catnb (Fig. 5c,d). A small but increased response to the VSV peptide-pulsed antigen-presenting cells was also seen in the LAT-G135D-expressing cells. This could reflect responses to endogenous self-peptides that the VSV-pulsed antigen-presenting cells also expressed. The percentages of IFN- $\gamma$ -producing cells in G135D<sup>+</sup> groups also increased compared with those in the wild-type groups (Fig. 5e,f). Thus, an aspartate residue preceding Y136 endowed mature T cells with the ability to be activated by low-affinity antigens and allowed at least one relevant self-peptide to become an agonist. Our data suggest that ZAP-70-mediated phosphorylation of LAT Y136 in primary mouse T cells may function as a critically important node involved in kinetic proofreading to enforce T cell ligand discrimination.

**T cell ligand discrimination is uniquely susceptible to the phosphorylation kinetics of LAT Y132.** The kinetic proofreading model predicts that proper ligand discrimination can be achieved by a series of gated biochemical events. In addition to the proofreading node involving LAT Y132 shown here, co-receptor scanning and delivery of Lck can also influence T cell ligand discrimination<sup>26</sup>. To experimentally compare the relative contributions of co-receptor scanning and G131–Y132 of LAT in TCR signaling, we again used the OT-I<sup>+</sup> Jurkat cells and OVA APL systems. We used OT-I<sup>+</sup> LAT-deficient Jurkat cells that did or did not express human CD8 (hCD8), and ectopically expressed wild-type LAT or the G131D mutant (termed J.OT-I.hCD8neg.LAT.WT or J.OT-I.hCD8neg.LAT.G131D, respectively). With these cells, we performed experiments as we did in Fig. 3. The presence of hCD8 seemed to enhance the number of cells responding towards OVA peptide or the partial agonists Q4R7, T4, or Q4H7, compared with cells lacking hCD8, but did not alter the EC<sub>50</sub> value of cell responses towards the low-affinity peptide G4 or self-peptide Catnb (Supplementary Fig. 7b,c). Thus, G131–Y132 of LAT creates an important TCR signaling bottleneck that is distinct from the previously reported time delay generated by co-receptor scanning<sup>26</sup>.

To investigate whether the slow phosphorylation of Y132 in LAT is a unique rate-limiting step to control ligand discrimination, we explored the possibility that any of the other four individual tyrosine residues in LAT (that are phosphorylated more efficiently than Y132) could similarly function as 'artificial' TCR signaling bottlenecks to further improve T cell ligand discrimination. We expressed 'GY series' LAT mutants in J.OT-I<sup>+</sup>.hCD8<sup>+</sup> LAT-deficient cells (termed J.OT-I.LAT.G126Y127, J.OT-I.LAT.G170Y171, J.OT-I.LAT.G190Y191, or J.OT-I.LAT.G225Y226, respectively). Interestingly, these mutants and wild-type LAT showed similar CD69 expression levels after stimulation with OVA or the partial agonists Q4R7 or T4-pulsed T2-K<sup>b</sup> cells (Supplementary Fig. 7d). The artificial attenuation of phosphorylation at LAT tyrosines other than Y132 did not influence OT-I TCR sensitivity or specificity, although there is probably redundancy in binding interactions with other SH2-containing proteins at the other phosphorylation sites. Thus, T cell ligand discrimination is preferentially controlled by the slow phosphorylation of LAT Y132 and probably depends on the importance of events downstream of PLC- $\gamma$ 1.

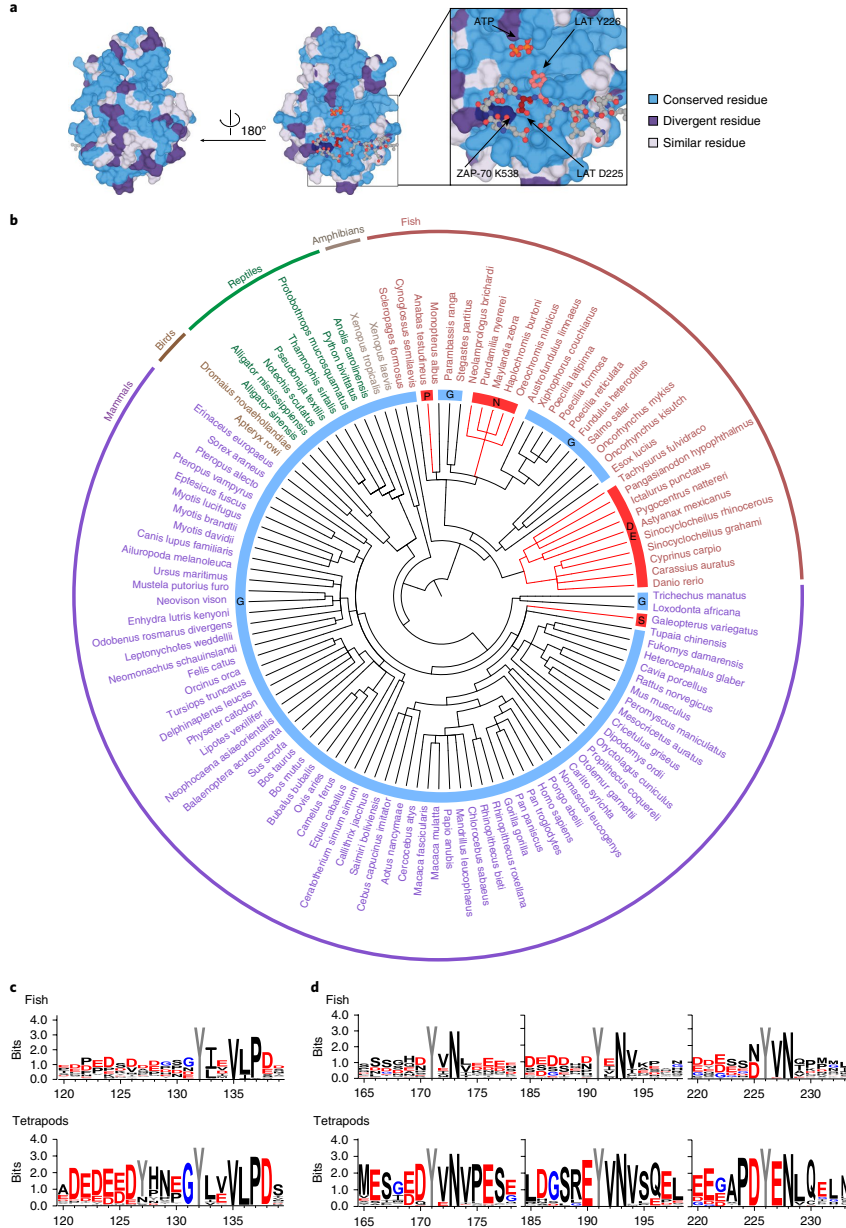
**Divergence at the LAT Y132 phosphosite in fish lineages may reflect temperature-sensitive signaling.** The slow phosphorylation kinetics of Y132 can be largely attributed to a –1 glycine residue, which cannot form critical interactions with a conserved lysine residue (K538) in the substrate-binding site of the ZAP-70 catalytic domain<sup>15,16</sup>. K538 and other positively charged residues in the ZAP-70 active site are conserved across all jawed vertebrates (Fig. 6a)<sup>15</sup>, suggesting that the substrate-binding mode of ZAP-70 is conserved in these organisms. The glycine residue at position 131 in LAT is also highly conserved across jawed vertebrates, consistent with a conserved regulatory role for slow LAT Y132 phosphorylation (Fig. 6b,c). Interestingly, a 'better neighbor' preceding Y132, such as asparagine, aspartate, or glutamate, is present in some fish (Fig. 6b). Among the other key tyrosine residues in LAT that get phosphorylated, there is also a relative lack of sequence conservation at the –1 positions among fish (Fig. 6d). However, throughout jawed vertebrate evolution, the preceding sequence is dominated by a negatively charged residue and lacking in any positively charged residues, consistent with the features preferred by ZAP-70 for tyrosine phosphorylation (Fig. 6d).

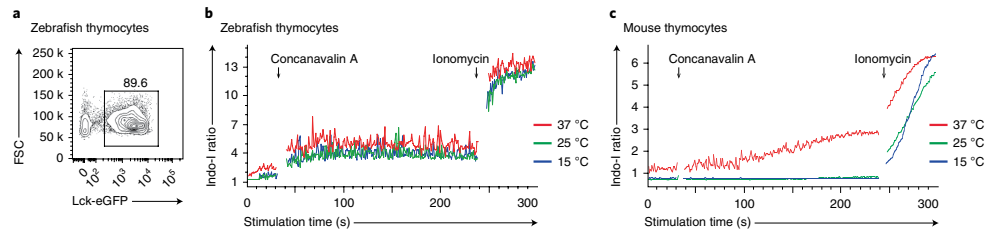
Given our data on the critical role of the slow kinetics of Y132 phosphorylation for T cell ligand discrimination, we wondered why G131 is not completely conserved in fish. Based on our data in mammalian T cells, the other three amino acids observed at position 131 in fish LAT sequences (aspartate, glutamate, and asparagine) should speed up the phosphorylation of Y132 and enhance calcium responses towards low concentrations of anti-CD3 stimuli (data for G131N not shown). We therefore questioned why some fish would tolerate faster phosphorylation of this tyrosine if it might impair ligand discrimination.

**Fig. 6 | LAT Y132 probably represents a conserved kinetic proofreading step in tetrapodal T cells.** **a**, Sequence conservation between the human and zebrafish ZAP-70 kinase domains. The kinase domains of human and zebrafish ZAP-70 are 65% identical. Conservation is mapped onto a model of the human ZAP-70 kinase domain bound to a peptide surrounding LAT Y226 (ref. 15). The surface of the kinase domain is colored based on which residues are identical (blue), have physicochemical similarity (light purple), or are unconserved (purple), between the human and zebrafish sequences. The peptide is shown in ball and stick representation, with LAT Y226 and the –1 residue (D225) is shown in red. The conserved ZAP-70 active site residue that coordinates LAT D225, K538, is shown in dark blue. Residues in the substrate-binding region, particularly those that contact the –1 substrate residue, are highly conserved between human and zebrafish sequences. **b**, Phylogenetic tree showing taxonomic relationships between various jawed vertebrate species, highlighting species with a non-glycine residue at position 131 in LAT. Relationships are derived from the NCBI Taxonomy dataset<sup>14</sup>. Species that do not have a glycine residue preceding Y132 in LAT are highlighted in red. These species typically have an aspartate (D), glutamate (E), asparagine (N), proline (P), or serine (S) residue at the –1 position as indicated in the inner circle. Note that LAT sequences were not readily identifiable in most bird species, aside from emu (*Dromaius novaehollandiae*) and kiwi (*Apteryx rowi*), suggesting possible loss of the canonical jawed vertebrate LAT gene in most birds. More details can be found in Supplementary Table 1. **c**, Sequence conservation of regions flanking LAT Y132 among fish and tetrapods. The positions are numbered using human LAT isoform 2 as a reference. **d**, Sequence logo of amino acid conservation in the regions of LAT spanning Y171, Y191, or Y226. The positions are numbered using human LAT isoform 2 as a reference. Sequence conservation in fish (top) or tetrapods (bottom) is shown.

Fish have a more limited antigen receptor repertoire than do mammals<sup>30</sup>, and are also generally cold-blooded<sup>31</sup>. We considered the possibility that better Y132 phosphorylation kinetics might

provide certain immune fitness advantages for these fish, as their body temperatures are probably lower than those of mammals. To test the effect of temperature on the ability of T cells to induce





**Fig. 7 | Cold temperature does not impair the ability of zebrafish thymocytes to trigger calcium flux in response to stimulation.** **a**, Representative contour plot of *lck-egfp* transgene zebrafish thymocytes. Data are representative of at least three experiments. The number in the contour plot indicates the percentage of GFP<sup>+</sup> cells. **b**, Representative calcium flux of Lck-eGFP<sup>+</sup> zebrafish thymocytes treated with 10  $\mu\text{g ml}^{-1}$  concanavalin A. Zebrafish thymocytes were loaded with the calcium indicator dye Indo-1, and incubated at 25°C, 37°C, or 15°C before being used for experiments. Concanavalin A was added at 30 s and ionomycin was added at 240 s. Data are representative of three independent experiments. **c**, Representative calcium responses of mouse thymocytes treated with 10  $\mu\text{g ml}^{-1}$  concanavalin A. Mouse thymocytes were loaded with the calcium indicator dye Indo-1, and incubated at 37°C, 25°C, or 15°C before they were used for experiments. Concanavalin A was added at 30 s and ionomycin was added at 240 s. Data are representative of two independent experiments.

calcium mobilization, we compared mouse and zebrafish thymocytes. Zebrafish have a naturally occurring aspartate preceding the tyrosine residue in LAT that is homologous to human Y132 and mouse Y136 (Fig. 6b). We used zebrafish that carry an *lck:egfp* transgene to harvest the zebrafish thymi and identify thymocytes (Fig. 7a). Since no monoclonal antibodies are currently available to stimulate zebrafish TCRs or CD3 (ref. <sup>23</sup>), we stimulated zebrafish or mouse thymocytes with concanavalin A, a plant lectin that depends on TCR expression to induce calcium increases in Jurkat T cells<sup>33,34</sup>. Interestingly, temperature change had little impact on concanavalin A responses of Lck-GFP<sup>+</sup> zebrafish thymocytes (Fig. 7b). By contrast, mouse thymocytes, which have a glycine preceding Y136, did not respond to concanavalin A stimulation at lower temperatures (Fig. 7c and Supplementary Fig 8). Importantly, when the cells were treated with ionomycin, zebrafish and mouse thymocytes had similar maximal calcium responses, although responses were delayed in mouse thymocytes incubated at a reduced concentration (Fig. 7c).

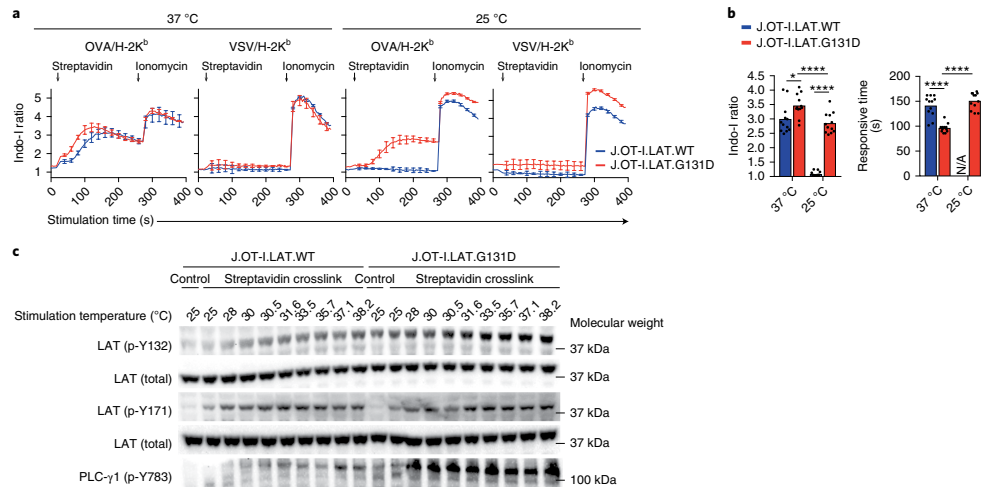
Next, we tested whether G131D-expressing Jurkat cells may gain the temperature resistance properties seen in zebrafish thymocytes. We used biotinylated OVA H-2K<sup>b</sup> monomers followed by cross-linking with streptavidin to stimulate J.OT-I.LAT.WT or J.OT-I.G131D cells. Notably, J.OT-I.LAT.WT cells were more vulnerable to the change in temperature than were J.OT-I.LAT.G131D cells (Fig. 8a,b). At room temperature, crosslinking of OVA H2-K<sup>b</sup> was unable to induce calcium flux in wild-type LAT-expressing cells, whereas the change in temperature had minimal impairment on G131D-expressing J.OT-I<sup>+</sup> cells. Next, we used immunoblots to examine LAT phosphorylation of J.OT-I.LAT.WT or J.OT-I.LAT.G131D cells stimulated with biotin-labeled OVA monomers, followed by streptavidin crosslinking, across different temperatures. Although wild-type LAT was phosphorylated in response to stimulation at temperatures close to 37°C, we could not detect the phosphorylation of Y132 at 25°C or 28°C (Fig. 8c). By contrast, at 25°C stimulation, we could detect phosphorylation at LAT tyrosine residues that have aspartate at the -1 position (Y171 or G131D preceding Y132), although this was much weaker than under stimulation at 37°C (Fig. 8c). Interestingly, we also observed an increase in basal phosphorylation of LAT Y132 and PLC- $\gamma$ 1 Y783 in J.OT-I.LAT.G131D cells, compared with those in J.OT-I.LAT.WT cells (Fig. 8c). Since we did not observe a similar increase in basal phosphorylation of Y132 in experiments that used anti-CD3 as the stimulus, the increase in basal phosphorylation here could be due to the prelabeling of cells with biotinylated OVA monomers at room temperature.

Our sequence analyses and comparison of temperature effects on calcium responses in mouse versus zebrafish thymocytes, or wild-type LAT versus G131D-expressing OT-I<sup>+</sup> Jurkat cells suggest that slow LAT Y132 phosphorylation has been selected for in most jawed vertebrate lineages, and is almost fixed in tetrapods. Some fish species, such as zebrafish, seem to have evolved to have faster phosphorylation of Y132, which may be required to enable signaling at the range of water temperatures in which these animals live in the wild (Supplementary Fig 9).

## Discussion

The balance of T cell sensitivity and specificity requires TCR discrimination of agonist pMHC from self-MHC, which can differ by as little as a factor of ten in their affinities for the TCR<sup>35</sup>. The kinetic proofreading model proposes that signal accuracy can be achieved by accepting some tolerable time delay through a series of reversible biochemical modifications before the commitment step that triggers a response. Here, we have shown that LAT functions as a critical time-keeper through constraints placed by a single residue, G131, which attenuates ZAP-70-mediated phosphorylation of Y132. The phosphorylation of Y132 is required for the recruitment, phosphorylation, and activation of PLC- $\gamma$ 1. The activation of PLC- $\gamma$ 1 is critical for the subsequent calcium increase and PKC and Ras activation, which mediate T cell cytokine production, proliferation, and effector responses. The molecular time delay at LAT Y132 is necessary for proper self-non-self discrimination, and our observations support the importance of slow Y132 phosphorylation in TCR kinetic proofreading.

Mutating G131 to aspartate leads to faster phosphorylation kinetics for Y132, but with negative consequences for ligand discrimination. Y132 is unique among the LAT phosphorylation sites in its ability to influence ligand discrimination, most likely because it is the only phosphorylation site that directly recruits PLC- $\gamma$ 1. The other four phosphorylation sites in LAT all have a YXNX motif, consistent with Grb2 or Gads recruitment sites<sup>17,36,37</sup>. Mutation of Y171, Y191, or Y226 has a minimal effect on T cell development and maturation<sup>38</sup>. By contrast, replacement of Y132 with phenylalanine disrupts thymic development<sup>39,40</sup>, and also leads to TCR-independent lymphoproliferation of T cells, suggesting that PLC- $\gamma$ 1 signals may maintain 'balanced' cell signaling to ensure an appropriate T cell response<sup>39-42</sup>. Thus, Y132 in LAT is a potentially unique and important bottleneck, to temporally regulate the recruitment of PLC- $\gamma$ 1, with help from other tyrosine residues (probably through Gads-SLP-76 preassembly on LAT to stabilize PLC- $\gamma$ 1 binding)<sup>17,38,43,44</sup>.



**Fig. 8 | Expression of LAT G131D endows T cells with the zebrafish thymocyte-like ability to promote calcium mobilization at reduced temperature.**  
**a**, LAT-deficient JOT-I.hCD8<sup>+</sup> cells that were reconstituted with wild-type LAT or G131D mutant LAT were used for the calcium assays. Cells were labeled with the calcium-sensitive dye Indo-1, washed, and labeled with biotinylated OVA-bound I-K<sup>b</sup> monomers or control VSV-bound I-K<sup>b</sup> monomers at room temperature for 30 min. Cells were then used for calcium assays and stimulated by the addition of streptavidin. Calcium traces were recorded for 400 s at 37 °C (left two panels) or 25 °C (right two panels). Data are representative of two independent experiments (mean  $\pm$  s.d.,  $n=3$  technical replicates). **b**, The bar graphs (left) depict the mean of the maximal calcium peak for cells at different temperatures (mean  $\pm$  s.d.,  $n=12$  samples from four independent experiments) as in **a**. \* $P=0.0145$ , \*\*\* $P=0.0007$ , \*\*\*\* $P<0.0001$ , two-tailed Mann-Whitney U test. Bar graphs (right) summarize the response time to reach the peak calcium responses (mean  $\pm$  s.d.,  $n=12$  technical replicates). \*\*\*\* $P<0.0001$ , two-tailed Mann-Whitney U test. Wild-type LAT-expressing JOT-I<sup>-</sup> cells did not respond to OVA/H-2K<sup>b</sup> stimulation at 25 °C, and therefore were not included for analysis (labeled as N/A). **c**, LAT-deficient JOT-I.hCD8<sup>+</sup> cells that were reconstituted with wild-type LAT or G131D mutant LAT were used for the experiments. Cells were labeled with biotinylated OVA-bound I-K<sup>b</sup> monomers (1:100) at room temperature for 30 min. Cells were then aliquoted and transferred to PCR tubes, stimulated with the addition of streptavidin, and then incubated at room temperature (25 °C), 28 °C, or in a PCR machine with a gradient of temperatures (30–39 °C) for 10 min. The reaction was stopped by the addition of 10 $\times$  lysis buffer and used for immunoblot analysis. Blots were probed with antibodies of the indicated specificities. Data are representative of at least four independent experiments.

Although artificial attenuation of LAT phosphorylation at individual tyrosine residues other than Y132 did not influence signaling sensitivity, we expect that combinations of –1 glycine substitutions at LAT Y171, Y191, or Y226 might perturb T cell sensitivity.

There may be several events involved in kinetic proofreading, each of which could contribute to the time delay required for ligand discrimination<sup>26,45,46</sup>. Very recently, using optogenetic methods, two groups implicated immediate downstream events of PLC $\gamma$ 1 activation, calcium and diacylglycerol increases, in kinetic proofreading<sup>45,46</sup>. Notably, our study has identified PLC $\gamma$ 1 recruitment as an important contributor to kinetic proofreading that might have actionable therapeutic implications by providing a means for enhancing T cell responses to weaker agonists against pathogens that elicit weak responses, or to weak agonist peptides displayed by tumors. However, a tradeoff might be the possibility of auto-reactivity. Interestingly, the LAT G131D mutation has a stronger effect than the G131E mutation in all of our data. Based on a previous study<sup>16</sup>, we speculate that a –1 aspartate residue is the optimal shape and charge to coordinate a series of lysine residues near the substrate-binding pocket. Extending the acidic side chain by an extra methyl group would slightly disrupt this geometry.

The presence of a glycine residue preceding human Y132 creates a very poor substrate for ZAP-70 (ref. 15). Although some fish have more optimal residues preceding their homologous site in LAT, it is

striking that almost all tetrapodal LAT molecules examined have a glycine at this position. This could be the result of a strong selective pressure that was more relaxed in fish. Interestingly, other tyrosine residues of LAT have been under strong selection pressure in tetrapods to become good ZAP-70 substrates. G131–Y132 is the only position that has become an evolutionarily conserved poor substrate for ZAP-70 in tetrapods, which might reflect the need for optimal ligand discrimination.

We therefore questioned why some fish have not adopted this same strategy for ligand discrimination. One major difference between tetrapods and fish is the maintenance of their body temperatures. Mammals are warm-blooded, whereas fish are cold-blooded, and the temperature of amphibians and reptiles can vary greatly depending on the environment. Various enzymes, including kinases, are sensitive to the temperature<sup>47,48</sup>. Thus, some fish may require a more optimal ZAP-70 substrate to phosphorylate their LAT Y132 homologous sequences to activate PLC $\gamma$ 1 when in cold water. Zebrafish T cells have a limited TCR repertoire, and they are more cross-reactive to self-antigens than are mammalian T cells<sup>30</sup>. This may be one strategy to compensate for their limited and self-cross-reactive TCR repertoire, but allow for protective T cell immunity to foreign antigens<sup>30</sup>. This increased self-reactivity of zebrafish T cells may be constrained by the prominence of regulatory T cells to prevent auto-reactivity. T and B cell-mediated adaptive immunity evolved approximately 500 million years ago,



with the emergence of jawed vertebrates<sup>49,50</sup>. Since then, different organisms may have adapted slight variations on this system, as our analyses suggest for LAT phosphorylation. More comparisons of the sequences and activities of T cell signaling molecules across the animal kingdom are likely to reveal new mechanisms for the control of T cell activation.

#### Online content

Any methods, additional references, Nature Research reporting summaries, source data, statements of code and data availability and associated accession codes are available at <https://doi.org/10.1038/s41590-019-0502-2>.

Received: 13 March 2019; Accepted: 20 August 2019;

Published online: 14 October 2019

#### References

- Feinerman, O., Germain, R. N. & Altan-Bonnet, G. Quantitative challenges in understanding ligand discrimination by  $\alpha\beta$  T cells. *Mol. Immunol.* **45**, 619–631 (2008).
- Brameshuber, M. et al. Monomeric TCRs drive T cell antigen recognition. *Nat. Immunol.* **19**, 487–496 (2018).
- Chakraborty, A. K. & Weiss, A. Insights into the initiation of TCR signaling. *Nat. Immunol.* **15**, 798–807 (2014).
- Huang, J. et al. A single peptide-major histocompatibility complex ligand triggers digital cytokine secretion in CD4<sup>+</sup> T cells. *Immunity* **39**, 846–857 (2013).
- Cui, W. & Mehta, P. Identifying feasible operating regimes for early T-cell recognition: the speed, energy, accuracy trade-off in kinetic proofreading and adaptive sorting. *PLoS One* **13**, e0202331 (2018).
- McKeithan, T. W. Kinetic proofreading in T-cell receptor signal transduction. *Proc. Natl Acad. Sci. USA* **92**, 5042–5046 (1995).
- Dustin, M. L. Stop and go traffic to tune T cell responses. *Immunity* **21**, 305–314 (2004).
- Lo, W. L. & Allen, P. M. Self-peptides in TCR repertoire selection and peripheral T cell function. *Curr. Top. Microbiol. Immunol.* **373**, 49–67 (2014).
- Siller-Farfan, J. A. & Dushkek, O. Molecular mechanisms of T cell sensitivity to antigen. *Immunol. Rev.* **285**, 194–205 (2018).
- Germain, R. N. Computational analysis of T cell receptor signaling and ligand discrimination—past, present, and future. *FEBS Lett.* **584**, 4814–4822 (2010).
- Gaud, G., Lesourne, R. & Love, P. E. Regulatory mechanisms in T cell receptor signalling. *Nat. Rev. Immunol.* **18**, 485–497 (2018).
- Courtney, A. H., Lo, W. L. & Weiss, A. TCR signaling: mechanisms of initiation and propagation. *Trends Biochem. Sci.* **43**, 108–123 (2018).
- Balagopalan, L., Kortum, R. L., Coussens, N. P., Barr, V. A. & Samelson, L. E. The linker for activation of T cells (LAT) signaling hub: from signaling complexes to microclusters. *J. Biol. Chem.* **290**, 26422–26429 (2015).
- Andreotti, A. H., Schwartzberg, P. L., Joseph, R. E. & Berg, L. J. T-cell signaling regulated by the Tec family kinase, Itk. *Cold Spring Harb. Perspect. Biol.* **2**, a002287 (2010).
- Shah, N. H. et al. An electrostatic selection mechanism controls sequential kinase signaling downstream of the T cell receptor. *Elife* **5**, e20105 (2016).
- Shah, N. H., Lobel, M., Weiss, A. & Kunyan, J. Fine-tuning of substrate preferences of the Src-family kinase Lck revealed through a high-throughput specificity screen. *Elife* **7**, e35190 (2018).
- Houtman, J. C., Houghtling, R. A., Barda-Saad, M., Toda, Y. & Samelson, L. E. Early phosphorylation kinetics of proteins involved in proximal TCR-mediated signaling pathways. *J. Immunol.* **175**, 2449–2458 (2005).
- Schoenborn, J. R., Tan, Y. X., Zhang, C., Shokat, K. M. & Weiss, A. Feedback circuits monitor and adjust basal Lck-dependent events in T cell receptor signaling. *Sci. Signal.* **4**, ra59 (2011).
- Zhang, W., Sloan-Lancaster, J., Kitchen, J., Tribble, R. P. & Samelson, L. E. LAT: the ZAP-70 tyrosine kinase substrate that links T cell receptor to cellular activation. *Cell* **92**, 83–92 (1998).
- Stoica, B. et al. The amino-terminal Src homology 2 domain of phospholipase C $\gamma$ 1 is essential for TCR-induced tyrosine phosphorylation of phospholipase C $\gamma$ 1. *J. Immunol.* **160**, 1059–1066 (1998).
- Songyang, Z. et al. SH2 domains recognize specific phosphopeptide sequences. *Cell* **72**, 767–778 (1993).
- Lo, W. L. et al. Lck promotes Zap70-dependent LAT phosphorylation by bridging Zap70 to LAT. *Nat. Immunol.* **19**, 733–741 (2018).
- Rosette, C. et al. The impact of duration versus extent of TCR occupancy on T cell activation: a revision of the kinetic proofreading model. *Immunity* **15**, 59–70 (2001).
- Hogquist, K. A. et al. T cell receptor antagonist peptides induce positive selection. *Cell* **76**, 17–27 (1994).
- Hogquist, K. A. et al. Identification of a naturally occurring ligand for thymic positive selection. *Immunity* **6**, 389–399 (1997).
- Stepanek, O. et al. Coreceptor scanning by the T cell receptor provides a mechanism for T cell tolerance. *Cell* **159**, 333–345 (2014).
- Sun, S., Zhang, X., Tough, D. F. & Sprent, J. Type I interferon-mediated stimulation of T cells by CpG DNA. *J. Exp. Med.* **188**, 2335–2342 (1998).
- Shen, S., Zhu, M., Lau, J., Chuck, M. & Zhang, W. The essential role of LAT in thymocyte development during transition from the double-positive to single-positive stage. *J. Immunol.* **182**, 5596–5604 (2009).
- Donnelly, M. L. et al. Analysis of the aphthovirus 2A/2B polyprotein ‘cleavage’ mechanism indicates not a proteolytic reaction, but a novel translational effect: a putative ribosomal ‘skip’. *J. Gen. Virol.* **82**, 1013–1025 (2001).
- Covacu, R. et al. System-wide analysis of the T cell response. *Cell Rep.* **14**, 2733–2744 (2016).
- Flajnik, M. F. A cold-blooded view of adaptive immunity. *Nat. Rev. Immunol.* **18**, 438–453 (2018).
- Conrad, M. L., Davis, W. C. & Koop, B. F. TCR and CD3 antibody cross-reactivity in 44 species. *Cytom. A* **71**, 925–933 (2007).
- Weiss, A., Shields, R., Newton, M., Manger, B. & Imboden, J. Ligand-receptor interactions required for commitment to the activation of the interleukin 2 gene. *J. Immunol.* **138**, 2169–2176 (1987).
- Weiss, A., Imboden, J., Shoback, D. & Stobo, J. Role of T3 surface molecules in human T-cell activation: T3-dependent activation results in an increase in cytoplasmic free calcium. *Proc. Natl Acad. Sci. USA* **81**, 4169–4173 (1984).
- Juang, J. et al. Peptide-MHC heterodimers show that thymic positive selection requires a more restricted set of self-peptides than negative selection. *J. Exp. Med.* **207**, 1223–1234 (2010).
- Bartelt, R. R. & Houtman, J. C. The adaptor protein LAT serves as an integration node for signaling pathways that drive T cell activation. *Wiley Interdiscip. Rev. Syst. Biol. Med.* **5**, 101–110 (2013).
- Houtman, J. C. et al. Binding specificity of multiprotein signaling complexes is determined by both cooperative interactions and affinity preferences. *Biochem. (Mosc.)* **43**, 4170–4178 (2004).
- Zhu, M., Janssen, E. & Zhang, W. Minimal requirement of tyrosine residues of linker for activation of T cells in TCR signaling and thymocyte development. *J. Immunol.* **170**, 325–333 (2003).
- Aguado, E. et al. Induction of T helper type 2 immunity by a point mutation in the LAT adaptor. *Science* **296**, 2036–2040 (2002).
- Sommers, C. L. et al. A LAT mutation that inhibits T cell development yet induces lymphoproliferation. *Science* **296**, 2040–2043 (2002).
- Kortum, R. L. et al. A phospholipase C- $\gamma$ 1-independent, RasGRP1-ERK-dependent pathway drives lymphoproliferative disease in linker for activation of T cells-Y136F mutant mice. *J. Immunol.* **190**, 147–158 (2013).
- Miyaji, M. et al. Genetic evidence for the role of Erk activation in a lymphoproliferative disease of mice. *Proc. Natl Acad. Sci. USA* **106**, 14502–14507 (2009).
- Lin, J. & Weiss, A. Identification of the minimal tyrosine residues required for linker for activation of T cell function. *J. Biol. Chem.* **276**, 29588–29595 (2001).
- Zhang, W. et al. Association of Grb2, Gads, and phospholipase C- $\gamma$ 1 with phosphorylated LAT tyrosine residues. Effect of LAT tyrosine mutations on T cell antigen receptor-mediated signaling. *J. Biol. Chem.* **275**, 23355–23361 (2000).
- Yousefi, O. S. et al. Optogenetic control shows that kinetic proofreading regulates the activity of the T cell receptor. *Elife* **8**, e42475 (2019).
- Tischer, D. K., . & Weiner, O. D. Light-based tuning of ligand half-life supports kinetic proofreading model of T cell signaling. *Elife* **8**, e42498 (2019).
- Tang, M. A., Motoshima, H. & Watanabe, K. Cold adaptation: structural and functional characterizations of psychrophilic and mesophilic acetate kinase. *Protein J.* **33**, 313–322 (2014).
- Saavedra, H. G., Wrabl, J. O., Anderson, J. A., Li, J. & Hilser, V. J. Dynamic allostery can drive cold adaptation in enzymes. *Nature* **558**, 324–328 (2018).
- Flajnik, M. F. & Kasahara, M. Origin and evolution of the adaptive immune system: genetic events and selective pressures. *Nat. Rev. Genet.* **11**, 47–59 (2010).
- Hirano, M., Das, S., Guo, P. & Cooper, M. D. The evolution of adaptive immunity in vertebrates. *Adv. Immunol.* **109**, 125–157 (2011).
- Pelosi, M. et al. Tyrosine 319 in the interdomain B of ZAP-70 is a binding site for the Src homology 2 domain of Lck. *J. Biol. Chem.* **274**, 14229–14237 (1999).
- Thill, P. A., Weiss, A. & Chakraborty, A. K. Phosphorylation of a tyrosine residue on Zap70 by Lck and its subsequent binding via an SH2 domain may be a key gatekeeper of T cell receptor signaling in vivo. *Mol. Cell. Biol.* **36**, 2396–2402 (2016).

53. Lo, W. L., Solomon, B. D., Donermeyer, D. L., Hsieh, C. S. & Allen, P. M. T cell immunodominance is dictated by the positively selecting self-peptide. *Elife* **3**, e01457 (2014).
54. Sayers, E. W. et al. Database resources of the National Center for Biotechnology Information. *Nucleic Acids Res.* **37**, D5–D15 (2009).

#### Acknowledgements

We thank A. Roque (University of California, San Francisco) for animal husbandry, S. Muratcioglu (University of California, Berkeley) for providing the GFP-labeled PLC- $\gamma$ 1 tandem N-SH2 protein, the NIH Tetramer Core Facility for providing the OVA and APL peptide-loaded H-2K<sup>b</sup> monomers or OVA-loaded H-2A<sup>b</sup> tetramers, the UCSF Parnassus Flow Cytometry Core for maintaining the BD FACSAria II, R. Mathieu (Boston Children's Hospital) and the BCH Department of Hematology/Oncology Flow Cytometry Research Facility for technical assistance, B. Au-Yeung (Emory University), P. Allen and D. Donermeyer (Washington University in St. Louis), and G. Morris and L.-F. Lu (University of California, San Diego) for critical feedback on the manuscript. The work was supported by the Jane Coffin Childs Fund 61–1560 (to W.-L.L.), the Damon Runyon Cancer Research Foundation DRG 2198-14 and DFS 31-18 (to N.H.S.), the Czech Science Foundation 19-03435Y (to O.S.), the Howard Hughes Medical Institute (to A.W. and J.K.) and NIH, NIAID P01 AI091580-06 (to A.W. and J.K.), 1R37AI114575 (to A.W.), and DRC Center Grant P30 DK063720 (UCSF Parnassus Flow Cytometry Core). All data to understand and access the conclusions of this study are available in the main text, the supplementary materials, and the indicated repositories.

#### Author contributions

W.-L.L., N.H.S., J.K., and A.W. were responsible for conceptualization; W.-L.L., N.H.S., S.A.R., L.I.Z., J.K., and A.W. were responsible for the methodology; W.-L.L., N.H.S., S.A.R., and I.R.F. carried out the investigations; W.-L.L., N.H.S., S.A.R., and A.W. wrote the original draft; W.-L.L., N.H.S., S.A.R., V.H., I.R.F., W.Z., O.S., L.I.Z., J.K., and A.W. reviewed and edited the manuscript; W.Z., V.H., and O.S. provided resources; L.I.Z., J.K., and A.W. supervised the study; and W.-L.L., N.H.S., W.Z., O.S., L.I.Z., J.K., and A.W. acquired funding.

#### Competing interests

The authors declare no competing interests.

#### Additional information

**Supplementary information** is available for this paper at <https://doi.org/10.1038/s41590-019-0502-2>.

**Correspondence and requests for materials** should be addressed to A.W.

**Peer review information** Laurie A. Dempsey was the primary editor on this article and managed its editorial process and peer review in collaboration with the rest of the editorial team.

**Reprints and permissions information** is available at [www.nature.com/reprints](http://www.nature.com/reprints).

**Publisher's note** Springer Nature remains neutral with regard to jurisdictional claims in published maps and institutional affiliations.

© The Author(s), under exclusive licence to Springer Nature America, Inc. 2019

## Methods

**Experimental models.** *Animals.* The C57BL/6 mice were housed in the specific pathogen-free facilities at the University of California, San Francisco. The ERCre<sup>+</sup>LAT<sup>fl</sup>:OT-1 mice were maintained at Duke University. Mice were treated according to protocols that were approved by University of California, San Francisco veterinary committees, or by Duke University animal care ethics committee, and are in accordance with National Institutes of Health (NIH) guidelines. Both male and female mice, 6–12 weeks of age, were used in the studies. Zebrafish were maintained in accordance with Boston Children's Hospital Institutional Animal Care and Use Committee protocols and in line with Animal Resources at Children's Hospital (ARCH) guidelines. Tg(*lck:eGFP*) was previously described<sup>35</sup>. Male and female zebrafish between 2 and 4 months post-fertilization were used in all studies.

**Cell lines.** The human leukemic Jurkat T cell line, Jurkat variants with LAT deficiency, ZAP-70 deficiency, or ITK deficiency, and T2-K<sup>o</sup> cells were maintained in RPMI culture medium supplemented (Thermo Fisher Scientific) with 5% FBS (Omega Scientific) and 2 mM glutamine (Thermo Fisher Scientific). For additional drug selection, LAT-deficient Jurkat variants that were reconstituted with wild-type LAT or various mutant LAT constructs were maintained in 0.5 mg ml<sup>-1</sup> of the aminoglycoside geneticin (G418, Santa Cruz Biotech), the Csk-AS Jurkat variant was maintained in 10 μg ml<sup>-1</sup> blasticidin (Thermo Fisher Scientific).

**Antibodies.** Antibodies are listed in Reporting Summary and Supplementary Note.

**Sequence alignments and analysis.** Sequences of LAT orthologs from various jawed vertebrates were identified as described previously<sup>36</sup>. Briefly, human LAT was used as a query sequence for an initial protein–protein BLAST search using the NCBI non-redundant protein database<sup>36,37</sup>. This initial search yielded mostly mammalian sequences, as well as a few fish, amphibian, and reptile sequences that were annotated to be LAT orthologs. These non-mammalian LAT sequences were used as queries in subsequent BLAST searches. Putative orthologous tyrosine phosphosites were identified in the C-terminal approximately 100 amino acids of each LAT sequence based on two criteria: they matched the SH2 binding motifs, and they occurred in the order seen for known human and mouse LAT phosphosites. The sequences surrounding individual putative phosphosites across all orthologs were manually aligned, and this local alignment was visualized using the online tool WebLogo<sup>38</sup>.

**LAT sequences of fish, birds, reptiles, and mammals.** The sequences are listed in Supplementary Table 1.

**Protein expression and purification, and in vitro phosphorylation assays.** Please see Supplementary Note.

**Generation of ZAP-70-deficient or ITK-deficient Jurkat variants.** The ZAP-70-deficient or ITK-deficient Jurkat variants were generated using CRISPR-Cas9 technology as previously described<sup>39</sup>. In brief, guide single guide RNAs (sgRNAs) against human ZAP70, or ITK coding regions were cloned into the pU6-(BbsI)-CBh-Cas9-T2A-BFP vector (Addgene, plasmid 64323), and electroporated into Jurkat T cells. The sgRNA sequences used in these studies were as follows: sgRNA nucleotide sequences against ZAP70: pair 1, 52-CACCGCATCGAGCAGGGCAAGCGGA-32 and 52-AAACTCCGCTTGCCCTGCTCGATGC-32; pair 2, 52-CACCGTTCGGGTGGACACTCTGGT-32 and 52-AAACACCAGAGTGTCACCCGAAC-32. sgRNA nucleotide sequences against ITK: pair 1, 52-CACC GATACCTTGAAGATCGTCATG-32 and 52-AAACATGACGATCTCAAAGTATC-32; pair 2, 52-CACCGAAGCGGACTTTAAAGTTCGA-32 and 52-AAACTCGAACCTTAAAGTCCGCTTC-32.

**Reconstituted LAT-deficient Jurkat with LAT mutants.** LAT-deficient Jurkat cells were generated in our previous study<sup>22</sup> and were used for reconstitution with pEF-vectors that express wild-type LAT, G131D, or G131E mutants by electroporation (Bio-Rad Laboratories).

**Intracellular calcium measurements.** Calcium mobilization was measured using a Flex Station II (Molecular Probes) as previously described<sup>22</sup>. More details can be also found in the Supplementary Note. In brief, 1 × 10<sup>7</sup> Jurkat variants were washed with PBS twice, and loaded with 1 μM Indo-1 AM calcium indicator dye (Thermo Fisher Scientific) individually at 37 °C for 30 min in 2 ml RPMI medium. 5 × 10<sup>5</sup> cells (100 μl) were washed twice again and transferred into individual wells in a flat-bottom 96-well plate. The temperature in the Flex Station II was set to 37 °C and each plate was incubated in the Flex Station II for 5 min before the experiment was started. The cells were first left unstimulated for 30 s to record basal levels of fluorescence intensities, followed by the addition of anti-CD3 (clone OKT3, Weiss Lab) at 30 s and the addition of ionomycin (Thermo Fisher Scientific) at a later time point as specified in corresponding figure legends, or incubated with 1:100 dilution of OVA- or APL-loaded biotinylated pMHC monomers (NIH Tetramer Core Facility) at 37 °C for 30 min in the pre-warmed Flex Station II. Indo-1 fluorescence ratios were recorded for 30 s to obtain the baseline relative

calcium levels, followed by the addition of streptavidin (10 μg ml<sup>-1</sup>, Jackson ImmunoResearch) at 30 s and this was followed by the addition of ionomycin (Thermo Fisher Scientific) at 240 s. Data were imported into GraphPad Prism software (version 7) for analysis and production of graphs.

**Jurkat variants stimulated by concanavalin A at different temperatures.** Jurkat variants were loaded with 1 μM of the Indo-1 calcium indicator dye at 25 °C for 30 min. After loading, cells were washed twice with PBS, resuspended in HBSS at a concentration of 5 × 10<sup>6</sup> cells per ml, and then transferred to a flat-bottom 96-well plate (5 × 10<sup>5</sup> cells per well) to record calcium-dependent fluorescence changes using the Flex Station II. The experiments started from a temperature of 25 °C, which gradually increased throughout the experiments up to 37 °C. Each time, after the temperature of the Flex Station II reached the pre-set temperature, the temperature was maintained for an extra few minutes before each experiment started. Concanavalin A was dissolved in double-distilled water at 10 mg ml<sup>-1</sup> as a stock solution, which was further diluted in PBS to prepare four working solutions (120 μg ml<sup>-1</sup>, 40 μg ml<sup>-1</sup>, 12 μg ml<sup>-1</sup>). The Indo-1 fluorescence changes were recorded for 30 s to obtain the baseline calcium level, followed by the addition of concanavalin A at 30 s, and the calcium-dependent fluorescence changes were recorded for another 4.5 min. Data were imported into GraphPad Prism software (version 7) for analysis and production of graphs.

**Intracellular calcium measurements by flow cytometry.** *Mouse CD8 T cells stimulated by OVA- or APL-loaded biotinylated pMHC monomers.* Naive OT-1<sup>+</sup> CD8 T cells were isolated and transduced with retrovirus expressing wild-type LAT-P2A-BFP or G135D LAT-P2A-BFP. Cells were loaded with 1 μM of the calcium indicator dye Indo-1 and 0.02% Pluronic F-127 (Thermo Fisher Scientific) at 37 °C in RPMI medium for 30 min, washed twice with PBS, and then labeled with 1:100 dilution of biotinylated OVA/H-2K<sup>b</sup>, T4/H-2K<sup>b</sup>, G4/H-2K<sup>b</sup>, or VSV/H-2K<sup>b</sup> monomers (NIH Tetramer Core Facility) at 37 °C for 30 min. Cells were then subjected to flow cytometry-based calcium assays. Indo-1 cell-associated fluorescence was first recorded for 30 s to obtain a baseline and then monitored after additions. Streptavidin (10 μg ml<sup>-1</sup>) was added at 30 s. Ionomycin was added at 240 s.

**Zebrafish thymocytes stimulated by concanavalin A at different temperatures.** Ice water immersion was used to euthanize the zebrafish before dissection of the thymus. Thymi were dissected from 15 or 16 zebrafish bilaterally into 800 μl of dissection solution: HBSS (no Ca<sup>2+</sup>, no Mg<sup>2+</sup>) with 0.2% FBS. After all of the thymi were collected, the solution was pipetted 15–20 times and filtered, followed by filtration through a pre-moistened 40 μm cell strainer. Next, the cells were centrifuged at 400 g for 5 min at 25 °C. The cell pellet was washed with 800 μl of dissection solution, centrifuged at 400 g for 5 min, and resuspended at 2.2 × 10<sup>6</sup> cells per ml in assay buffer (HBSS with Ca<sup>2+</sup> and Mg<sup>2+</sup>, 20 mM HEPES at pH 7.4). Indo-1-AM (Millipore Sigma) was pre-mixed 1:1 with Pluronic F-127 (Thermo Fisher Scientific) and added to the cell suspension at a final concentration of 1 μM Indo-1, 0.02% Pluronic F-127, and 0.18% DMSO, and vortexed immediately. After incubating in the dark for 30 min at 28.5 °C, the cells were washed twice with assay buffer, centrifuged at 400 g for 5 min at room temperature, and then resuspended at a final concentration between 1.6 × 10<sup>6</sup> and 3.5 × 10<sup>6</sup> cells per ml in assay buffer. The cells were incubated at 15 °C, 25 °C, and 37 °C using Eppendorf thermomixers (Eppendorf) for 10–15 min before running on an LSRFortessa (BD Biosciences). Baseline calcium-dependent fluorescence was determined over a 30 s interval before the addition of stimulus: concanavalin A (final concentration 10 μg ml<sup>-1</sup>, Millipore Sigma) followed by the addition of ionomycin at 240 s to a final concentration of 1 μM.

**Mouse thymocytes stimulated with concanavalin A at different temperatures.** Thymi from C57BL/6 mice were harvested and prepared as single cell suspension in RPMI. Cells were labeled with 1 μM Indo-1 at 37 °C for 30 min, washed twice with PBS, and then resuspended in HBSS at the concentration of 1 × 10<sup>7</sup> cells per ml. The cells were incubated at 37 °C in a water bath, at room temperature, or at 15 °C in a pre-cooled benchtop centrifuge for at least 15 min before the experiment started. The calcium-dependent Indo-1 fluorescence was recorded on an LSRFortessa (BD Biosciences). The fluorescence was first recorded for 30 s to obtain a baseline level, and then cells were stimulated with concanavalin A at 30 s, followed by stimulation with ionomycin at 240 s. The concanavalin A was purchased through the same vendor and lot number as the calcium experiments performed with zebrafish thymocytes.

**Immunoblot analysis.** Immunoblot analysis was performed as previously described<sup>22</sup> and more details could be found in the Supplementary Note.

**CD69 activation assay.** The J.OT-1.hCD8<sup>+</sup> or J.OT-1.hCD8neg series of Jurkat derivative cells expressing wild-type LAT or G131D or G131E variants were used in the experiments. A series of titrated concentrations of OVA or APL peptides was incubated with T2-K<sup>o</sup> cells (2.5 × 10<sup>6</sup> cells per well) in flat-bottom 96-well plates at 37 °C for 1 h. 2.5 × 10<sup>5</sup> cells of J.OT-1.hCD8<sup>+</sup> or J.OT-1.hCD8neg series of Jurkat derivative cells were added into each well of the 96-well plate that contained the

peptide-pulsed T2-K<sup>o</sup> cells. The plates were incubated at 37°C for around 16 h. For mouse OT-I<sup>+</sup> CD8 or OT-II<sup>+</sup> CD4 cells, cells were prepared and transduced to express wild-type or G135D LAT. Splenocytes from TCR  $\alpha$ -deficient mice were used as antigen-presenting cells.  $5 \times 10^5$  cells per well of TCR  $\alpha$ -deficient splenocytes were pulsed with titrated concentrations of OVA or APL peptides, and cultured with  $5 \times 10^5$  cells of the transduced mouse T cells at 37°C for around 16 h. Upregulation of CD69 was analyzed on an LSRFortessa (BD Biosciences) the next day.

**Phospho-ERK activation assay.** T2-K<sup>o</sup> cells ( $2.5 \times 10^5$  cells per well) were pulsed with titrated concentrations of OVA or APL peptides in U-bottom 96-well plates and incubated at 37°C for 1 h. Individual clones of Jurkat derivative cells were barcoded by labeling each clone with differently titrated concentrations of CellTrace Violet (Thermo Fisher Scientific). Jurkat derivative cells expressing wild-type LAT were labeled with 2.5  $\mu$ M CellTrace Violet in PBS at 37°C for 20 min in the dark, whereas G131D- or G131E-expressing cells were labeled with 0.1  $\mu$ M or 0.5  $\mu$ M of CellTrace Violet, respectively. Complete medium was then added to the cells for another 5 min of incubation at 37°C, and cells were washed with ice-cold PBS, resuspended in PBS to a concentration of  $2.5 \times 10^6$  cells per ml, and kept on ice.  $2.5 \times 10^5$  cells of the barcoded Jurkat derivatives were added into each well that contained the peptide-pulsed T2-K<sup>o</sup> cells. During the whole process the plates remained on ice. Cells were mixed well, and the plate was quickly centrifuged at 2,200 r.p.m. at 4°C for 30 s. The plate was then moved to a 37°C water bath for 5 min to start the stimulation. The stimulation was stopped by the direct addition of 4% formaldehyde (final concentration of 2%). The plate was incubated at 25°C for 30 min for formaldehyde fixation. Cells were washed once with FACS buffer (2% FBS, 1 mM EDTA in PBS buffer), and permeabilized in 90% ice-cold methanol overnight at 4°C. Cells were washed once with FACS buffer, rested in FACS buffer at 25°C for 30 min, and stained with anti-phospho-ERK (Cell Signaling Technology) for LSRFortessa analysis (BD Biosciences). For mouse T cells stimulated with OVA or APL-pulsed  $\alpha$ -deficient splenocytes, the procedures were similar to the experiments in Jurkat derivative cells, except that TCR  $\alpha$ -deficient splenocytes were used as antigen-presenting cells.

**IRF4 upregulation assay.** Mouse OT-I<sup>+</sup> CD8 or OT-II<sup>+</sup> CD4 cells were prepared and transduced to express wild-type or G135D LAT. Cells were rested for 1 d before being used in the experiments. Splenocytes from  $\alpha$ -deficient mice ( $2.5 \times 10^5$  cells per well) were mixed with titrated concentrations of OVA or APL peptides and mouse T cells, and incubated at 37°C for approximately 16 h at 37°C. Cells were washed once with FACS buffer (2% FBS, 1 mM EDTA in PBS buffer), stained for CD4 or CD8, washed in FACS buffer, and then fixed and permeabilized in eBioscience Transcription Factor Staining Buffer (Thermo Fisher Scientific). Cells were stained with anti-IRF4 (BioLegend) and analyzed by LSRFortessa (BD Biosciences).

**IFN- $\gamma$  secretion assay.** Mouse OT-I<sup>+</sup> CD8 or OT-II<sup>+</sup> CD4 cells were prepared and transduced to express wild-type or G135D LAT. A 48-well plate was coated with a 1:100 dilution of OVA- or APL-loaded biotinylated monomers the day before. Cells were washed and rested for 1 d in complete media without IL-2 before being used in the experiments. Cells were stimulated overnight at 37°C and harvested for IFN- $\gamma$  secretion analysis using an IFN- $\gamma$  secretion assay (Miltenyi Biotec) and assessed by LSRFortessa (BD Biosciences).

**Production of lentivirus or retrovirus expressing wild-type or G135D LAT.** Murine wild-type *Lat* was cloned into the pHR backbone under the expression of the *Efla* promoter. The murine G135D-LAT mutant was generated using a QuickChange Lightning site-directed mutagenesis kit (Agilent Technologies). A C-terminal P2A self-cleaving peptide followed by mCherry was incorporated to assess transduction efficiency and expression levels. Packaging vector pCMV dR8.91, envelope vector pMD 2.G, and pHR.WT-LAT.P2A.mCherry or pHR.G135D-LAT.P2A.mCherry constructs were transiently co-transfected into LX-293T cells using TransIT-LT1 reagent (Mirus Bio). Supernatants containing virus particles were collected 48 h after transfection, filtered, and concentrated by PEG 8000 precipitation. The virus particles were resuspended in PBS and stored at -80°C. For retrovirus-transduced experiments, murine WT-LAT or G135D-LAT were cloned into the pMSCV vectors individually, along with a C-terminal P2A self-cleaving peptide followed by BFP to help determine transduction efficiency

and monitor expression level. The Phoenix-Eco packaging cell line was transduced using Lipofectamine 2000 (Thermo Fisher Scientific). 48 h after transfection, the supernatants were harvested for experimental use. The viral supernatants were prepared freshly for each experiment.

**Retroviral transduction of mouse peripheral CD8 or CD4 T cells.** Naive mouse CD8 or CD4 T cells were isolated using biotinylated antibody cocktails (a mixture of anti-CD4 or anti-CD8, together with anti-CD19, anti-B220, anti-CD11b, anti-CD11c, anti-DX5, anti-TER119, and anti-CD24) and magnetic bead-mediated negative selection (anti-biotin Miltenyi iBeads, Miltenyi Biotec). The retroviral supernatants (prepared freshly for every experiment) were first mixed with Lipofectamine (final concentration of 8  $\mu$ g ml<sup>-1</sup>) and IL-2 (final concentration of 50 U ml<sup>-1</sup>), and incubated at 25°C for 20–30 min. In a 24-well plate,  $1 \times 10^6$  T cells were incubated with 1 ml retroviral supernatants, lipofectamine, and IL-2 per well. The plate was wrapped in saran wrap and centrifuged at 460 g for 1 h at 25°C. The plate was then moved to a 37°C incubator. BFP expression was monitored by LSRFortessa (BD Biosciences) and can be seen 24 h after transduction.

**Tamoxifen treatment and lentiviral transduction of mouse peripheral CD8<sup>+</sup> T cells.** CD8<sup>+</sup> T cells from spleens of ERCre<sup>+</sup>OT-I<sup>+</sup>LAT<sup>+</sup> mice were prepared, and naive CD44<sup>hi</sup>CD62L<sup>lo</sup>V $\alpha$ 2<sup>+</sup> CD8<sup>+</sup> cells were sorted using a FACSAria II (BD Biosciences). Naive CD8<sup>+</sup> T cells were cultured in a 24-well plate with 5  $\mu$ g ml<sup>-1</sup> plate-bound anti-CD3 (clone 2C11, Weiss Lab) and 5  $\mu$ g ml<sup>-1</sup> soluble anti-CD28 (clone 37.51, Weiss Lab) overnight at 37°C. A non-tissue culture-treated 24-well plate was coated with 3  $\mu$ g RetroNectin (Takara Bio) in 250  $\mu$ l PBS per well at 25°C for 2 h, blocked with 2% BSA at 25°C for 30 min, and then bound with concentrated lentivirus particles by centrifuging at 460 g for 1 h at 25°C and washed with PBS. The next day, activated CD8<sup>+</sup> T cells were added to the RetroNectin-coated, lentivirus-bound plates and centrifuged at 460 g for 5 min at 25°C, and incubated at 37°C overnight in the presence of mouse IL-2 (10 ng ml<sup>-1</sup>) and 50 nM 4-hydroxytamoxifen (Millipore Sigma) for 4 d. Tamoxifen-mediated deletion of endogenous LAT can be monitored by the expression of GFP, and the transduction efficiency can be monitored by the expression of mCherry. Cells were rested in the complete medium without IL-2 a day before being used in experiments.

**Quantification and statistical analysis.** Statistical analysis was applied to technical replicates, or biologically independent mice for each experiment. All experiments described in this study have been performed at least twice, and the exact numbers of independent experiments with similar results are indicated in the figure legends. All statistical analyses of experiments were performed using non-parametric, two-tailed Mann-Whitney U tests. GraphPad Prism 6 Software (GraphPad Software) was used for data analysis and representation. All bar graphs show means with overlaid scatter dots, or error bars (indicating s.d.), to show the distribution of the data, as indicated in each figure legend. *P* values for comparisons are provided as exact values or as *P* < 0.0001. 95% confident intervals were used to determine statistically significant *P* values.

**Reporting Summary.** Further information on research design is available in the Nature Research Reporting Summary linked to this article.

#### Data availability

Further information and requests for resources and reagents should be directed to, and will be fulfilled by, the corresponding author.

#### References

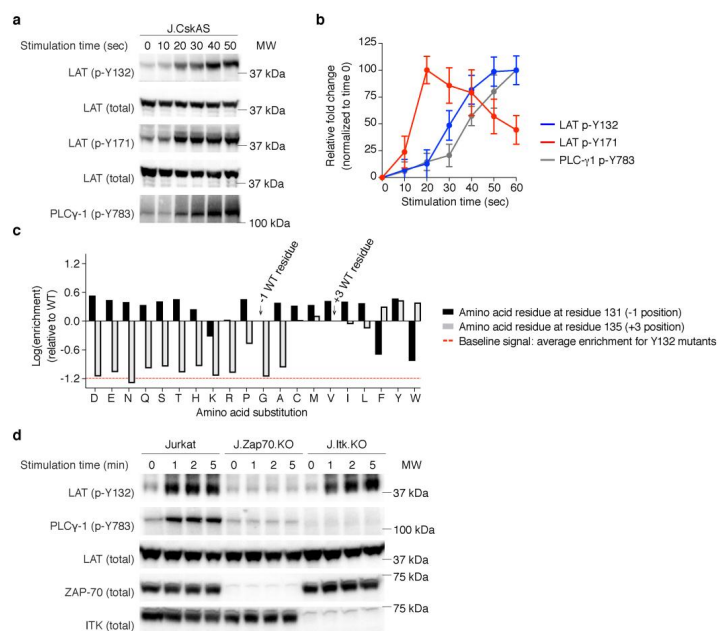
- Langenau, D. M. et al. In vivo tracking of T cell development, ablation, and engraftment in transgenic zebrafish. *Proc. Natl Acad. Sci. USA* **101**, 7369–7374 (2004).
- Altschul, S. F., Gish, W., Miller, W., Myers, E. W. & Lipman, D. J. Basic local alignment search tool. *J. Mol. Biol.* **215**, 403–410 (1990).
- Pruitt, K. D., Tatusova, T. & Maglott, D. R. NCBI Reference Sequence (RefSeq): a curated non-redundant sequence database of genomes, transcripts and proteins. *Nucleic Acids Res.* **33**, D501–D504 (2005).
- Crooks, G. E., Hon, G., Chandonia, J. M. & Brenner, S. E. WebLogo: a sequence logo generator. *Genome Res.* **14**, 1188–1190 (2004).

In the format provided by the authors and unedited.

## Slow phosphorylation of a tyrosine residue in LAT optimizes T cell ligand discrimination

Wan-Lin Lo<sup>1</sup>, Neel H. Shah<sup>2,10</sup>, Sara A. Rubin<sup>3,4</sup>, Weiguo Zhang<sup>5</sup>, Veronika Horkova<sup>6</sup>,  
Ian R. Fallahee<sup>2</sup>, Ondrej Stepanek<sup>6</sup>, Leonard I. Zon<sup>3,4,7</sup>, John Kuriyan<sup>2,8</sup> and Arthur Weiss<sup>1,9\*</sup>

<sup>1</sup>Division of Rheumatology, Rosalind Russell and Ephraim P. Engleman Arthritis Research Center, Department of Medicine, University of California, San Francisco, San Francisco, CA, USA. <sup>2</sup>Department of Molecular and Cell Biology, University of California, Berkeley, Berkeley, CA, USA. <sup>3</sup>Harvard Stem Cell Institute, Harvard University, Cambridge, MA, USA. <sup>4</sup>Stem Cell Program and Division of Hematology/Oncology, Boston Children's Hospital and Dana-Farber Cancer Institute; Program in Immunology, Harvard Medical School, Boston, MA, USA. <sup>5</sup>Department of Immunology, Duke University Medical Center, Durham, NC, USA. <sup>6</sup>Institute of Molecular Genetics of the Czech Academy of Sciences, Prague, Czech Republic. <sup>7</sup>Howard Hughes Medical Institute, Boston Children's Hospital and Harvard University, Boston, MA, USA. <sup>8</sup>Howard Hughes Medical Institute, University of California, Berkeley, Berkeley, CA, USA. <sup>9</sup>Howard Hughes Medical Institute, University of California, San Francisco, San Francisco, CA, USA. <sup>10</sup>Present address: Department of Chemistry, Columbia University, New York, NY, USA. \*e-mail: [art.weiss@ucsf.edu](mailto:art.weiss@ucsf.edu)



**Supplementary Figure 1**

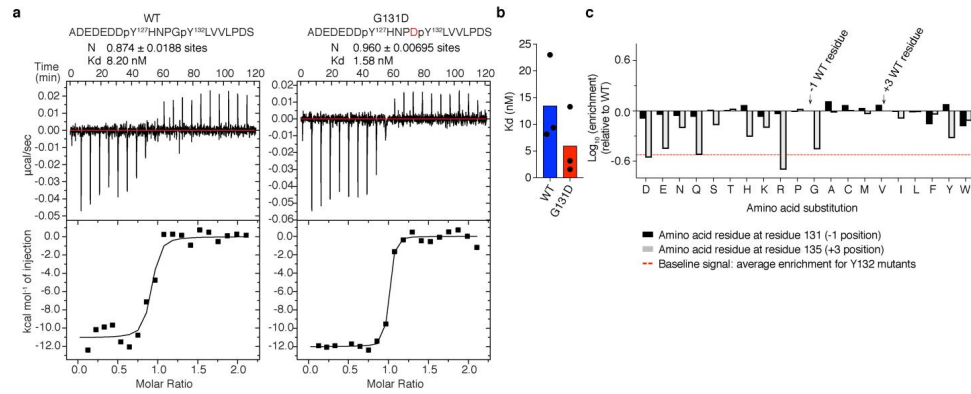
ZAP-70-mediated phosphorylation of LAT Y132 is a slow signal event.

**a.** J.CskAS Jurkat cells were treated with the PP1 analog, 3-iodo-benzyl-PP1, for various periods (sec) of time. Lysates were subjected to immunoblot analysis of p-Y171, p-Y132 of LAT or p-Y783 of PLC-γ1. Total LAT is used as a loading control. Note the same lysates were run on two separate gels to blot for p-Y171 and p-Y132.

**b.** The relevant bands in each immunoblot were quantified by Image Lab. The signal intensity was normalized to the 0 sec time point first and then further normalized as the fraction of maximal responses. The experiments were performed seven times. The brackets represent the standard deviation (mean ± s.d.; n = 7).

**c.** Representative bar graphs of phosphorylation of Y132 by ZAP-70. Data are derived from a high-throughput phosphorylation screen using the ZAP-70 kinase domain and a peptide library spanning LAT residues 120-139, in a Y127F background, as reported in previously (Shah et al., 2016). This subset of the data from the full screen shows the impact of every amino acid substitution at residues 131 (-1 position) and 135 (+3 position) on the ability of ZAP-70 to phosphorylate Y132. Data are shown on a log<sub>10</sub>-scale relative to the parent ("wild-type") sequence (glycine at 131 and valine at 135). A positive value indicates enhancement of phosphorylation relative to the parent sequence, a value close to zero indicates no impact on phosphorylation efficiency, and a negative value indicates that the substitution reduced the efficiency of phosphorylation. The screen shows that most -1 substitutions enhance phosphorylation by ZAP-70, relative to a -1 glycine, and that ZAP-70 strongly prefers to phosphorylate substrates with a +3 hydrophobic residue. The average effect of mutations at Y132 are shown by a red dotted horizontal line to demonstrate the magnitude of the most negatively-perturbing substitutions (i.e. the signal floor of the assay). This high-throughput screen was done once.

**d.** CRISPR-Cas9 was used to generate ZAP-70-deficient Jurkat cells (J.Zap70.KO) or ITK-deficient Jurkat cells (J.Itk.KO). Cells were stimulated with anti-TCR mAb (C305) at 37°C for a time course of 1, 2, or 5 min. Lysates were then subjected to immunoblot analysis as indicated. Data are representative of four independent experiments.



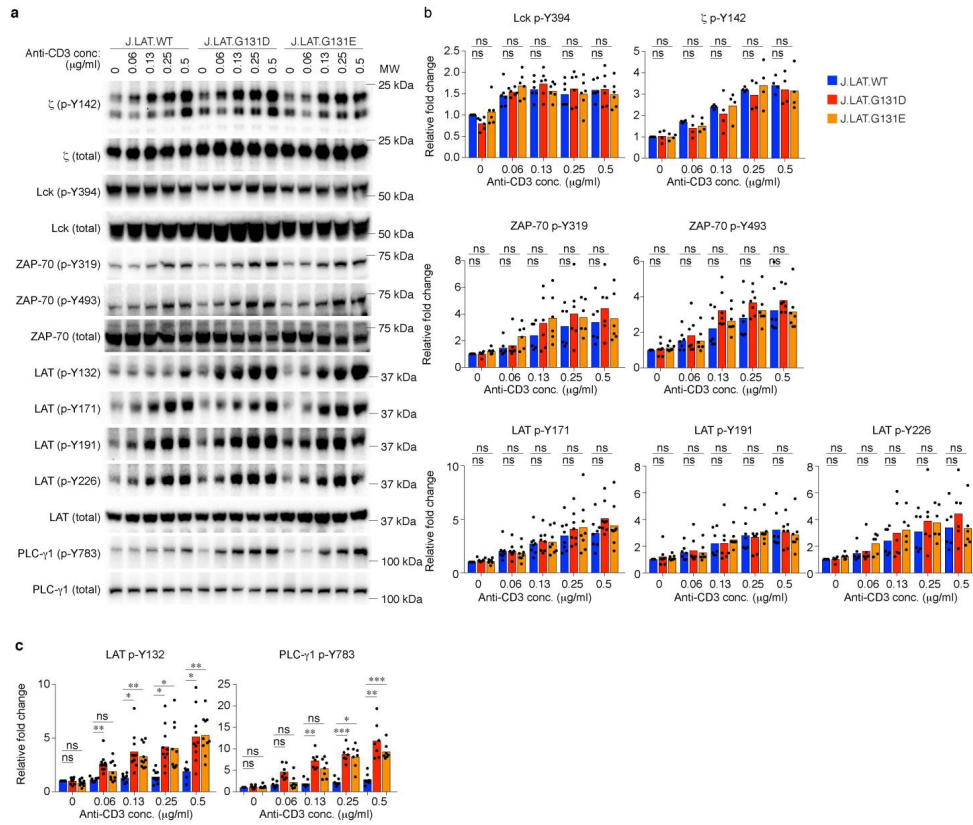
### Supplementary Figure 2

G131-p-Y132 exhibits comparable binding affinity to the PLC-γ1 N-SH2 domain as does a peptide with aspartate preceding p-Y132.

**a.** Graphs showing the raw data and binding isotherms from isothermal titration calorimetry for representative measurements of LAT p-Y132 peptides binding to the PLC-γ1 N-terminal SH2 domain. The calorimeter cell contained the SH2 domain at a concentration of 3 μM, and the peptide (30 μM) was delivered in 16 injections. Peptide sequences are given above the graphs.

**b.** Bar graph showing the mean binding affinities from three independent experiments as in (a). Each symbol represents one independent experimental result. ns, not significant; two-tailed Mann-Whitney test. The center values presented the mean.

**c.** Data derived from a high-throughput binding screen using the PLC-γ1 N-terminal SH2 domain and a phospho-peptide library containing all single point mutations in LAT residues 120-139, in a Y127F background and with a phosphorylated Y132 residue. This subset of the data from the full screen shows the impact of every amino acid substitution at residues 131 (-1 position) and 135 (+3 position) on the ability of the PLC-γ1 N-terminal SH2 domain to bind to p-Y132. Data are shown on a log<sub>10</sub>-scale relative to the parent ("wild-type") sequence. A positive value indicates enhancement in binding relative to the parent sequence, a value close to zero indicates no impact on binding affinity, and a negative value indicates that the substitution reduced the binding affinity. The average effect of mutations at Y132 is shown by a red dotted horizontal line to demonstrate the magnitude of the most negatively-perturbing substitutions (*i.e.* the signal floor of the assay). The screen shows that binding to the PLC-γ1 N-terminal SH2 domain is largely unaffected by the identity of the -1 residue, whereas it has a strong preference for hydrophobic residues at the +3 position, as described previously (Songyang et al., 1995). This high-throughput screen was done once.



**Supplementary Figure 3**

G131D or E does not impact activation of ZAP-70 and Lck.

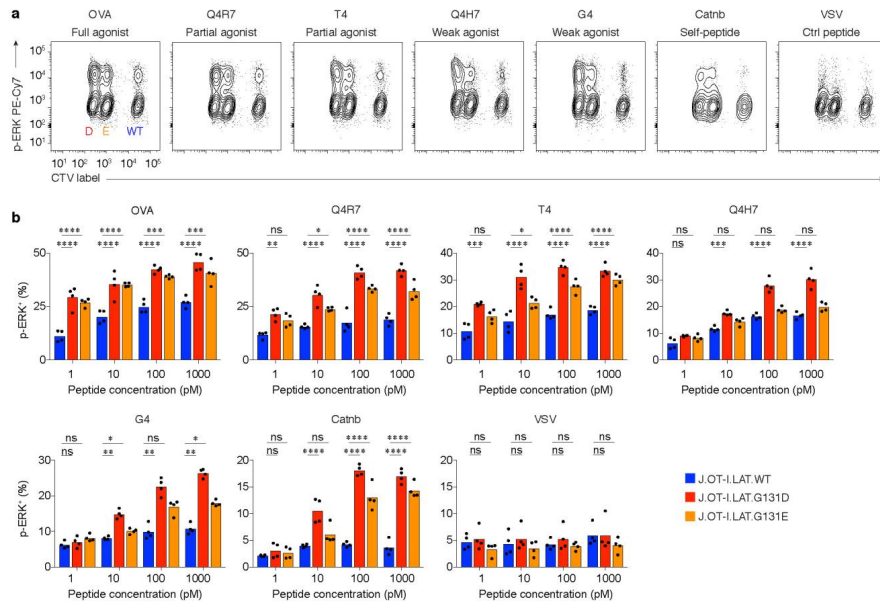
**a.** Immunoblot analysis of J.LAT.WT, J.LAT.G131D, or J.LAT.G131E cells stimulated with a range of titrated anti-CD3 for one minute at 37°C. Lysates were prepared and run on 12% NuPage Bis-Tris protein gels, and subjected to immunoblot analysis with various anti-pY or anti-total protein as indicated. Data are representative of at least six independent experiments.

**b.** Bar graphs depicting the fold change of phospho-tyrosines of specific proteins (as indicated) of J.LAT.WT, J.LAT.G131D, or J.LAT.G131E cells following stimulation with titrated concentrations of anti-CD3. Each symbol represents the analysis of one experiment. The lines above the bar graphs represent the significance of standard deviations (mean; n = 6 for Lck p-Y394, ZAP-70 p-Y319, LAT p-Y191, LAT p-Y226; n = 7 for ZAP-70 Y493; n = 8 for LAT p-Y171; n = 4 for ζ p-Y142). ns = not significant. For Lck p-Y394, WT vs D from left to right:  $P = 0.2751$ ;  $P = 0.9989$ ;  $P = 0.9923$ ;  $P = 0.9933$ ;  $P > 0.9999$ ; WT vs E from left to right:  $P > 0.9999$ ;  $P = 0.9847$ ;  $P = 0.9565$ ;  $P = 0.9933$ ;  $P > 0.9999$ ;  $P = 0.9987$ ; For ζ p-Y142, WT vs D from left to right:  $P > 0.9999$ ;  $P = 0.9378$ ;  $P = 0.9988$ ;  $P = 0.9996$ ;  $P = 0.9932$ ; WT vs E from left to right:  $P > 0.9999$ ;  $P = 0.9119$ ;  $P > 0.9999$ ;  $P > 0.9999$ ;  $P > 0.9999$ ; For ZAP-70 p-Y319, WT vs D from left to right:  $P > 0.9999$ ;  $P = 0.9958$ ;  $P = 0.7575$ ;  $P = 0.6990$ ;  $P = 0.1022$ ; WT vs E from left to right:  $P = 0.5233$ ;  $P = 0.5144$ ;  $P = 0.4558$ ;  $P = 0.3149$ ;  $P = 0.9968$ ; For ZAP-70 p-Y493, WT vs D from left to right:  $P > 0.9999$ ;  $P = 0.9180$ ;  $P = 0.4685$ ;  $P = 0.3701$ ;  $P = 0.9789$ ; WT vs E from left to right:  $P = 0.8176$ ;  $P > 0.9999$ ;  $P = 0.9429$ ;  $P = 0.7203$ ;  $P > 0.9999$ ; For LAT p-Y171, WT vs D



from left to right:  $P = 0.2263$ ;  $P > 0.9999$ ;  $P = 0.9997$ ;  $P = 0.9986$ ;  $P = 0.7571$ ; WT vs E from left to right:  $P = 0.9852$ ;  $P = 0.9801$ ;  $P > 0.9999$ ;  $P = 0.9994$ ;  $P = 0.9983$ ; For LAT p-Y191, WT vs D, from left to right:  $P = 0.9995$ ;  $P = 0.6763$ ;  $P = 0.9994$ ;  $P = 0.9999$ ;  $P > 0.9999$ ; WT vs E, from left to right:  $P = 0.9998$ ;  $P = 0.9996$ ;  $P > 0.9999$ ;  $P = 0.9998$ ;  $P = 0.9998$ ; For LAT p-Y226, WT vs D, from left to right:  $P > 0.9999$ ;  $P = 0.9984$ ;  $P > 0.9999$ ;  $P > 0.9999$ ;  $P = 0.9869$ ; WT vs E, from left to right:  $P = 0.3200$ ;  $P = 0.9887$ ;  $P = 0.9985$ ;  $P > 0.9999$ ;  $P > 0.9999$ . One-way ANOVA test.

c. Bar graphs depicting the fold change of LAT p-Y132 or PLC- $\gamma$ 1 p-Y783 of J.LAT.WT, J.LAT.G131D, or J.LAT.G131E cells following stimulation with titrated concentrations of anti-CD3. The relevant bands in each immunoblot were quantified by Image Lab. The signal intensity of LAT p-Y132 or PLC- $\gamma$ 1 p-Y783 was normalized to the total protein (LAT or PLC- $\gamma$ 1) first and then normalized to the 0 sec time point of J.LAT.WT cells' response. The experiments were performed at least six times. Each symbol represents the analysis of one experiment. The lines above the bar graphs represent the significance of the standard deviations (mean  $n = 10$  for LAT p-Y132;  $n = 7$  for PLC- $\gamma$ 1 p-Y783). For LAT p-Y132 statistical analysis: \*\* $P = 0.0098$  (WT vs D at 0.06  $\mu\text{g/ml}$ ); \* $P = 0.0305$  (WT vs D at 0.13  $\mu\text{g/ml}$ ); \* $P = 0.0121$  (WT vs D at 0.25  $\mu\text{g/ml}$ ); \* $P = 0.0359$  (WT vs D at 0.5  $\mu\text{g/ml}$ ); \*\* $P = 0.0036$  (WT vs E at 0.06  $\mu\text{g/ml}$ ); \* $P = 0.0420$  (WT vs E at 0.13  $\mu\text{g/ml}$ ); \*\* $P = 0.0022$  (WT vs E at 0.5  $\mu\text{g/ml}$ ); ns = not significant:  $P > 0.9999$  (WT vs D at 0  $\mu\text{g/ml}$ );  $P = 0.8161$  (WT vs E at 0  $\mu\text{g/ml}$ );  $P = 0.2517$  (WT vs E at 0.06  $\mu\text{g/ml}$ ). For PLC- $\gamma$ 1 p-Y783 statistical analysis: \*\* $P = 0.00206$  (WT vs D at 0.13  $\mu\text{g/ml}$ ); \*\*\* $P = 0.0005$  (WT vs D at 0.25  $\mu\text{g/ml}$ ); \* $P = 0.0305$  (WT vs D at 0.5  $\mu\text{g/ml}$ ); \* $P = 0.0483$  (WT vs E at 0.25  $\mu\text{g/ml}$ ); \*\*\* $P = 0.0026$  (WT vs E at 0.5  $\mu\text{g/ml}$ ); ns = not significant:  $P > 0.9999$  (WT vs D at 0  $\mu\text{g/ml}$ );  $P > 0.9999$  (WT vs E at 0  $\mu\text{g/ml}$ );  $P = 0.2593$  (WT vs D at 0.06  $\mu\text{g/ml}$ );  $P > 0.9999$  (WT vs E at 0.06  $\mu\text{g/ml}$ );  $P = 0.2843$  (WT vs E at 0.13  $\mu\text{g/ml}$ ); One-way ANOVA test.

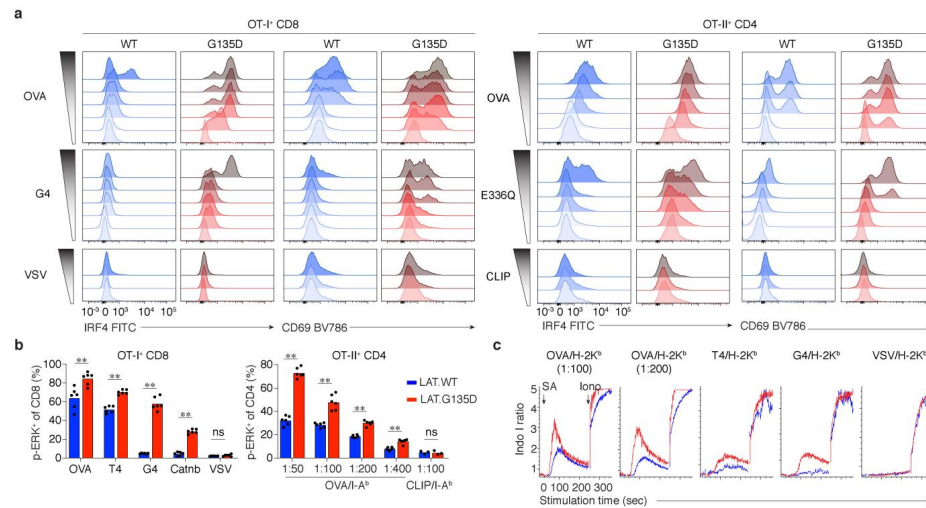


**Supplementary Figure 4**

The expression of G131D or E promotes the activation of ERK in response to weak OVA APL stimulation

**a.** Representative contour plot of ERK phosphorylation of G131D (left population), G131E (middle population), or WT LAT (right population) expressing J.OT-I<sup>h</sup>CD8<sup>+</sup> Jurkat variants as in Fig. 4a,b. Ligands used for stimulation are indicated above the plots.

**b.** Bar graphs depicting the percent of p-ERK<sup>+</sup> cells as shown in Fig. 4b,c. The percent of p-ERK<sup>+</sup> cells at peptide concentration at 1000 pM represents the gated population in Fig. 4b. Each symbol represents one experiment (n = 4). Data are compiled from four independent experiments. The statistical analysis for cells stimulated with OVA peptide: \*\*\*P = 0.0001 (WT vs E at 100 pM); \*\*\*P = 0.0002 (WT vs E at 1000 pM); \*\*\*\*P = <0.0001. For cells stimulated with Q4R7 peptide: \*P = 0.0159; \*\*P = 0.0019; \*\*\*\*P = <0.0001; ns, not significant P = 0.0838. For cells stimulated with T4 peptide: \*P = 0.0298; \*\*\*P = 0.001; \*\*\*\*P = <0.0001; ns, not significant P = 0.1385. For cells stimulated with Q4H7 peptide: \*\*\*P = 0.0009; \*\*\*\*P = <0.0001; ns, not significant P = 0.4285 (WT vs D at 1 pM); P = 0.8305 (WT vs E at 1 pM); P = 0.4731 (WT vs E at 10 pM); P = 0.6343 (WT vs E at 100 pM); P = 0.2393 (WT vs E at 1000 pM); For cells stimulated with G4: \*\*P = 0.0035 (WT vs D at 10 pM); \*\*P = 0.0048 (WT vs D at 100 pM); \*\*P = 0.0030 (WT vs D at 1000 pM); \*P = 0.0192 (WT vs E at 10 pM); \*P = 0.0358 (WT vs E at 1000 pM); ns, not significant: P = 0.9978 (WT vs D at 1 pM); P = 0.2937 (WT vs E at 1 pM); P = 0.3008 (WT vs E at 100 pM). For cells stimulated with Catnb peptide: \*\*\*\*P = <0.0001; ns, not significant P = 0.9967 (WT vs D at 1 pM); P > 0.9999 (WT vs E at 1 pM); P = 0.6354 (WT vs E at 10 pM). For cells stimulated with VSV peptide: ns, not significant: P > 0.9999 (WT vs D at 1 pM); P = 0.8635 (WT vs D at 10 pM); P = 0.9991 (WT vs D at 100 pM); P > 0.9999 (WT vs D at 1000 pM); P = 0.9658 (WT vs E at 1 pM); P > 0.9999 (WT vs E at 10 pM); P = 0.9998 (WT vs E at 100 pM); P = 0.9688 (WT vs E at 1000 pM); One-way ANOVA test.



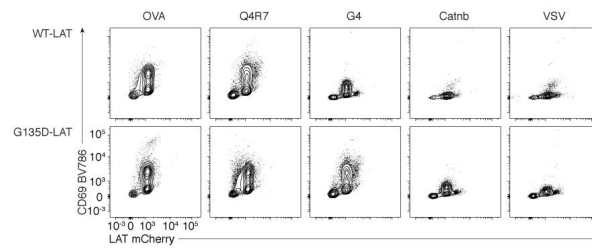
### Supplementary Figure 5

Substitution of G135D in LAT enables the activation of T cells by low affinity antigen in a gain-of-function manner.

**a.** Naive OT-I<sup>+</sup> CD8 T cells (left panels) were isolated and transduced with retrovirus expressing wild-type LAT-P2A-BFP or G135D LAT-P2A-BFP. Cells were rested for one day before they were subjected to stimulation with various peptides-pulsed TCR C $\alpha$ -deficient splenocytes over a range of peptide concentrations (10  $\mu$ M, 3  $\mu$ M, 1  $\mu$ M, 0.3  $\mu$ M, 0.1  $\mu$ M, 0  $\mu$ M for OVA or G4 peptide; 10  $\mu$ M, 1  $\mu$ M, 0  $\mu$ M for VSV peptide). Or, naive OT-II<sup>+</sup> CD4 T cells were used for experiments. OT-II<sup>+</sup> CD4 T cells were stimulated with agonist OVA- or partial agonist E336Q-pulsed splenocytes overnight (10  $\mu$ M, 3  $\mu$ M, 1  $\mu$ M, 0.1  $\mu$ M, 0  $\mu$ M for OVA or E336Q peptide; 10  $\mu$ M, 1  $\mu$ M, 0  $\mu$ M for CLIP peptide). Representative histograms are shown. Peptides used for stimulation are indicated at the left. The expression of IRF4 or CD69 was analyzed. Data are representative of three independent experiments.

**b.** Statistical analysis of p-ERK activation for OT-I<sup>+</sup> CD8 T cells (left) or OT-II<sup>+</sup> CD4 T cells (right) as experiments done in (a). TCR C $\alpha$ -deficient splenocytes were pulsed with 1  $\mu$ M of OVA, T4, or G4 peptide, 10  $\mu$ M of Catnb peptide or 10  $\mu$ M of VSV peptide. Each symbol represents an independent replicate (mean  $\pm$  s.d.). \*\* $P$  = 0.0043 (OVA); \*\* $P$  = 0.0022 (T4, G4, Catnb); ns: not significant  $P$  = 0.3095. Mann-Whitney test. Statistical analysis of p-ERK induction of OT-II<sup>+</sup> T cells was shown on right. Each symbol represents an independent replicate ( $n$ =6 samples from two independent experiments). \*\* $P$  = 0.0022; ns: not significant  $P$  > 0.9999. Two-tailed Mann-Whitney test.

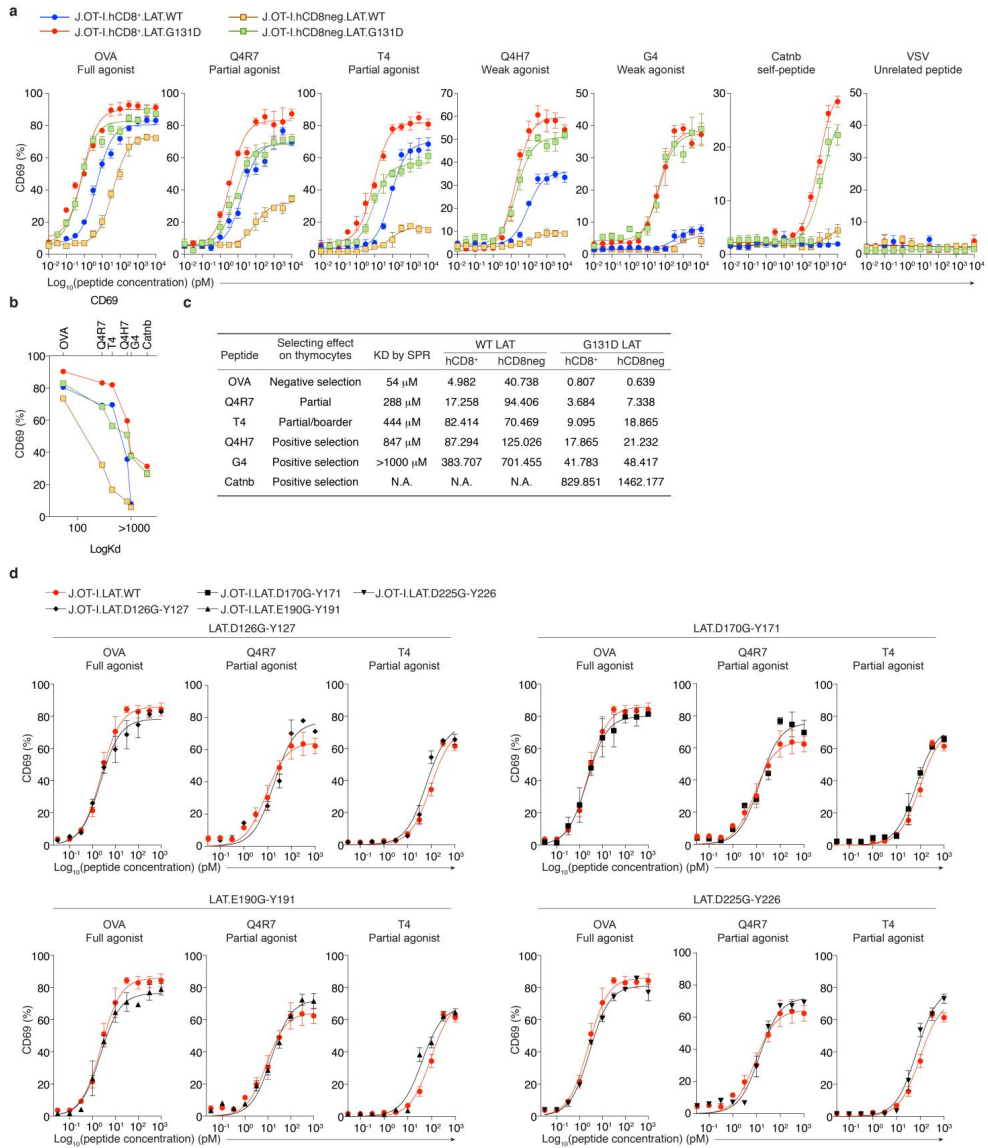
**c.** Cells were prepared as in (a) to retrovirally express wild-type LAT-P2A-BFP or G135D LAT-P2A-BFP, loaded with the calcium-sensitive dye Indo-1, and incubated with 1:100 or 1:200 biotinylated OVA/H-2K<sup>b</sup>, or 1:100 T4/H-2K<sup>b</sup>, G4/H-2K<sup>b</sup>, or VSV/H-2K<sup>b</sup> monomers. Cells were then moved to 37°C and subjected to flow cytometry-based calcium assays. Cells were first recorded for 30 sec to obtain a baseline calcium level. Streptavidin (SA) was added at the 30th sec. Ionomycin (Iono) was added at the 240th sec. Representative calcium traces are shown. Monomers used for stimulation are indicated above the calcium plots. Data are representative of two independent experiments.



**Supplementary Figure 6**

Peripheral T cells ectopically expressing the mutant G135D LAT exhibit a lower responsive threshold while stimulated with weak ligands or self-peptides.

Flow cytometric analysis of CD69 upregulation and mCherry expression in GFP<sup>+</sup>Vα2<sup>+</sup>CD8<sup>+</sup> T cells after stimulation with different peptide-pulsed splenocytes (as indicated on top of the contour plots) as in **Fig. 5**. The GFP<sup>+</sup> mCherry-negative population did not express the transduced LAT and, thus, did not respond to peptide stimulation. Data are representative of three experiments.



Supplementary Figure 7

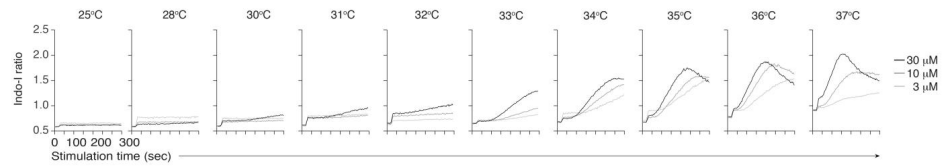
T cell ligand discrimination is preferentially regulated at LAT Y132.

**a.** CD8-negative or positive LAT-deficient J.OT-I<sup>+</sup> Jurkat variants were reconstituted with wild-type LAT or G131D LAT (J.OT-I<sup>+</sup>.hCD8neg.LAT.WT, J.OT-I<sup>+</sup>.hCD8neg.LAT.G131D, J.OT-I<sup>+</sup>.hCD8<sup>+</sup>.LAT.WT, or J.OT-I<sup>+</sup>.hCD8<sup>+</sup>.LAT.G131D). Cells were stimulated with T2-K<sup>D</sup> antigen-presenting cells pulsed with OVA peptide, OVA APL peptides, self-peptide Catnb, or VSV control peptide over a wide range of peptide concentrations as in Fig. 3. The percentage of cells that are CD69<sup>+</sup> is plotted against peptide concentration (mean  $\pm$  s.d; n = 3 technical replicates). Data are representative of three experiments.

**b.** Statistical analysis of CD69 upregulation as in (a) with the stimulation of 10 nM of each peptide (mean; n = 3 technical replicates). Data are representative of three experiments.

**c.** LogEC50 analysis of CD69 induction assays as in (a).

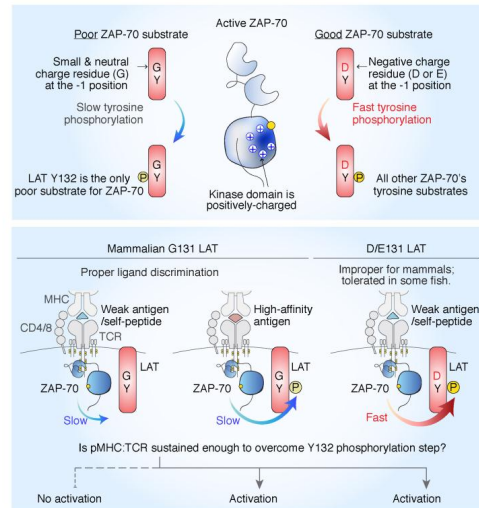
**d.** LAT-deficient J.OT-I<sup>+</sup> hCD8<sup>+</sup> Jurkat variants were reconstituted with wild-type LAT or D126G-Y127, D170G-Y171, E190G-Y191, or D225G-Y226 LAT. Cells were subjected to CD69 induction assays as in (a). The percentage of cells that are CD69<sup>+</sup> is plotted against peptide concentration (mean  $\pm$  s.d; n = 3 technical replicates). Data are representative of two experiments.



### Supplementary Figure 8

Temperature effect on mouse thymocyte calcium responses.

Con A-induced calcium responses in  $5 \times 10^5$  mouse thymocytes per well in a 96 well plate. The cells were loaded with the calcium-sensitive dye Indo-1 at room temperature, washed and rested, and then used to record calcium responses using a Flex Station II. Indo-1 loaded cells were first analyzed for 30 sec to obtain the baseline ratio of bound to unbound calcium, and then stimulated with various concentrations of Con A (as color-coded; treatment was added at the 30th sec) for 5 min at various temperatures. Representative calcium traces are shown. Data are representative of two independent experiments.



**Supplementary Figure 9**

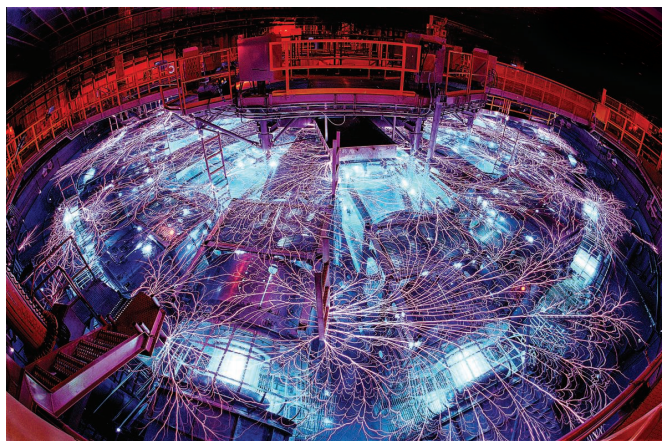
Schematic summary depicting the role of LAT residue 131 in controlling T cell signaling.

The top panel builds upon structural and biochemical analyses of ZAP-70 substrate recognition, which revealed that G131 in human LAT attenuates the rate of Y132 phosphorylation relative to that of other tyrosine phosphorylation events on LAT. The bottom panel depicts the implication for T cell ligand selectivity of the naturally slow Y132 phosphorylation found in mammalian T cells relative to more efficient Y132 phosphorylation in G131D/E mutant T cells and some fish T cells. The G131D mutation facilitates Y132 phosphorylation but also promotes self-reactivity. Mammals use G131 to attenuate Y132 phosphorylation for better ligand discrimination. Our results raise the possibility that some fish may utilize different LAT phosphorylation kinetics than most jawed vertebrates to alter the T cell activation threshold and achieve immune-fitness advantages in their environments for better T cell ligand discrimination.



## **Attachment 8**

A LoCK at the T cell Dock



The Z pulsed-power facility used for calibrating terapascal pressures has a diameter of 37 m.

essential for comparing the different laboratory measurements, all the more so because the samples are probed over different temperatures and time scales by the different high-pressure methods. Fratanduono *et al.*'s pressure-volume measurements using both pulsed-power and laser-driven compression show that the two technologies, which can differ by an order of magnitude or more in sample dimensions and compression time, are in good agreement with each other (3). They also find general accord with diamond-cell reports but are able to provide improvements for the necessarily extrapolated calibrations of past experiments.

It is both reassuring and impressive that measurements made over time scales spanning 12 orders of magnitude, from  $10^{-8}$  s for laser-driven compression to  $10^4$  s or more for static high-pressure experiments, are in such good agreement with each other. Calibration allows completely independent experiments to be compared and even combined, not only validating but also substantially enhancing results because each method has its advantages and drawbacks. Short duration in the dynamic measurements invites nonequilibrium effects, whereas small samples and large stress gradients in the static experiments challenge reproducibility and quantification.

One of the key reasons that robust calibration is essential is that these experiments provide tests of first-principles quantum mechanical calculations of material properties. To be clear, theory and experiment are closely symbiotic, with the laboratory work being guided by quantum calculations, which also help in the interpretation and application of the experimental results. At the same time,

experiments provide important validation for theory, and discrepancies between theory and experiment help guide improvements in both. Working at extreme conditions, the community is moving toward more reliable predictions of material properties and phase stability at ambient conditions, advancing technology as well as fundamental understanding. The work also helps us to better understand planets, the platforms on which life can establish itself and evolve. ■

#### REFERENCES AND NOTES

1. One terapascal corresponds to 10 million atmospheres pressure.
2. R. Jeanloz *et al.*, *Proc. Natl. Acad. Sci. U.S.A.* **104**, 9172 (2007).
3. D. E. Fratanduono *et al.*, *Science* **372**, 1063 (2021).
4. One electron volt = 96.5 kJ/mol.
5. Y. Ma *et al.*, *Nature* **458**, 182 (2009).
6. The electron-charge density becomes concentrated between the sodium ion cores at high pressure, so that the metal effectively transforms into a "salt" of Na<sup>+</sup> cations bound to e<sup>-</sup> anions of increased charge density but without a nucleus.
7. Hartree's atomic unit of energy,  $E_h = \hbar^2 / (m a_0^2) = 27$  eV, is the potential energy drawing the electron to the nucleus in the Bohr atom, and the unit of pressure is simply the energy density  $E_h / a_0^3$  derived on dimensional grounds.
8. M. Miao, Y. Sun, E. Zurek, H. Lin, *Nat. Rev. Chem.* **4**, 508 (2020).
9. C. J. Pickard, R. J. Needs, *J. Phys. Condens. Matter* **21**, 452205 (2009).
10. L. Stixrude, *Phys. Rev. Lett.* **108**, 055505 (2012).
11. J. E. McMahon, M. A. Morales, C. Pierleoni, D. M. Ceperley, *Rev. Mod. Phys.* **84**, 1607 (2012).
12. N. Dubrovinskaia *et al.*, *Sci. Adv.* **2**, e1600341 (2016).
13. E. Snider *et al.*, *Nature* **586**, 373 (2020).
14. R. F. Smith *et al.*, *Nature* **511**, 330 (2014).
15. A. L. Kritcher *et al.*, *Nature* **584**, 51 (2020).

#### ACKNOWLEDGMENTS

I have benefitted from discussions with G. W. Collins, D. E. Fratanduono, N. Y. Yao, and E. Zurek. This work was supported by the National Nuclear Security Administration Center for Matter under Extreme Conditions and the National Science Foundation Physics Frontier Center for Matter at Atomic Pressure.

10.1126/science.abi8015

#### IMMUNOLOGY

## A LoCK at the T cell dock

Topology of T cell receptor-antigen binding constrains T cell activation

By Veronika Horkova and Ondrej Stepanek

The stimulation of T cells with foreign or self-antigens plays a central role in the adaptive immune responses to infection and cancer but also in autoimmunity. T cells use a sophisticated molecular machinery to recognize and respond to cognate antigens. On page 1056 of this issue, Zareie *et al.* (1) examine the productive and unproductive engagement of the T cell receptor (TCR) with antigens by focusing on binding orientation. The polarity of the interaction affects recruitment of key signaling molecules to the TCR. This topology thus constrains T cell immune responses.

Most immune receptors are encoded in the germline DNA. Evolution fine-tuned them to recognize germline-encoded endogenous ligands (such as cytokines, secreted immunoregulatory proteins) or conserved exogenous ligands (such as bacterial products). By contrast, genes encoding the TCR and B cell receptor (BCR) are rearranged in each lymphocyte independently. Clonal selection of lymphocytes during maturation and in the immune response mimics the evolutionary adaptations on a scale of an individual organism.

Whereas the BCR recognizes the antigen directly, a canonical TCR recognizes an antigenic peptide fragment presented by the major histocompatibility complex (MHC) on the surface of a host cell. Therefore, the TCR ligand consists of a germline-encoded component (MHC) and a highly variable antigen (peptide). This bivalent character stirred debate about whether peptide-MHC (pMHC) recognition is determined by inherent properties of the germline-encoded segments of the TCR or by the selection processes during T cell development (2). There is a clear germline bias of the TCR repertoire toward MHC recognition that is manifested by a relatively high percentage of self-pMHC-specific TCRs in the preselection repertoire

Laboratory of Adaptive Immunity, Institute of Molecular Genetics of the Czech Academy of Sciences, 14220 Prague, Czech Republic. Email: ondrej.stepanek@img.cas.cz

Downloaded from <http://science.sciencemag.org/> on June 4, 2021

PHOTO: MONIKAR/REUTERS/IMAGINATION

(3, 4). Yet the majority of developing T cells do not recognize self-pMHC, indicating a role for T cell selection in shaping the self-MHC-restricted TCR repertoire.

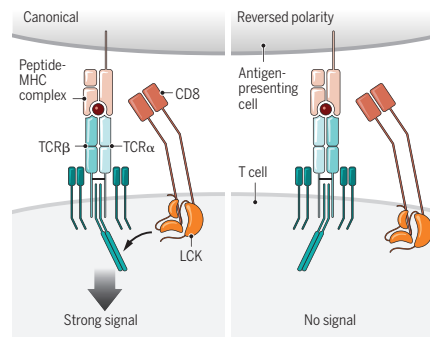
Engagement between a TCR and a cognate pMHC triggers TCR signaling that instructs cell fate decisions. During T cell development in the thymus, self-antigens evoke strong, weak, or negligible TCR signals that lead to T cell death (negative selection), survival (positive selection), or death “by neglect,” respectively. In mature T cells, strong TCR signaling stimulates proliferation and effector immune responses. TCR signaling is initiated by tyrosine phosphorylation of the TCR complex by the intracellular enzyme LCK (lymphocyte-specific protein tyrosine kinase). However, the mechanism of how antigen binding induces the intracellular signaling steps is still unresolved. Although not essential for TCR activation, invariant co-receptors CD4 and CD8 facilitate TCR signaling by binding to MHC class II (MHCII) and class I (MHCI), respectively. The co-receptors deliver LCK to the TCR complex to enhance positive (5) and negative selection (6) of immature T cells and TCR sensitivity in mature T cells (7). The sequestration of LCK by co-receptors shapes the self-MHC-restricted T cell repertoire by preventing maturation of T cells specific for MHCI/II-independent antigens (8).

Various TCRs associated with their cognate pMHC ligands exhibit similar, but not identical, binding orientation (9). High-affinity TCR-pMHC interactions with deviated (10) or even reversed docking symmetries (11) do not trigger TCR signaling. Zareie *et al.* explored the phenomenon of unproductive antigen engagement by comparing three murine TCRs that interact with an MHCI-restricted influenza antigen (H-2D<sup>b</sup>-NP<sub>396</sub>) in the canonical orientation and two TCRs that bind the same antigen in the reversed docking polarity (see the figure). T cells that recognized the reverse orientation did not respond to influenza infection in mice. Only canonical antigen docking recruited CD8 to the proximity of the TCR signaling motifs. Whereas CD8-LCK interaction activated a conventional TCR, it prevented the activation of a TCR recognizing the antigen with reversed docking polarity. The authors concluded that CD8 sequestered LCK and made it inaccessible for TCR-pMHC pairs with reversed docking polarity.

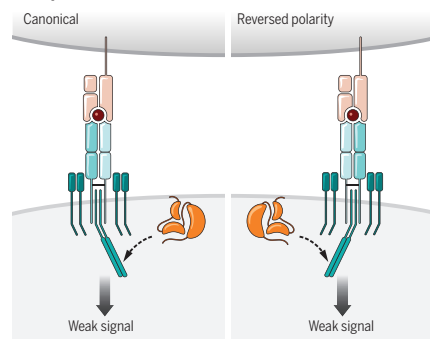
### Productive docking

The polarity of T cell receptor (TCR) binding to its cognate peptide ligand [presented by the major histocompatibility complex (MHC)] dictates whether lymphocyte-specific protein tyrosine kinase (LCK) phosphorylates the TCR and initiates signaling. Absence of CD8 alters LCK availability and results in weak signaling regardless of docking polarity.

#### Normal CD8-LCK interaction



#### Disrupted CD8-LCK interaction



The major finding of this study is that it provides an explanation for productive versus unproductive TCR-pMHC interactions by the engagement of CD8-LCK. Overall, CD8-LCK not only increases TCR sensitivity and skews the T cell repertoire toward pMHC/II recognition (8) but also restricts the orientation of productive TCR-pMHC docking (11). Two productive TCR-pMHC interactions with reversed docking orientation have been described in humans (12), suggesting that the mechanism proposed by Zareie *et al.* might not apply to CD4 co-receptor-mediated signaling. However, too few TCR-pMHC/II pairs with reversed docking polarity have been characterized so far to make any general conclusions.

A previous study characterized three productive and one unproductive human

TCR-pMHC interaction with conventional docking geometries (13). The most pronounced difference was that only the productive TCR-pMHC pairs formed catch bonds, which are stabilized by mechanical force. Catch-bond formation also predicted signaling in two pMHCII-restricted TCRs (13). Recruited CD8-LCK stabilizes the TCR-pMHC interaction, which enables suboptimal antigens to form catch bonds (14). Zareie *et al.* observed that canonical productive TCR-pMHC interactions formed catch bonds, whereas unproductive interactions with reversed docking polarity did not. Although TCRs with canonical and reversed docking polarity exhibited comparable time of antigen binding at 10-pN force, their differential ability to form catch bonds could be important. The catch bond might not just prolong antigen engagement but might also trigger conformational changes that promote TCR activation (15). However, Zareie *et al.* observed that the exclusion of CD8 resulted in comparable responses of the canonical and reversed docking polarity TCRs without affecting their differential ability to form catch bonds.

The connections between the roles of co-receptors and LCK in initiating TCR signaling, promoting catch-bond formation, and constraining the productive TCR-pMHC/II orientation are key emerging questions. Although there is no clear physiological role for unproductive TCR binding, such interactions are informative about TCR signaling itself. Understanding of mechanistic details of TCR activation are instrumental for rationalizing the design of antigenic receptors for immunotherapy. ■

#### REFERENCES AND NOTES

1. P. Zareie *et al.*, *Science* **372**, abc9124 (2021).
2. K. C. Garcia, *Trends Immunol.* **33**, 429 (2012).
3. B. D. McDonald, J. J. Bunker, S. A. Erickson, M. Oh-Hora, A. Bendelac, *Immunity* **43**, 859 (2015).
4. S. H. Krovit, J. W. Kappler, P. Marrack, L. Gapin, *Proc. Natl. Acad. Sci. U.S.A.* **116**, 22252 (2019).
5. B. Erman *et al.*, *J. Immunol.* **177**, 6613 (2006).
6. O. Stepanek *et al.*, *Cell* **159**, 333 (2014).
7. A. Drobnak *et al.*, *EMBO J.* **37**, 98518 (2018).
8. F. Van Laethem *et al.*, *Cell* **154**, 1326 (2013).
9. J. Rossjohn *et al.*, *Annu. Rev. Immunol.* **33**, 169 (2015).
10. J. J. Adams *et al.*, *Immunity* **35**, 631 (2011).
11. S. Gras *et al.*, *Immunity* **45**, 749 (2016).
12. D. X. Beringer *et al.*, *Nat. Immunol.* **16**, 1153 (2015).
13. L. V. Sibener *et al.*, *Cell* **174**, 672 (2018).
14. J. Hong *et al.*, *Nat. Immunol.* **19**, 1379 (2018).
15. C. Zhu, W. Chen, J. Lou, W. Rittase, K. Li, *Nat. Immunol.* **20**, 1269 (2019).

10.1126/science.abj2937